NDOT Research Report

Report No: RDT03-033

CREEP AND SHRINKAGE LOSSES IN HIGHLY VARIABLE CLIMATES (Final Report)

September 2003

Prepared by Research Division
Nevada Department of Transportation
1263 South Stewart Street
Carson City, Nevada 89712

TECHNICAL REPORT DOCUMENTATION PAGE

1. Report No. **RDT 03-033**	2. Government Accession No.	3. Recipient's Catalog No.
4. Title and Subtitle Creep and Shrinkage Losses in Highly Variable Climates	5. Report Date April 2003	
	6. Performing Organization Code	
7. Author(s) M. Saiid Saiidi and Cole Mortensen	8. Performing Organization Report No.	
9. Performing Organization Name and Address Department of Civil Engineering/258 University of Nevada, Reno Reno, Nevada 89557	10. Work Unit No.	
	11. Contract or Grant No. P133-99-803	
12. Sponsoring Agency Name and Address Nevada Department of Transportation 1263 S. Stewart Street Carson City, NV 89712	13. Type or Report and Period Covered 1-2001 to 6-30 2002	
	14. Sponsoring Agency Code	
15. Supplementary Notes		

16. Abstract

This study had several objectives, including studying the effects of aggregate type and climate on creep and shrinkage losses, determining and quantifying the effects of moist-curing concrete (after prestressing), and proposing necessary revisions to the current AASHTO equations for creep and shrinkage loss prediction. In Reno and Las Vegas, twelve post-tensioned concrete beams made with local aggregates were monitored for creep and shrinkage losses along with a number of cylinder specimens that were monitored for creep and shrinkage strains independently. At each location, two box girders were left indoors exposed to a more stable environment, and two box girders and two solid beams were left outdoors exposed to precipitation and a wider varying environment. Of each pair of beams, one beam was kept moist for two weeks after prestressing (moist-curing) and one beam was not.

Testing and analysis found that moisture can increase the stiffness of aged concrete by 20%, possibly reducing creep and shrinkage losses. Aggregate type was found to influence concrete susceptibility to creep and shrinkage losses and the effects of moisture. Testing and analysis also

found that in some cases the lifetime creep and shrinkage losses calculated from measured extrapolated surface strains exceeded the losses predicted by current prestress loss prediction methods from AASHTO, Naaman, and Nawy. Based on these findings, necessary revisions to the AASHTO equations for creep and shrinkage losses were proposed.

17. Key Words	18. Distribution Statement
Aggregate type, climate on creep & shrinkage, moist-curing concrete, prestressing , post tensioned concrete beams, box girders, concrete stiffness, relative humidity, creep/shrink cylinders	Unrestricted. This document is available through the National Technical Information Service, Springfield, VA 21161

19. Security Classif. (of this report)	20. Security Classif. (of this page)	21. No. Of Pages	22. Price
Unclassified	Unclassified	178	

ABSTRACT

This study had several objectives, including studying the effects of aggregate type and climate on creep and shrinkage losses, determining and quantifying the effects of moist-curing concrete (after prestressing), and proposing necessary revisions to the current AASHTO equations for creep and shrinkage loss prediction. In Reno and Las Vegas, twelve post-tensioned concrete beams made with local aggregates were monitored for creep and shrinkage losses along with a number of cylinder specimens that were monitored for creep and shrinkage strains independently. At each location, two box girders were left indoors exposed to a more stable environment, and two box girders and two solid beams were left outdoors exposed to precipitation and a wider varying environment. Of each pair of beams, one beam was kept moist for two weeks after prestressing (moist-curing) and one beam was not.

Testing and analysis found that moisture can increase the stiffness of aged concrete by 20%, possibly reducing creep and shrinkage losses. Aggregate type was found to influence concrete susceptibility to creep and shrinkage losses and the effects of moisture. Testing and analysis also found that in some cases the lifetime creep and shrinkage losses calculated from measured extrapolated surface strains exceeded the losses predicted by current prestress loss prediction methods from AASHTO, Naaman, and Nawy. Based on these findings, necessary revisions to the AASHTO equations for creep and shrinkage losses were proposed.

ACKNOWLEDGEMENTS

This study was sponsored by the Nevada Department of Transportation (NDOT) and the Federal Highway Administration (FHWA) grant # P133-99-803. However, the findings of the study do not necessarily represent the views of NDOT or FHWA. Mr. Bill Crawford, the Chief Bridge Engineer at NDOT and the staff of the NDOT Bridge Division are thanked for all of their help. Committee members Dr. David Sanders and Dr. Yanyao Jiang are thanked for their involvement in the project. Dr. Ashraf Ahmed, and Mr. Mohammad Hasan are thanked for the countless ours spent collecting data and helping with the Las Vegas end of the study. Thanks to the lab technicians, Mr. Jesus Pedroarena, Dr. Patrick Laplace, Mr. Paul Lucas, and Mr. John Drumm, for their invaluable help on the study. Mr. Jessen Mortensen, Ms. Catherine French, Dr. Nagi Abo-Shadi, Mr. Erik Reinhardt, and Mr. John Ziegler are also thanked for all of their help during the design and construction portion of the study.

TABLE OF CONTENTS

Page

LIST OF TABLES

LIST OF FIGURES

CHAPTER 1
INTRODUCTION

1.1 Introductory Remarks

An important aspect of the design of prestressed concrete is the prediction of prestress losses over the lifetime of the prestressed element. These losses consist of two basic types, instantaneous and time-dependent. Instantaneous losses consist of stress losses in the prestressing steel due to anchorage set, friction with the grout duct, and elastic shortening. Time-dependent losses include losses due to the relaxation of the prestressing steel, creep of concrete, and shrinkage of concrete. Unlike the instantaneous losses that occur at the time of tensioning, time-dependent losses occur over the lifetime of the structure, and are affected by variations in relative humidity, precipitation, and temperature. These losses also vary with the size and shape of a member, initial stress in the prestressing steel, material properties, as well as aggregate type used in the concrete mix. Accurate estimation of these losses is critical in the design of prestressed concrete, as they can affect the lifetime performance of the structure. Unexpected losses can result in excessive deflections, lower cracking loads, and wider cracking under service load conditions.

Nevada typically has a dry desert climate and is subject to very high variations in temperature and relative humidity. Throughout the course of the study discussed in this report, the average relative humidity for Reno was 46.6%, with a daily high of 100% and a daily low of 6%. On average the relative humidity in Reno would cover a range of 45%, with a maximum difference between the high and low relative humidity in a single day of 83%. Las Vegas showed a similar trend with an average relative humidity of 32%, with a daily high of 100% and a daily low of 7%. The maximum range that the relative humidity covered in a single day for Las Vegas was 77%, with an average daily relative humidity fluctuation of 24.3%. These statistics show how unpredictable the climate in these areas can be. This wide range of relative humidity can affect the creep and shrinkage losses in these regions, making accurate loss estimation difficult since the current design guidelines are based on studies that were performed under constant relative humidity.

1.2 Previous Research

Prestressing concrete is a procedure that has been around since the late 1800's, and since then many extensive studies have been done in laboratory environments that have lead the way for the current procedures used to predict the losses of prestress in the prestressing strands for both instantaneous and time-dependent losses. These studies have been performed using many different independent variables, finding that the shape and size of a member, the aggregate used in the concrete mix, the initial stress value, the age of the concrete, the admixtures used in the concrete, and the temperature and relative humidity that the concrete is exposed to are all variables that affect the losses seen in

prestressed members. Some of these tests date back to the 1930's. The current prediction procedures have equations based on the results of these tests.

During World War II, higher strength steel emerged and technology improved allowing prestressed concrete to become a more widely used procedure in bridge design. In the years following World War II, many of the bridges in western and central Europe were designed and rebuild using the concept of prestressing. In 1943, Schorer[1] published a method of predicting prestress losses, which calculated shrinkage as a function of relative humidity and creep as a function of relative humidity and initial stress. The current method of predicting creep and shrinkage losses specified by AASHTO[2] was reportedly based on Shorer's work. The current AASHTO equation for shrinkage is a function of relative humidity and the equation for creep is a function of initial stress.

In 1965, a study by Keeton[3] had a significant impact on the development of more sophisticated creep and shrinkage loss prediction methods. Keeton tested many different specimens of several shapes and sizes under varying conditions including steam-curing and moist curing (before prestress), varying levels of relative humidity, and varying levels of initial stress. The results were reported to have been the basis of the development of the equations that factor the ultimate creep and shrinkage values used in the current methods by ACI Committee 209[4], Naaman[5], and Nawy[6].

During the following years, many studies were performed to increase the understanding of the variables that influence the properties of concrete. Neville[7] suggested that the stiffness of concrete (Modulus of Elasticity, E) is affected by moisture, and that stiffness of wet concrete is approximately 24% higher than dry concrete stiffness. This phenomenon is also mentioned in Mehta and Monterio[8] who state that the stiffness of wet concrete is 15% higher than the stiffness of dry concrete. Mehta and Monterio also state that the compressive strength concrete is also affected by moisture, being approximately 15% lower in wet concrete than dry. They also point out that the type of aggregate used in the concrete mix can affect the stiffness of concrete. The sensitivity of concrete stiffness to moisture can affect prestress losses.

In more recent times, some emphasis has been placed on studying the actual losses experienced by specimens in the field exposed to varying climatic conditions. Mangoba et al.[9] discusses many of the recent research projects comparing the actual losses in prestressed bridges to the losses predicted by accepted methods. Several of these tests done on full-scale post-tensioned box girder bridges including Mangoba et al. lead to the development of the study presented in this document.

In 1989, Saiidi and Shields[10, 11] studied the Golden Valley Bridge in Reno. The bridge was a single-span, post-tensioned box girder that was instrumented with electric resistance strain gages and mechanical gages and was monitored for two and a half years. The mechanical gages used in the study were installed along the depth of the girder to monitor the strain distribution throughout the section. Prestress losses were calculated using the AASHTO Specifications and Naaman's time-step method and then compared to

the lifetime losses extrapolated from the measured data. The extrapolated losses were 60% higher than the losses calculated using the AASHTO method and 30% higher than the losses calculated using Naaman's method.

In 1994, Saiidi et al.[12, 13] studied the Greenway Bridge in Las Vegas. The single-span, post-tensioned box girder was instrumented with electric resistance strain gages and mechanical gages. The mechanical gages were installed at the level of the instrumented strain gages. The lifetime losses extrapolated from the measured data were also compared to the methods suggested by AASHTO and Naaman. The estimated losses using the AASHTO method were conservative by 40%, and the estimated losses using Naaman's method showed good correlation.

Mangoba et al. studied four bridges in the Reno area stressed on different dates at the South Meadows Interchange, the Mount Rose Interchange, the Zolezzi Lane Grade Separation, and the Old Virginia Road Grade Separation. The four post-tensioned box girder bridges were instrumented with mechanical strain gages. The South Meadows Interchange and the Mount Rose Interchange were two-span bridges and theZolezzi Lane Grade Separation were single span bridges. Mangoba et al. found that AASHTO overestimated losses in the Zolezzi and the Mount Rose bridges by 31% and 7%, respectively. They also found that the losses in the South Meadows and Old Virginia bridges were underestimated by AASHTO by 7% and 30%, respectively. It was noted that the Zolezzi Lane and Old Virginia bridges were exposed to unusual conditions following stressing. For the first week following stressing, the bridge at Old Virginia Road was subject to a significant drop in RH, which is believed to be responsible for the excessive loss. In contrast, the Zolezzi Lane Bridge was subjected to relatively high moisture and experienced low losses due to inadvertent dumping of water from a tanker truck and closure of drainpipes in the bottom slab of the box superstructure.

In 1996, further research was performed into the effects of aggregate type on creep, shrinkage, and elastic modulus. Alexander[4] studied concrete made from 23 different aggregate types. Alexander concluded that the values of creep, shrinkage, and elastic modulus can each vary by as much as 100%, depending on aggregate type.

The range of results from the studies performed prior to 1999 as well as the noted and unknown effects of moisture on concrete after prestressing presented a need for a more controlled study to better understand the effects of some of the actual environmental conditions and aggregate sources.

Since the development of the study discussed in this document, research has continued into creep and shrinkage losses. In 2000, Robertson[15] presented a study on the correlation between field observations and creep and shrinkage models. Laboratory tests were performed on concrete used in the North Halawa Valley Viaduct in Hawaii. These tests found that losses experienced by the concrete made with basalt aggregate were underestimated by all of the models used for the comparison.

A new procedure by Gardner[16] for predicting creep and shrinkage in concrete uses the element size, relative humidity, 28-day specified strength, and the strength at the end of curing or at loading. The procedure emphasizes the importance of the elastic modulus of concrete, and states that the method is accurate within 25% regardless of casting temperature, curing, or admixtures in the concrete.

In 2000, a study by Sakata and Ayano[17] found that the ambient temperature and humidity to which concrete is exposed to can have a large influence on creep and shrinkage. They found that the effect of temperature has a larger influence on creep and shrinkage than the relative humidity, and the difference of the season in which concrete is cast can highly influence the magnitude of creep and shrinkage. It was also noted that creep can be heavily influenced by the temperature of curing water prior to prestress, and that concrete subjected to an increase in temperature is subject to higher shrinkage than concrete subjected to constant temperature.

1.3 Object and Scope

Previous studies conducted on concrete box girder bridges in Reno and Las Vegas have indicated that creep and shrinkage losses are often underestimated by current design methods. Due to differences in the bridges involved in these studies, pinpointing the causes and quantifying the results of these studies to produce more accurate design equations was difficult. From these studies several possible variables were identified as potentially having a large influence on creep and shrinkage losses. These variables were climate (relative humidity, temperature, and precipitation), aggregate type, and curing (discussed later).

This study had several objectives, including observe creep and shrinkage losses and propose necessary revisions to the current AASHTO equations for creep and shrinkage loss prediction, determine the effects of moist-curing prestressed concrete after the application of prestress, quantify the effects of this type of curing on box girders and solid beams, and to study the effects of aggregate and climate on creep and shrinkage losses in prestressed concrete.

Twelve prestressed concrete beam specimens, eight box girders and four solid beam specimens, were constructed and monitored in this study. The beams were studied in two locations, six in Reno and six in Las Vegas, which determined the aggregate used as well as the climate that the specimens were exposed to. At each location, two box girders were left indoors and two box girders and two solid beams were left outdoors. Of each pair of beams, one beam was moist-cured for a period of time following the application of prestress, and the other was not. Each beam was monitored with two different types of strain gages, mechanical and electric resistance gages. With each pair of beams, concrete cylinders were kept and were used to measure creep and shrinkage strains. Data were collected for at least 24 months for the box girders and 15 months for the solid beams. Prestress losses were then calculated from the strain data collected and then log-fit to estimate 40-year losses.

The extrapolated measured 40-year losses calculated were then compared to the values calculated by three current prestress loss prediction methods by: AASHTO, Naaman, and Nawy. The method presented by AASHTO, which is a method currently used in bridge design, calculates creep and shrinkage losses as a functions of initial stress and relative humidity. The methods by Naaman and Nawy are more complex, calculating creep and shrinkage losses as functions of many variables including initial stress, relative humidity, volume-to-surface ratio, and time, which have origins based on the recommendations of ACI Committee 209.

The effects of moist-curing were also investigated. Research indicated that the elastic modulus was influenced by moisture and could be a possible reason for the effects of moisture on prestress losses. Elastic modulus data were measured on one-year old concrete cylinders, dried and wet, and with other research an approximation for quantifying the effects of moisture on elastic modulus was developed.

CHAPTER 2
DESCRIPTION OF SPECIMENS

2.1 Introductory Remarks

There are twelve main specimens involved in this study, eight box girders and four solid beams. This chapter outlines describes selection of aggregates, the methods used to design the specimens, the materials used to construct the specimens, the construction process, and the test variables.

2.2 Aggregate Selection

Aggregate selection was based on several parameters. Modulus of elasticity, aggregate content, absorption, size, cleanness, and thermal expansion were among these parameters. Aggregates were selected based on suggested sources and the utilization of mix designs from the most commonly utilized companies providing aggregates for NDOT bridges. The aggregates chosen were selected as part of representative mix designs that demonstrated the most sensitivity to creep and shrinkage effects.

Different aggregate types and sources were considered for each of the Northern Nevada and Southern Nevada regions. Appendix A presents the summary of the aggregate selection study.

The final aggregate source selected for the north was All Lite Lockwood and Gopher Pit, which produce Metamorphic Andesite. In the south, since all of the plants produce essentially the same rock type for concrete, limestone was the aggregate chosen.

2.3 Box Girders

Important dates concerning the construction and stressing of the beam specimens are listed in Table 2.1.

2.3.1 Design

The design of the box girders was developed to model a single cell of a typical box girder bridge. The box girders are approximately one-quarter scale with dimensions that were selected based on AASHTO guidelines for prestressed concrete and ease of constructing and testing. The compressive stress limits in concrete outlined by AASHTO set a maximum stress of 55% of the concrete compressive strength at the time of stressing (f'_{ci}) and 40% of the concrete strength at 28 days. A concrete strength of 6 ksi (41.4 MPa) was chosen for the design of the girders.

The box girder final design was simply supported with an overall length of 12 ft. (3.658 m) and a clear span length of 11 ft. (3.353 m). The girders are 10 in. (254 mm) deep and 12 in. (304.8 mm) wide with 2.5 in. (63.5 mm) thick webs and 2 in. (50.8) thick

flanges. Each web in the box girder contains two prestressing tendons (four total per box girder). The prestressing tendons were to be centered about the midpoint of the web, spaced at 2.5 in. (63.5 mm) on center (Figs. 2.1-2.2).

The tendons were to be stressed to a level representative of the stress ratio commonly used in bridges. The box girder design was to allow the tendons to be stressed to 65% of their ultimate strength (f_{pu}) and to produce a maximum compressive force of 55% f'_{ci} in the mid-section of the girders.

Reinforcing in the girders consisted of #4 (∅12.7 mm) longitudinal reinforcing bars with #3 (∅9.5 mm) reinforcing bar stirrups spaced at 8 in. (203 mm). The end blocks of the girders had perimeter stirrups spaced at 3.5 in. (88.9 mm), with a grid of horizontal and vertical #4 (∅12.7 mm) reinforcing bar stirrups spaced at 3 in. (76.2 mm). The ends of each beam were capped with a 1 in. (25.4 mm) thick plate to distribute the stresses from the anchors.

2.3.2 Materials

Table 2.2 contains a summary of the materials used to construct the test specimens.

2.3.2.1 Prestressing Steel

The prestressing steel used in the box girders was 0.6 in. (15.2 mm) diameter, stress-relieved, seven-wire, grade 270 strands (ASTM A416). The material properties of the prestressing steel were measured at the NDOT Materials Division. The elastic modulus of the tendons was measured at 28100 ksi (193790 MPa), with an ultimate strength of 280 ksi (1930 MPa).

2.3.2.2 Concrete

The box girders were constructed with normal weight concrete. The aggregate used in the concrete for Reno was andesite, and limestone was the aggregate used in the concrete in Las Vegas. The concrete used to pour the Reno box girders had a twenty-eight day strength of 6.7 ksi (46.2 MPa). The twenty-eight day strength of the concrete used to pour the Las Vegas box girders was 3.8 ksi (26.2 MPa).

2.4 Solid beams

2.4.1 Design

The design of the solid beams was developed to produce a concrete stress of 45% of the 28-day concrete compressive strength with a single prestressing strand stressed to 70% of the ultimate strength of the prestressing steel. The final selection of the

dimensions for the solid beams were based on finding dimensions that would correspond to standard lumber dimensions to allow for more efficient construction.

The final beam design was a two-span beam. Each beam was 8 ft. (2.438 m) in length, with a cross-section 5.5 in. (139.7 mm) deep by 4.5 in. (12.7 mm) wide. Each beam contained a single prestressing strand, which passes through the centroid of the section (Figs. 2.3-2.4).

Reinforcing in the solid beams consisted of #3 (∅9.5 mm) longitudinal reinforcing bars in the corners of the cross-section with #3 (∅9.5 mm) perimeter stirrups spaced at 5 in. (127 mm). The ends of each beam were capped with a 1 in. (25.4 mm) thick steel plate to distribute the stresses from the anchors.

2.4.2 Materials

2.4.2.1 Prestressing Steel

The prestressing steel used in the solid beams was the same as the prestressing steel used in the box girders (Table 2.2).

2.4.2.2 Concrete

The solid beams were constructed with normal weight concrete. The aggregates used in the concrete were andesite and limestone for Reno and Las Vegas, respectively. The concrete used to pour the Reno solid beams had a twenty-eight day strength of 4.1 ksi (28.3 MPa). The twenty-eight day strength of the concrete used to pour the Las Vegas solid beams was 5.8 ksi (40.0 MPa).

2.5 Cylinders

Concrete test cylinders (6 in. (152 mm) by 12 in. (305 mm)) were poured with each batch of concrete. The cylinders were used to perform several different tests, including concrete strength, creep, shrinkage, and elastic modulus. Each set of beams had a set of cylinders for strength testing, and a set of cylinders exposed to the same environment for shrinkage data. The box girders also had a set of cylinders exposed to the same environment and stressed in creep frames for creep data. Extra cylinders from the Reno Box Girder pour were used for elastic testing discussed in Chapter 4.

2.6 Construction

The box girders were constructed in wooden forms. The hollow section of the box was created using Styrofoam that was cut to produce a hollow section of the proper dimensions. The foam needed to be in the proper location after the concrete was poured, so it was held in place vertically by wire strung horizontally across the forms and by

wooden framework and horizontally by the bolts used to hold the prestressing strands in place (see Fig. 2.5).

The box girders were poured upside down in layers. The bottoms of the forms were poured up to the wires used to keep the foam in the proper location. The foam was then inserted into the rebar cages, and the sides of the beams were then poured around the foam. A wooden framework was then placed on top of the foam in the center of each beam to keep the foam from rising in the concrete and to produce the access hole to the box. The box girders were then vibrated both in the concrete and along the outside of the forms to eliminate air voids.

The solid beams were also constructed in wooden forms. Since the design of the solid beams was much less complex, they were all cast at once. Once the solid beams were poured, the concrete was vibrated both directly and along the outside of the forms to ensure that there would be no air voids.

There were separate pours for each of the test groups. The Reno specimens were made from concrete mixed at the lab in a 6 $ft.^3$ (0.17 m^3) capacity mixer. The box girders total of six batches were mixed, five batches of 6 $ft.^3$ (0.17 m^3) and one batch of 4.5 $ft.^3$ (0.13 m^3) feet. The solid beams required a single 6 $ft.^3$ (0.17 m^3) batch of concrete to complete the pour.

The Las Vegas concrete was ordered. Therefore it took a single batch to pour the box girders, and a single batch to pour the solid beams.

2.7 Test Variables

There were many variables used in this study (summarized in Table 2.3). Since the project is a study into the effects of aggregate and climate on creep and shrinkage, location was one of the major variables. There were two locations used in the project, Reno and Las Vegas. These locations reflect the locations of the greatest number of bridges in Nevada.

The locations dictated aggregate use, as the aggregates chosen were those that would most commonly be used in these locations in prestressed concrete bridges. In Reno, the aggregate chosen was metamorphic andesite from All-Lite Lockwood and fines from Gopher Pit. In Las Vegas, the aggregate chosen was limestone, since all of the sources in Las Vegas supply this aggregate.

The locations also dictated climate. Two of the box girders in both Reno and Las Vegas were kept outside, exposed to the local climate, and two of the box girders at each location were kept inside buildings to expose the beams to a more stable climate. The solid beams at each location were kept outside. As a result, the outdoor specimens were subjected to precipitation, whereas the indoor specimens were not.

Another variable was the type of specimen. This study utilized two main specimen types, box girders and solid beams.

The final variable for the study was referred to as curing, however it is a curing of the beams following the stressing of the prestressing steel. Studies have shown that the greatest amount of prestress losses due to creep and shrinkage occur in the first few months and that moist concrete can be up to 30 % stiffer than dry concrete. Previous studies have also indicated that prestressed concrete that is moistened following the application of prestress performs better. Therefore, to further explore this phenomenon, one specimen was moistened daily or twice daily for the first two weeks following prestressing and one specimen was kept dry, for the pairs of specimens at each location and climate.

2.7.1 Naming Convention

In order to distinguish between test specimens, a naming convention was developed as seen in Table 2.3. The first two letters of each specimen's name correspond to the specimen location, Reno (RN) and Las Vegas (LV). The third letter of each specimen's name corresponds to the exposure climate, indoor (I) and outdoor (O). The fourth letter of each specimen's name corresponds to the curing of the specimen, moist (M) and air (A). Finally, the last letter of each specimen's name corresponds to the type of specimen, solid beam (S) and Box Girder (B).

CHAPTER 3
INSTRUMENTATION

3.1 Introductory Remarks

In this study the time-dependent losses in prestressed concrete members were monitored using several different methods. The first method was the use of electric resistance strain gages bonded directly to the prestressing strands. The second method was mechanical strain gages mounted on the concrete surface. Finally, concrete cylinder samples taken from the pours for each of the beam specimens were monitored for creep and shrinkage losses.

3.2 Box Girders

3.2.1 Equipment

The electric strain gages used originally in the box girders were manufactured by Measurements Group, Inc. The gages were of type EA-06-125AD-120, 120-Ohm resistance, 2.07 $\pm$ 0.5 % strain gage factor, and + 1.2 $\pm$ 0.2 % transverse sensitivity. These gages were originally installed in all of the box girders. However, due to loss of gages during an initial attempt at tensioning the Las Vegas box girders another gage type was mounted on the prestressing strands. Those gages were made by Tokyo Sokki Kenkyujo Co., Ltd., and purchased from Texas Measurements, Inc. The gages were of type FLG-1-11, 120-Ohm resistance, and 2.07 $\pm$ 1 % strain gage factor.

The electrical strain gage data from the Reno box girders was collected using a MEGADAC Data Acquisition System, manufactured by OPTIM Electronics. The electrical strain gage data from Las Vegas box girders was collected using a National Instruments Data Acquisition System.

The mechanical strain gages mounted on the box girders were made by the L. S. Starret Company. The gages were mounted on the beams to have an 18 in. (457 mm) gage length. The gages were dial gages with a range of 0.4 in. (10 mm) and sensitivity to 0.0001 in. (0.0025 mm).

3.2.2 Instrumentation

Each strand was instrumented with three electric gages. The gages were installed on alternating wires of each strand (Fig. 3.1). The installation of electric gages was done in several steps. First, the surface of each wire, in the strand where a gage was to be located, was cleaned to ensure an effective bond. The tendons were packed in grease inside a plastic sheath, so the plastic was stripped and the grease was removed. The strain gage locations were then sanded and polished, and cleaned using an acidic solution followed by a basic solution.

The original electric strain gages were bonded to the prestressing strands using a M-BOND AE-15 kit from Measurements Group, Inc. The additional gages used in the Las Vegas box girders were bonded using a cyanoacrylate adhesive manufactured by Tokyo Sokki Kenkyujo Co., Ltd., and purchased from Texas Measurements, Inc. All the gages were then covered with Teflon tape, butyl rubber, neoprene rubber, and finally electrical tape. Figure 3.2 shows the instrumented strands. These coatings were used as a precautionary measure to help avoid damaging the gages during tensioning. The sections of tendon that were exposed were then covered with rubber hose to help protect the gages. The tendons were then placed in the forms, and the beams were poured.

The original electric gages in the Las Vegas box girders were not used because they were damaged during the initial attempt to tension the strands. In these girders, a new bearing plate (plate 2) was added at one end of the box girders, supported by steel pipe that covered the tendons and gages (Fig. 3.3 and 3.4). The anchorages were then anchored against plate 2 transferring the compressive load through the pipes to the first plate (plate 1). Since the tendons were unbonded and the stress is uniform through the length of the tendon, an external section of tendon that measure the same strain was created. This external section was where the second set of gages was mounted (Fig. 3.1 and 3.5). By using this method, the electric gages were protected during the final tensioning.

The mechanical dial gages were attached to the webs of the box girders at mid-span by drilling into the concrete and using concrete anchors. A system of nuts and bolts and a 0.25 in. (6.35 mm) diameter steel rod were assembled to produce the strain gage (Fig. 3.6). Sections of PVC pipe were capped then cut to produce covers to protect the gages from accidental bumping or other environmental hazards (Fig. 3.7).

3.2.3 Data Collection Schedule

The data collection schedule for the box girders was daily for the first week, followed by weekly readings for the remainder of the first month, and then monthly for the remainder of the study.

3.3 Solid Beams

3.3.1 Equipment

The electric strain gages used for the solid beams were the same type of gages as the second set that were used on the Las Vegas box girders. The electrical strain gage data from the solid beams were collected using a National Instruments Data Acquisition System.

The mechanical strain gages mounted on the solid beams were made by the L. S. Starret Company. The gages were mounted on the beams to have a 42 in. (1.067 m) gage

length (Fig. 3.8). The gages were dial gages with a range of 0.4 in. (10 mm) and sensitivity to 0.0001 in. (0.0025 mm).

3.3.2 Instrumentation

The instrumentation process for the electric gages was similar to the box girders. The tendons and the bonding surface were prepared in the same fashion. The strain gages were bonded to the prestressing strands using the same adhesive that was used for the second set of gages used on the Las Vegas box girders, and the gages were then covered and protected in a similar fashion.

A method similar to the strain gage retrofit for the Las Vegas box girders was used for the solid beams. To limit electric gage loss, the gages were bonded to the tendons outside of the concrete section. The force was transferred from the anchorages through a plate and a steel pipe to the plate on the ends of the beams. The pipes allowed the gages to be bonded to a tensioned section of the tendon without being damaged through the tensioning process (Fig. 3.9 and 3.10).

The mechanical dial gages were attached to the tops of the solid beams in a fashion similar to the box girders. Sections of PVC fence posts were cut and bolted on to the tops of the beams to prevent the gage from damage (Fig. 3.11).

3.3.3 Data Collection Schedule

Data was collected for the solid beams daily for the first two weeks, weekly for the rest of the first month, and monthly for the rest of the study.

3.4 Cylinders

3.4.1 Equipment

During each concrete pour, a number of 6 in. x 12 in. (152 mm x 305 mm) concrete cylinder specimens were cast. These cylinders were used for concrete strength tests, modulus of elasticity tests, and collecting creep and shrinkage data at each beam location. Each beam set had three cylinders that were tested to determine the 28-day concrete compressive strength. Each pair of box girders had five cylinders poured from the same concrete located in the same environment, two creep and three shrinkage. Three shrinkage cylinders accompanied each pair of solid beams. The cylinders were left exposed to the environment at each location, and were not subjected to the same moist curing that part of the beam specimens were.

The creep cylinders were kept in a frame that was stressed at the same time as the corresponding beam specimens. The cylinders were loaded to a stress slightly higher than the stress in the concrete at the centroid of the prestressing tendons in typical bridge girders. A jack and pump were used to stress the pair of cylinders to a stress of 2 ksi

(13.8 MPa)(Fig. 3.12). Spring washers were used in each frame to help maintain the stress on the cylinders. The spring washers used were part number K2750-K-275, manufactured by Key Bellevilles, Inc.

3.4.2 Instrumentation

Each cylinder was fitted with two aluminum tabs that served as reading points spaced for an 8 in. (203 mm) gage length (Fig. 3.13). The tabs were attached using a five-minute epoxy. A multi-position strain gage, model 35-2882, from ELE International, was used in the reading points to determine the strains in each cylinder. The multi-position gage had a range of 0.2 in. (5.1 mm), gradations to 0.0001 in. (0.0025 mm), and accuracy to 0.0005 in. (0.013 mm).

3.4.3 Data Collection Schedule

The data collection schedule for the cylinders varied depending on the tests performed on each cylinder. Data was collected from the creep and shrinkage cylinders at the same time that the prestress data from the corresponding beams was taken. Concrete strength tests were performed at seven days, fourteen days, and twenty-eight days after pouring. The cylinders used in the elasticity modulus testing were weighed daily until they reached a constant weight, at which time data was taken. Chapter 4 describes the objective and results for the elasticity modulus test.

3.5 Temperature and Relative Humidity

Each time that data was collected, temperature and relative humidity were measured using a Dickson DH121 Data Logger. The data logger has a temperature range of –30 to +120 °F (-34 to 50°C), with a temperature accuracy of ± 1.8 °F (± 1 °C). The relative humidity range for the data logger is 0 to 90 %, with an accuracy of ± 2 %.

CHAPTER 4
THEORETICAL ANALYSIS OF PRESTRESS LOSS

4.1 Introductory Remarks

The following chapter outlines the methods used to predict and compare prestress loss to the measured data and the possible ways of modifying those methods to produce a more accurate model. This study utilizes three main methods of predicting prestress loss. The first method of loss prediction is the AASHTO method[2], which is currently used by NDOT. The other two are time-step methods proposed by Naaman[5] and Nawy[6].

The creep and shrinkage losses in the beams are the only types of losses that the beam instrumentation monitors. Losses such as anchorage set and friction are not monitored since the first data point is taken after these losses have occurred. Losses due to relaxation of prestressing steel are also not monitored, since they are losses in stress without a change in strain. With this in mind, the creep and shrinkage values from the afore mentioned methods were the only losses considered in the prediction of prestress losses.

This chapter discusses the theory used in this study, covering some of the current prediction methods, possible explanations for creep and shrinkage losses being affected by moisture, and methods used to evaluate the validity some of the equations used in the current prediction methods.

4.2 Description of Methods

4.2.1 AASHTO

The refined estimates of time-dependent losses in the Standard Specifications for Highway Bridges of AASHTO was used for comparison in this study. The following is an overview of the procedure presented by.

Shrinkage Loss, Δf_{pSH}

$$\Delta_{pSH} = 0.80(17.0 - 0.150RH) \text{ (ksi)}$$

$$\Delta_{pSH} = 0.80(117 - 1.03RH) \text{ (MPa)} \qquad (4.1)$$

RH = average annual ambient relative humidity (%)

Creep Loss, Δf_{pCR}

$$\Delta_{pCR} = 12.0f_{cgp} - 7.0\Delta f_{cdp} \qquad (4.2)$$

f_{cgp} = concrete stress at center of gravity of prestressing steel at transfer
Δf_{cdp} = change in prestress in concrete stress at center of gravity of prestressing steel due to permanent loads, with the exception of the load acting at the time the prestressing force is applied.

4.2.2 Time-Step Methods

The time-step methods allow prestress losses to be calculated for different periods of time, which lends itself to comparison with measured data, as the method can be used to predict losses on any day that data was taken. The time-step methods are more complex than the AASHTO method because they utilize more of the variables that affect prestress losses. Both of the time-step methods used in this study were based on the recommendations of ACI Committee 209[4].

For the purposes of this study, only the creep and shrinkage losses were compared with the measured data. However, since relaxation of the prestressing steel affects the amount of stress that the concrete is experiencing, without a change in length, relaxation was included when calculating creep losses and not when comparing to the measured data.

For calculation and comparison purposes, each time-step was taken to coincide with the time interval used in collecting data. The ultimate losses were found for 40 years. For projected loss calculations, the time-steps were taken at monthly intervals beyond the last data point up to 1000 days, beyond which the time-step was changed to yearly intervals for the remainder of the forty-year lifetime.

Different from Naaman whose method predicts only loss over a certain period of time, the method proposed by Nawy determines the total prestress losses at anytime beyond the time of prestressing. See Appendix B for a thorough description of these methods, including the variables used.

4.3 Effect of Moisture on Elastic Modulus

In the study by Mangoba et al.[9], as mentioned earlier, the losses in the Zollezi Lane Grade Separation were significantly lower than the other bridges involved in the study and the losses predicted by AASHTO and Naaman. These lower losses were a result of the bridge being soaked with water following tensioning. Water is expected to reduce shrinkage in new concrete, but the Zollezi Lane Grade Separation was 64 days old when post-tensioning occurred. An investigation occurred to determine why water had such an effect on the performance of aged concrete. The basic material properties of concrete were searched and two properties were found to be influenced by moisture. Mehta and Monteiro[8] state that the concrete compressive strength (f'_c) of wet concrete is 15% lower than dry concrete, and that the elastic modulus (E) of wet concrete is 15% higher than dry concrete. However, since a lower compressive strength would have a detrimental affect on the creep and shrinkage losses, the concrete property responsible for

the decreased losses would have to be the elastic modulus. Neville[7] suggests an increase in stiffness of 24 % for wet concrete versus dry, Mehta and Monteiro claim a 15 % increase in stiffness.

Five concrete cylinders from the Reno box girder pour were subjected to elastic modulus testing. At the time of testing, the cylinders were eleven months old. The testing consisted of a series of cycles. Each cycle consisted of a period of drying followed by an elastic test and a period of wetting followed by an elastic test. The cylinders were dried in an oven at 212°F (100°C). The cylinders were periodically weighed to help determine when they had dried completely. When the cylinders reached a constant weight between measurements, they were assumed to be dry and they were then tested. After testing, the cylinders were put in a moist room, where the relative humidity is 100%. In the moist room, the cylinders were also subjected to some direct moisture from the misters. The cylinders were left in the moist room for about a week and then weighed to determine how much water they had absorbed. They were then tested again.

For the elastic modulus test, ASTM CT-170 was used. Since the cylinders were to be placed in an oven and the moist room, some concern was raised about using capping compound on the cylinders. Neoprene testing pads were seen as an acceptable alternative to capping compound. Unfortunately, the test setup for ASTM CT-170 does not work with neoprene pads, so the test procedure was modified slightly. ASTM CT-170 utilizes a 10 in. (254 mm) gage length, but in order to make the test work with the neoprene testing pads the gage length was shortened to 9 in. (229 mm).

The measured data averaged for the five cylinders are shown in Fig. 4.1. From these tests, an increase in the elastic modulus of concrete due to moisture of 18% was found. This increase was within the range of 15 to 24% reported by others[7, 8]. An increase in the elastic modulus of 20% was chosen to develop an equation to possibly quantify the effect on prestress losses.

The 20% increase in elastic modulus was for a relative humidity of 100%. To determine how the elastic modulus is affected by moisture, the model by Ramachandran et. al.[18] was used. The authors describe the effects of relative humidity on the elastic modulus of cement paste (not concrete). They suggest that the elastic modulus of cement paste is not affected by moisture up to 50 % relative humidity. Above 50 % relative humidity, the elastic modulus increases to 154 % of the dry elastic modulus, which can be seen in Fig. 4.2. The curve from that study was scaled to show an increase of 20 % at 100% relative humidity and an equation for the elastic modulus in concrete was developed (Fig. 4.2):

$$X = 0.000093RH^2 - 0.0101RH + 1.2766 \qquad (4.4)$$

In which X is the factor to adjust the elastic modulus.

This equation creates a coefficient to multiply by the elastic modulus to produce a modified elastic modulus for concrete subjected to a relative humidity greater than 50 %. Using this new equation to modify the elastic modulus in the Naaman's time-step method, the effects of relative humidity on prestress losses are estimated. Figure 4.3 demonstrates the effects of one week and two-week periods of exposure to relative humidity in a box girder with properties based on the box girders in this study. From this figure, moist curing (relative humidity at approximately 100%) the beam for two weeks following the application of prestress can reduce the long-term prestress loss compared to the losses expected at the ambient humidity by 18%, and an abnormally dry period in the first two weeks can increase prestress losses by 12%. This figure shows the effects of relative humidity lower than 50% as varying the long-term losses, which is a result of using a varying relative humidity in the time-step method and not the modified elastic modulus.

4.4 Creep and Shrinkage Factors

Another possible method of modifying current models to produce better accuracy was to adjust the creep and shrinkage factors in time-step analysis. These factors were traced to a study performed at the U. S. Naval Civil Engineering Laboratory by John R. Keeton[3] in the early 1960's. The data produced from this study was analyzed until it was clear how the factors were developed, and then the measured creep and shrinkage data were used to try to evaluate the current factors.

An initial comparison between the Navy data and the data collected from the cylinders was performed using various plots of relative humidity versus creep and shrinkage strains. These plots consisted of creating a curve based on the Navy data, from the specimens with similar characteristics to those of the cylinders, for each day that data were taken. Data collected in the present study were then plotted on the same chart for comparison. Figures 4.4 to 4.21 show the results. For example, Figure 4.4 shows a plot of the Navy shrinkage data taken at day one of the study along with the data measured from the shrinkage cylinders monitored in this study. The figure uses the same naming convention as the beam specimens, using –S to indicate a shrinkage cylinder specimen (-C for creep cylinder specimens), for example, RNOB-S is the Reno outdoor box girder shrinkage cylinder data.

The next step was to develop a curve similar to the one produced from the Navy data. Due to a limited amount of data in the present study covering a narrow range, a second point had to be selected to help create a more accurate curve. The Navy data was studied, and it was determined that the values of shrinkage varied the least from day to day at 100% RH, therefore the Navy data for RH=100% for each day was selected as the second point to produce a curve. The broken line in each curve goes through the average point for the cylinders and the Navy data point for RH=100%. The same procedure was followed for the creep cylinders. The results for both shrinkage and creep can be seen in Figs. 4.4-4.21.

The next step was to create an equation for a correction factor that would factor creep as a function of RH similar to the coefficients used in the time-step methods (Appendix B) and recommended by ACI Committee 209. To do this a strain value had to be selected to normalize each curve. The ACI-209 coefficients for both creep and shrinkage produce a value of 1 at a relative humidity of 40%. Therefore, at 40% relative humidity, the calculated creep value would equal the ultimate creep value. Since these equations were based on a very extensive study, the creep strain at 40% in each of the broken lines was used to normalize each line. The normalized lines for creep are shown in Fig. 4.22. These lines were then averaged, producing a new line that would include the data measured in this study (Fig. 4.22).

From this average line, an equation was produced. Equation 4.5 is the equation produced for creep (Fig. 4.22).

$$K_{ch} = 1.28 - 0.007\ RH \qquad (4.5)$$

RH = relative humidity (%)

Equation 4.5 is almost exactly the formula for the creep factor recommended by ACI Committee 209 and currently used in time-step methods (Eq. 4.6).

$$K_{ch} = 1.27 - 0.0067\ RH \qquad (4.6)$$

The shrinkage data, despite the wide spread data, produced similar results with the average line (Eq. 4.7) (Fig. 4.23).

$$K_{sh} = 1.39 - 0.0098\ RH \qquad (4.7)$$

Equation 4.6 is also almost exactly the equation currently used for the shrinkage factor for relative humidity of less than 80% (Eq. 4.8).

$$K_{sh} = 1.4 - 0.01\ RH \qquad (4.8)$$

From these comparisons, it was concluded that the existing equations for the relative humidity factors for creep and shrinkage are appropriate, and that no modification is necessary.

CHAPTER 5
MEASURED RESULTS AND COMPARISON WITH THEORETICAL RESULTS

5.1 Introductory Remarks

The data collected form the beam and cylinder specimens are presented in this chapter. The values of stress at each date of collection were then compared to what the time-step methods, discussed in the previous chapter, predicted at that date. The stress values were also fit with a logarithmic curve and this curve was used to predict what the stress loss would be over forty years. These values were compared to what the time-step methods predicted at forty years, as well as what the AASHTO method predicted. This chapter discusses the results of these comparisons.

5.2 Prestressing and Measuring Data

5.2.1 Prestressing

The tendons in the box girders were stressed one at a time following a diagonal sequence. The prestress force was monitored during prestressing using the electrical strain gages. Prestressing force was applied in two steps. Approximately 70% of the target prestress was applied during the first step on all four tendons, and the remainder was applied in the second step. To compensate for immediate losses due to elastic shortening and anchorage set, the force at time of release was allowed to exceed the target by approximately ten percent.

One tendon in LVOA was damaged during an initial tensioning attempt, so the remaining tendons were stressed to help distribute the prestress more evenly. The tendon in the opposite corner from the damaged tendon was stressed to a lower value than the remaining two tendons, to help move the centroid of stress in the section closer to the centroid of the section.

Stressing of the solid beams was straightforward. The tendons in the solid beams were also overstressed to compensate for the immediate losses.

5.2.2 Measuring Data

The data were collected in the form of surface strains, both on the concrete and the prestressing tendons. The strain values from the beam specimens were then multiplied by the modulus of elasticity for the prestressing tendons, 28100 ksi (193790 MPa), to determine the stress in the tendons.

At the time of data collection, temperature and relative humidity readings were taken. For a complete variation climate throughout the length of the study, data from the

National Climatic Data Center[19] were obtained (Figs. 5.1 and 5.2). The plots contain daily precipitation measurements as well as the maximum and minimum relative humidity values taken at the Reno International Airport in Reno and McCarren International Airport in Las Vegas, respectively.

5.2.2.1 Thermal Corrections

The temperature values taken at the time of data collection were used to compensate for thermal expansion in the gages. All temperature corrections were made, by calculating the difference in temperature from the time of initial stressing to the time of data collection and multiplying it by the difference in thermal coefficients of expansion for the two materials used in each type of gage. This value was the strain correction that would be applied to negate the effects of temperature. The data from mechanical strain gages were corrected using the difference between the thermal coefficients of expansion for concrete ($6.0 * 10^{-6}$ / °F) and aluminum ($1.3 * 10^{-5}$ / °F) (steel ($7.0 * 10^{-6}$ / °F) for the Reno box girders).

The thermal corrections for the electric resistance strain gages were done differently, since the manufacturers suggest a fourth-order relationship between the temperature and the apparent thermal strain (Figs. 5.3 and 5.4). The apparent thermal strain value from the gages was subtracted from the thermal strain value produced from the coefficient of thermal expansion for steel and the difference in temperature.

5.2.3 Data Presentation

Data measured from the study was viewed in several different ways. The prestress was plotted for each specimen throughout the length of the study to illustrate how the stress levels in the specimens fluctuated with time. Since the major focus of this project was to observe prestress losses, the data was also plotted in a chart showing prestress loss levels throughout the study. It was not possible to tension each beam to the same stress, so the prestress losses were normalized and plotted as a percentage of initial stress to allow for a more reasonable comparison among specimens.

Because of the variation among data, the charts mentioned above were created for the data collected from both types of gages as well as the average of the two. The average prestress values read from each type of gage were also plotted against each other with the average of the two types of gages, to demonstrate the correlation between the two types of gages. The average stress values per tendon were also plotted against each other to monitor how the tendons responded relative to each other.

To develop the 40-year prestress values from the data, a logarithmic curve was fit to the data. Only monthly data points were considered since including the daily points in the first few weeks after prestressing tended to give more weight to the data for the first few weeks, diluting the effects of the data taken later in the study.

5.3 Measured Data

5.3.1 Reno Specimens

5.3.1.1 Box Girders

5.3.1.1.A Measured Data

The Reno box girders were poured on August 12, 1999, and were stressed on January 12, 2000. The period of data collection for the beams lasted 938 days, a little over two and a half years. Table 5.1 contains the initial prestress values and the 40-year extrapolated values for the electric gage readings, mechanical gage readings, and the average of the two.

The outdoor moist-cured girder (RNOMB) had an initial stress value of 173.1 ksi (1193 MPa). The average of the gage readings suggest an extrapolated loss of 20.1% or 34.8 ksi (240 MPa). The electric resistance strain gage readings suggest a 40-year loss of 34.7 ksi (240 MPa) or 20.1%, and the mechanical gages suggest a 20.2% loss or 34.9 ksi (241 MPa).

The outdoor air-cured girder (RNOAB) showed an average 24.2% loss of the initial stress of 169.2 ksi (1166 MPa) with an extrapolated measured loss of 40.9 ksi (282 MPa). The log-fit curves from the electric gages and mechanical gages predict a loss of 21.9% and 26.4%, respectively, with losses of 37.0 ksi (255 MPa) and 44.7 ksi (308 MPa).

The average extrapolated measured loss for the indoor moist-cured girder (RNIMB) was 47.2 ksi (325 MPa), or 24.8% of the initial prestress of 190.1 ksi (1311 MPa). The 26.1% loss or 49.5 ksi (342 MPa) projected from the electric gages is slightly higher than the 23.6% loss or 44.8 ksi (309 MPa) projected from the mechanical gages.

The indoor air-cured box girder (RNIAB) had an average extrapolated loss of 22.8% of the initial stress of 166.5 (1148 MPa), with a loss of 37.9 ksi (261 MPa). This average is from an electric gage projection of a 21.9% loss or 36.5 ksi (251 MPa) and a mechanical gage projection of a 23.6% loss or 39.3 ksi (271 MPa).

5.3.1.1.B Discussion

Figures 5.5 and 5.6 show the measured temperature and relative humidity values taken near the Reno box girders at the time of data collection. From these charts, the approximate difference in climate between the indoor and outdoor pairs of box girders can be observed. The temperature readings throughout the length of the study show a cyclical behavior with the changing seasons, even for the indoor beams. From the temperature and relative humidity plots, the indoor measurements tended to remain more stable while the outdoor measurements covered a much broader range of values.

To allow for a better idea of how much moisture the outdoor specimens were exposed to following the application of prestress, the maximum and minimum relative humidity and precipitation for the first three months, as collected at the Reno International Airport, were plotted (Fig. 5.7). For the first two months the outdoor box girders were subjected to higher than average relative humidity as well as precipitation. This figure also indicates that the outdoor air-cured beam was exposed to quite a bit of moisture as well as a higher relative humidity, which could have been enough to partially moist-cure the beam. The high relative humidity during this time affect all of the beams, including the indoor air-cured beam.

Figure 5.8 shows the prestress value in each beam as read from the electric gages, Fig. 5.9 shows the values from the mechanical gages, and Fig. 5.10 shows the average values from the two types of gages. The readings from the electric gages tend to be slightly more jagged whereas the mechanical gage data shows a smoother prestress loss progression. From these figures, the effects of the environment on the beams can be clearly seen. The cyclical behavior in the outdoor beams is due to the ambient humidity and precipitation during the course of the year. The prestress values decrease during the hot dry summer months, when a reduction in the volume of the concrete due to the loss of moisture reduces the prestress. Some of the losses are regained during the winter months when the ambient humidity is higher and precipitation is more frequent. The indoor beams were not subjected to precipitation and highly varying relative humidity, and show prestress loss at a smoother rate.

The effects of moisture can also be seen in Figs. 5.11 –5.13, which illustrate the value of creep and shrinkage loss throughout the length of the study for the electric gages, mechanical gages, and the average of the two gages, respectively.

A better idea of how the beams performed relative to each other can be obtained from Figs. 5.14-5.16, which plot the prestress loss as a percentage of initial stress. From these figures the effects of the environment can be observed. During the winter months, the outdoor beams regain some of the lost prestress, and show lower losses than the indoor beams. During the dry summer months, the prestress losses in the outdoor beams increase and in some cases exceed the losses experienced by the indoor beams. Figure 5.15 shows the normalized prestress loss as read from the dial gages, and clearly shows the effects of the seasonal moisture as the outdoor beam data oscillates about the indoor beam data.

The data illustrated in Figs. 5.14-5.16 gives varying results when studying the effects of the moist-curing. From the electric gage data, contrary to expectations RNIMB shows higher losses than RNIAB, but the mechanical gage data shows the beams to be experiencing the same losses. The data from the outdoor beams indicate that the moist-curing has indeed decreased the prestress loss experienced by RNOMB, and that moist-curing was beneficial.

Comparisons were also made to evaluate the instrumentation. Figure 5.17 shows a comparison of the prestress measurements from each type of gage for RNOMB. From this figure, a very good correlation between the electric gage data and the mechanical gage data can be observed. The electric gage readings for each tendon were also plotted against each other to make sure that the readings coincided (Fig. 5.18). RNOMB only had readings from two tendons due to gages damaged during prestressing and the course of the study. Similar plots for the rest of the beams are shown in Figs. 5.19-5.24. Overall, there was very good correlation between the gages, so for the comparisons made between the measured and the calculated data, the average between the two types of gages was used.

5.3.1.2 Solid Beams

5.3.1.2.A Measured Results

The Reno solid beam specimens were poured on February 20, 2001, were stressed on May 23, 2001, and monitored for 455 days ending August 21, 2002. Both beams were placed outdoors. Table 5.2 lists a summary of the extrapolated creep and shrinkage losses from the electric resistance strain gages, the mechanical gages, and the average of the two types of gages.

The moist-cured outdoor solid beam (RNOMS) had an electrical gage loss projection of a 9.9% loss or 24.5 ksi (169 MPa) and a mechanical gage projection of a 9.9% loss of 24.6 ksi (170 MPa), which averaged an extrapolated measured loss or 24.6 ksi (169 MPa) or 9.9% of the initial stress of 248.5 ksi (1148 MPa).

The air-cured solid beam (RNOAS) was initially stressed to 214.4 ksi (1478 MPa), and the 40-year projections suggest a 9.6% loss or 20.6 ksi (142 MPa). The electric gages suggest a 40-year loss of 28.2 ksi (194 MPa) or 13.1% of the initial stress. The mechanical gages suggest a 40-year loss of 13.0 ksi (90 MPa) or 6.1% of the initial stress.

5.3.1.2.B Discussion

Figures 5.25 and 5.26 show the measured temperature and relative humidity readings, respectively, at the time of each data collection. Figure 5.27 shows the relative humidity and precipitation, as collected from the Reno International Airport, for the solid beams in the two months following prestressing (values for the third month were unavailable). The prestress loss progression can be seen for the two types of gages and the average of the two in Figs. 5.28-5.30. At around 40 days, the beams were exposed to precipitation as well as higher relative humidity, and as a result, the beams show a slight increase in prestress as shown in Figs. 5.28-5.30. From these figures the seasonal effects of relative humidity and moisture can be seen in the fluctuation of the prestress forces.

Figures 5.31-5.33 show the measured prestress loss values for the solid beams, and Figs. 5.34-5.36 contain the prestress loss as a percentage of initial stress. From these figures, an indication of poor correlation between the mechanical gages and the electrical gages can be seen. The losses measured from the electric gages in Figs. 5.31 and 5.34 suggest that the air-cured beam experienced larger prestress losses than the moist-cured beam. Figs. 5.32 and 5.35, which suggest that the moist-cured beam has experienced higher losses, contradict this trend.

Figures 5.37 and 5.38 compare the mechanical gage and the electrical gage results. From these figures, a difference of up to about 23 ksi (159 MPa) can be seen between the two types of gages. Correlation between the two types of gages is good before 150 days and after 330 days. At 150 days, the temperature begins to decrease and the relative humidity begins to increase, based on what was seen in the Reno box girders, the stresses in the tendons should have increased. At about 220 days, the opposite occurs, the temperatures increase and the relative humidity decreases, and the stresses in the tendons should have decreased. Since the mechanical gages show data that corresponds to these observations, the data was seen as being a more accurate representation of the prestress in the solid beams and was used in comparisons with the theoretical models.

5.3.1.3 Cylinder Specimens

A total of ten cylinders were instrumented from the box girder pour in Reno. Four of these cylinders were used as creep cylinders, and the remaining six were instrumented as shrinkage cylinders. Two creep and three shrinkage cylinders were kept near the indoor box girders, and the same was done for the outdoor box girders.

The cylinder data were measured at the same time that data were collected from the box girders. Since the creep cylinders experience creep in addition to shrinkage, the average shrinkage value from the shrinkage cylinders in the same location was subtracted from the strain experienced by the creep cylinders to determine the creep strain. The results from these measurements are displayed in Tables 5.3 and 5.4. The calculated results in Tables 5.3 and 5.4 are explained later in this chapter.

The outdoor creep cylinders in Reno suggest a 40-year extrapolated strain value of 1299 microstrain. The indoor creep cylinders show similar results with a 40-year extrapolated result of 1373 microstrain. Figure 5.39 illustrated the progression of the creep in the both sets of cylinders throughout the study. The average creep values along with the trend line used to project the 40-year estimates are illustrated in Fig. 5.40. From the trend line in these figures, the indoor cylinders experienced slightly higher creep than the outdoor cylinders.

The shrinkage cylinders from the Reno box girders show very low shrinkage values, with the outdoor cylinders actually suggesting expansion over time. It is important to point out that in Figs. 5.41 and 5.42 an oscillation in the data has affected the log-fit curves giving unreliable projections. In Fig. 5.41 the shrinkage data begins to

increase as expected, until around 300 days, when the shrinkage readings drop, and some of them actually show expansion in the cylinders. This is further reinforced by comparing the shrinkage experienced by these cylinders over time to the climate data shown in Fig. 5.1. From this comparison, the oscillation in the shrinkage cylinder data is shown to coincide with the seasonal oscillation in relative humidity and precipitation. For the first fifty days, higher relative humidity and precipitation can be observed in Fig. 5.1, which is reflected in the slight decrease in shrinkage (expansion) seen in Fig. 5.42. For the next two hundred days, the relative humidity and precipitation are lower and Fig. 5.42 reflects the effects of lower moisture in an increase in shrinkage. These trends are seen to continue throughout the study, with the lowest shrinkage values occurring at about 750 days, which was when Fig. 5.1 shows the highest day of precipitation as well as some of the highest relative humidity.

The data from the indoor shrinkage cylinders projects a 40-year value of 256 microstrain. The data from the outdoor shrinkage cylinders indicates an expansion in the concrete. The 40-year projected shrinkage value for these cylinders is –223 microstrain (223 microstrain expansion). Figure 5.41 demonstrates the change in length due to shrinkage with time, and Fig. 42 shows the average values for the shrinkage cylinders along with the trend line used for 40-year projections.

Three cylinders from the Reno solid beam specimen pour were instrumented and used to monitor shrinkage values in the solid beam specimens. The shrinkage trends for these cylinders can be seen in Fig. 5.43, with the average value and the log-fit curve in Fig. 5.44. From these figures, a phenomenon similar to the cylinders from the box girder pour can be seen. Throughout the course of the year, the effects of moisture can be seen. Since the beams were stressed in May, they dried over the summer, and exhibited an increase in shrinkage. When the cylinders were exposed to winter's relative humidity and precipitation, they began to regain some of the lost shrinkage and started to demonstrate expansion by around 150 days after stressing. Then, as winter again turned to spring then summer, the cylinders again started to exhibit signs of shrinkage. The effects of moisture can again be seen in the first 90 days of data collection. From Fig. 5.27, an increase in precipitation and relative humidity can be seen at about 30 days, which in turn causes a decrease in shrinkage, which explains the spike in the shrinkage at approximately the same time in the shrinkage data. Again, an oscillation like this makes the curve-fit values unreliable. Similar to the outdoor cylinders from the box girder pour, the average shrinkage values for these cylinders projected a 40-year shrinkage value of –213 microstrain (213 microstrain expansion).

Since an ultimate shrinkage value could not be accurately measured from the shrinkage cylinders monitored from the two beam specimen pours, two sets of supplemental cylinders were also monitored for shrinkage in Reno. A total of ten cylinders, two different pours of five cylinders apiece, were instrumented and data was collected immediately following the removal of the cylinder molds.

The first set was poured October 25, 2001, and the first data points were taken November 8, 2001. The cylinders were monitored for 271 days, ending on August 6, 2002. This set of cylinders was left outside, exposed to precipitation. Data were generally taken at weekly intervals. Temperature and relative humidity data were taken at the time of each data collection, and Figs. 5.45 and 5.46 show the results from those readings. Figure 5.47 illustrates the relative humidity and precipitation measurements taken at the Reno airport for the first three months. Figure 5.48 illustrates the progression of shrinkage over time for each cylinder, and from this figure, you can see that these cylinders expanded in the first three months as a result of being exposed to snow several times. Looking at the climate data in Fig. 5.47 as well as the shrinkage values in Fig. 5.48, a definite relationship between shrinkage and moisture can be clearly seen. Figure 5.49 shows the average shrinkage for all five cylinders, as well as the logarithmic fit trend line. From this trend line, we can expect a 40-year shrinkage value of 963 microstrain, however, due to the moisture in the beginning affecting the log-fit curve, this value may be a bit low.

The second set of cylinders monitored was handled slightly different than the first. These cylinders were poured December 28, 2001, and the data were first collected January 17, 2002. These cylinders were monitored for 201 days ending on August 8, 2002. The cylinders were instrumented with two sets of aluminum reading tabs on the opposite sides of the cylinders, and the readings were averaged to produce the shrinkage value at the time of data collection. These cylinders were also kept in a shed near the first set of cylinders, so they were exposed to the same relative humidity and temperature, but were sheltered from precipitation. Figures 5.50 and 5.51 show the temperature and relative humidity values at the time of each data collection, and the daily precipitation and extreme relative humidity values for the first three months are shown in Fig.5.52. Figure 5.53 shows the shrinkage values for each cylinder individually, and Fig. 5.54 shows the average shrinkage values as well as a logarithmic fit trend line. The trend line shown in Fig. 5.54 suggests a 40-year shrinkage value of 2264 microstrain, which could be a bit high since from Figs. 5.53 the shrinkage values appear to be leveling off between 1600 and 1700 microstrain.

5.3.2 Las Vegas Specimens

Data for the Las Vegas beams were collected by the UNLV staff and sent to Reno in raw form. The data were then processed and incorporated in this document.

5.3.2.1 Box Girders

5.3.2.1.A Measured Results

The Las Vegas box girders were poured on October 22, 1999, and were stressed August 8, 2000. The last set of data was collected on August 16, 2002, making the total length of monitoring 743 days or a little over two years. The initial prestress values and

the 40-year extrapolated values for the electric gage readings, mechanical gage readings, and the average of the two are included in Table 5.5.

The outdoor moist-cured girder (LVOMB) had an initial stress value 136.4 ksi (940 MPa). The average of the gages suggest an extrapolated loss of 25.3% or 34.4 ksi (237 MPa). The mechanical gage readings suggest a loss of 13.3 ksi (92 MPa) or 9.8%, but the extrapolated electric gage losses suggest a 55.5 ksi (383 MPa) loss (40.7% of the initial stress). Compared to the other beams, the loss in LVOMB is high. Table 5.5 shows that the extrapolated electric gage loss is approximately twice the others, whereas the loss from the mechanical gages is comparable. The electric gage data for LVOMB was hence considered to be unreliable.

For the indoor moist-cured girder (LVIMB), a projected loss of 20.0% or 32.0 ksi (221 MPa) from the electric gages and a projected loss of 6.8% or 10.8 ksi (75 MPa) from the mechanical gages averaged a projected loss of 21.4 ksi (148 MPa), or 13.4% of the initial prestress value of 160.0 ksi (1103 MPa).

The electric gages from the indoor air-cured girder (LVIAB) suggest an extrapolated measured loss of 19.9% or 29.4 ksi (203 MPa), and the mechanical gages suggest an extrapolated measured loss of 9.0% or 13.3 ksi (92 MPa). The average of the two gages suggests an extrapolated loss of 14.4% of the initial stress of 148.1 (1021 MPa) with a loss of 21.4 ksi (148 MPa).

5.3.2.1.B Discussion

Figures 5.55 and 5.56 show the measured values of temperature and relative humidity, respectively, taken throughout the study. The climate in the lab was not adequately controlled due to an electric malfunction. Since the two sets of beams were exposed to very close to the same relative humidity and temperature, the only difference between the indoor and outdoor box girders was the precipitation, and direct sunlight.

It was also determined that the ambient temperature readings were not accurate in estimating the temperature of the beams exposed to direct sunlight during most of the summer, the outdoor beams could not be touched by hand. This made it difficult to correct for thermal effects on the instrumentation. The climate data taken at the McCarren International Airport in Las Vegas for the first three months following the application of prestress is shown in Fig. 5.57.

The prestress values in each beam, as read from the electric gages, are illustrated in Fig. 5.58, the values from the mechanical gages are shown in Fig. 5.59, and the values from the averages of the two types of gages are illustrated in Fig. 5.60. From these figures, the effects of the environment are not as obvious as the Reno box girders, however a slight cyclical behavior can be observed in the plot from the mechanical gages (Fig. 5.59) for the outdoor girders. These figures also show an increase in prestress in the indoor girders during the first few weeks. This increase coincides with an increased

humidity shown in Fig. 5.56 during the first few weeks following prestressing, before the malfunction in the heating and air system in the lab. From that point on the indoor box girders demonstrate prestress loss at a fairly constant rate.

Figure 5.57 shows that the Las Vegas box girders were exposed to an increased relative humidity as well as precipitation at about 25 days and again at about 85 days. The results can be seen in the data readings taken from the dial gages as increasing prestress at about 85 days and a decreased rate of loss at about 25 days. The decreased rate of loss at about 25 days is also evident in the electric gage readings.

The electric gage and mechanical gage readings are plotted against each other in Fig. 5.67. This figure shows a very large difference between the two gages, which was discussed earlier. The electric gage readings on each tendon were also compared (Fig. 5.68), but no discrepancies were found. Similar plots were created for the rest of the beams (Figs. 5.67-5.74), and the two types of gages didn't correlate well. Since it was not possible to determine what gage type was more correct, the average of the two types of gages was taken as being somewhat representative of the actual values for comparison with theory.

5.3.2.2 Solid Beams

5.3.2.2.A Measured Results

The Las Vegas solid beams were poured on February 2, 2001 and stressed on April 5, 2001. After a monitoring the beams for 498 days, the last date of data collection was August 16, 2002. The initial stress values and the 40-year extrapolated prestress loss values for the electric gages, mechanical gages, and an average of the two are listed in Table 5.6.

The moist-cured solid beam (LVOMS) suggested an averaged extrapolated loss of 17.5 ksi (121 MPa) or 8.5% of the initial prestress value. The mechanical gages for this beam however suggest a value of 23.8 ksi (164 MPa), 11.6% of the initial prestress value. The electric gages show a much lower trend, suggesting a value of 11.2 ksi (77 MPa) or 5.5 % of the initial prestress value.

The air-cured solid beam (LVOAS) suggested an averaged extrapolated loss of 13.8 ksi (95 MPa), which is 6.4% of the initial prestress value. The mechanical gages suggest a larger loss of 19.3 ksi (133 MPa), 8.9% of the initial prestress value. The electric gages for LVOAS also show a lower loss of 8.4 ksi (58 MPa) or 3.8% of the initial prestress value.

Between January 29, 2002 and March 15, 2002, the lab where the electric gages were setup to be read was renovated, and the gage wires were damaged in the process, making the gage data unreliable. Therefore, the data of the last data set considered for the electric gages was January 29, 2002.

5.3.2.2.B Discussion

Figures 5.75 and 5.76 illustrate the temperature and relative humidity data taken from the solid beam data. Figure 5.77 plots the climate data taken at the McCarren International Airport in Las Vegas, for the first three months of data collection. Figures 5.78-5.80 show the prestress values read from the electric gages, the mechanical gages, and an average of the two. The solid beam behavior in the figures mentioned above shows an increase in prestress during the two weeks of monitoring, which could be due to precipitation. With the exception of the initial variation of prestress, the prestress loss progression remained fairly constant.

Figures 5.81-5.86 illustrate the prestress loss and the normalized prestress loss. From these figures, the two beams experienced losses that remained fairly similar. Contrary to what was expected, the data from the air-cured solid beam suggests lower losses than the data from the moist-cured solid beam.

The prestress values measured from the two types of gages also did not correlate well. Up to a 20 ksi (183 MPa) difference between the readings from the two types of gages was noted. No clear correlation between the strain data and climate data could be found. UNLV staff reported slippage problems with the end bearing of the mechanical gage rods. Therefore, only the electric gage readings were used to compare the data to the estimated prestress losses.

5.3.2.3 Cylinder Specimens

Like the Reno box girders, there were a total of ten cylinders instrumented from the Las Vegas box girder pour. Again, four cylinders were kept in creep frames (two indoor and two outdoor) and six cylinders were kept as shrinkage cylinders (three indoor and three outdoor). The data for the Las Vegas cylinders was also measured at the same time as the corresponding beam specimens. The final results from these measurements are listed in Tables 5.7 and 5.8. The calculated results in Tables 5.7 and 5.8 are explained later in this chapter.

Data from the indoor creep cylinders in Las Vegas suggested a 40-year extrapolated strain value of 1608 microstrain. The outdoor creep cylinders show an extrapolated strain value of 1213 microstrain. Figure 5.89 shows the creep strain progression for the individual cylinders over the length of the study, and Fig. 5.90 shows the average creep strain progression for the two sets along with a log-fit trend line. These figures show that the outdoor creep cylinders generally experienced smaller strains due to creep.

Like the Reno cylinder specimens, comparisons can be made between the climatic data illustrated in Figs. 5.56 and 5.57 and the shrinkage values measured in the shrinkage

cylinders (Figs. 5.91 and 5.92). These comparisons also show that during periods of moisture, the cylinders respond by expanding and reversing the effects of shrinkage

The shrinkage cylinders show expansion from the first day of data collection. The indoor shrinkage cylinders suggest a 40-year extrapolated shrinkage value of –1122 microstrain, or an expansion of 1122 microstrain. Upon further investigation into the ultimate shrinkage value, Fig. 5.92 shows both the indoor and the outdoor cylinders to remain close to or below –500 microstrain.

The negative shrinkage value for the cylinders from the Las Vegas box girder pour are due to the response of the concrete to seasonal changes. From data discussed earlier, the effects of seasonal variations can be seen in the response of the concrete. Typically, the concrete shows higher shrinkage values during the summer months, some of which is recovered during the winter and spring. The Las Vegas box girder specimens were stressed on August 3 and data collection began. August would be one of the final months during the summer, when the shrinkage is the highest, and following August would be months bringing higher relative humidity and precipitation (as can be seen in Fig. 5.2), making the concrete recover some of the losses due to shrinkage. Therefore, from the data collected, the expansion of the cylinders (negative shrinkage) could be attributed to the time of year that data collection began.

A total of five cylinders from the solid beam pour in Las Vegas were instrumented and monitored in conjunction with the beams. These cylinders were instrumented and monitored for shrinkage strain values. The cylinders were kept outside along with the solid beam specimens. Similar to the box girder shrinkage cylinders, the solid beam cylinders show an extrapolated 40-year strain value of –122 microstrain (122 microstrain expansion). Figures 5.93 and 5.94 illustrate the shrinkage trend for each cylinder as well as the average value and the log-fit trend line.

On December 4, 2001, seven more supplemental cylinders were poured in Las Vegas. The cylinders were split into two groups, three indoor and 4 outdoor, and were monitored starting December 15, 2001. The temperature and relative humidity plots for the outdoor cylinders are located in Figs. 5.95 and 5.96. The climatic data taken for the first three months is located in Fig. 5.97. Figures 5.98 and 5.99 show the shrinkage values for individual cylinders as well as the average values and log-fit trend line. Contrary to the shrinkage data from the beam specimen cylinders, the supplemental cylinders show shrinkage, with a 40-year extrapolated shrinkage value of 491 microstrain for the indoor cyinders and 160 microstrain for the outdoor cylinders. The temperature and relative humidity plots for the indoor cylinders are located in Figs. 5.100 and 5.101. The shrinkage values for the individual cylinders and the average value with a log-fit trend line for the indoor cylinders are located in Figs. 5.102 and 5.103. Tabulated results from the supplemental cylinders can be found in Table 5.8.

Here again the extrapolated 40-year shrinkage strain is positive further reinforcing the observation made about the cylinders that were studied along with the box girders.

5.4 Comparison of Measured and Theoretical Results

As mentioned previously, one of the objectives of this study is to compare current methods of predicting prestress losses with actual data from prestressed concrete specimens in highly varying climate similar to Reno and Las Vegas. For the purposes of this study, three methods were used for comparison against measured results. Methods from the American Association of State Highway and Transportation Officials (AASHTO)[2], Naaman[5], and Nawy[6] were chosen for use in this study. The portions of these methods used are described in the previous chapter and are explained in detail in Appendix B.

The three prediction methods are all used for lifetime loss comparisons, however, the methods proposed by Naaman and Nawy allow prestress losses to be predicted periodically throughout the lifetime of a structure. For this study, comparisons were made between the predictions from Naaman and Nawy and the measured losses at the time of each data collection.

During the comparison process, Naaman's method was modified slightly in two ways in an attempt to develop more accurate results. The first way that the method was modified was by using the average measured humidity between two dates for that period of time, instead of the recommended 50% for Reno and 27% for Las Vegas. The second way was to modify the elastic modulus using the equation suggested in the previous chapter, along with the varying relative humidity. For moist-cured specimens a relative humidity of 100% was used for the period following tensioning.

Both of these modifications had only a small effect on the results. By varying the relative humidity, the projected losses for the moist-cured beams was reduced slightly, but increased slightly for the air-cured beams, since the average relative humidity was almost always below 50%. Varying the elastic modulus in the prediction method also had minimal effects on the projected loss, since with the exception of the moist-curing the average relative humidity was below 50% where the elastic modulus is unaffected.

5.4.1 Reno Specimens

Summaries of the comparisons between the measured and theoretical results are located in Tables 5.1, 5.2, and 5.9.

As mentioned earlier, the time-step methods utilize more variables to allow for a more accurate estimation of prestress loss. Even though these equations take into account a wide range of variables, these variables are general and based on averages. They do not take into account varying climate, a period of very dry weather followed by a period of very moist weather would produce an average value that would be about mid-range. Sakata and Ayano[17] show that when the concrete is exposed to climate can have a significant impact on creep and shrinkage losses. Another factor that is just averaged is

the aggregate used to make the concrete. The study by Alexander[4] shows the effect that aggregate type can have on creep and shrinkage losses.

From the comparison between the actual data collected from the beam specimens and the losses predicted by the time-step methods, it was found that the analytical methods underestimate the Reno box girder losses. As discussed previously, several approaches were taken to adjust the equations used in these methods to produce more accurate prestress loss estimates in Nevada. Adjusting the elastic modulus (E) for moisture affected the predicted results, but the results still did not accurately predict the prestress losses. From Will and Sanders[20], experimental study had indicated that the elastic modulus for the aggregates produced at All-Lite was approximately 65% of the value of elastic modulus calculated from ACI 318. The equation that Will recommends for All-Lite aggregate is the following.

$$E = 36500\sqrt{f'_c} \text{ (psi)}$$

$$E = 3030\sqrt{f'_c} \text{ (MPa)} \qquad (5.1)$$

By using this equation for the concrete that was made with All-Lite aggregates, the values predicted by the time-step methods become more accurate. The method suggested by Naaman went from underestimating the losses in the Reno box girders by an average of 39% to only underestimating the losses by an average of 12%.

For the comparisons discussed in this chapter, Equation 5.1 was used in the calculation of losses for the Reno beams using the time-step methods.

5.4.1.1 Box Girders

The results from the comparison of the measured data and the theoretical methods for the box girders can be seen in Table 5.1, Table 5.9, and Fig. 5.104. The measured losses discussed in this section refer to the average extrapolated loss from the measured mechanical and electric gage data. Figures 5.105-5.108 show the comparisons between the measured prestress and the predicted prestress throughout the course of the study. These figures not only show Nawy and Naaman's methods but they show the two adjustments to Naaman's method and where they fall with respect to the measured data. Only creep and shrinkage losses are shown.

The AASHTO method under-predicted the creep and shrinkage losses in the Reno box girders by an average of 10%. The method under-predicted the outdoor beams by an average of 6% and the indoor beams by an average of 14%. Of the four Reno box girders, RNOMB was the only girder for which the AASHTO method overestimated the losses. The AASHTO method overestimated the extrapolated measured loss by 2%. The AASHTO method under-predicted the losses in RNOAB by 14%, the losses in RNIMB by 19%, and the losses in RNIAB by 9%.

The method suggested by Naaman under-predicted the losses in the Reno box girders by an average of 12%, underestimating the outdoor girders by 9% and the indoor girders by 16%. The method accurately predicted the losses in RNOMB with an estimate of 34.7 ksi (239 MPa), but underestimated the losses in RNOAB by 17%, RNIMB by 20%, and RNIAB by 11%.

Nawy's method overestimated the losses in the Reno box girders by an average of 6%, overestimating the outdoor girders by an average of 11% and the indoor girders by an average of 2%. The method only underestimated the losses in one box girder, RNIMB, which was 3% under the measured extrapolated loss. RNOMB was overestimated by 21%, RNOAB was overestimated by 1%, and RNIAB was overestimated by 7%.

5.4.1.2 Solid Beams

The data from the solid beam specimens projected losses that in all cases were overestimated by the current prediction methods. This is attributed to the volume-to-surface ratio of the solid beams versus the box girders. The volume-to-surface ratio of the box girders was 0.75, while the volume-to-surface ratio for the solid beams was 1.25. Overall comparisons of the methods used can be observed in Fig. 5.109, Table 5.2, and Table 5.9. The prestress values in comparison to the values predicted by the time-step methods proposed by Naaman and Nawy for each day of data collection are plotted in Figs. 5.110 and 5.111.

The creep and shrinkage losses in the solid beams were overestimated by the AASHTO method by an average of 84%. The estimated loss for RNOMS overestimated the measured extrapolated losses by 37%, and the estimated loss for RNOAS overestimated the measured extrapolated loss by 131%.

The method suggested by Naaman overestimated the creep and shrinkage losses in the solid beams by an average of 178%. The method overestimated the losses in RNOMS by 109% and RNOAS by 248%.

The method proposed by Nawy overestimated the creep and shrinkage losses in the solid beams by an average of 181%, overestimating RNOMS by 112% and RNOAS by 252%.

5.4.1.3 Cylinder Specimens

A summary of the comparison of the Reno cylinder specimens is located in Tables 5.3 and 5.4. The cylinder data were compared using the coefficients for both creep and shrinkage suggested by Naaman and the values calculated from the collected data. The shrinkage coefficient from the collected data was simply the 40-year projected value, and the creep coefficients were calculated by taking the projected 40-year value

divided by the initial strain. For moist-cured concrete Naaman suggests an ultimate shrinkage value of 600 microstrain for moist-cured concrete and an ultimate creep value based on the values for C_{CU} as shown in Table B.2.

The creep cylinders in Reno were taken from the box girder pour. The creep coefficient projected from the indoor cylinders of 1.87 was overestimated by 22% with a value of 2.27 calculated from Naaman. The creep coefficient projected from the outdoor cylinders of 2.93 was 23% higher than the calculated value of 2.27.

The oscillation in the shrinkage data from the beam specimen pours made it difficult to draw any conclusions from the cylinder data.

The supplemental cylinders for Reno both have higher projected shrinkage coefficients than the coefficient suggested by Naaman. The exposed cylinders have an extrapolated measured loss of 963 microstrain, which is underestimated by the suggested value by 38%. This value however, could be low since the cylinders were exposed to precipitation during the first weeks following the initial date of data collection. From Fig. 5.48 an increasing trend in shrinkage can be seen. This increasing trend, along with a final shrinkage value of 1065 microstrain, suggests that the actual 40-year shrinkage value may be slightly higher than the current projected value.

The sheltered cylinders suggest the opposite. The final shrinkage value measured read 1629 microstrain, and from Fig. 5.53 the shrinkage seems to be stabilizing between 1600 and 1700 microstrain, which contradicts the 40-year log fit that suggests 2264 microstrain. The shrinkage coefficient suggested by Naaman is 74% smaller than the 40-year projected value.

5.4.2 Las Vegas Specimens

5.4.2.1 Box Girders

Similar to the Reno box girders, a summary of the results may be found in Table 5.5, Table 5.10, and Fig. 5.112. Figures 5.113-5.116 illustrate the comparison between the measured data and the methods suggested by Naaman and Nawy as well as the two modifications that were made to Naaman's method for each data collection date.

Unlike the Reno box girders, the current prediction methods overestimated the losses in the Las Vegas box girders.

The difference in the readings between the mechanical gages and the electrical gages, as seen in Table 5.5 and Table 5.10 makes it difficult to discern which gage is more correct or if the average is an accurate representation of the prestress actual prestress values. However, from the data collected, AASHTO is still conservative with respect to the data collected from the gages for all of the girders with the exception of the electrical gage reading in LVOMB, which at 55.5 ksi (383 MPa) would be a loss of 41%

of the initial stress in the beam, which indicates unreliable data as discussed earlier. This is also the case when comparing the data from the box girders to the methods suggested by Naaman and Nawy.

From the averages of the collected data, the AASHTO method overestimated the losses in the Las Vegas box girders considerably. The method suggested by Naaman also overestimated the losses in the box girders by a large margin. Similar results were found using the method suggested by Nawy. The relatively small losses in Las Vegas are in agreement with the low time dependent losses observed in the field in the Las Vegas area (Saiidi et al.[12, 13]).

5.4.2.2 Solid Beams

The Las Vegas solid beams also show some of the same results as the Reno solid beams. The Las Vegas solid beam losses were also overestimated by the current prediction methods. This is attributed to the volume-to-surface ratio, as mentioned earlier in this chapter, as well as the overall lower losses seen in Las Vegas, which could be due to the aggregate used in the concrete mixes. Figure 5.117, Table 5.6, and Table 5.10 contain comparisons of the estimated prestress values using the different methods. Figure 5.118 and 5.119 contains the prestress comparison with the different time-step methods throughout the study.

The mechanical gages for the Las Vegas solid beams were not considered as discussed earlier. The data in Table 5.6 show that all analytical methods overestimated the losses for the Las Vegas solid beams.

5.4.2.3 Cylinder Specimens

The comparisons made from the cylinder data were performed similar to the comparisons of the Reno cylinder specimens. The results from these comparisons can be seen in Tables 5.7 and 5.8.

The calculated creep coefficient for the creep cylinders was 2.92. This value was 3% higher than the measured coefficient of 2.85 for the indoor creep cylinders, and 15% lower than the measured creep coefficient of 3.43 for the outdoor creep cylinders.

Similar to the Reno cylinder specimens from the beam pours, the oscillation in the shrinkage data due to moisture makes it difficult to draw any accurate conclusion from the measured data.

The supplemental cylinders, however, show more realistic shrinkage values. The indoor shrinkage cylinders show an extrapolate shrinkage value of 491 microstrain which is overestimated by the suggested value of 600 microstrain by 22%. The outdoor cylinders averaged a lower shrinkage value of 160 microstrain, which is overestimated by the suggested value by 276%.

5.5 Concluding Remarks

From the comparisons made in this chapter, several observations may be made. For the climate and aggregate in the Reno area, the current methods of predicting prestress losses are conservative for specimens with higher volume-surface ratios. However, for specimens with lower volume-surface ratios, the current methods were unconservative in the estimates calculated for the prestress losses. For the climate and aggregate in the Las Vegas area, the current prediction methods are adequate.

The comparisons made in this chapter show that continuing moisture has a lasting effect on the creep and shrinkage losses in prestressed concrete. The precipitation in conjunction with higher relative humidity can reduce creep and shrinkage in prestressed concrete throughout the lifetime of the structure. As discussed earlier, the indoor beams generally showed larger losses over time than the outdoor beams, which were subjected to a more varying climate and precipitation. This could be even more evident in areas of higher average annual ambient relative humidity and precipitation.

Since studies have shown the effects of relative humidity above 50% on the stiffness of concrete and since the differences between no precipitation (indoor specimens) and very little precipitation and generally low relative humidity are observable, the current prediction methods could prove to be even more conservative in regions with more moisture.

The age of the concrete at the time of stressing of the specimens was relatively high, thus reducing the shrinkage losses. Had the beams been stressed at an earlier age, the projected measured losses would have been higher making AASHTO predictions even less conservative. Chapter 6 presents a modification to AASHTO equations to improve the loss estimates.

CHAPTER 6
DESIGN IMPLICATIONS

6.1 Introductory Remarks

The following chapter discusses how the findings in this study would affect the current design and construction techniques used. Three topics are discussed, the adjusted elastic modulus for the All-Lite aggregates, the suggested adjustments to AASHTO for bridge design in Northern Nevada, and the effect of moisture on creep and shrinkage losses.

6.2 Elastic Modulus

As mentioned in Chapter 4, the study performed by Will and Sanders[20] shows that the elastic modulus for All-Lite aggregate is 65% of what ACI 318 predicts. From Will and Sanders, the suggested modulus of elasticity for this aggregate source is best modeled by Eq. (4.3).

$$E = 36500\sqrt{f'_c} \text{ (psi)}$$

$$E = 3030\sqrt{f'_c} \text{ (MPa)} \qquad (4.3)$$

By using this equation for the concrete that was made with All-Lite aggregates, the values predicted by the time-step methods become more accurate. Table 6.1 contains the results produced from the method suggested by Naaman[5] for the Reno box girders for both ACI 318 method and Eq. 4.3. As can be seen in Table 6.1, the results from this analysis show that the predicted prestress losses went from underestimating the measured extrapolated losses by 30-45% to underestimating by 0-20%. The method suggested by Naaman went from underestimating the losses in the Reno box girders by an average of 39% to only underestimating the losses by an average of 12%. While these numbers are still unconservative, they show that the elastic modulus equation suggested by Will and Sanders is significantly more accurate than the equation from ACI 318 for the aggregate from All-Lite Pit.

Not only could this have an impact on the estimation of prestress losses, but using an inaccurate elastic modulus would also show poor results in all deflection calculations.

6.3 Revisions to AASHTO

One of the objectives of this study was to analyze the measured data and propose any necessary revisions to the current AASHTO method. The data discussed in the previous chapter showed that the AASHTO provisions for creep and shrinkage losses can be unconservative for the Reno box girders (specimens with a lower volume-to-surface ratio), and that a revision of the equations is necessary.

6.3.1 Shrinkage Losses

Before developing a modification to the current AASHTO equations, the origin of the equations was searched. The AASHTO equations are reported to have been based on the work by Shorer[1]. Therefore, Shorer equations in conjunction with the current AASHTO equations and data extrapolated from the concrete cylinders were studied to help develop possible revisions.

The AASHTO equation for long-term shrinkage loss in pre-tensioned members is:

SH = 17000 – 150 * RH (psi)

SH = 117 – 1.03 * RH (MPa) (4.1)

In which RH = relative humidity (%)

The relationship for Eq. 4.1 is shown in Fig. 6.1. For post-tensioned concrete, the equation is multiplied by a factor of 0.8. This basic form was preserved in the development of the new equation. Shorer's equation produces a line with nearly twice the loss as what AASTHO equation predicts (Fig. 6.1).

SH = 225 – 2.25 * RH (MPa)

SH = 32625 – 326.5 * RH (psi) (4.2)

The extrapolated data from the shrinkage cylinders was averaged to develop an ultimate shrinkage value for the concrete used, and to produce an equation with a format similar to that of AASHTO and Shorer. Since the data from the cylinders did not cover a sufficiently wide range of RH, they were not seen as being adequate to develop an equation solely on the average of these points. Therefore, an ultimate shrinkage value of 800 microstrain was assumed to be the value at 0% humidity. This value was based on the ultimate shrinkage values suggested by ACI 209[4] (780 microstrain) and the Prestressed Concrete Institute[21] (820 microstrain). To develop an equation, another data point was needed; therefore the ultimate shrinkage at 100% relative humidity was taken to be zero. Using these two data points a new equation was developed.

SH = 159 – 1.59 * RH (MPa)

SH = 23000 – 230 * RH (psi) (6.1)

This equation was taken to be for pre-tensioned concrete, and by multiplying this equation by 0.8 the equation for post-tensioned concrete was produced. Figure 6.1 shows a comparison of the shrinkage equations.

6.3.2 Creep Losses

The equation the AASHTO method suggests for predicting creep losses is:

$$CR = 12\, f_{cir} - 7\, \Delta f_{cds} \qquad (4.2)$$

In which f_{cir} = concrete stress at center of gravity of prestressing steel at transfer

Δf_{cds} = change in prestress in concrete stress at center of gravity of prestressing steel due to superimposed permanent loads.

Shorer's equation for creep loss estimate depends not only on the prestresses present in the concrete, but the ambient RH.

$$CR = 41.47 * \frac{(125 - RH)}{100} * f_{cir} \qquad (6.2)$$

Similar to what was done for shrinkage, the extrapolated creep data were used along with the 13.8 MPa (2000 psi) that the creep cylinders were stressed to develop a new equation. Since the beams used in this study had no superimposed loading after prestressing, only the first term in Eq. 4.2 was manipulated. The resulting equation was:

$$CR = 17\, f_{cir} - 7\, \Delta f_{cds} \qquad (6.3)$$

Equation 6.3 would increase estimate of creep loss by 40% compared to the AASHTO method. It was felt that the limited number of measured data points in this study could not justify such a large increase, and hence, a value of 15 was chosen for the coefficient of the first term leading to the following final proposed equation:

$$CR = 15\, f_{cir} - 7\, \Delta f_{cds} \qquad (6.4)$$

Figures 6.2 and 6.3 illustrate the comparisons in creep values based on the equations discussed above. Since Schorer's equation for creep was a function of both relative humidity and initial stress, the equations were compared in two different ways. Equation 6.2 shows how the creep loss varies with respect to relative humidity, and the variation of Shorer's equation can be clearly seen. Figure 6.3 illustrates how the creep loss varies with initial stress. These figures show that the equations produced in this study predict losses slightly larger than the losses predicted by AASHTO.

Tables 6.2 and 6.3 show the total creep and shrinkage loss predictions based on the proposed equations. The existing AASHTO equations underestimated the losses in RNOAB, RNIAB, and RNOMS, with the maximum difference being 22%. With the proposed equations the estimates of creep and shrinkage losses are conservative for all the beams.

6.3.3 Proposed Loss Estimates Used in Actual Bridges

To further investigate the performance of the revised equations, they were used to estimate the losses in four actual bridges studied in Mangoba et al.[9]. The predicted values were then compared to the measured extrapolated values reported in that study.

Mangoba et al. studied four post-tensioned box girder bridges in the Reno area stressed on different dates at the South Meadows Interchange, the Mount Rose Interchange, the Zolezzi Lane Grade Separation, and the Old Virginia Road Grade Separation. The South Meadows Interchange and the Mount Rose Interchange were two-span bridges and theZolezzi Lane Grade Separation were single span bridges. The four bridges were instrumented with mechanical strain gages, and the stress loss measured was extrapolated to estimate 40-year losses, which were compared to the AASHTO estimates.

The results from this comparison are summarized in Table 6.4. The revised equations improve estimate of prestress losses. For the South Meadows interchange, the equations take the predicted values from being unsafe by 5% to safe by 17%. The Mount Rose Interchange and the Zolezzi Lane Grade Separation become more conservative. The Old Virginia Road Grade Separation improves from being unconservative by 32% to being unconservative by 16%.

6.4 Moist-Curing of Concrete

Another objective of this study was to quantify the effects of moisture following the application of prestress. In Mangoba et al.'s study, the effects of moisture on creep and shrinkage losses in prestressed concrete were observed inadvertently in the Zolezzi Lane Grade Separation, which experienced lower losses due to heavy exposure to moisture, and in the Old Virginia Road Grade Separation, which experienced higher losses due to a period of dry climate following tensioning.

From the experimental work done on cured concrete cylinders and the adjustments made to the elastic modulus in the time-step methods, discussed in Chapter 4, the effects of moisture on prestress losses can also be clearly seen, in that added moisture increases the stiffness of the concrete and decreases the susceptibility to creep and shrinkage losses.

From the beam specimens, the effects of moisture on the prestress losses have not been so clear. From the Reno outdoor beam specimens, the moist-curing seems to have improved the performance of RNOMB and RNOMS. However, with the indoor box girders, the difference is unnoticeable, which suggests that added moisture following the initial moist-curing helps to perpetuate the effects. In Las Vegas, the moist-curing was probably not as extensive as it should have been since the beams were only wet once a day the hot August temperature in Las Vegas. The solid beams also seemed less

susceptible to moisture in general, which could be due to the difference in volume-to-surface ratios.

From the studies discussed in this section, the effects of moist-curing can still have a major effect on the performance of prestressed concrete, and would be a useful tool in improving the performance of prestressed concrete structures.

CHAPTER 7
SUMMARY AND CONCLUSIONS

7.1 Summary

Prestress losses in post-tensioned beam specimens were monitored in this study to determine the effects of a variety of variables on creep and shrinkage losses. This study had several objectives, including observe creep and shrinkage losses and propose revisions to the current AASHTO equations for creep and shrinkage loss prediction, study the effects of moist-curing prestressed concrete after the application of prestress, quantify the effects of this type of curing on box girders and solid beams, and to determine the effects of aggregate and climate on creep and shrinkage losses in prestressed concrete.

The losses were measured in twelve prestressed concrete beam specimens; eight box girders and four solid beams. The specimens were studied in two locations, six in Reno and six in Las Vegas, each with local aggregate subjected to the local climate. At each location, two box girders were left indoors and two box girders and two solid beams were left outdoors. Of each pair of beams, one beam was moist-cured after the application of prestress, and the other was not. Each beam was monitored with two different types of strain gages, mechanical and electric resistance gages. With each pair of beams, concrete cylinders were kept and were used to measure creep and shrinkage strains. Data collection took place daily for the two weeks following the application of prestress, weekly after the first two weeks, and monthly after the first month. Prestress losses were then calculated from the strain data collected and then log-fit to estimate 40-year losses. The 40-year losses calculated were then compared to the values calculated by the methods presented by AASHTO[2], Naaman[5], and Nawy[6].

The effects of moist-curing on concrete stiffness were also investigated. Research indicated that the elastic modulus was susceptible to the effects of moisture and a possible reason for the effects of moisture on prestress losses. Elastic modulus tests were performed on one-year old concrete cylinders, dried and wet, and with other research results. An approximation for quantifying the effects of moisture on elastic modulus was developed. With this approximation and the method suggested by Naaman, a model was created that demonstrated the effects of moisture on creep and shrinkage losses.

7.2 Conclusions

The following conclusions were made based on the experimental and analytical results presented in this report:

1. The extrapolated measured creep and shrinkage losses for the Reno box girders suggested 40-year losses that were underestimated by the AASHTO method by an average of 10%.

2. The proposed revisions to AASHTO discussed in the previous chapter improve the accuracy of the predictions made for box girder specimens in the Reno area.

3. The method proposed by AASHTO was conservative in the estimation of creep and shrinkage losses for the Las Vegas box girders.

4. The method proposed by AASHTO was conservative in the estimation of creep and shrinkage losses for the solid beams, in part due to a higher volume-to-surface ratio compared to the box girders.

5. The method of estimating creep and shrinkage losses proposed by Nawy was conservative in estimating the creep and shrinkage losses for all but one of the specimens monitored in this study.

6. The long-term creep and shrinkage losses for the Reno box girders were underestimated by the prestress loss estimation method suggested by Naaman by an average of 12%, but the method was conservative for all other specimens.

7. The effects of moisture in the form of relative humidity and precipitation were greater in Reno than in Las Vegas. The effects of precipitation on the Las Vegas beam specimens were negligible.

8. The creep and shrinkage coefficients used in the time-step methods suggested by Naaman and Nawy that act as a function of relative humidity agreed with the coefficients derived in this study.

9. Concrete made with metamorphic andesite is more susceptible to creep and shrinkage losses as well as the effects of moisture than limestone.

7.3 Recommendations

The following recommendations were made based on the experimental and analytical results presented in this report:

1. Based on the data collected in this study, the following equations estimate creep and shrinkage losses when andesite aggregate (All-Lite aggregate source) are used in members subjected to the Reno climate:

Shrinkage Loss

$$SH = 23000 - 230 * RH \text{ (psi)}$$

$$SH = 159 - 1.59 * RH \text{ (MPa)}$$

Creep Loss

$CR = 15\ f_{cir} - 7\ \Delta f_{cds}$

In which, f_{cir} = concrete stress at center of gravity of prestressing steel at transfer and Δf_{cds} = change in prestress in concrete stress at center of gravity of prestressing steel due to superimposed permanent loads. These equations were developed using the format in the AASHTO Provisions to facilitate their adoption.

2. Moisture following the application of prestress has been shown to reduce long-term losses in prestressed concrete, in previous studies as well as the analytical research presented in this paper. Therefore, it is recommended to moist cure the members in the Reno area for two weeks after prestressing. Where this recommendation is followed, the current AASHTO equations may be used to estimate creep and shrinkage losses.

REFERENCES

1. Shorer, H., "Prestressed Concrete, Design Principles and Reinforcing Units", *ACI Journal*, V. 14, No. 6, June 1943, pp. 493-528.

2. American Association of State Highway and Transportation Officials (AASHTO), *Standard Specifications for Highway Bridges 16th Edition*, Washington, D.C., 1996.

3. Keeton, J. R., "Study of Creep in Concrete", *U.S. Naval Civil Engineering Laboratory Technical Report R 333 I-III*, Port Hueneme, California, 1965.

4. ACI Committee 209, *ACI Manual of Concrete Practice 1996*, American Concrete Institute, Detroit, Mich. 1996

5. Naaman, A. E., *Prestressed Concrete Analysis and Design*, J. Wiley &Sons, New York, 1987, pp. 337-345

6. Nawy, E. G., *Prestressed Concrete A Fundamental Approach 3rd Edition*, Prentice-Hall, New Jersey, 1996.

7. Neville, A. M., *Properties of Concrete 3rd Edition*, Pitman Books, 1981, pp. 363-366.

8. Mehta, P. K. and P. J. M. Monteiro, *Concrete Structure, Properties, and Materials 2nd Edition*, Prentice Hall, New Jersey, 1993, pp. 86-89.

9. Mangoba, N., M. Mayberry, M. and Saiidi, "Prestress Loss in Four Box Girder Bridges in Northern Nevada", *Civil Engineering Department, Report CCEER-99-2*, University of Nevada, Reno, 1999.

10. Saiidi, M. and J. Shields, "Direct Field Measurement of Prestress Losses in Box Girder Bridges", *Civil Engineering Department, Report CCEER-89-4*, University of Nevada, Reno, 1989.

11. Saiidi, M., J. Shields, D. O'Connor, and E. Hutchens, "Variation of Prestress Force in a Prestressed Concrete Bridge During the First 30 Months", *PCI Journal*, Precast / Prestressed Concrete Institute, Vol. 41, No. 5, September / October 1996, pp. 66-72.

12. Saiidi, M., E. Hutchens, and D. Gardella, "Prestress Losses in a Post-Tensioned R/C Box Girder Bridge in Southern Nevada", *Civil Engineering Department, Report CCEER-94-5*, University of Nevada, Reno, 1994.

13. Saiidi, M., E. Hutchens, and D. Gardella, "Bridge Prestress Losses in Dry Climate," *Journal of Bridge Engineering*, ASCE, Vol. 3, No. 3, August 1998, pp. 111-116.

14. Alexander, M. G., "Aggregate and the Deformable Properties of Concrete", *ACI Materials Journal*, ACI, Vol. 93, No. 6, November-December 1996

15. Robertson, I. N., "Correlation of Creep and Shrinkage Models with Field Observations", *The Adam Neville Symposium: Creep and Shrinkage-Structural Design Effects*, ACI, SP-194-09, May 2000

16. Gardner, N. J., "Provisions for Shrinkage and Creep of Concrete", *The Adam Neville Symposium: Creep and Shrinkage-Structural Design Effects*, ACI, SP-194-03, May 2000

17. Sakata, K. and T. Ayano, "Effect of Ambient Temperature and Humidity on Creep and Shrinkage of Concrete", *The Adam Neville Symposium: Creep and Shrinkage-Structural Design Effects*, ACI, SP-194-06, May 2000

18. Ramachandran, V. S., R. F. Feldman, and J. J. Beaudoin, *Concrete Science Treatise on Current Research*, Heyden, Philadelphia, 1981

19. National Climatic Data Center, NNDC Climate Data Online, http://cdo.ncdc.noaa.gov/plclimprod/plsql/poemain.poe. Accessed Aug. 26, 2002

20. Will, J. and D. Sanders, "High-Performance Using Nevada Aggregates", *Civil Engineering Department, Report CCEER-00-06*, University of Nevada, Reno, 2000

21. Prestressed Concrete Institute, *PCI Design Handbook, 5th Edition*, PCI, Chicago, 1999

Table 2.1 – Pouring and Stressing Dates

	Reno Box Girders	Reno Solid Beams	Las Vegas Box Girders	Las Vegas Solid Beams
Pour Date	8/12/1999	2/20/2001	10/22/1999	2/2/2001
28-day Date	9/9/1999	3/20/2001	11/19/1999	3/2/2001
Stress Date	1/12/2000	5/23/2001	8/3/2000	4/5/2001
Days From End of Curing	146	85	279	55

Table 2.2 – Material Properties

Material Properties		**Reno**		**Las Vegas**	
		Box Girders	**Solid Beams**	**Box Girders**	**Solid Beams**
Concrete	**28-day Strength**	6.7 ksi (46.2 MPa)	4.1 ksi (28.3 MPa)	3.8 ksi (26.2 MPa)	5.8 ksi (40.0 MPa)
	Aggregate	Metamorphic Andesite		Limestone	
Prestressing Steel	**Ultimate Strength**	280 ksi (1930.5 MPa)			
	Elastic Modulus	28100 ksi (193790 MPa)			

Table 2.3 – Test Variables

	Variables					
Location	Reno					
Climate	Indoor		Outdoor			
Curing	Air	Moist	Air		Moist	
Type	Box Girder		Box Girder	Solid Beam	Box Girder	Solid Beam
Label	**RNIAB**	**RNIMB**	**RNOAB**	**RNOAS**	**RNOMB**	**RNOMS**

Location	Las Vegas					
Climate	Indoor		Outdoor			
Curing	Air	Moist	Air		Moist	
Type	Box Girder		Box Girder	Solid Beam	Box Girder	Solid Beam
Label	**LVIAB**	**LVIMB**	**LVOAB**	**LVOAS**	**LVOMB**	**LVOMS**

Table 5.1 – Reno Box Girder Prestress Loss Comparison

ksi (MPa)		RNOMB	RNOAB	RNIMB	RNIAB
INITIAL STRESS		**173.1 (1193)**	**169.2 (1166)**	**190.1 (1311)**	**166.5 (1148)**
MEASURED EXTRAPOLATED (M. E.)	Electric Gages	34.7 (240)	37.0 (255)	49.5 (342)	36.5 (251)
	Mech. Gages	34.9 (241)	44.7 (308)	44.8 (309)	39.3 (271)
	Average	**34.8 (240)**	**40.9 (282)**	**47.2 (325)**	**37.9 (261)**
AASHTO	Creep	28.0 (193)	27.4 (189)	30.8 (212)	27.0 (186)
	Shrinkage	7.6 (52)	7.6 (52)	7.6 (52)	7.6 (52)
	Total	**35.6 (246)**	**35.0 (241)**	**38.4 (265)**	**34.6 (238)**
NAAMAN	Creep	30.7 (212)	30.0 (207)	33.6 (232)	29.6 (204)
	Shrinkage	4.0 (28)	4.0 (28)	4.0 (28)	4.0 (28)
	Total	**34.7 (239)**	**34.0 (235)**	**37.6 (259)**	**33.6 (231)**
NAWY	Creep	37.8 (261)	37.0 (255)	41.5 (286)	36.4 (251)
	Shrinkage	4.2 (29)	4.2 (29)	4.2 (29)	4.2 (29)
	Total	**42.0 (290)**	**41.1 (284)**	**45.7 (315)**	**40.5 (279)**
M. E.	% of Initial Stress	20.1	24.2	24.8	22.8
AASHTO		20.6	20.7	20.2	20.8
NAAMAN		20.0	20.1	19.8	20.2
NAWY		24.3	24.3	24.0	24.3
AASHTO / M. E.		1.02	0.86	0.81	0.91
NAAMAN / M. E.		1.00	0.83	0.80	0.89
NAWY / M. E.		1.21	1.01	0.97	1.07

Table 5.2 – Reno Solid Beam Prestress Loss Comparison

ksi (MPa)		RNOMS	RNOAS
INITIAL STRESS		**248.5 (1713)**	**214.4 (1478)**
MEASURED EXTRAPOLATED (M. E.)*	Electric Gages	24.5 (169)	28.2 (194)
	Mechanical Gages	24.6 (170)	13.0 (90)
	Average	**24.6 (169)**	**20.6 (142)**
AASHTO	Creep	26.0 (179)	22.5 (155)
	Shrinkage	7.6 (52)	7.6 (52)
	Total	**33.6 (232)**	**30.1 (207)**
NAAMAN	Creep	45.5 (314)	39.5 (273)
	Shrinkage	5.8 (40)	5.8 (40)
	Total	**51.3 (354)**	**45.3 (313)**
NAWY	Creep	45.5 (314)	39.5 (272)
	Shrinkage	6.3 (44)	6.3 (44)
	Total	**51.8 (357)**	**45.8 (316)**
M. E.*	% of Initial Stress	9.9	6.1
AASHTO		13.5	14.0
NAAMAN		20.7	21.1
NAWY		20.9	21.4
AASHTO / M. E.*		1.37	2.31
NAAMAN / M. E.*		2.09	3.48
NAWY / M. E.*		2.11	3.52

*Only measured extrapolated values from the mechanical gages were considered for comparisons.

Table 5.3 – Reno Creep Cylinder Comparison

RENO CREEP CYLINDER SPECIMENS		BOX GIRDER	
		Indoor	Outdoor
Projected Data (From Initial Data Reading)	40-Year (microstrain)	1373	1299
	ksi	38.6	36.5
	MPa	266	252
Measured Coefficients		1.87	2.93
Calculated Coefficients		2.27	
Calculated / Measured		1.22	0.77

Table 5.4 – Reno Shrinkage Cylinder Comparison

RENO SHRINKAGE CYLINDER SPECIMENS		BOX GIRDER		SOLID BEAM	SUPPLEMENTAL	
		Indoor	Outdoor	Outdoor	Exposed	Sheltered
Projected Data (From Initial Data Reading)	40-Year (microstrain)	256	-223	-213	963	2264
	ksi	7.2	-6.3	-6.0	27.1	63.6
	MPa	50	-43	-41	187	439
Measured Coefficients		0.000256	-0.000223	-0.000213	0.000963	0.002264
Calculated Coefficients		0.0006				
Calculated / Measured		2.35	-2.69	-2.81	0.62	0.26

Table 5.5 – Las Vegas Box Girder Prestress Loss Comparison

ksi (MPa)		LVOMB	LVOAB	LVIMB	LVIAB
INITIAL STRESS		**136.4 (940)**	**160.3 (1105)**	**160.0 (1103)**	**148.1 (1021)**
MEASURED EXTRAPOLATED (M. E.)*	Electric Gages	55.5 (383)	25.5 (176)	32.0 (221)	29.4 (203)
	Mech. Gages	13.3 (92)	12.7 (87)	10.8 (75)	13.3 (92)
	Average	**34.4 (237)**	**19.1 (131)**	**21.4 (148)**	**21.4 (148)**
AASHTO	Creep	22.7 (156)	20.2 (139)	25.9 (179)	23.9 (165)
	Shrinkage	10.4 (71)	10.4 (71)	10.4 (71)	10.4 (71)
	Total	**33.1 (228)**	**30.6 (211)**	**36.3 (250)**	**34.3 (236)**
NAAMAN	Creep	29.0 (200)	26.3 (182)	33.1 (228)	30.5 (211)
	Shrinkage	2.9 (20)	2.9 (20)	2.9 (20)	2.9 (20)
	Total	**31.9 (220)**	**29.2 (201)**	**35.9 (248)**	**33.4 (230)**
NAWY	Creep	27.1 (187)	25.4 (175)	31.0 (214)	28.6 (197)
	Shrinkage	2.4 (16)	2.4 (16)	2.4 (16)	2.4 (16)
	Total	**29.5 (203)**	**27.8 (191)**	**33.4 (230)**	**31.0 (213)**
M. E.*	% of Initial Stress	9.8	11.9	13.4	14.4
AASHTO		24.2	19.1	22.7	23.1
NAAMAN		23.4	18.2	22.5	22.6
NAWY		21.6	17.3	20.9	20.9
AASHTO / M. E.*		2.48	1.60	1.70	1.60
NAAMAN / M. E.*		2.39	1.53	1.68	1.56
NAWY / M. E.*		2.21	1.46	1.56	1.45

*Only measured extrapolated values from the mechanical gages were considered for LVOMB comparisons.

Table 5.6 – Las Vegas Solid Beam Prestress Loss Comparison

ksi (MPa)		LVOMS	LVOAS
INITIAL STRESS		**204.9 (1413)**	**217.5 (1500)**
MEASURED EXTRAPOLATED (M. E.)*	Electric Gages	11.2 (77)	8.4 (58)
	Mechanical Gages	23.8 (164)	19.3 (133)
	Average	**17.5 (121)**	**13.8 (95)**
AASHTO	Creep	21.5 (148)	22.8 (157)
	Shrinkage	10.4 (71)	10.4 (71)
	Total	**31.8 (219)**	**33.1 (228)**
NAAMAN	Creep	22.3 (154)	23.7 (163)
	Shrinkage	9.7 (67)	9.7 (67)
	Total	**32.1 (221)**	**33.4 (230)**
NAWY	Creep	22.0 (151)	23.3 (160)
	Shrinkage	8.4 (58)	8.4 (58)
	Total	**30.4 (210)**	**31.7 (219)**

M. E.*	% of Initial Stress	5.5	3.8
AASHTO		15.5	15.2
NAAMAN		15.7	15.4
NAWY		14.8	14.6

AASHTO / M. E.*	2.84	3.97
NAAMAN / M. E.*	2.86	4.00
NAWY / M. E.*	2.71	3.80

*Only measured extrapolated values from the electric gages were considered for comparisons.

Table 5.7 – Las Vegas Creep Cylinder Comparison

LAS VEGAS CREEP CYLINDER SPECIMENS		BOX GIRDER	
		Indoor	Outdoor
Projected Data (From Initial Data Reading)	40-Year (microstrain)	1608	1213
	ksi	45.2	34.1
	MPa	312	235
Measured Coefficients		2.85	3.43
Calculated Coefficients		2.92	
Calculated / Measured		1.03	0.85

Table 5.8 – Las Vegas Shrinkage Cylinder Comparison

LAS VEGAS SHRINKAGE CYLINDER SPECIMENS		BOX GIRDER		SOLID BEAM	SUPPLEMENTAL	
		Indoor	Outdoor	Outdoor	Indoor	Outdoor
Projected Data (From Initial Data Reading)	40-Year (microstrain)	-1122	-817	-122	491	160
	ksi	-31.5	-23.0	-3.4	13.8	4.5
	MPa	-217	-158	-24	95	31
Measured Coefficients		0.000256	-0.000223	-0.000122	0.000491	0.000160
Calculated Coefficients		0.0006				
Calculated / Measured		2.35	-2.69	-4.94	1.22	3.76

Table 5.9 – Reno Beam Specimen Percentage Loss Comparison

%		RNOMB	RNOAB	RNIMB	RNIAB	RNOMS	RNOAS
MEASURED EXTRAPOLATED (M. E.)*	Electric Gages	20.1	21.9	26.1	21.9	9.9	13.1
	Mechanical Gages	20.2	26.4	23.6	1.8	9.9	6.1
	Average	**20.1**	**24.2**	**24.8**	**22.8**	**9.9**	**9.6**
AASHTO / M. E.	Electric	102.6	94.5	77.5	94.8	137.2	106.6
	Mechanical	102.1	78.4	85.8	87.9	136.6	230.5
	Average	**102.3**	**85.7**	**81.4**	**91.2**	**136.9**	**145.8**
NAAMAN / M. E.	Electric	99.9	91.9	75.9	92.0	209.4	160.8
	Mechanical	99.4	76.2	84.0	85.3	208.6	347.7
	Average	**99.6**	**83.3**	**79.7**	**88.5**	**209.0**	**254.3**
NAWY / M. E.	Electric	120.9	111.1	92.2	111.1	211.5	162.6
	Mechanical	120.3	92.1	102.0	103.1	210.7	351.6
	Average	**120.6**	**100.7**	**96.8**	**106.9**	**211.1**	**257.1**

*Only the measured extrapolated values from the mechanical gages were considered for solid beam comparisons.

Table 5.10 – Las Vegas Beam Specimen Percentage Loss Comparison

%		LVOMB	LVOAB	LVIMB	LVIAB	LVOMS	LVOAS
MEASURED EXTRAPOLATED (M. E.)*	Electric Gages	40.7	15.9	20.0	19.9	5.5	3.8
	Mechanical Gages	9.8	7.9	6.8	1.8	11.6	8.9
	Average	**25.3**	**11.9**	**13.4**	**14.4**	**8.5**	**6.4**
AASHTO / M. E.	Electric	59.5	119.9	113.4	116.3	283.5	396.7
	Mechanical	248.1	241.3	335.7	256.6	133.9	171.9
	Average	**96.0**	**160.2**	**169.5**	**160.1**	**181.9**	**239.9**
NAAMAN / M. E.	Electric	57.5	114.6	112.3	113.5	285.8	399.9
	Mechanical	239.5	230.6	332.5	250.3	135.0	173.3
	Average	**92.7**	**153.2**	**167.9**	**156.2**	**183.4**	**241.8**
NAWY / M. E.	Electric	53.1	109.0	104.4	105.1	270.9	379.5
	Mechanical	221.3	219.3	309.2	231.9	128.0	164.5
	Average	**85.6**	**145.7**	**156.1**	**144.6**	**173.8**	**229.5**

*Only the measured extrapolated values from the mechanical gages were considered for LVOMB comparisons, and only the measured extrapolated values from the electric gages were considered for solid beam comparisons.

Table 6.1 – Prestress Loss Comparison Using Will's Elastic Modulus Equations

ksi (MPa)		RNOMB	RNOAB	RNIMB	RNIAB
MEASURED EXTRAPOLATED (M. E.)		34.8 (240.1)	40.9 (281.7)	47.2 (325.1)	37.9 (261.3)
NAAMAN'S TIME-STEP METHOD	LOSS (ACI 318)	24.2 (167.1)	23.8 (164.0)	26.2 (180.3)	23.5 (161.9)
	LOSS (WILL)	34.7 (239.2)	34.0 (234.6)	37.6 (259.3)	33.6 (231.4)
	ACI 318 / M. E.	0.70	0.58	0.55	0.62
	WILL / M. E.	1.00	0.83	0.80	0.89

Table 6.2 - Modified AASHTO Results for the Reno Box Girders

ksi (MPa)		RNOMB	RNOAB	RNIMB	RNIAB
Measured Extrapolated (M.E.)		34.8 (240.1)	40.9 (281.7)	47.2 (325.1)	37.9 (261.3)
AASHTO		35.6 (245.7)	35.0 (241.4)	38.4 (264.7)	34.6 (238.4)
Modified AASHTO	Shrinkage	9.2 (63.4)			
	Creep	35.1 (241.7)	34.3 (236.2)	38.5 (265.4)	33.7 (232.5)
	Total	44.3 (305.1)	43.5 (299.7)	47.7 (328.8)	42.9 (295.9)
AASHTO / M.E.		1.02	0.86	0.81	0.91
Mod. AASHTO / M.E.		1.27	1.06	1.01	1.13

Table 6.3 – Modified AASHTO Results for the Reno Solid Beams

ksi (MPa)		RNOMS	RNOAS
Measured Extrapolated (M.E.)		24.5 (169.0)	28.2 (194.3)
AASHTO		33.6 (231.8)	30.1 (207.2)
Modified AASHTO	**Shrinkage**	9.2 (63.4)	
	Creep	32.5 (224.3)	28.1 (193.5)
	Total	41.7 (287.7)	37.3 (256.9)
AASHTO / M.E.		1.37	1.07
Mod. AASHTO / M.E.		1.70	1.32

Table 6.4 – Modified AASHTO Results for the Bridges in Mangoba's Study

ksi (Mpa)		South Meadows Int.	Mt. Rose Int.	Zolezzi Lane G.S.	Old Virginia Road G.S.
Measured Extrapolated (M.E.)		**22.9 (158.2)**	**26.2 (180.4)**	**18.1 (124.7)**	**30.1 (207.7)**
Modified AASHTO	**Creep**	17.7 (122.0)	25.1 (173.2)	20.1 (138.4)	16.2 (111.8)
	Shrinkage	9.2 (63.4)	9.2 (63.4)	9.2 (63.4)	9.2 (63.4)
	Total	**26.9 (185.5)**	**34.3 (236.7)**	**29.3 (201.8)**	**25.4 (175.2)**
AASHTO		**21.8 (150.0)**	**27.7 (191.2)**	**23.7 (163.1)**	**20.6 (141.8)**
AASHTO / M. E.		0.95	1.06	1.31	0.68
MOD. AASHTO / M. E.		1.17	1.31	1.62	0.84

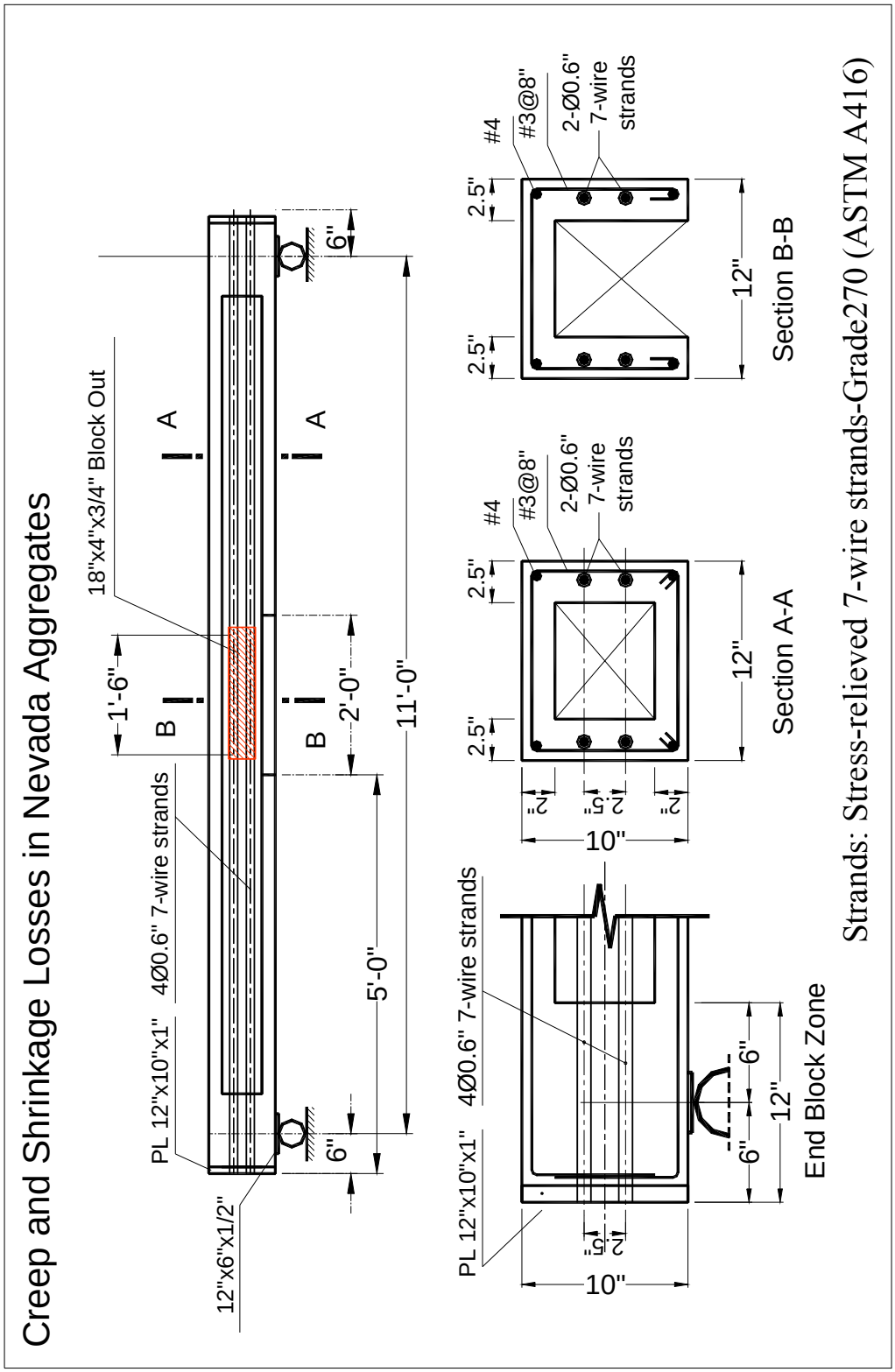

Figure 2.1 – Box Girder Plans in U.S. Customary Units

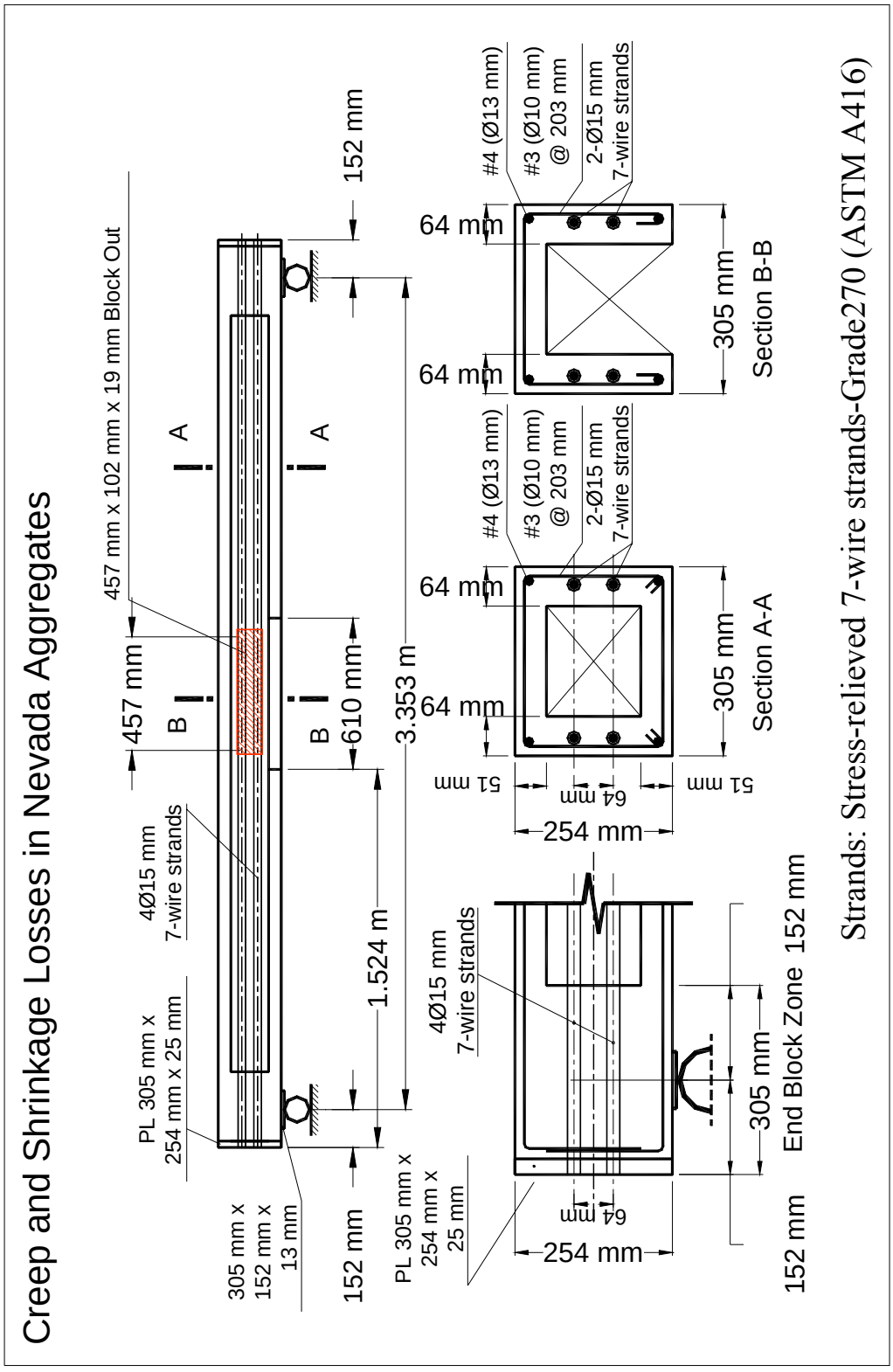

Figure 2.1 (continued) – Box Girder Plans in SI Units

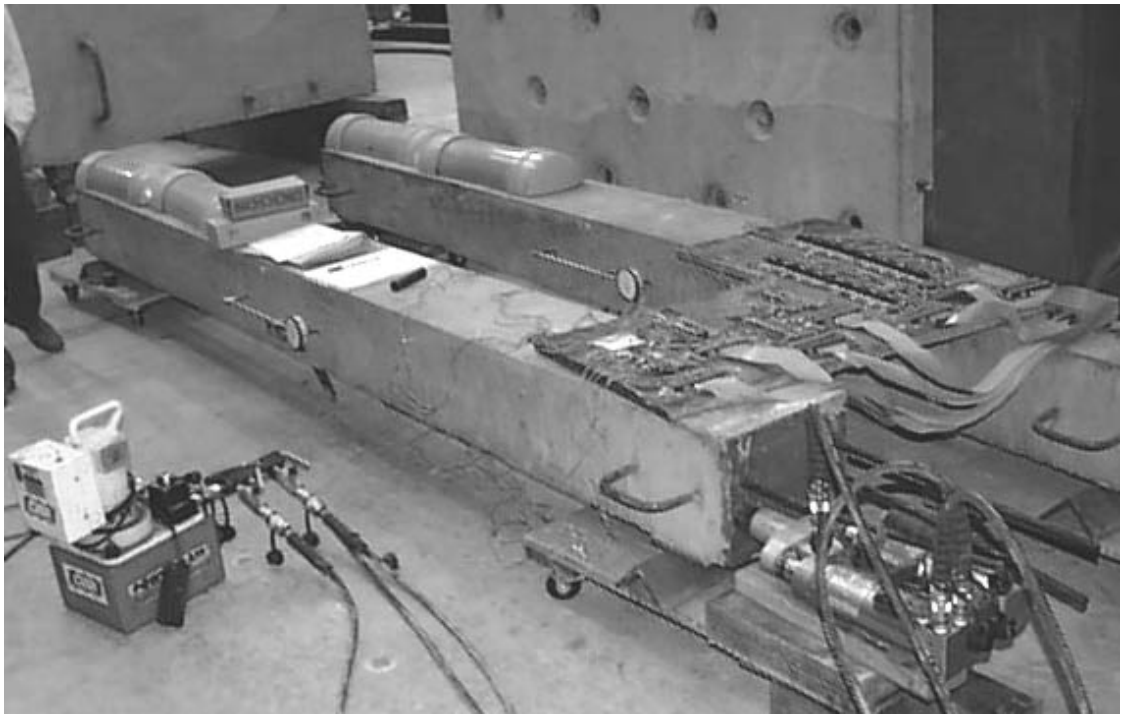

Figure 2.2 – Box Girders

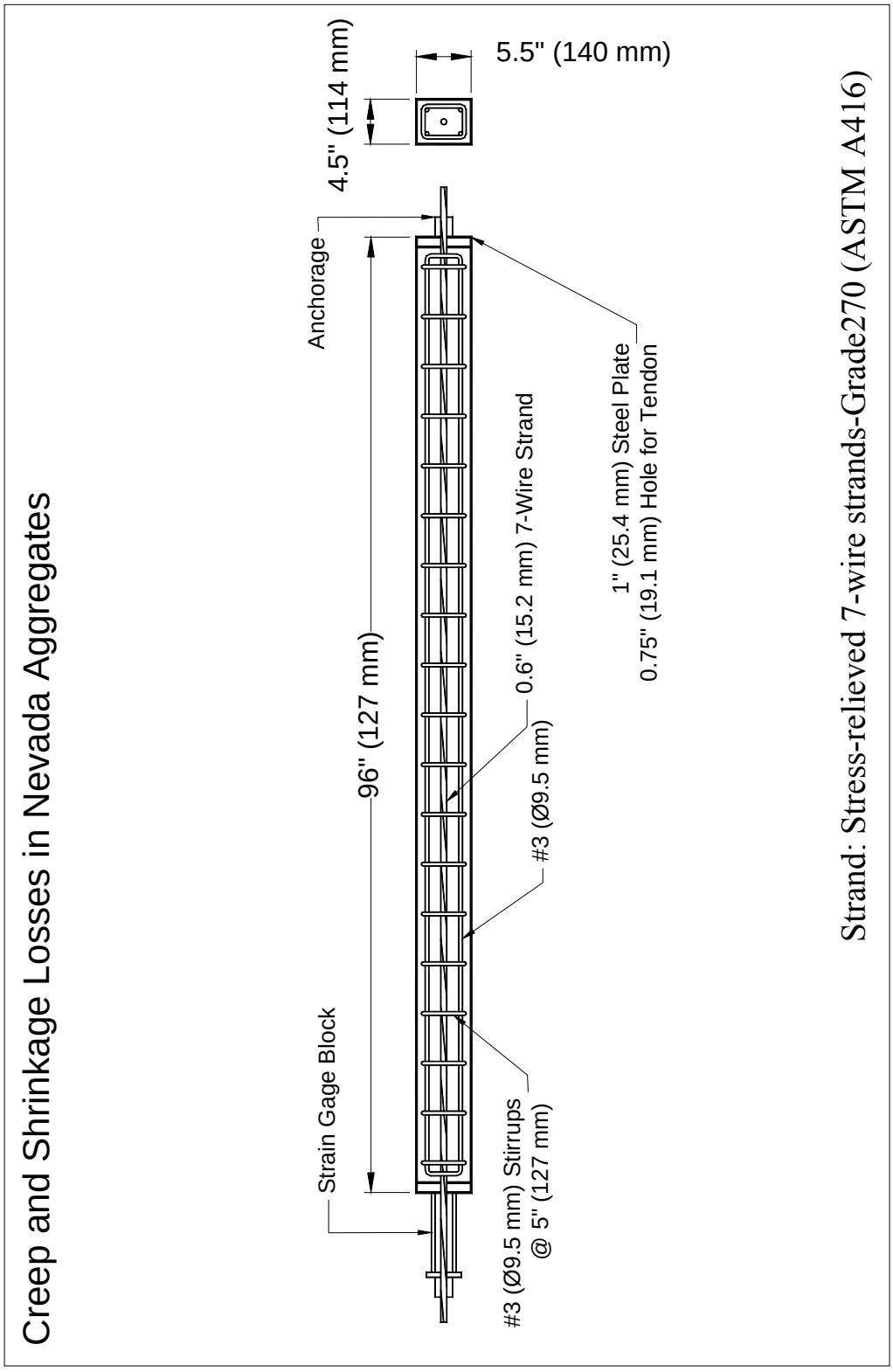

Figure 2.3 – Solid Beam Plans

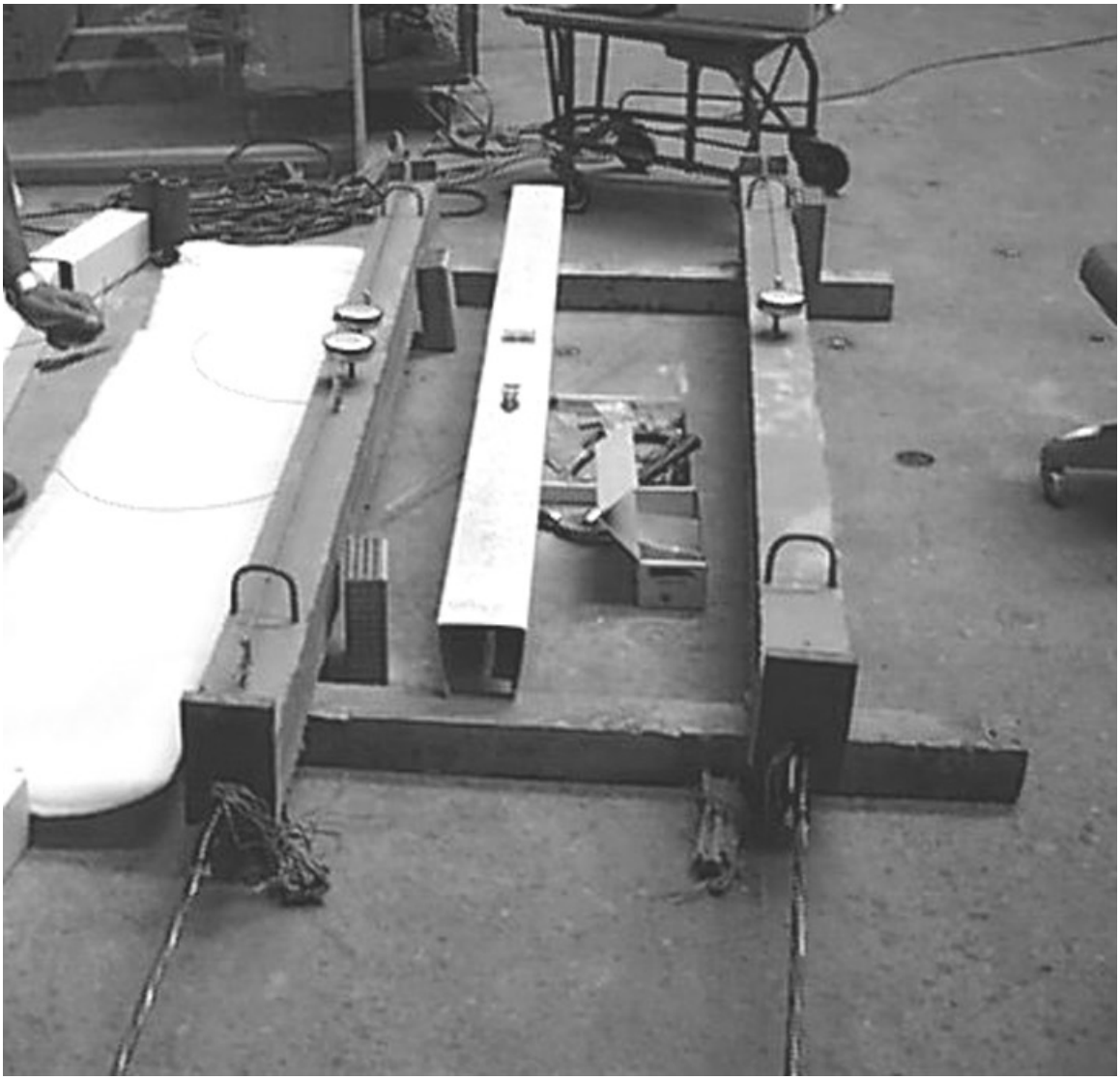

Figure 2.4 – Solid Beams

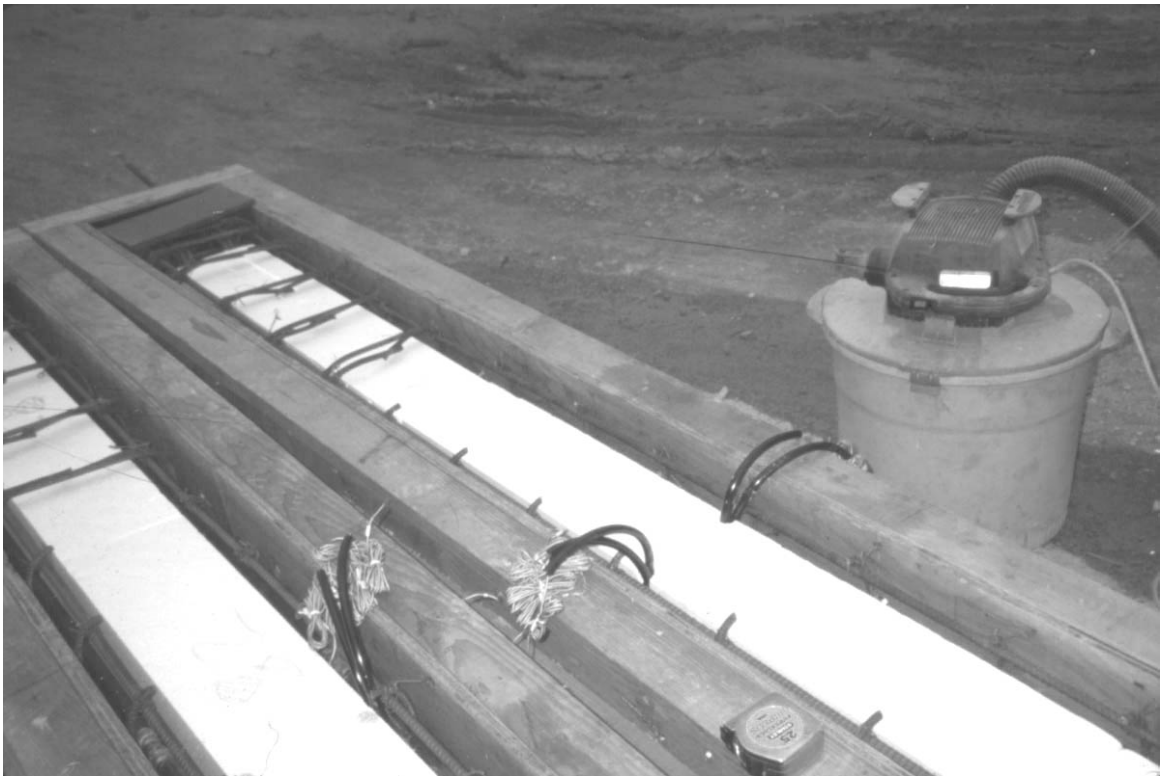

Figure 2.5 – Box Girders Under Construction

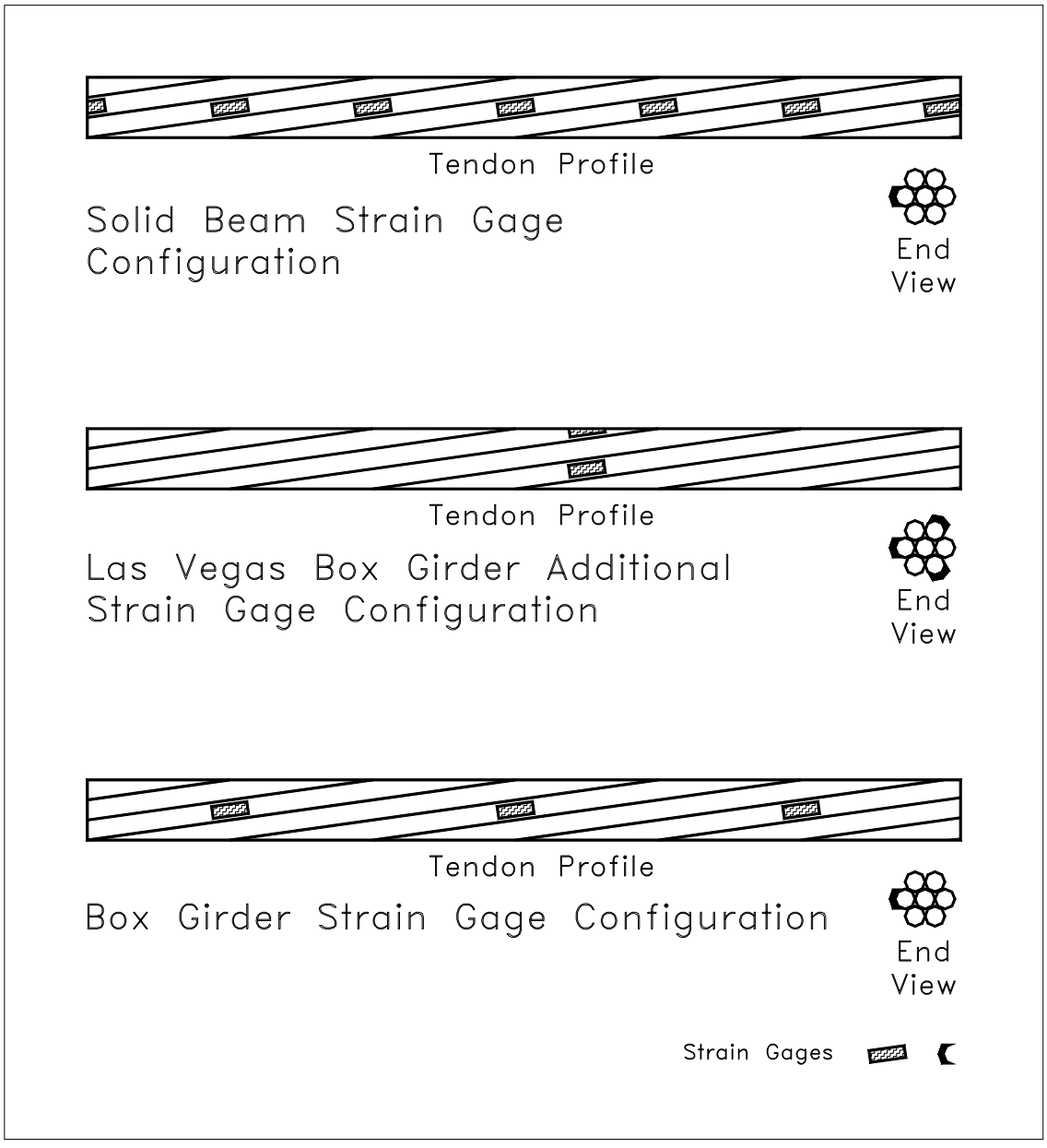

Figure 3.1 – Strain Gage Configuration

Figure 3.2 – Strain Gages on Box Girder Tendons

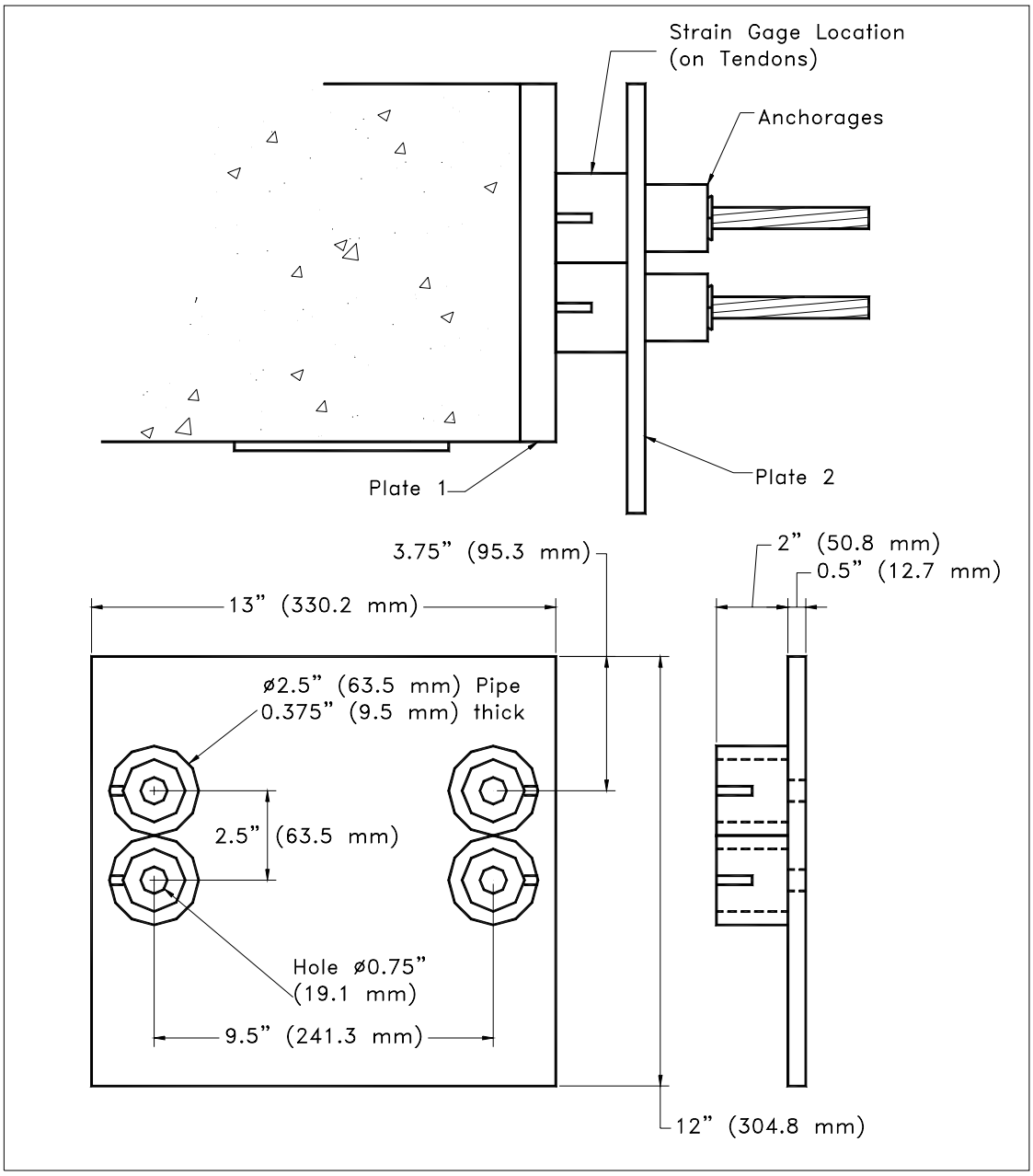

Figure 3.3 – Las Vegas Box Girder Strain Gage Plate Plans

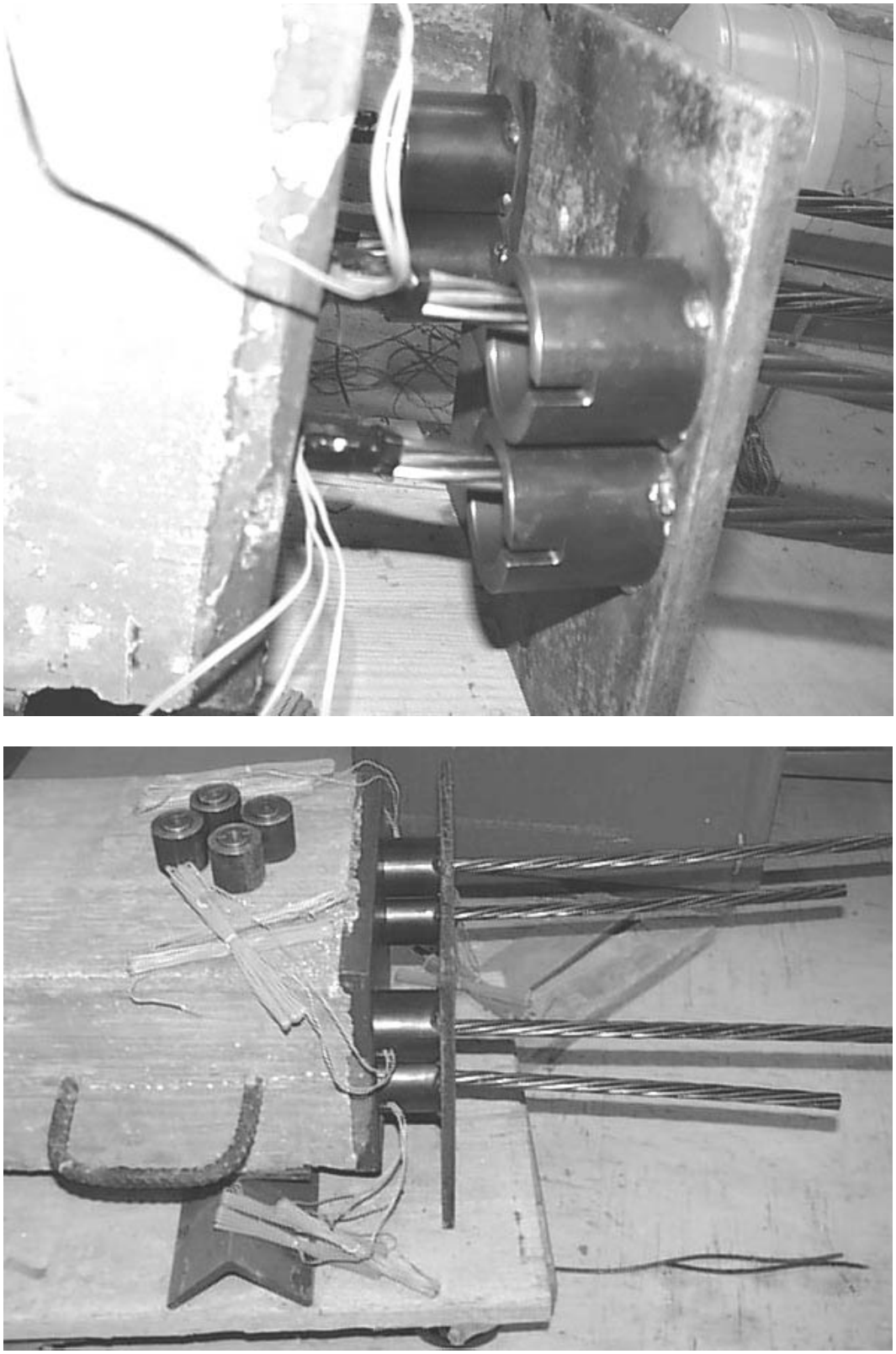

Figure 3.4 – Las Vegas Box Girder Strain Gage Plate

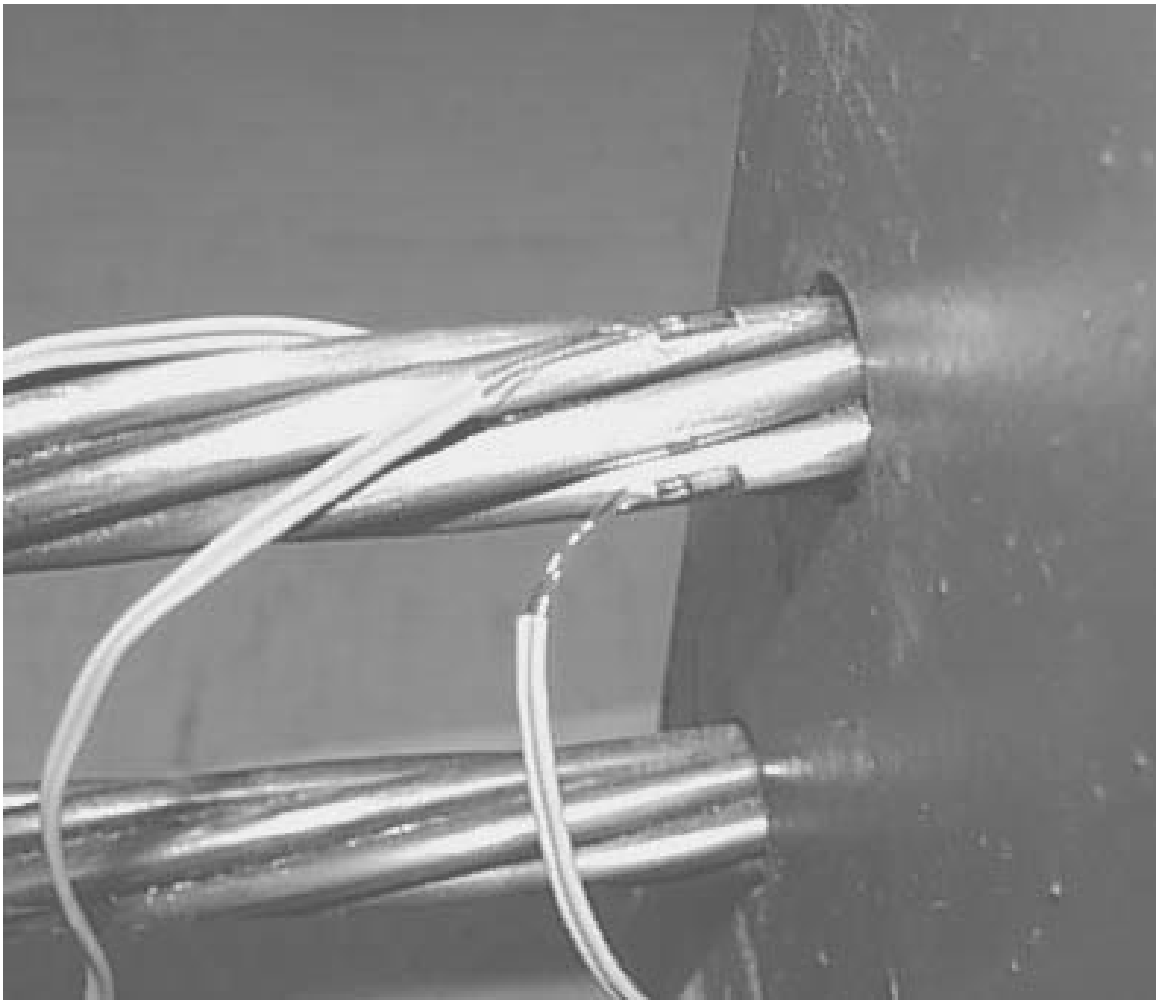

Figure 3.5 – Additional Las Vegas Box Girder Strain Gages

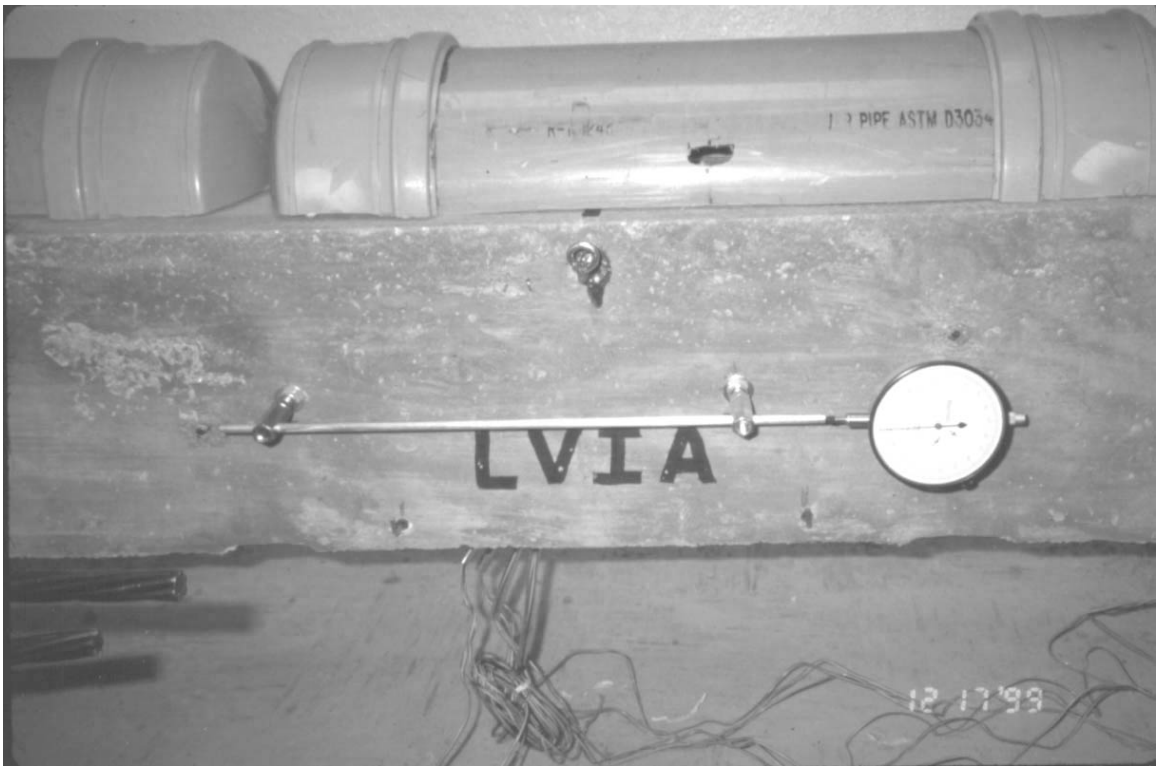

Figure 3.6 – Box Girder Mechanical Strain Gage

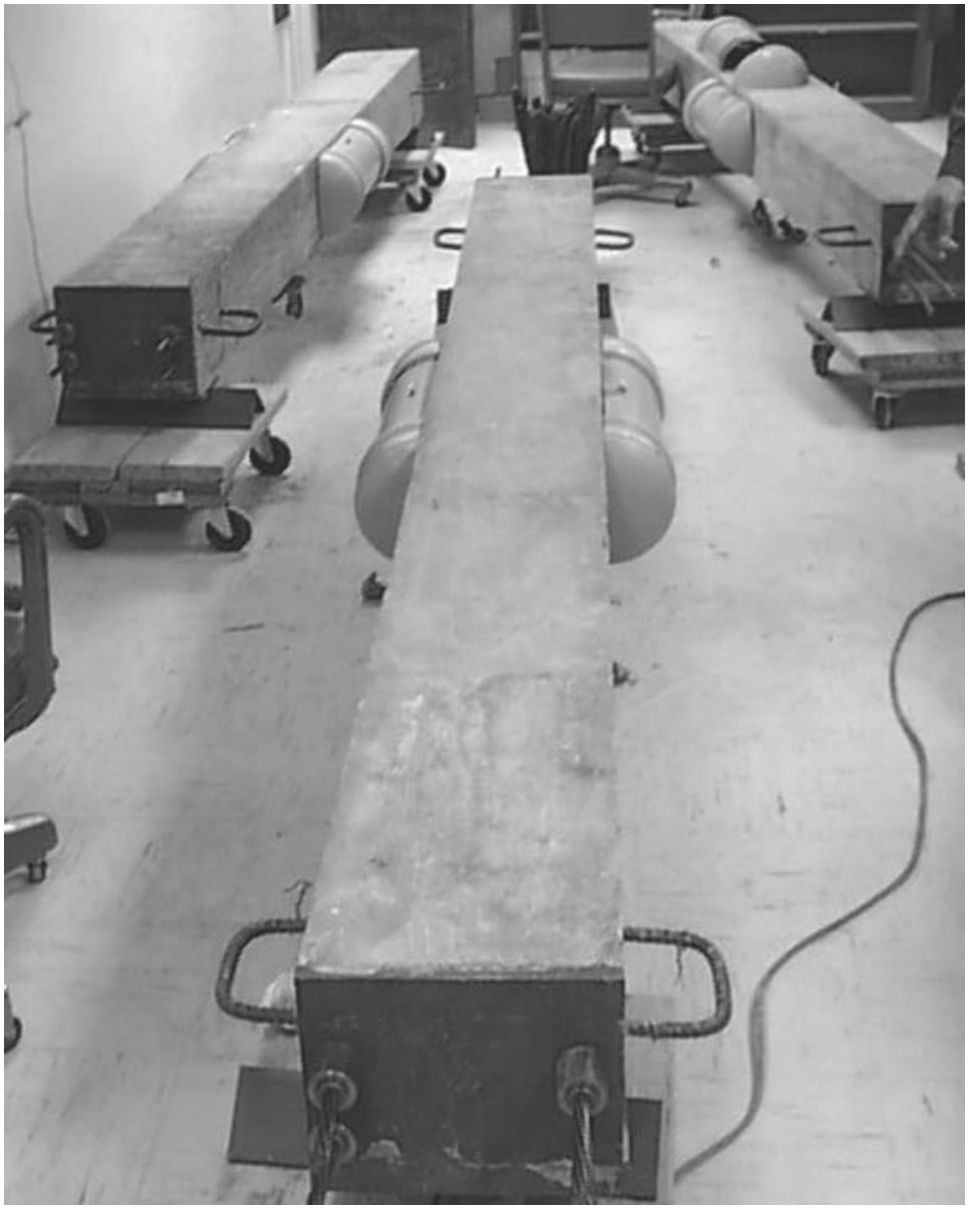

Figure 3.7 – Strain Gage Covers Over Box Girder Mechanical Gages

Figure 3.8 – Solid Beam Mechanical Strain Gages

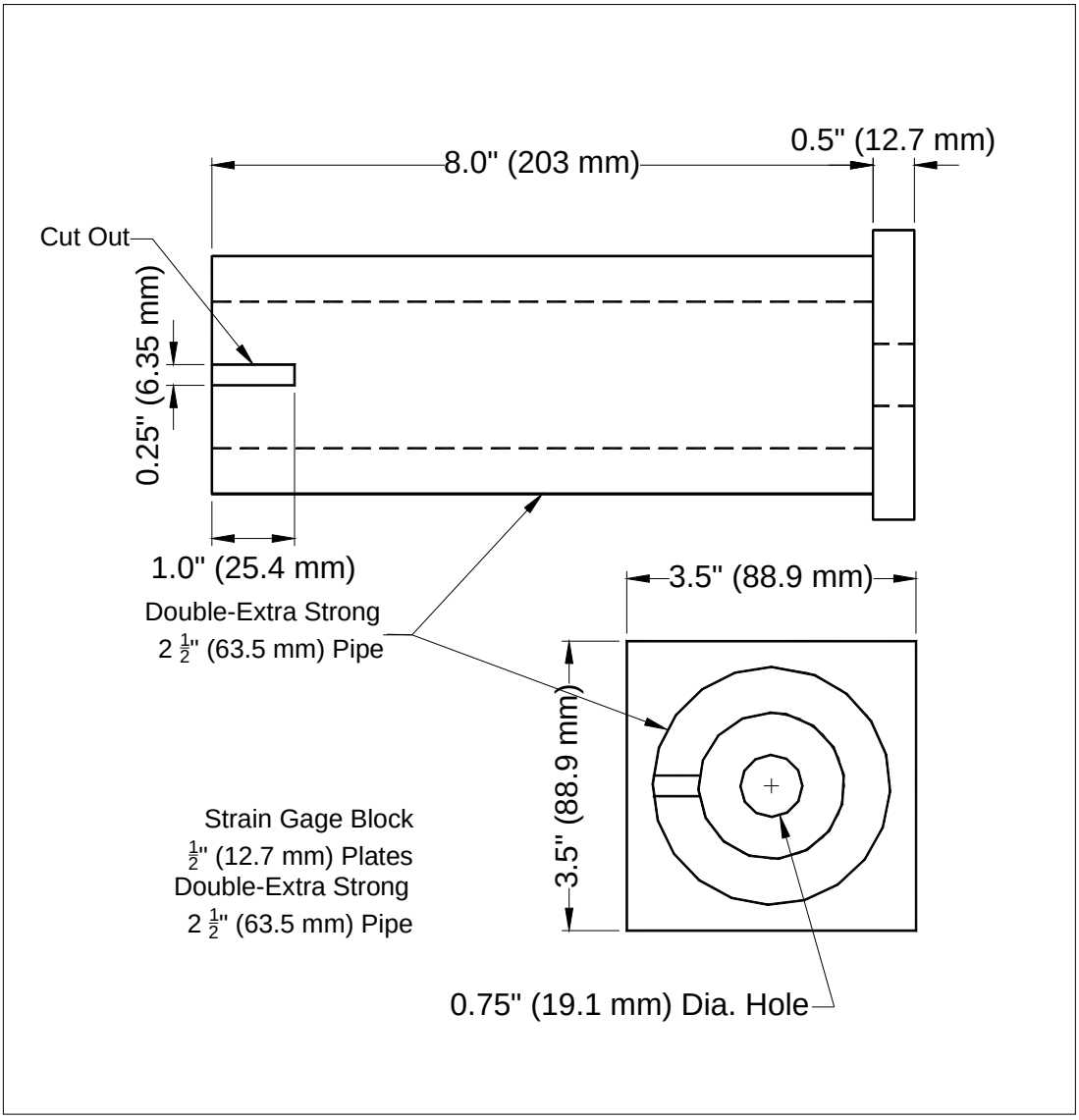

Figure 3.9 – Solid Beam Strain Gage Block Plans

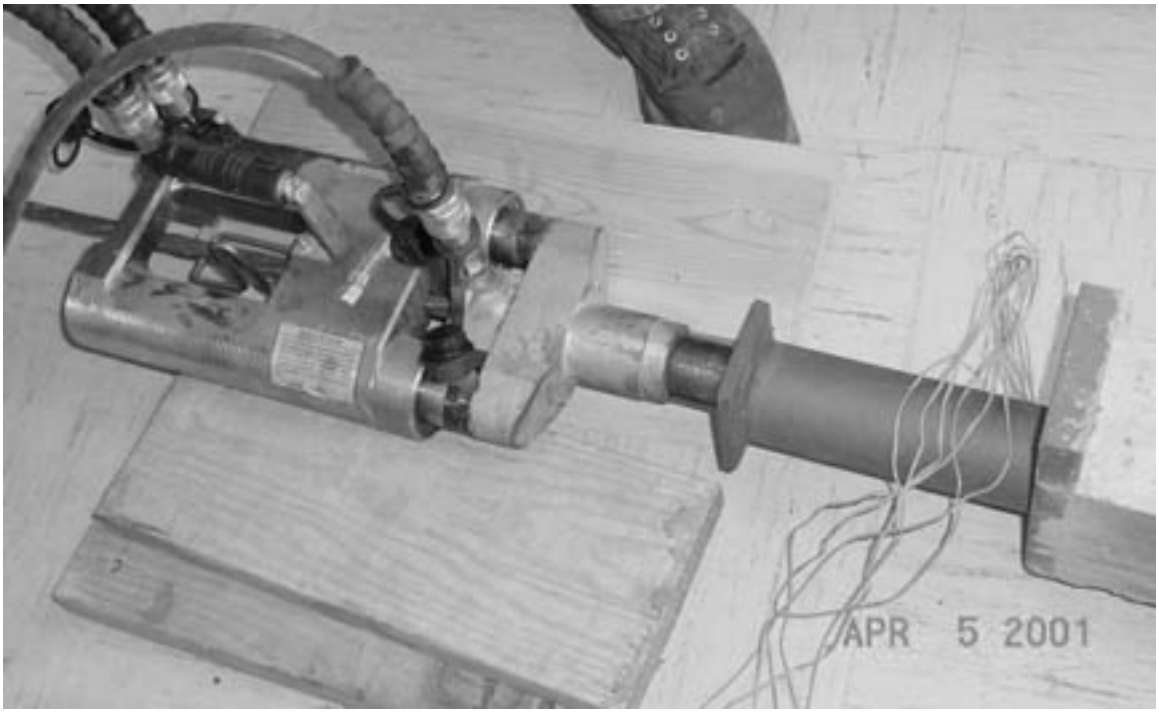

Figure 3.10 – Prestressing Jack on Solid Beam with Strain Gage Block

Figure 3.11 – Solid Beams with Mechanical Gage Cover and Batting for Moist Curing Prior to Gage Cover

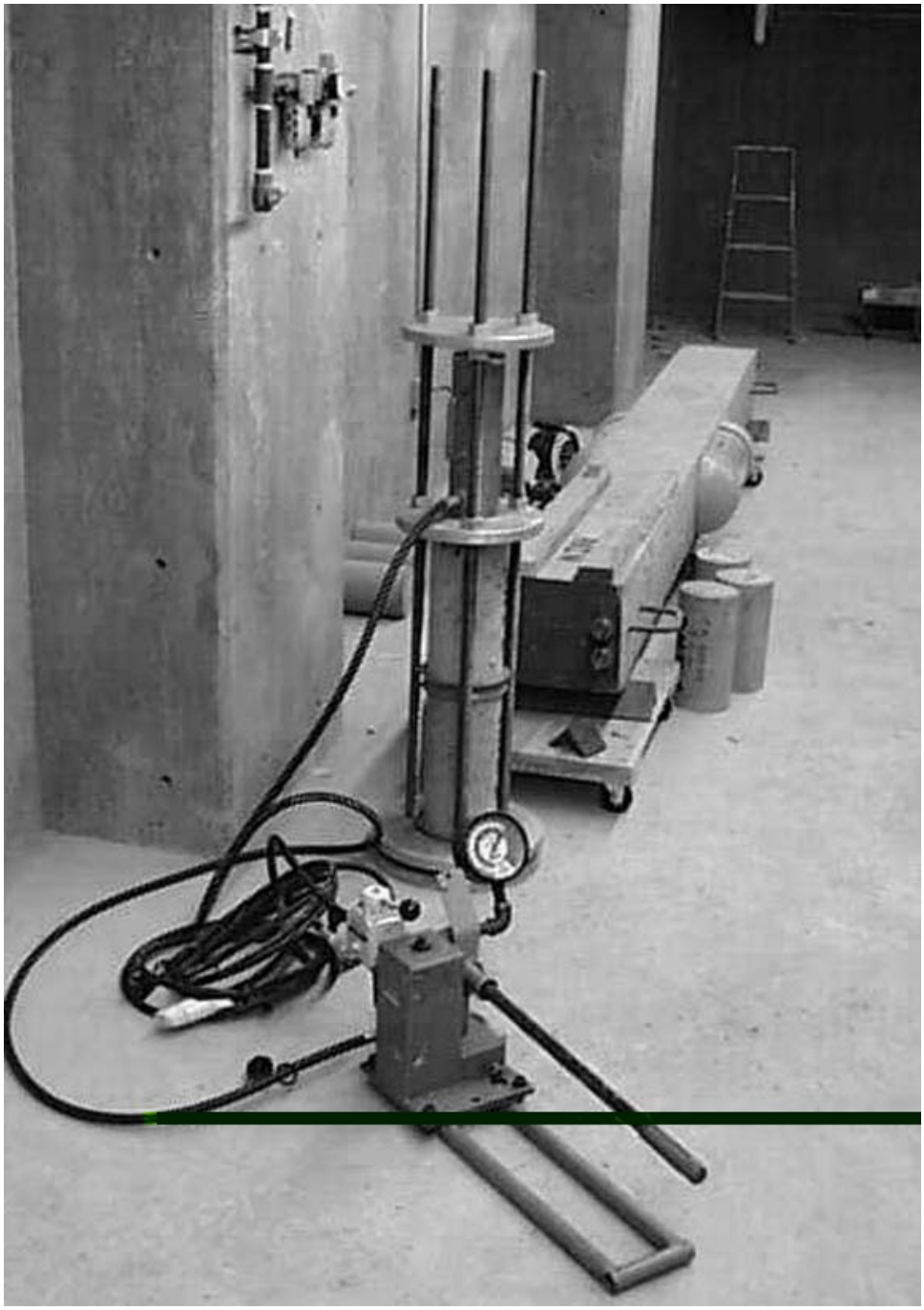

Figure 3.12 – Creep Frame, Jack, and Pump

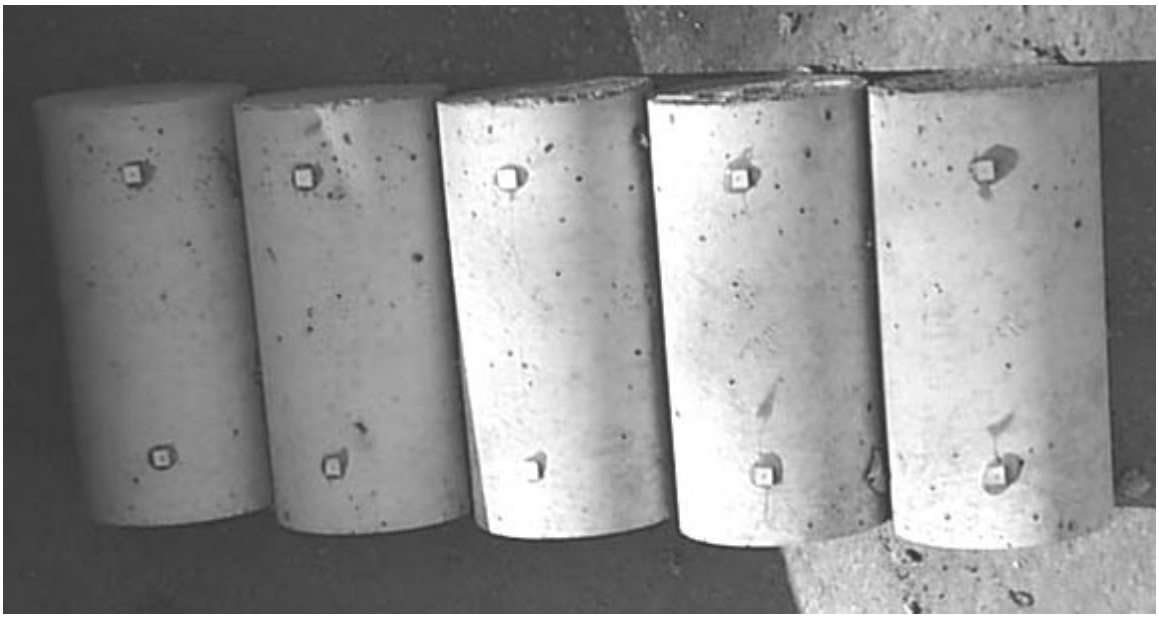

Figure 3.13 – Concrete Cylinders with Gage Tabs

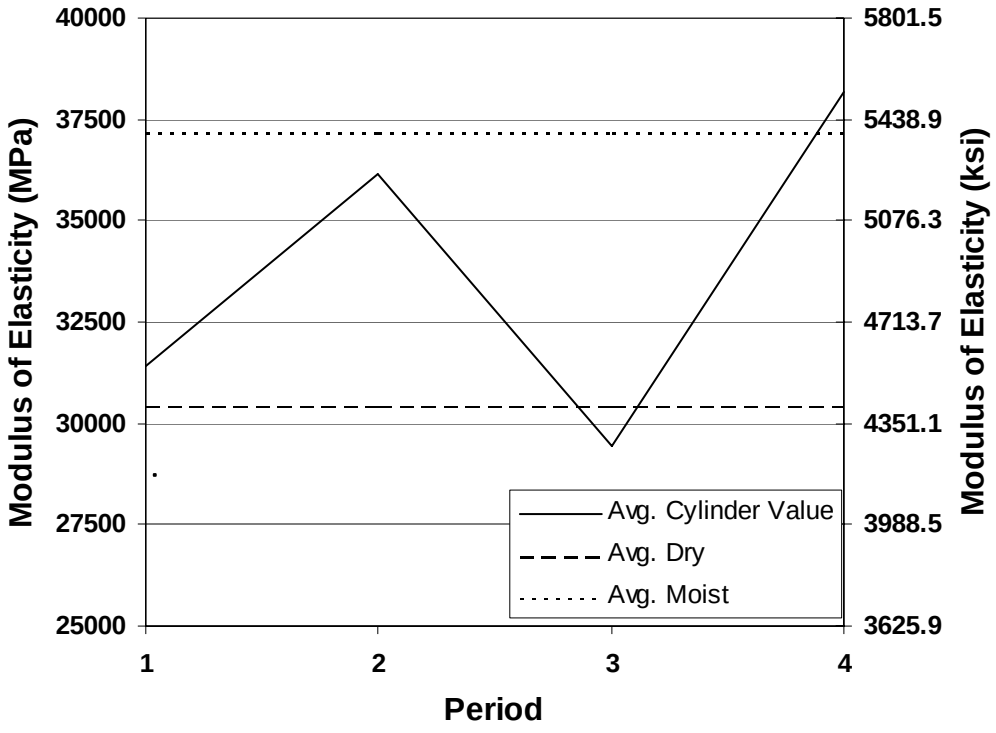

Figure 4.1 – Modulus of Elasticity Cycles

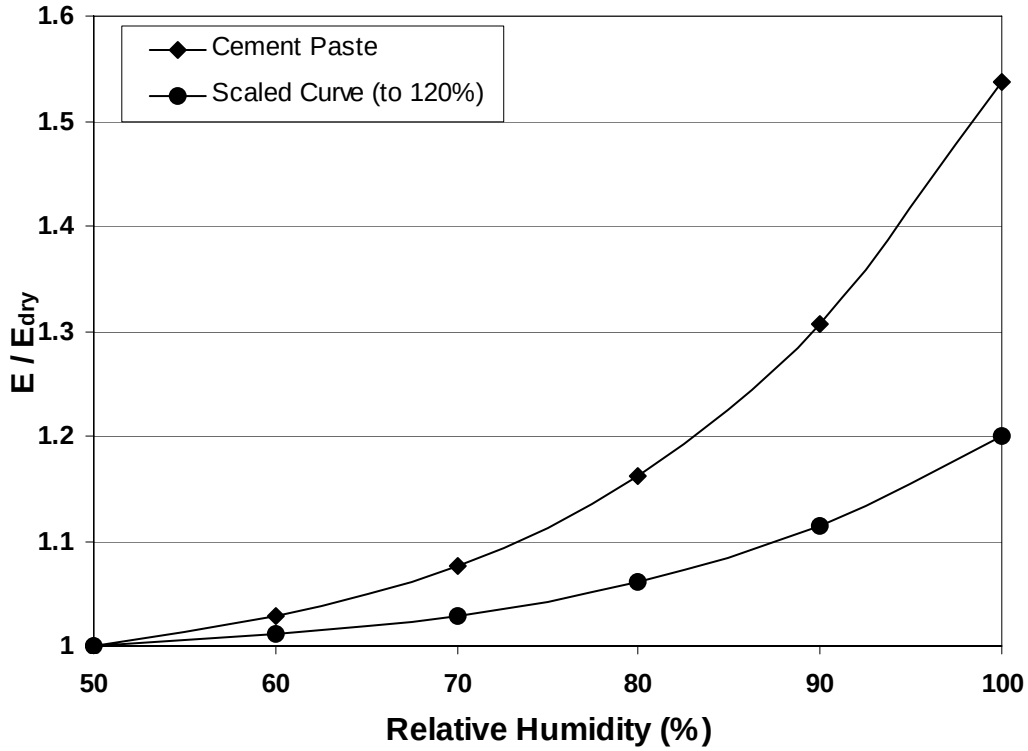

Figure 4.2 – Humidity Effect Curve

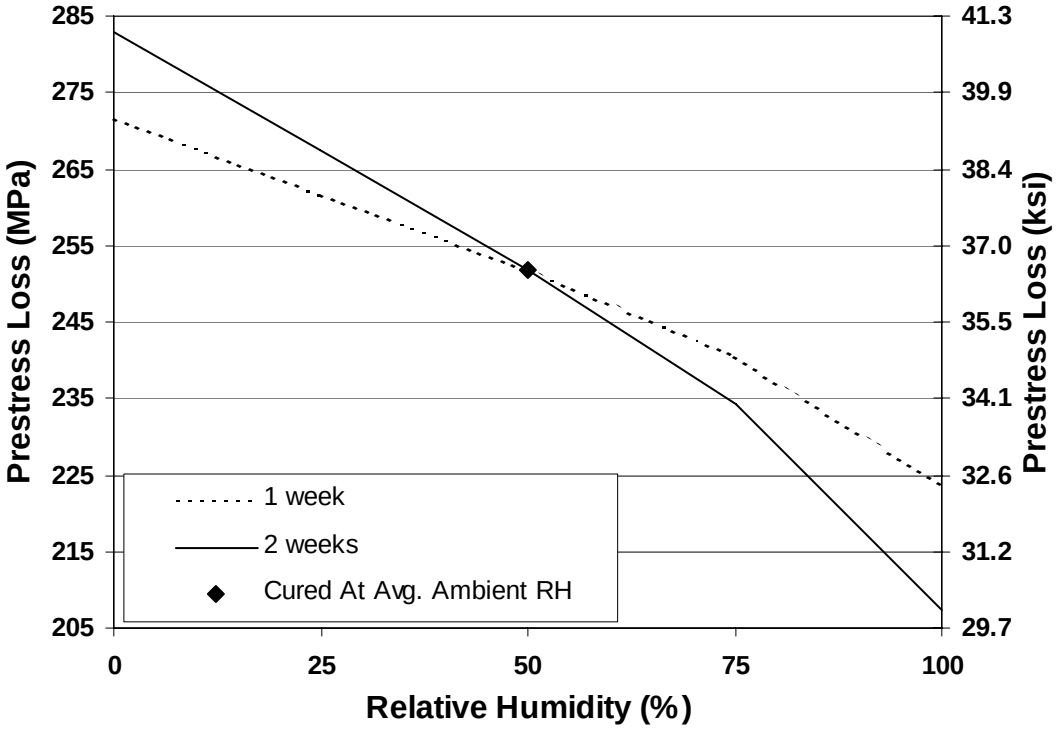

Figure 4.3 – Prestress Loss Comparison of Curing Times Using Modified Elastic Modulus

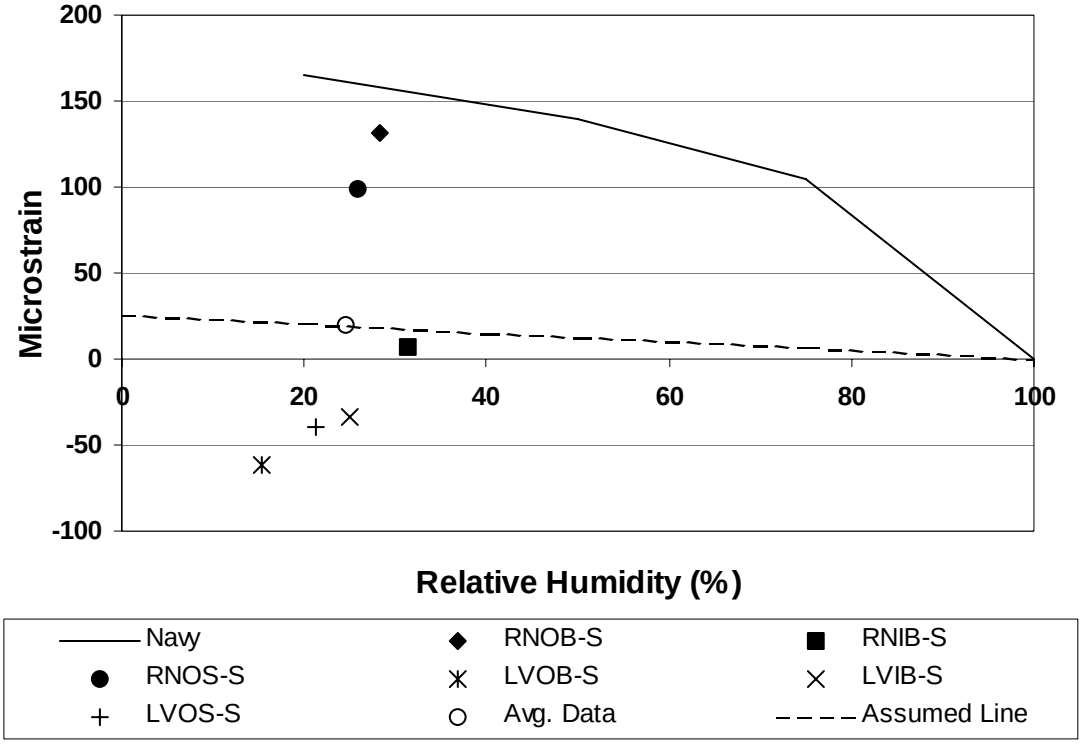

Figure 4.4 – Navy Shrinkage Data Comparison, Day 1

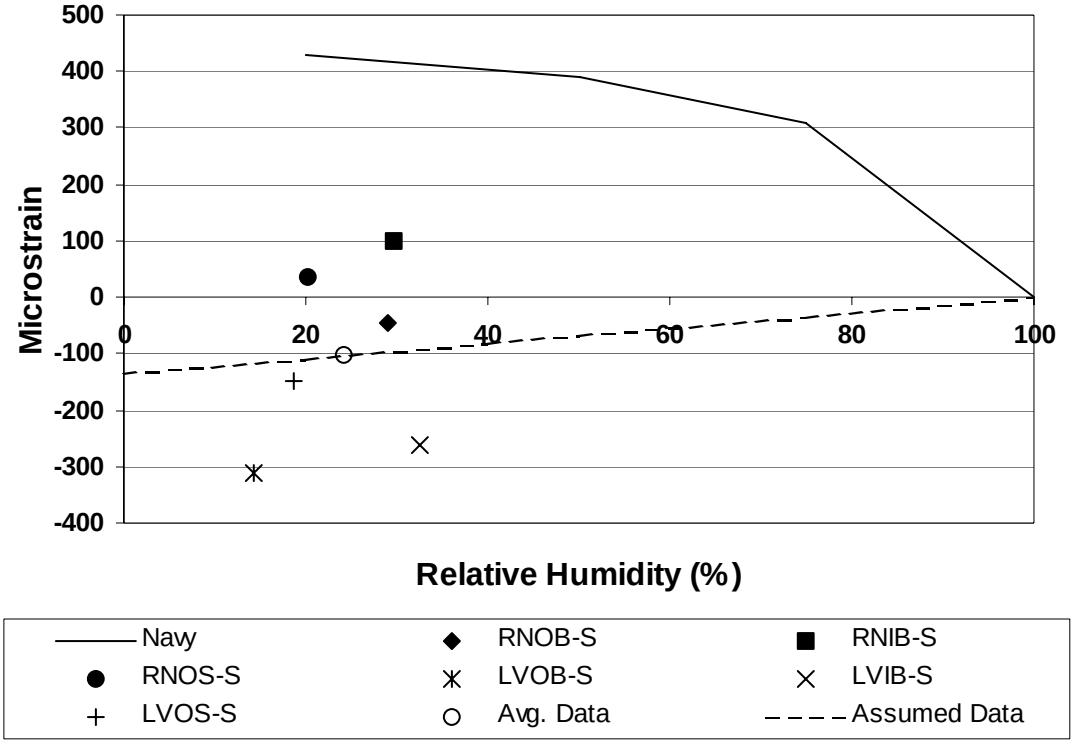

Figure 4.5 – Navy Shrinkage Data Comparison, Day 7

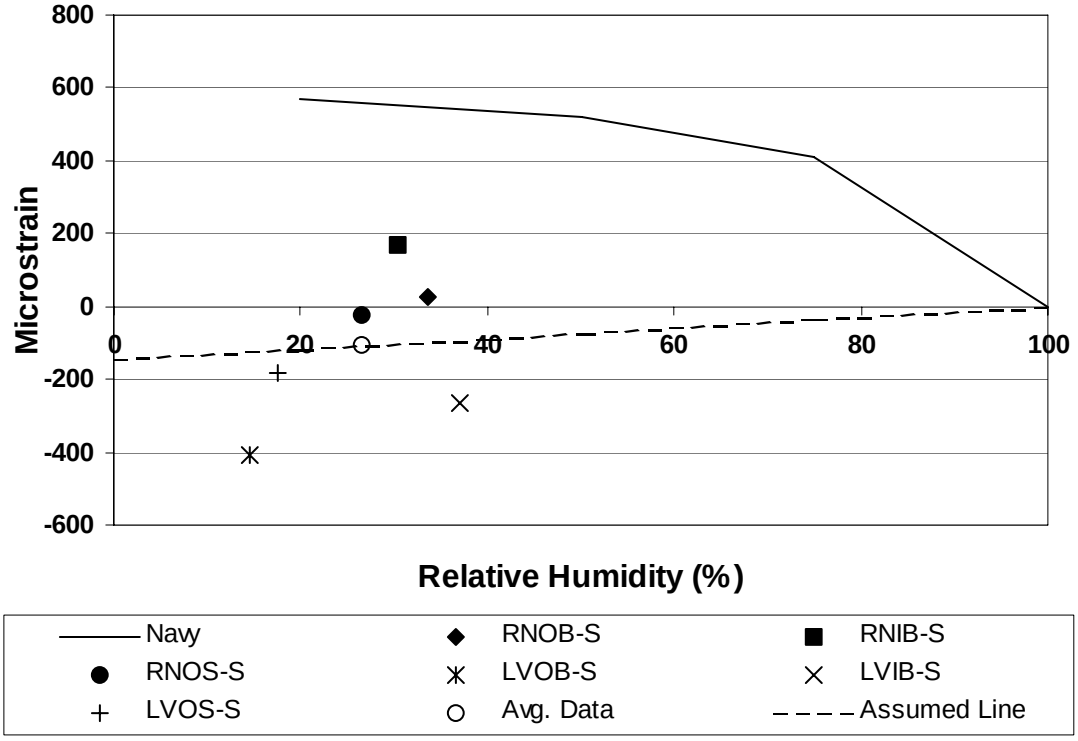

Figure 4.6 – Navy Shrinkage Data Comparison, Day 14

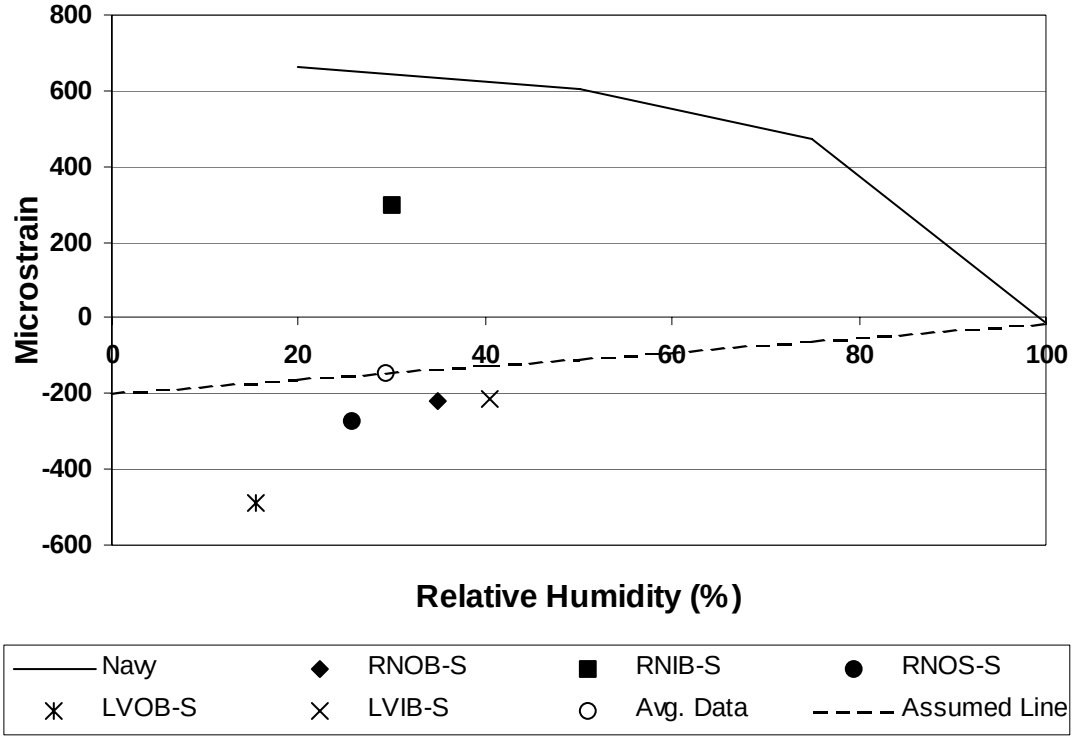

Figure 4.7 – Navy Shrinkage Data Comparison, Day 21

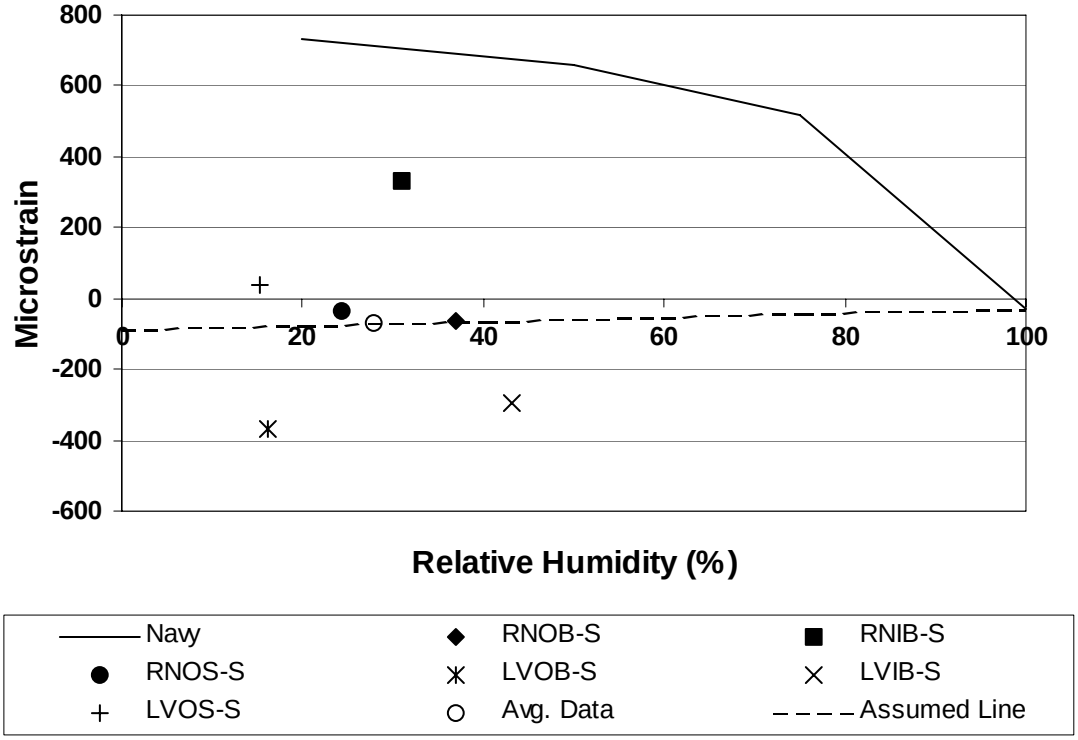

Figure 4.8 – Navy Shrinkage Data Comparison, Day 28

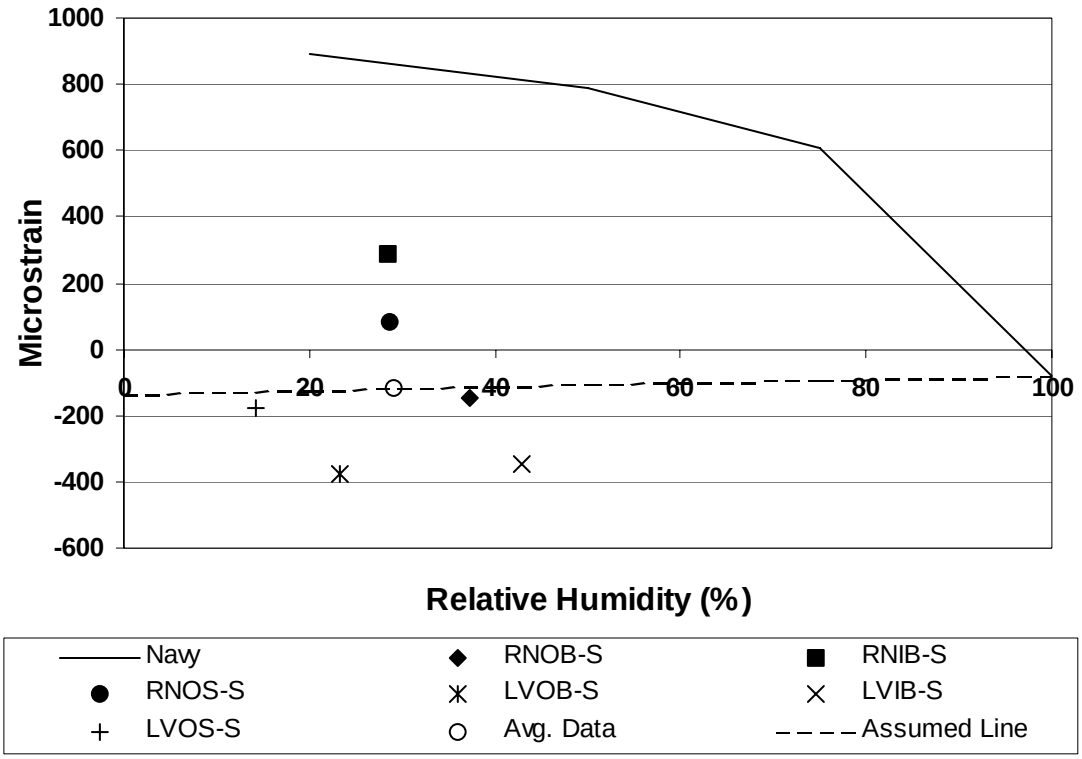

Figure 4.9 – Navy Shrinkage Data Comparison, Day 56

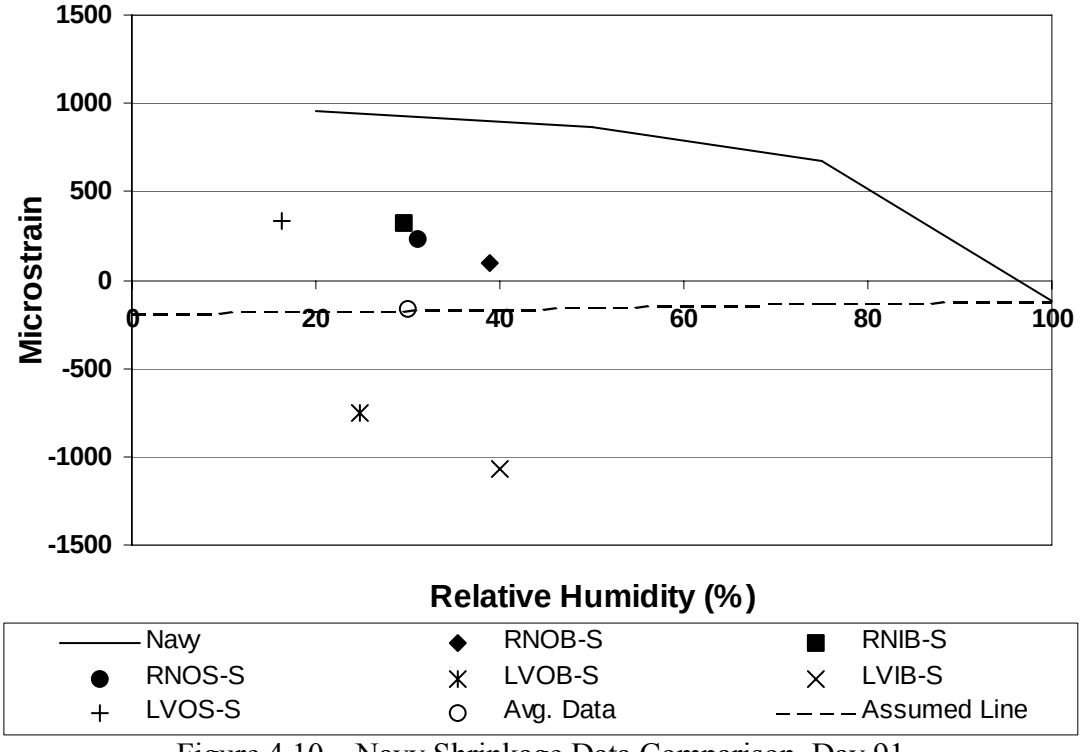

Figure 4.10 – Navy Shrinkage Data Comparison, Day 91

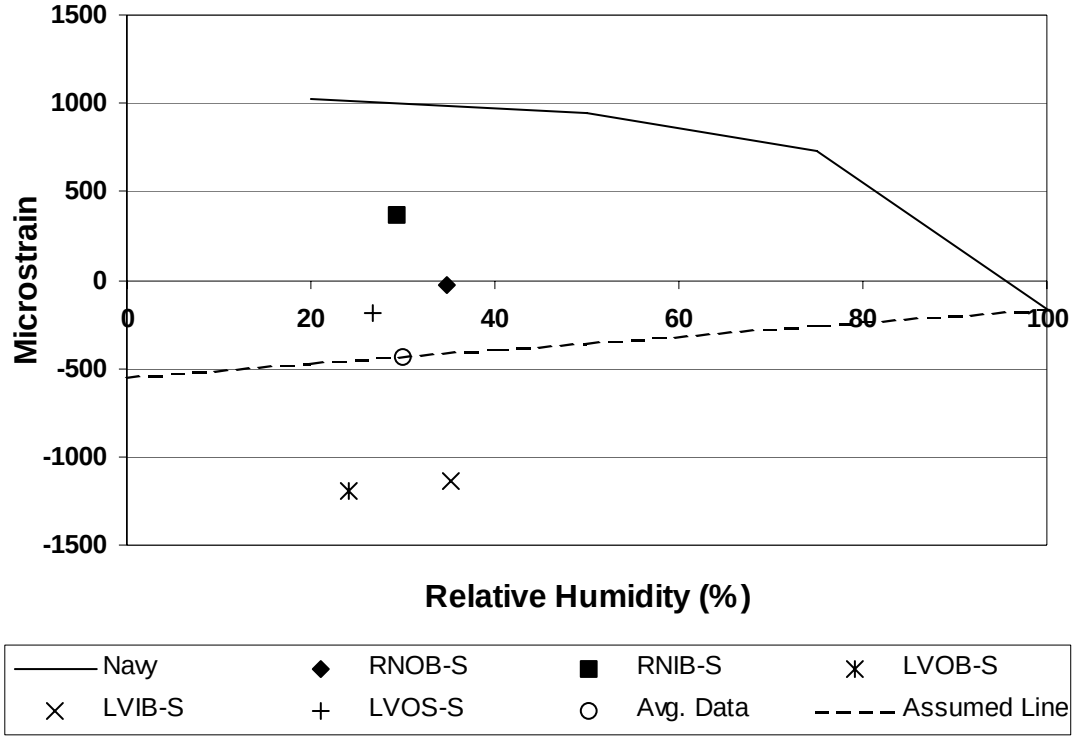

Figure 4.11 – Navy Shrinkage Data Comparison, Day 175

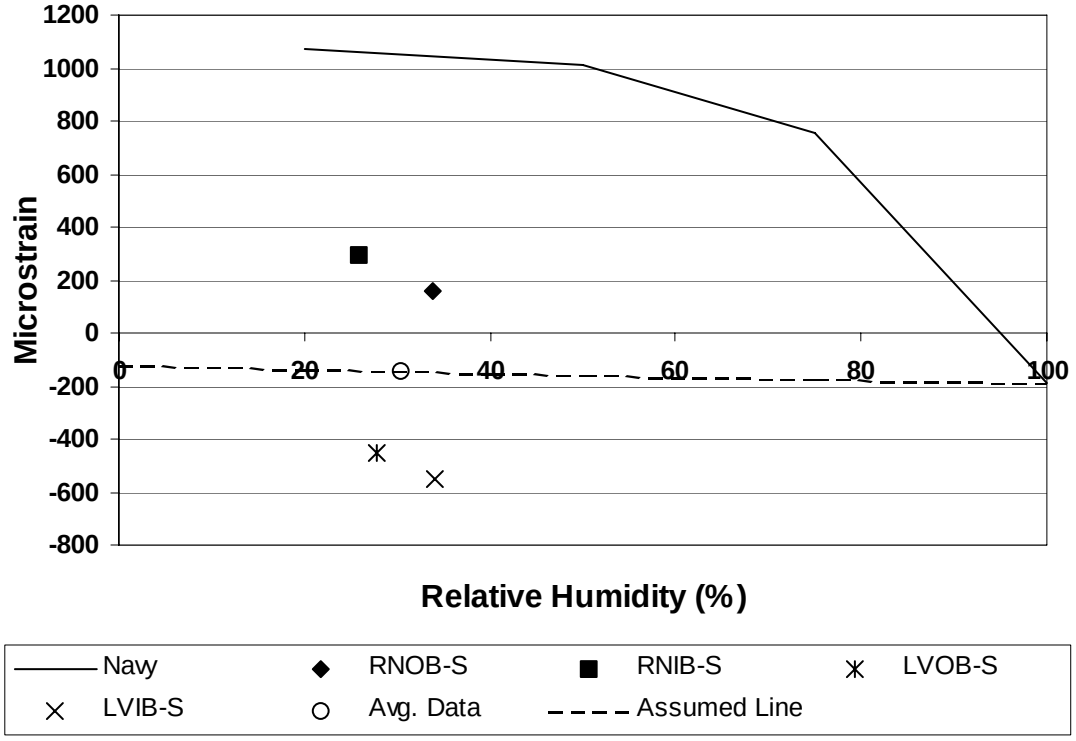

Figure 4.12 – Navy Shrinkage Data Comparison, Day 365

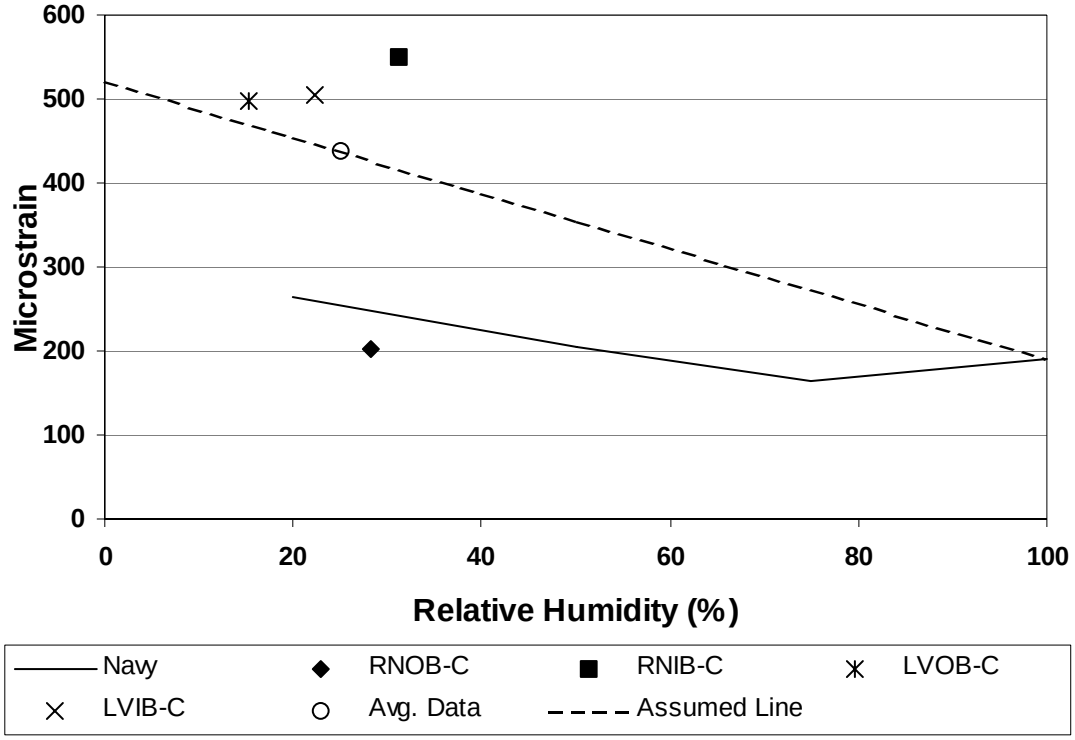

Figure 4.13 – Navy Creep Data Comparison, Day 1

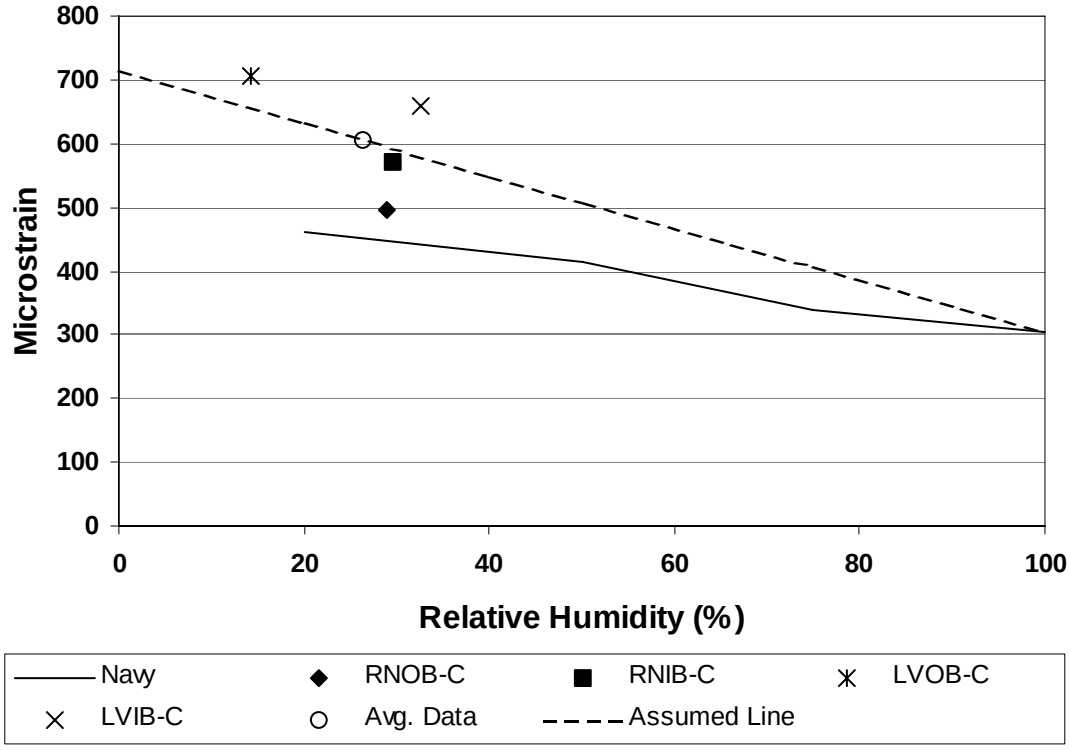

Figure 4.14 – Navy Creep Data Comparison, Day 7

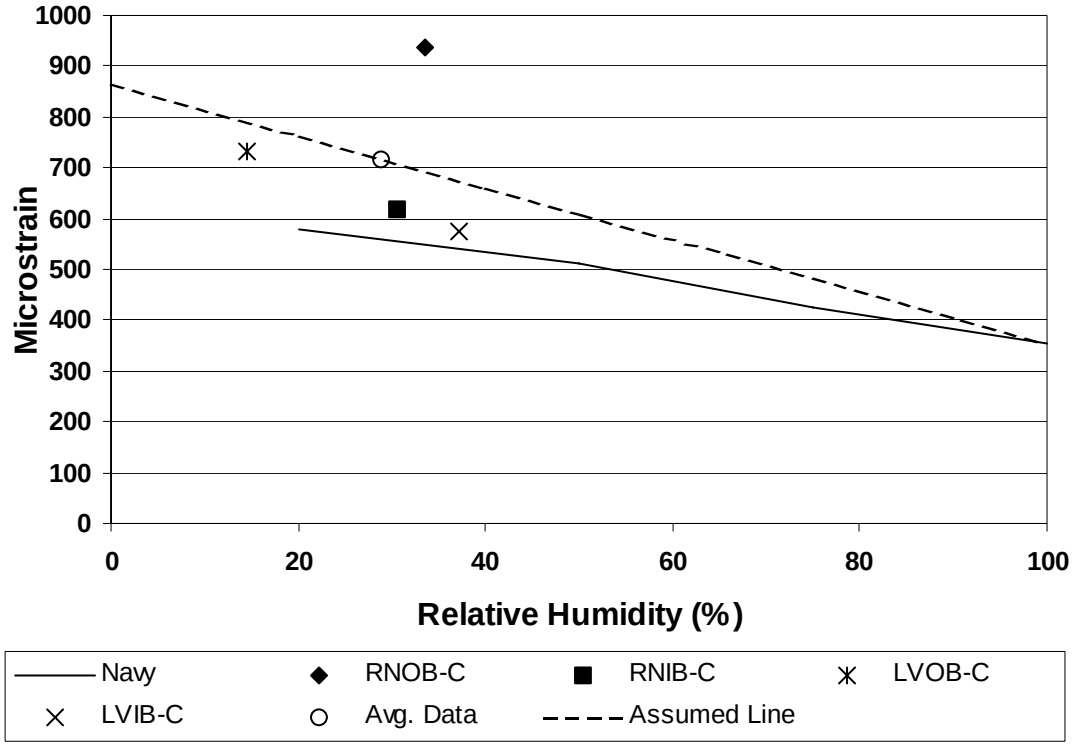

Figure 4.15 – Navy Creep Data Comparison, Day 14

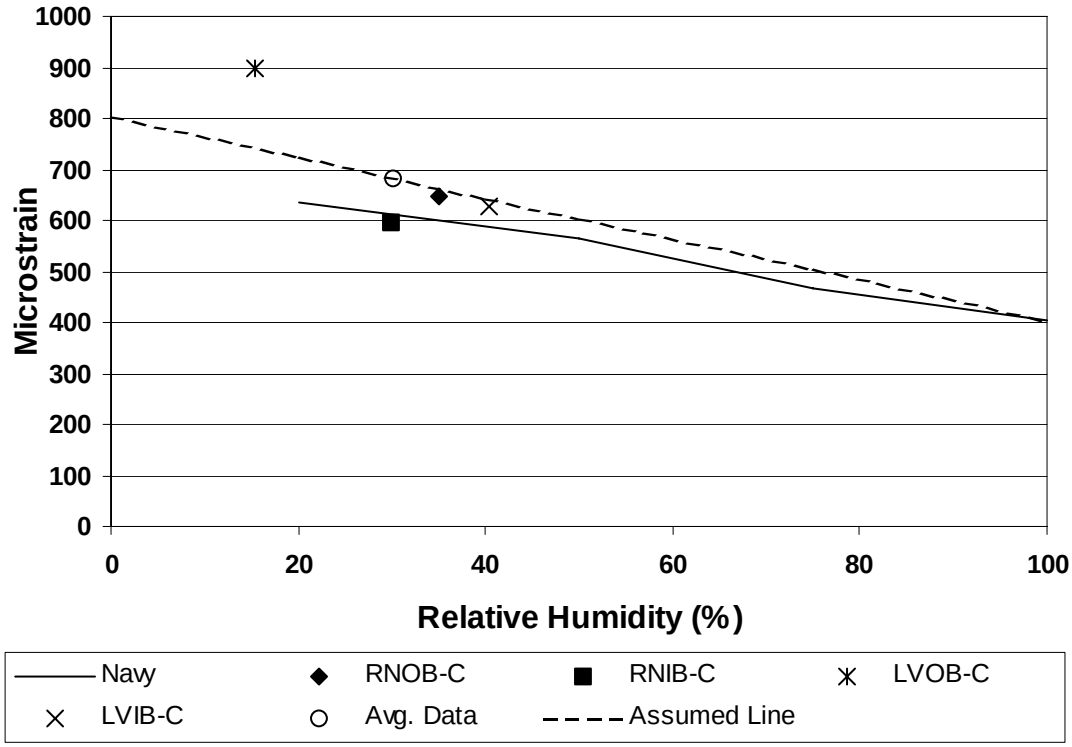

Figure 4.16 – Navy Creep Data Comparison, Day 21

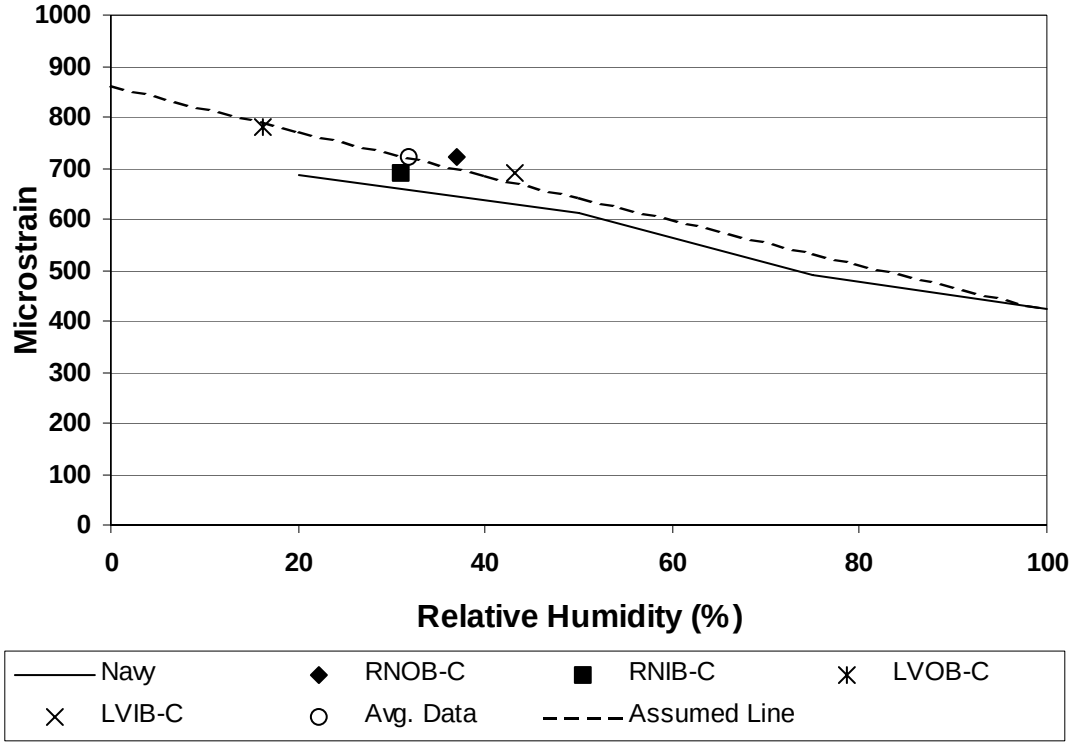

Figure 4.17 – Navy Creep Data Comparison, Day 28

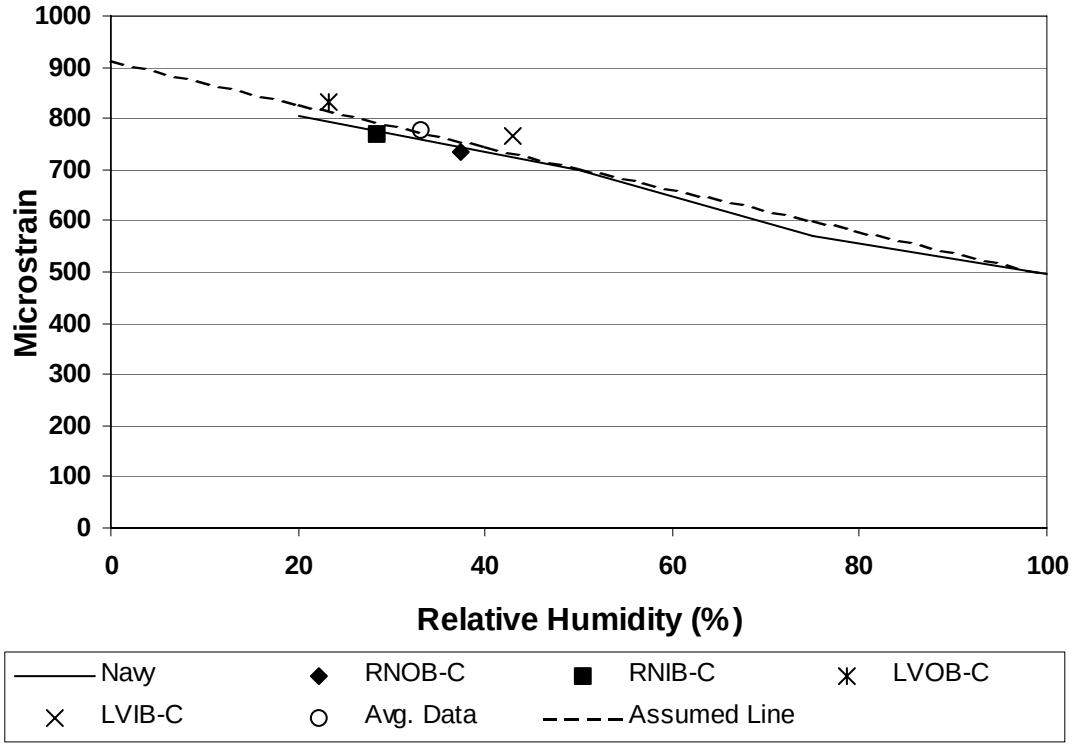

Figure 4.18 – Navy Creep Data Comparison, Day 56

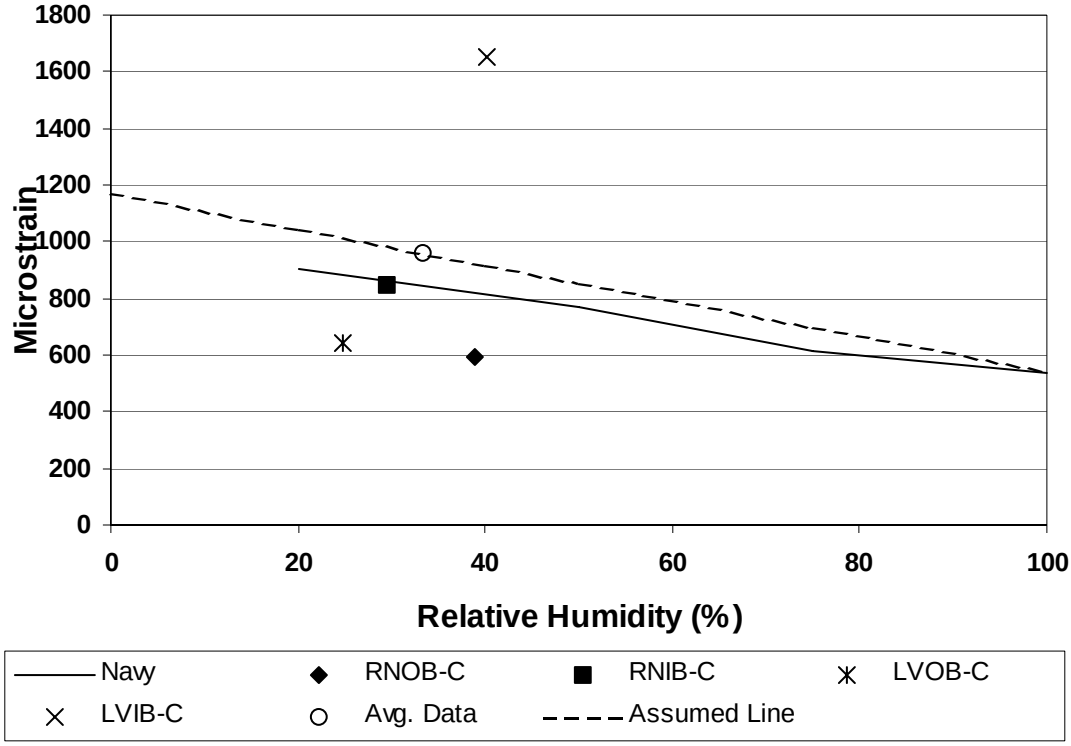

Figure 4.19 – Navy Creep Data Comparison, Day 91

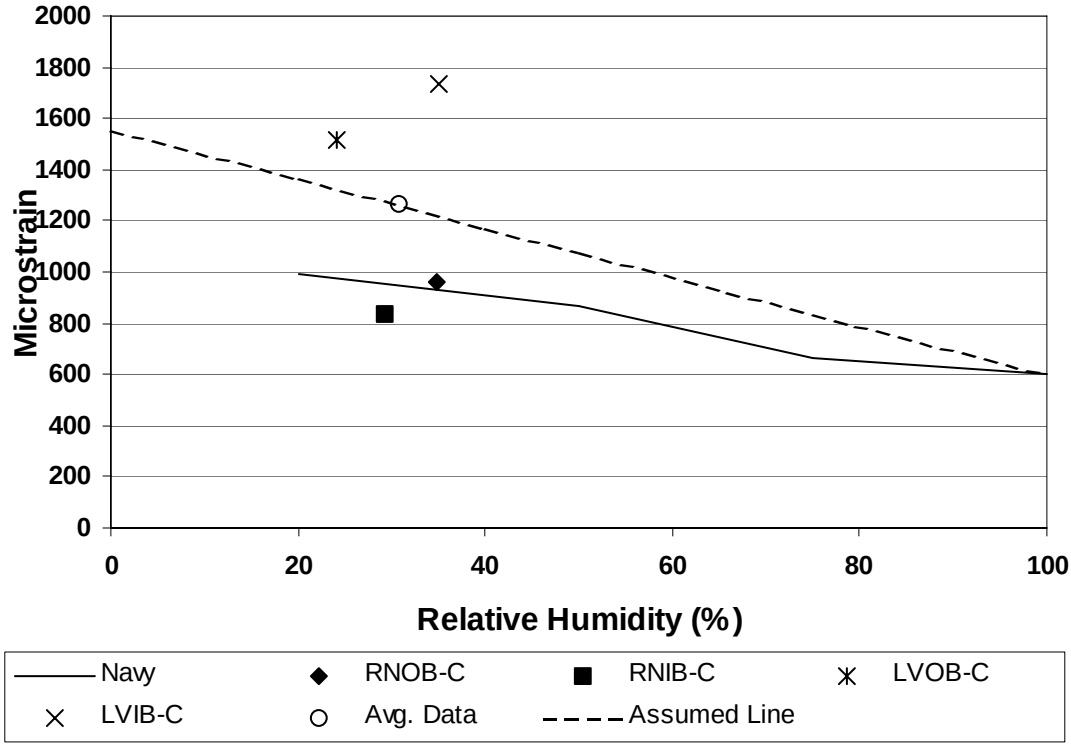

Figure 4.20 – Navy Creep Data Comparison, Day 175

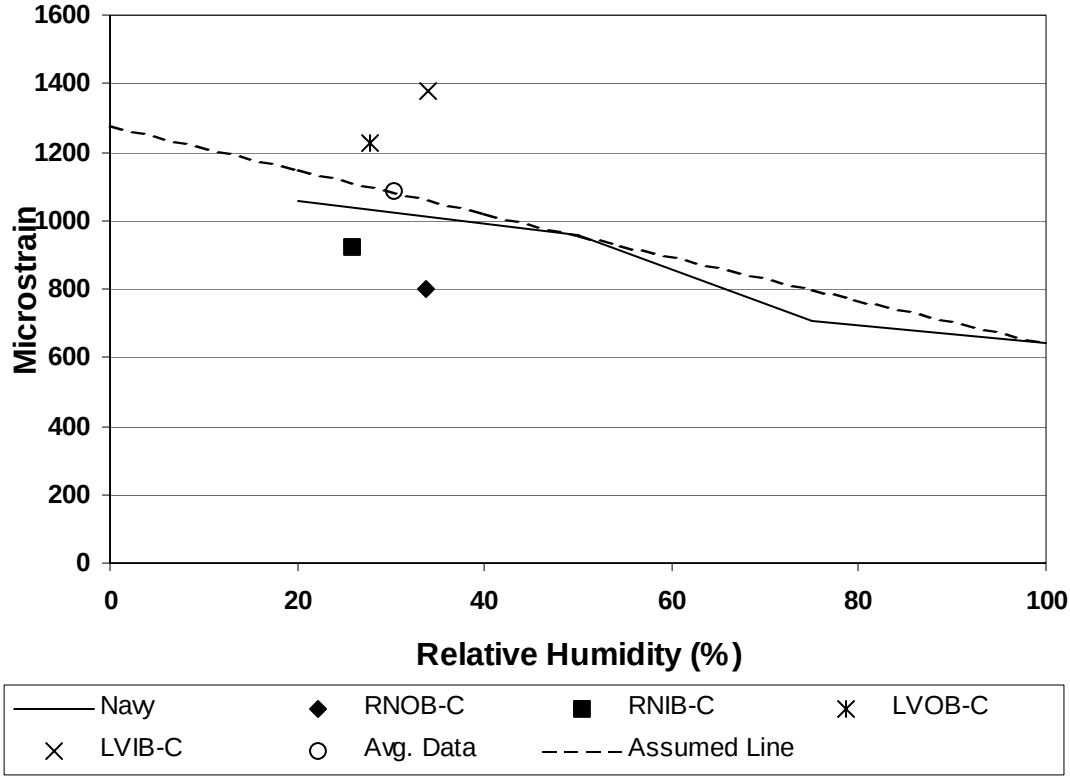

Figure 4.21 – Navy Creep Data Comparison, Day 365

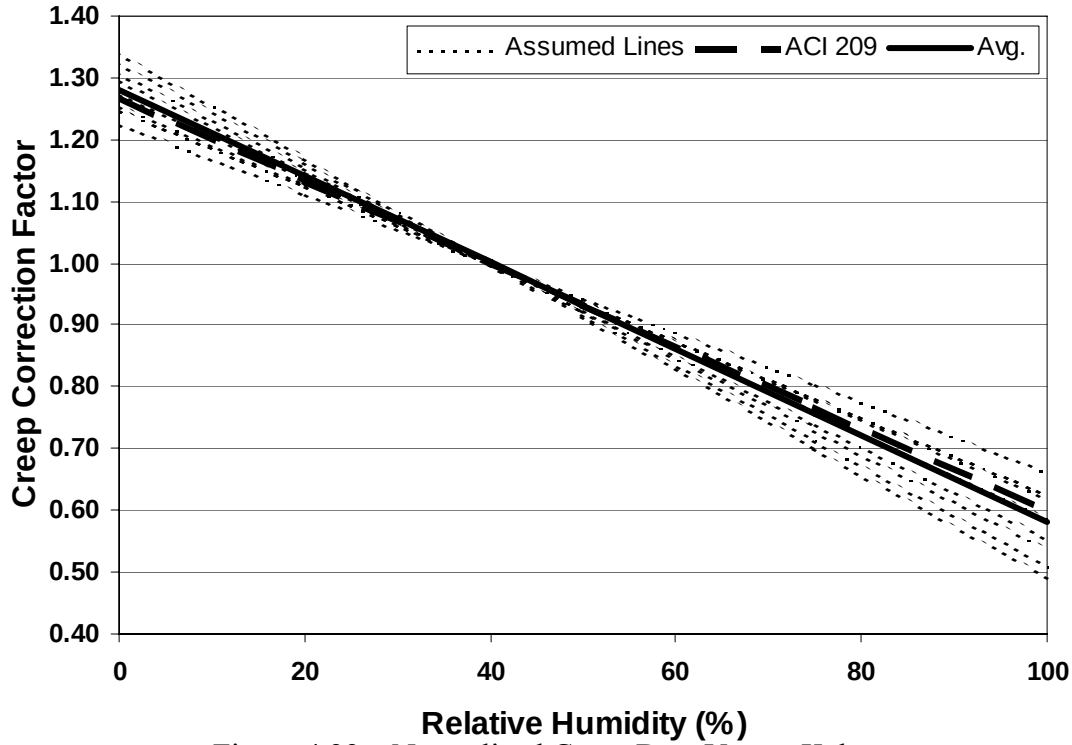

Figure 4.22 – Normalized Creep Data Versus Kch

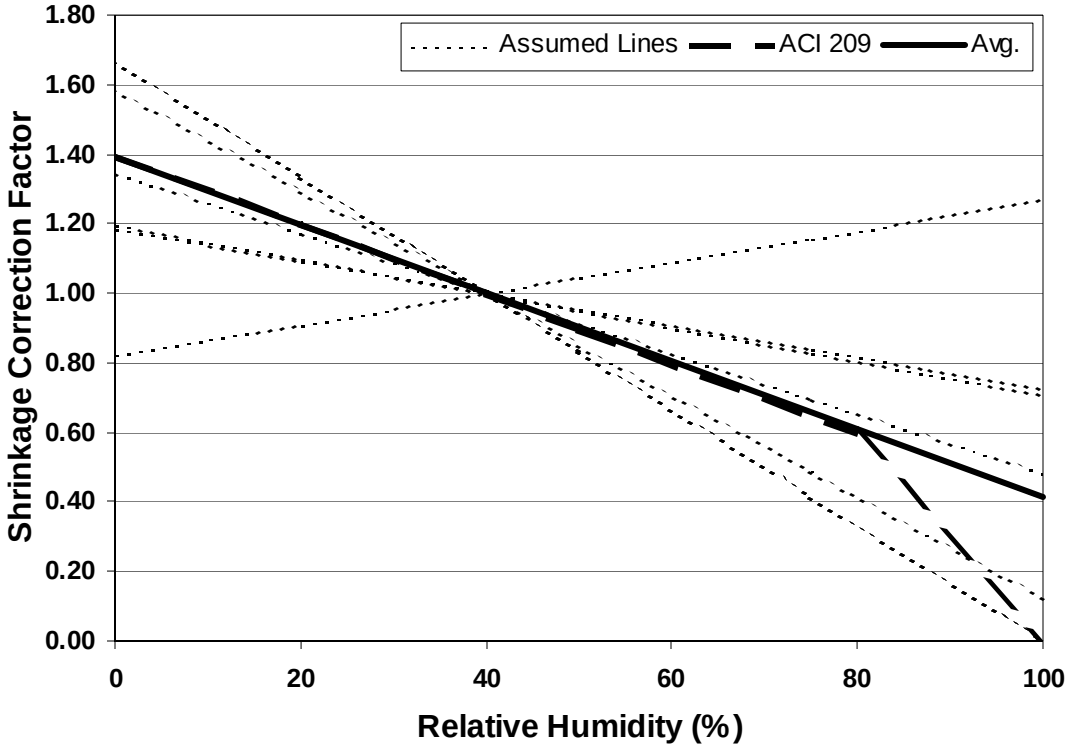

Figure 4.23 – Normalized Shrinkage Data Versus Ksh

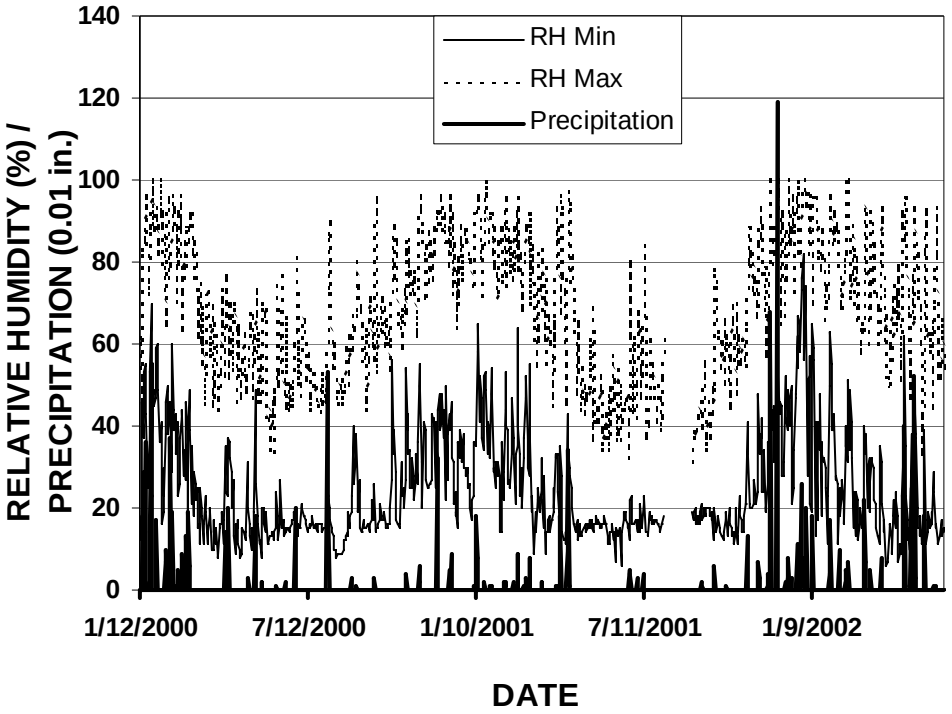

Figure 5.1 – Daily Climate Data Taken at the Reno Airport Throughout the Study

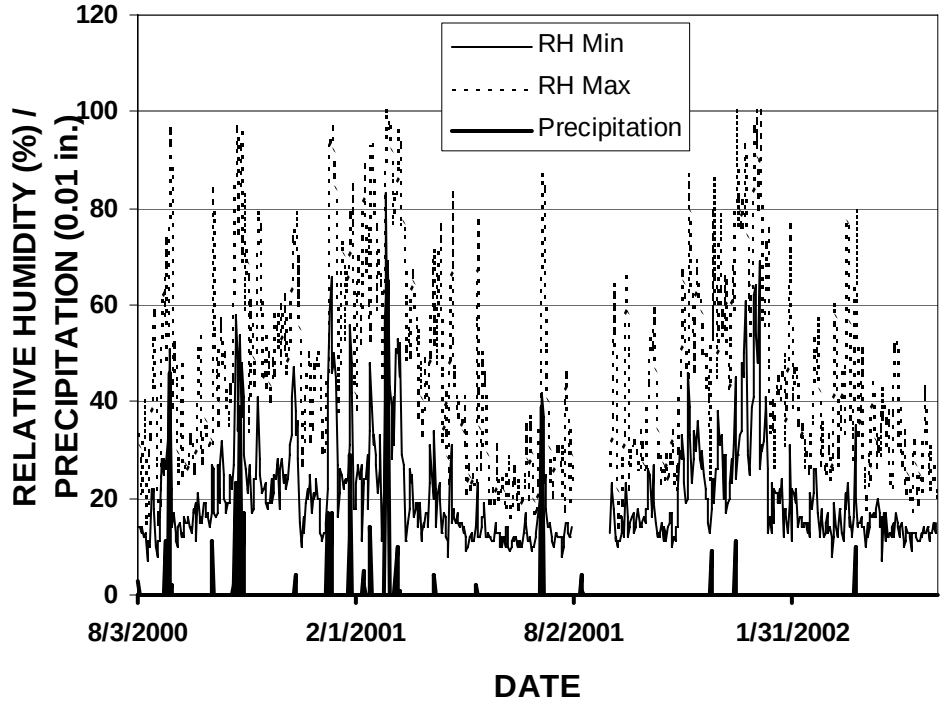

Figure 5.2 – Daily Climate Data Taken at the Las Vegas Airport Throughout the Study

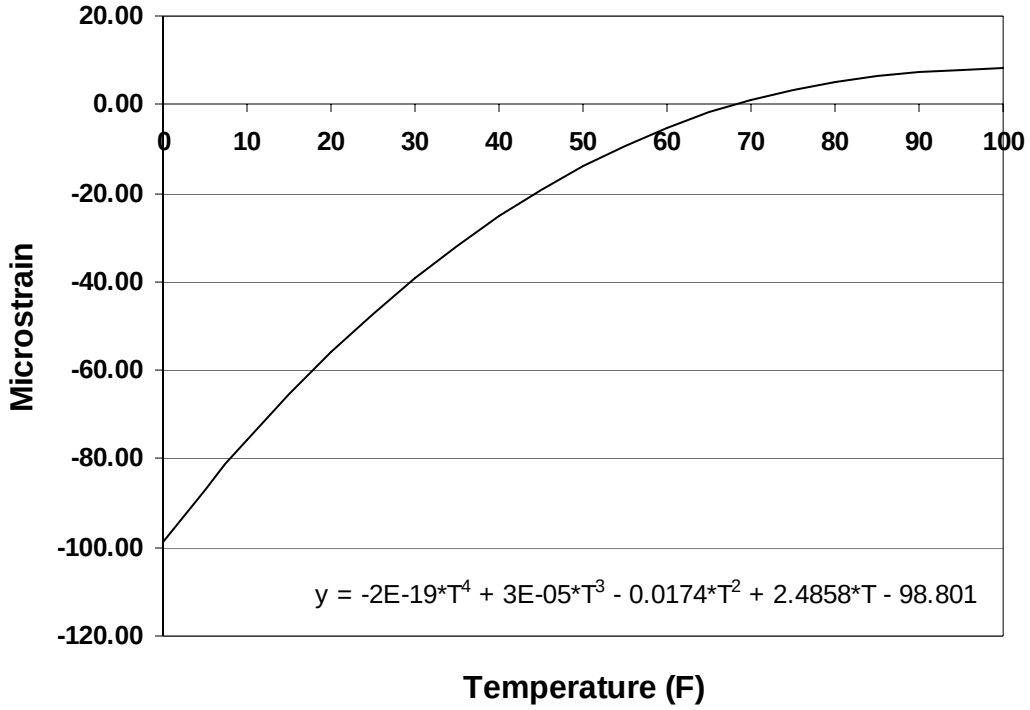

Figure 5.3 – Apparent Thermal Strain for TML Strain Gages

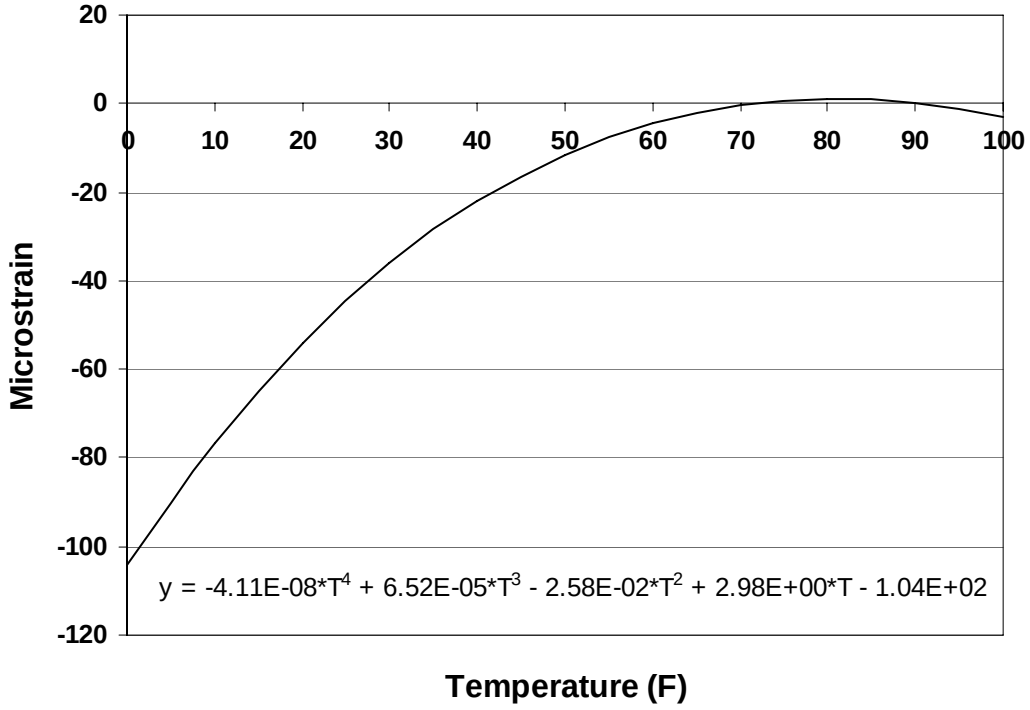

Figure 5.4 – Apparent Thermal Strain for Micro Measurements Strain Gages

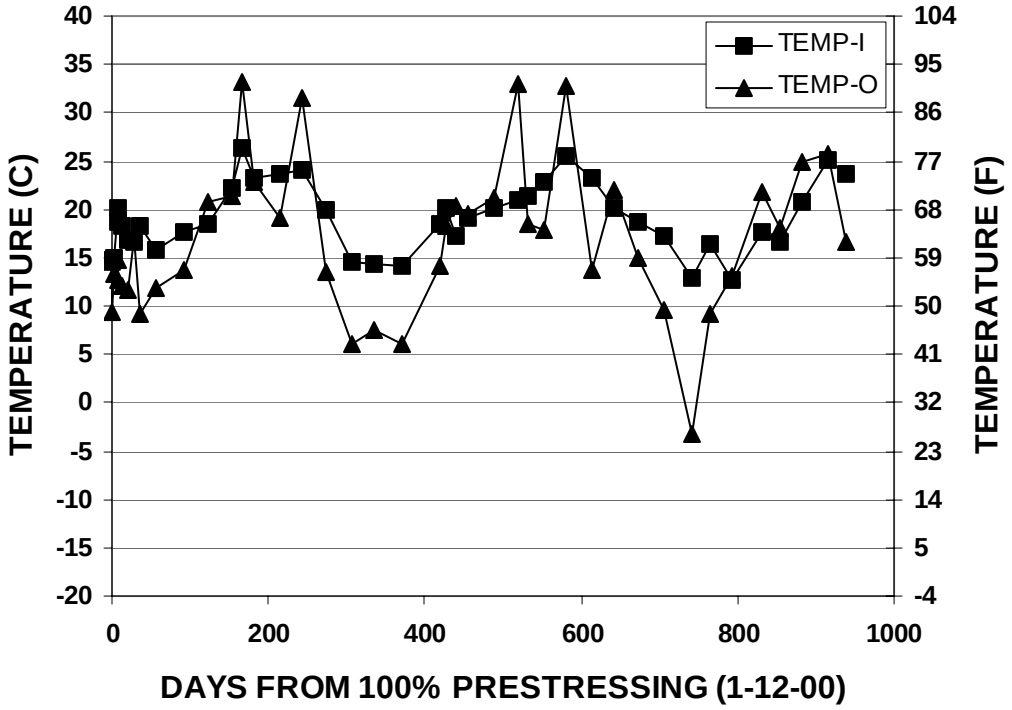

Figure 5.5 – Temperature Readings for the Reno Box Girder Specimens

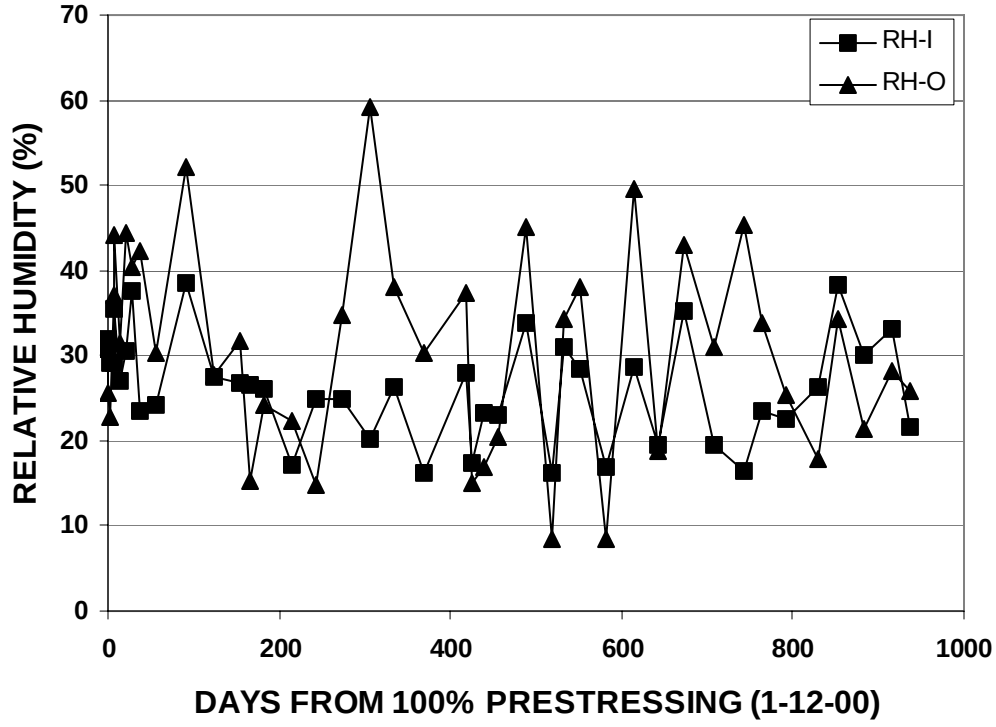

Figure 5.6 – Relative Humidity Readings for the Reno Box Girder Specimens

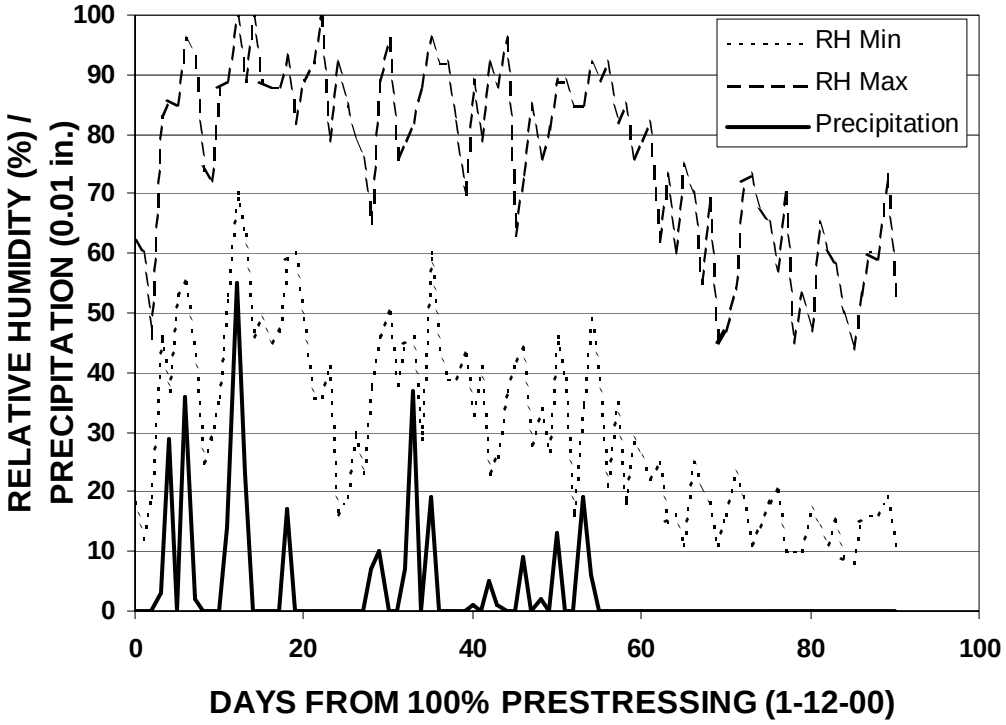

Figure 5.7 – Climate Data from the Reno Airport for the Three Months Following Tensioning of the Box Girders

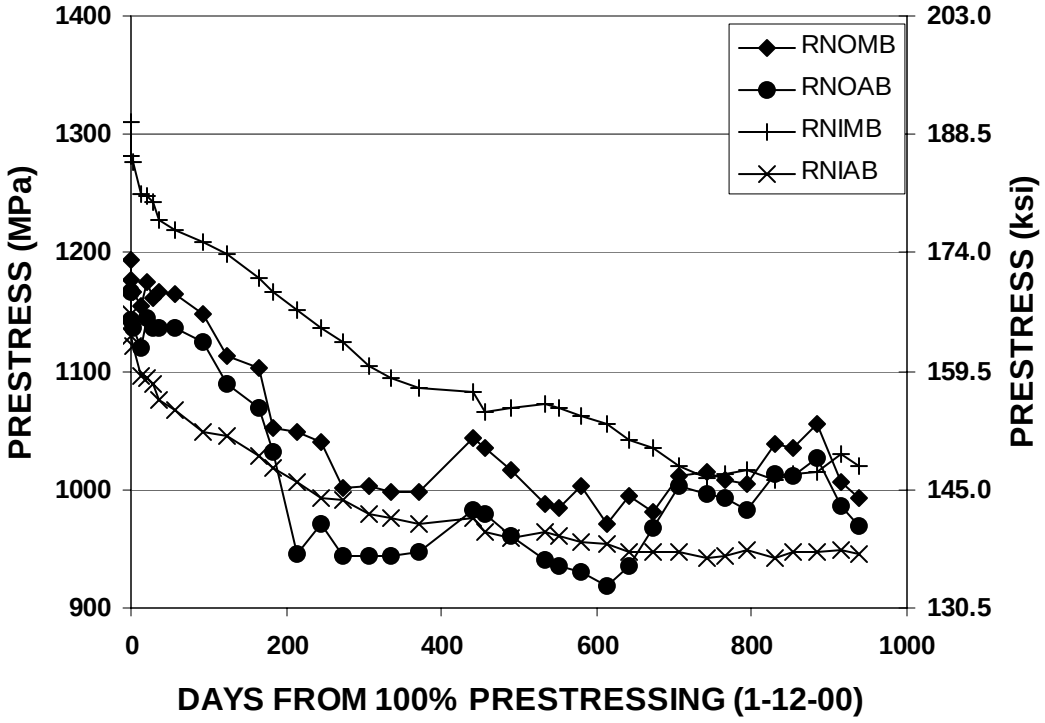

Figure 5.8 – Electric Gage Prestress Readings for the Reno Box Girders

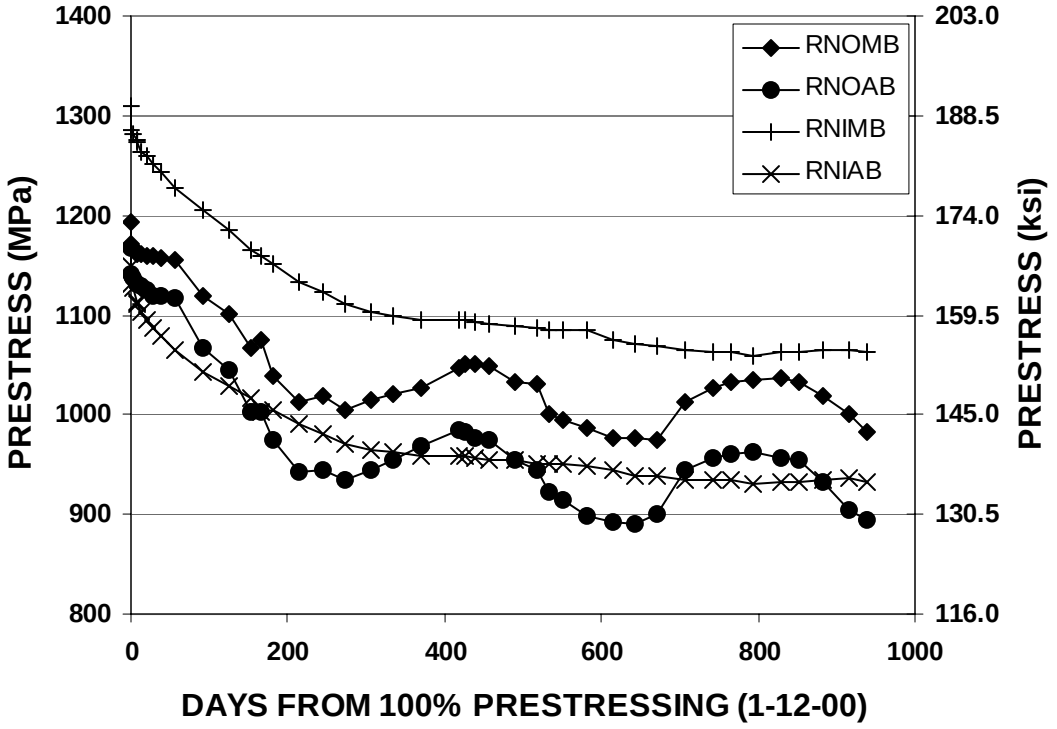

Figure 5.9 – Mechanical Gage Prestress Readings for the Reno Box Girders

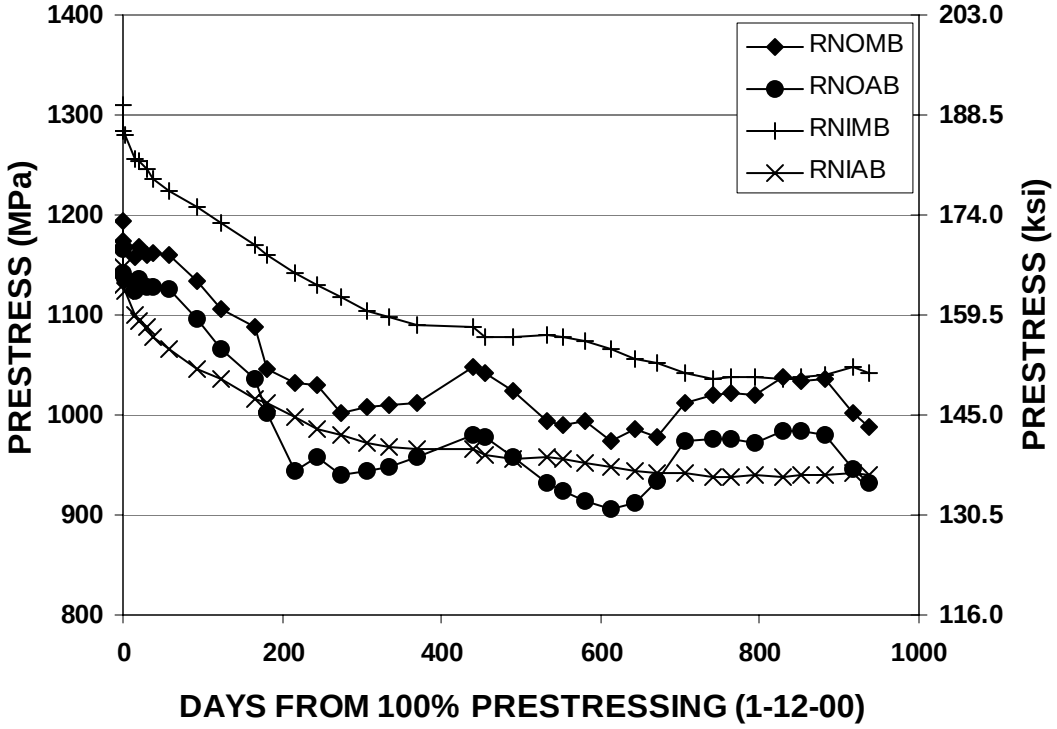

Figure 5.10 – Average Gage Readings for the Reno Box Girders

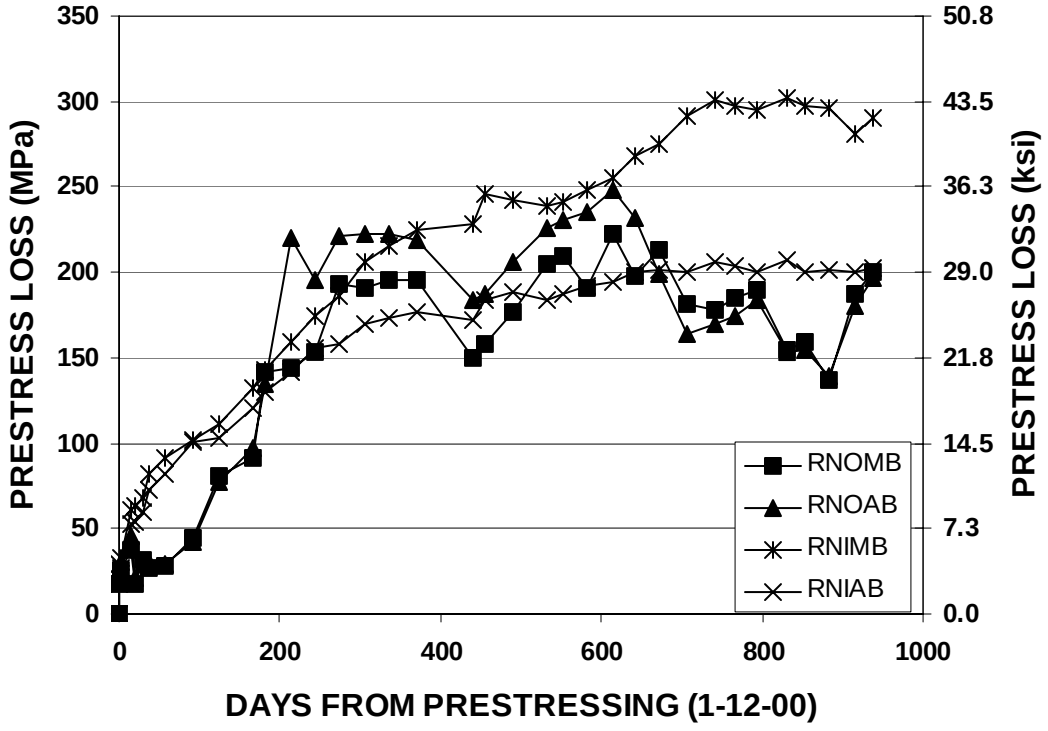

Figure 5.11 – Electric Gage Prestress Loss Readings for the Reno Box Girders

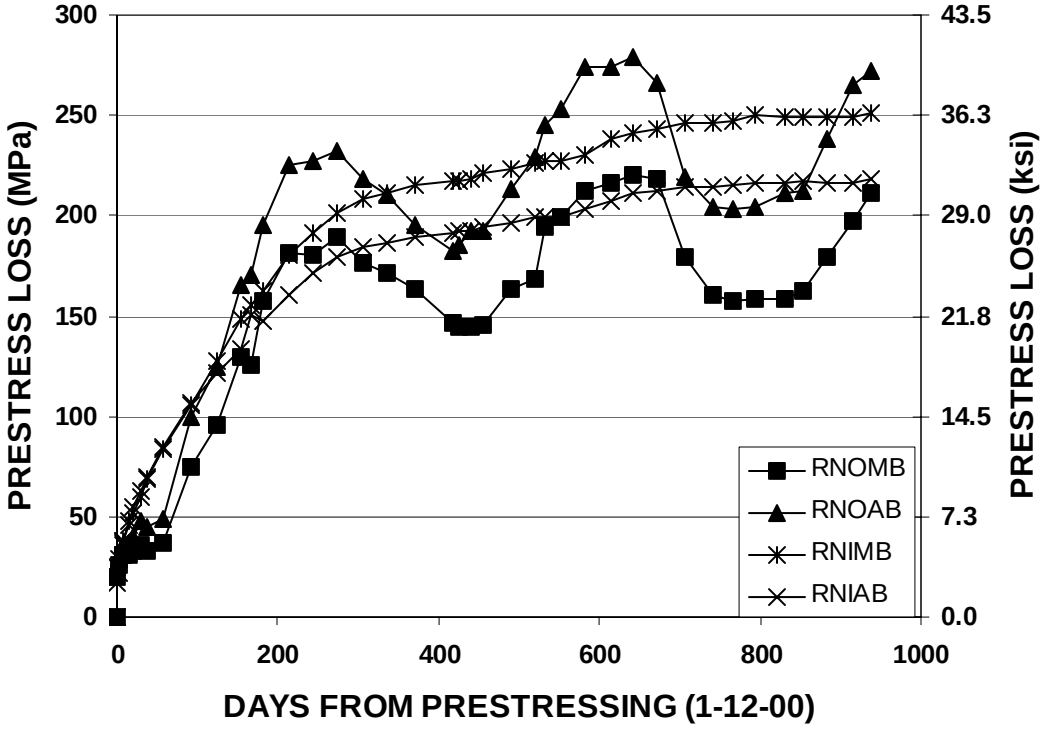

Figure 5.12 – Mechanical Gage Prestress Loss Readings for the Reno Box Girders

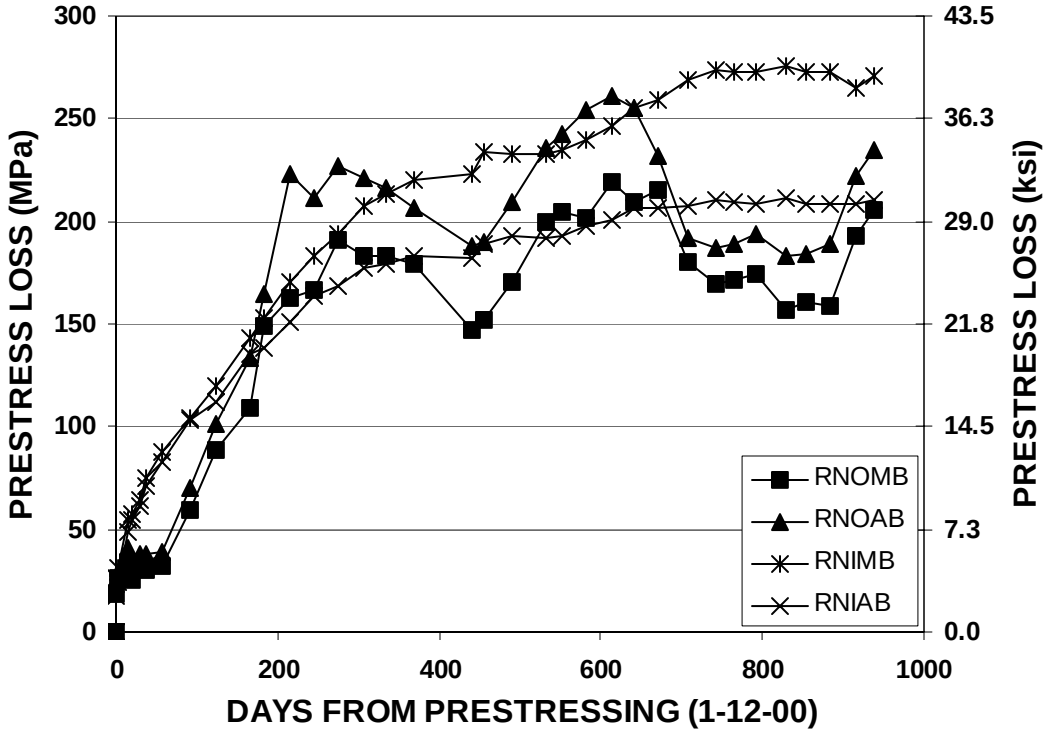

Figure 5.13 – Average Gage Prestress Loss Readings for the Reno Box Girders

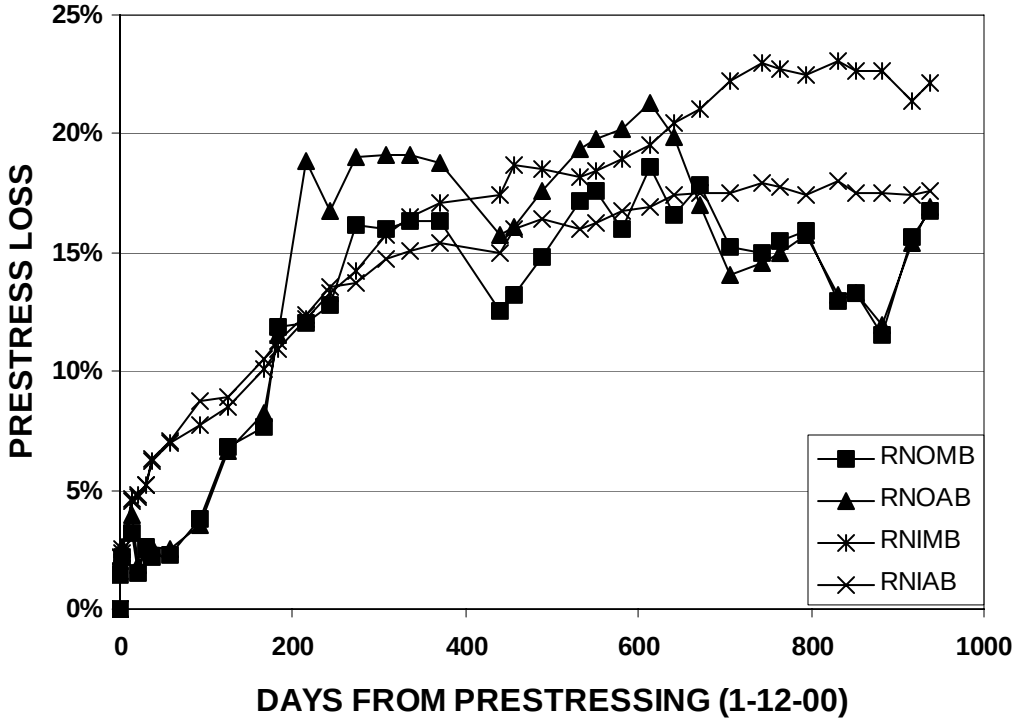

Figure 5.14 – Electric Gage Percentage Loss Readings for the Reno Box Girders

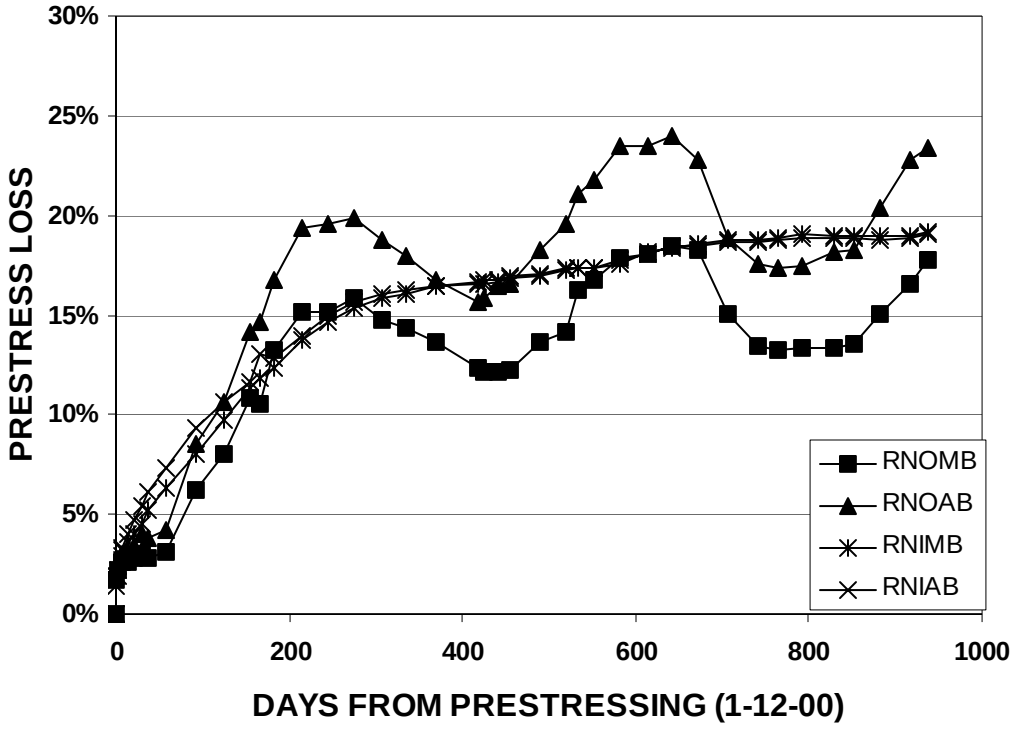

Figure 5.15 – Mechanical Gage Percentage Loss Readings for the Reno Box Girders

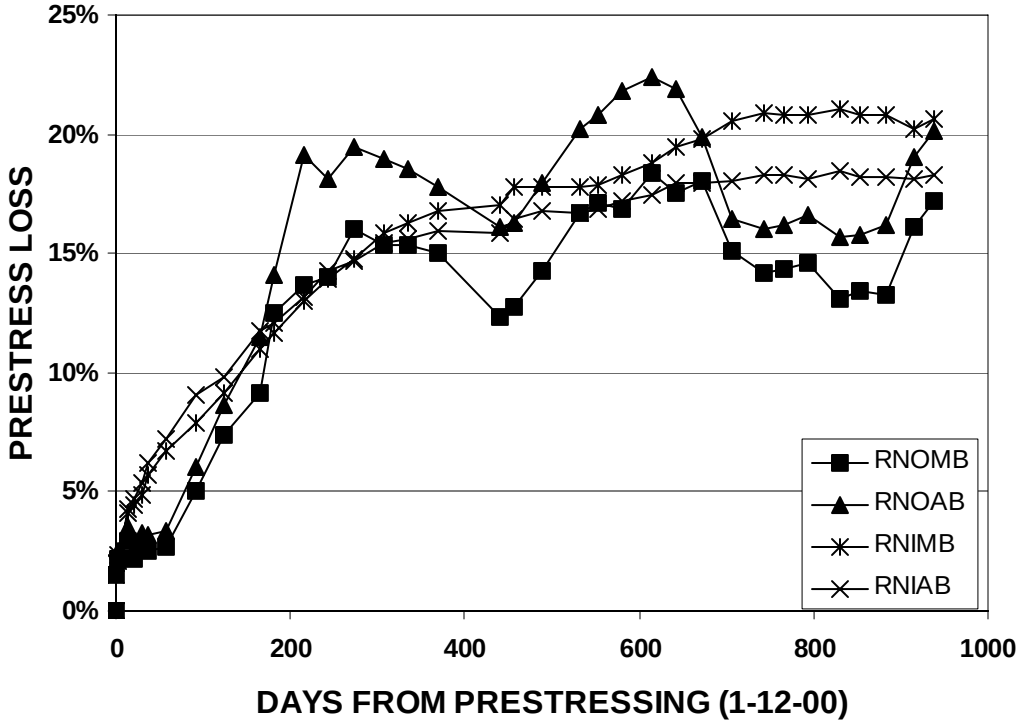

Figure 5.16 – Average Gage Percentage Loss Readings for the Reno Box Girders

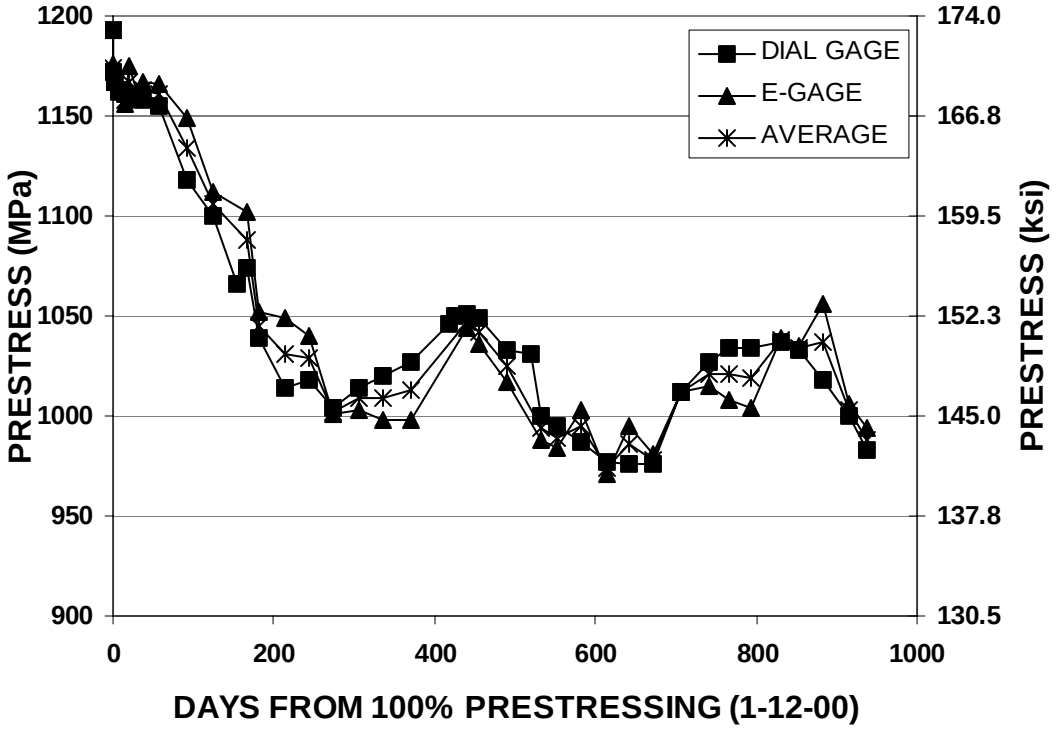

Figure 5.17 – RNOMB Gage Readings

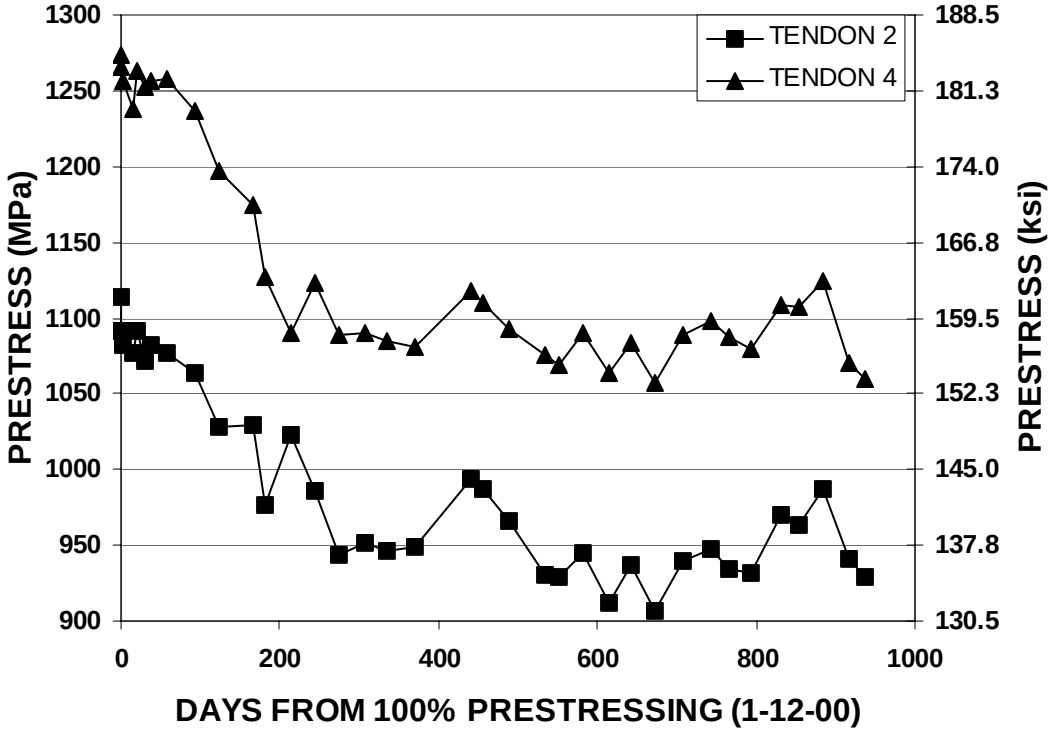

Figure 5.18 – RNOMB Electric Gage Readings Per Tendon

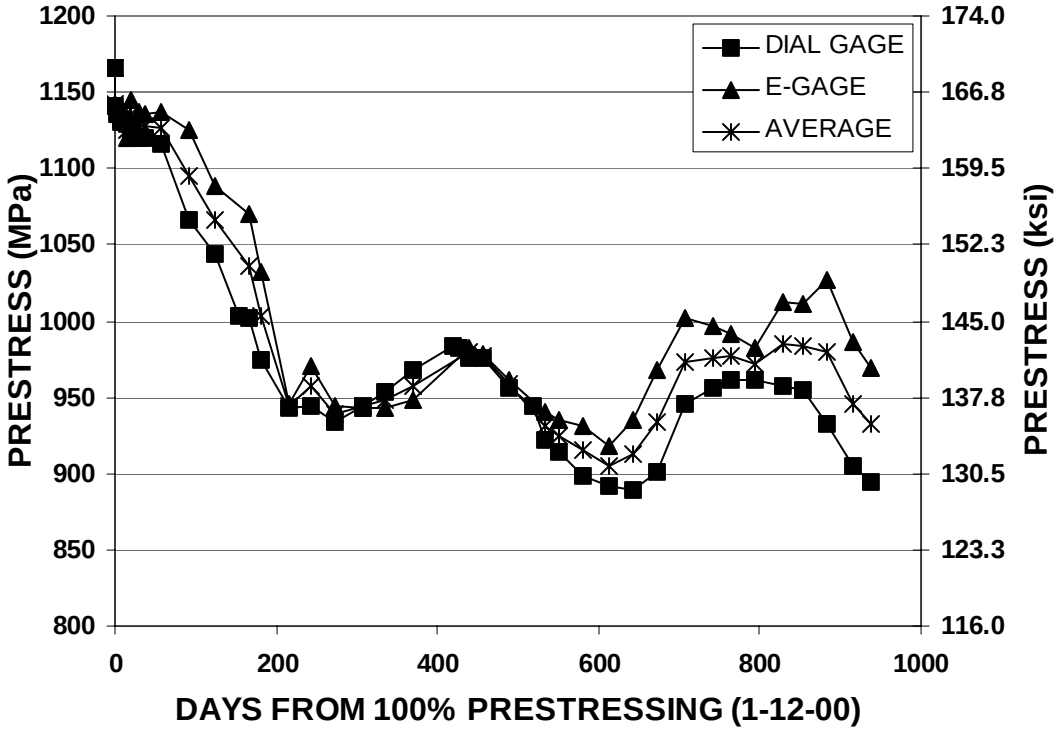

Figure 5.19 – RNOAB Gage Readings

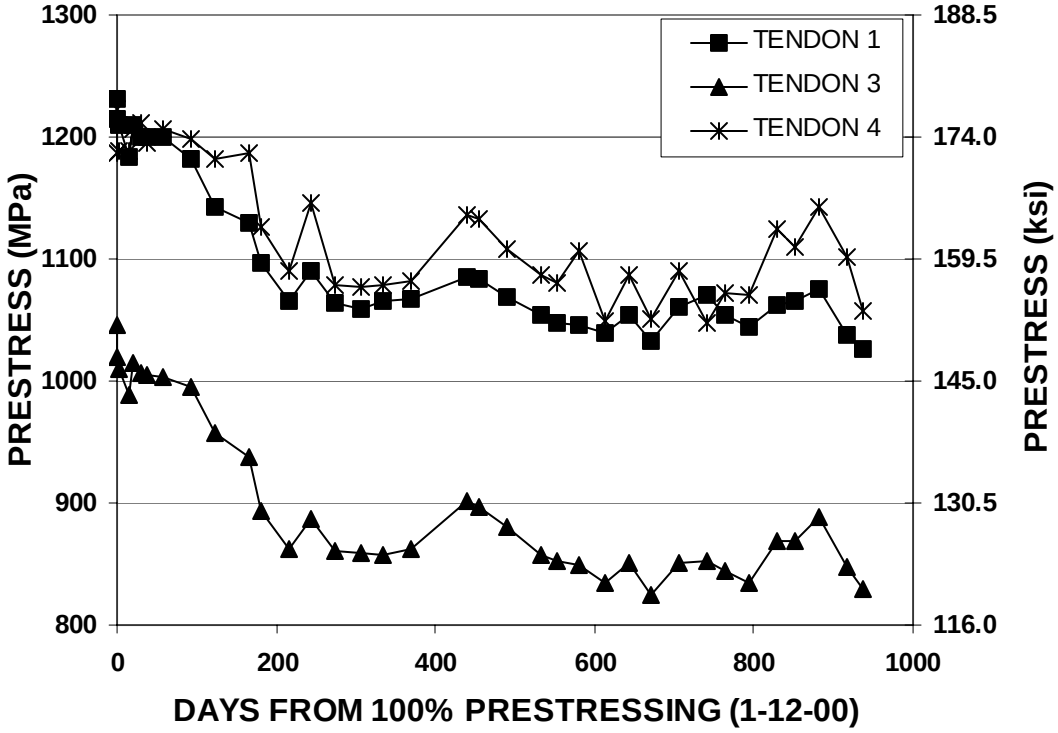

Figure 5.20 – RNOAB Electric Gage Readings Per Tendon

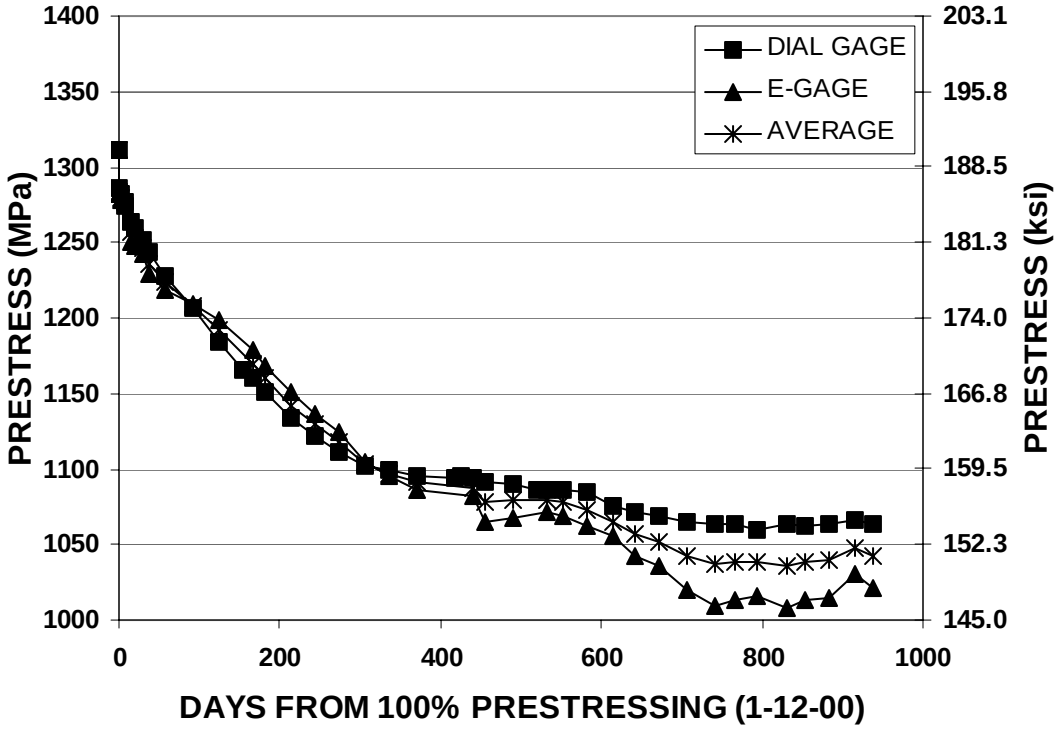

Figure 5.21 – RNIMB Gage Readings

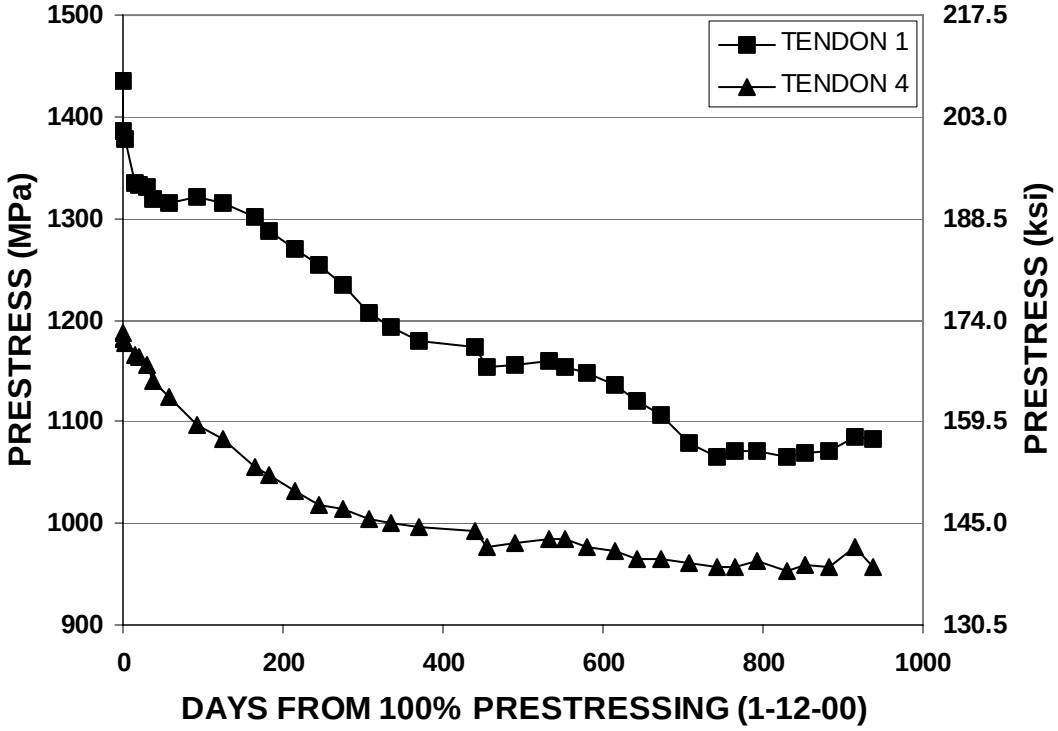

Figure 5.22 – RNIMB Electric Gage Readings Per Tendon

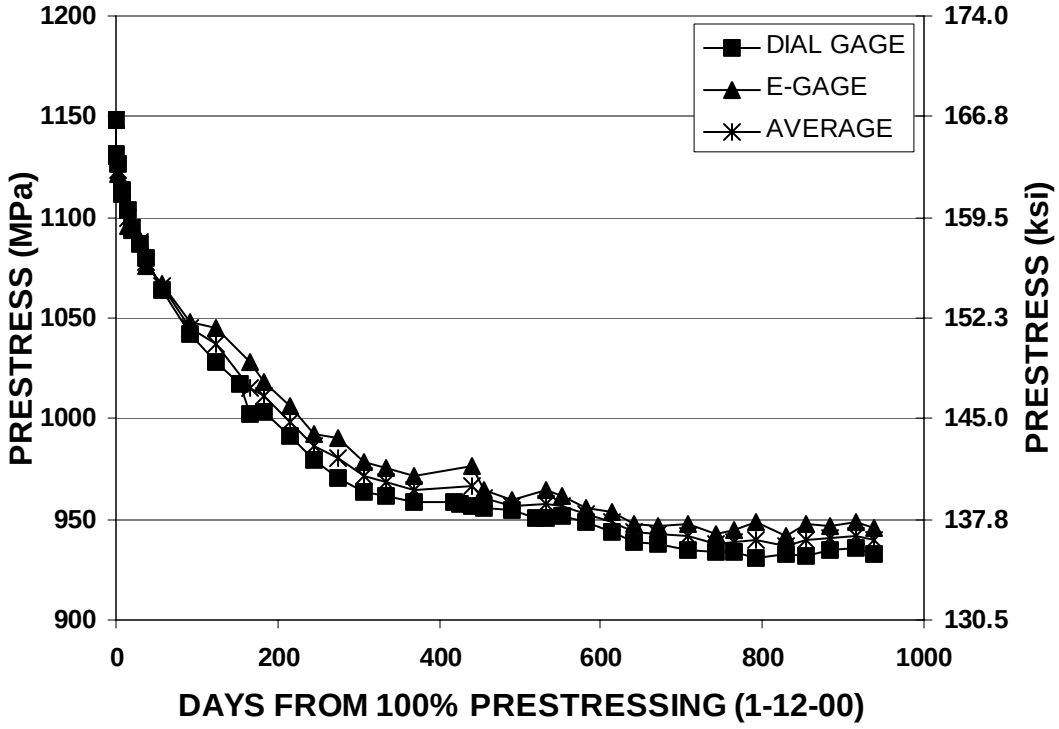

Figure 5.23 – RNIAB Gage Readings

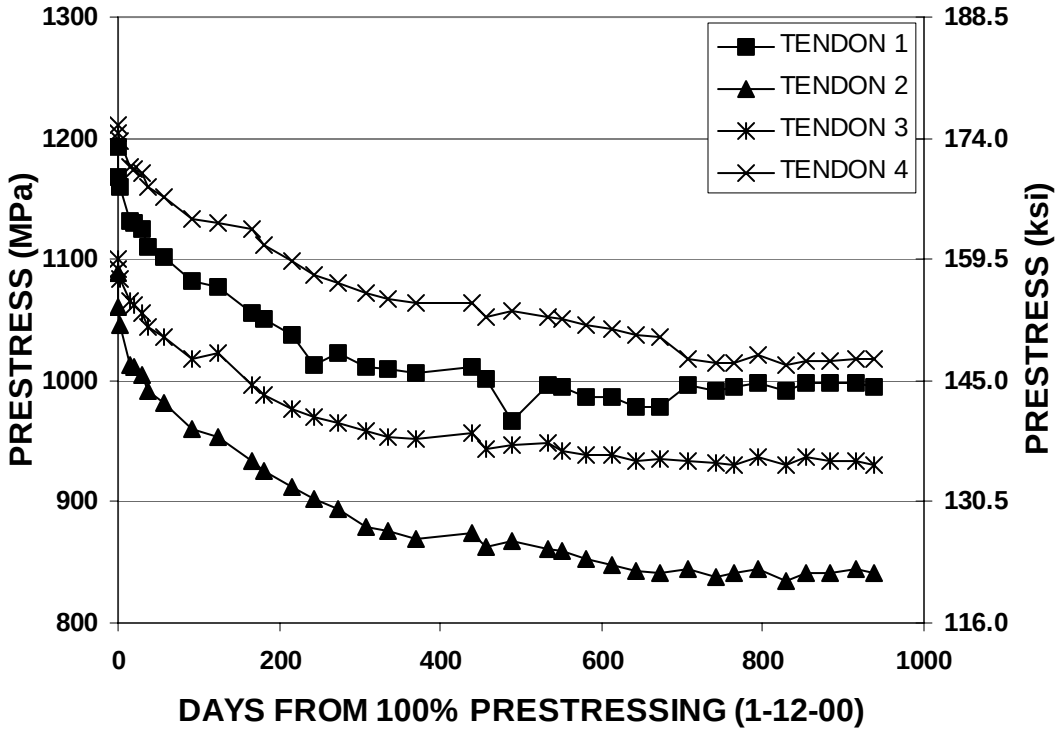

Figure 5.24 – RNIAB Electric Gage Readings Per Tendon

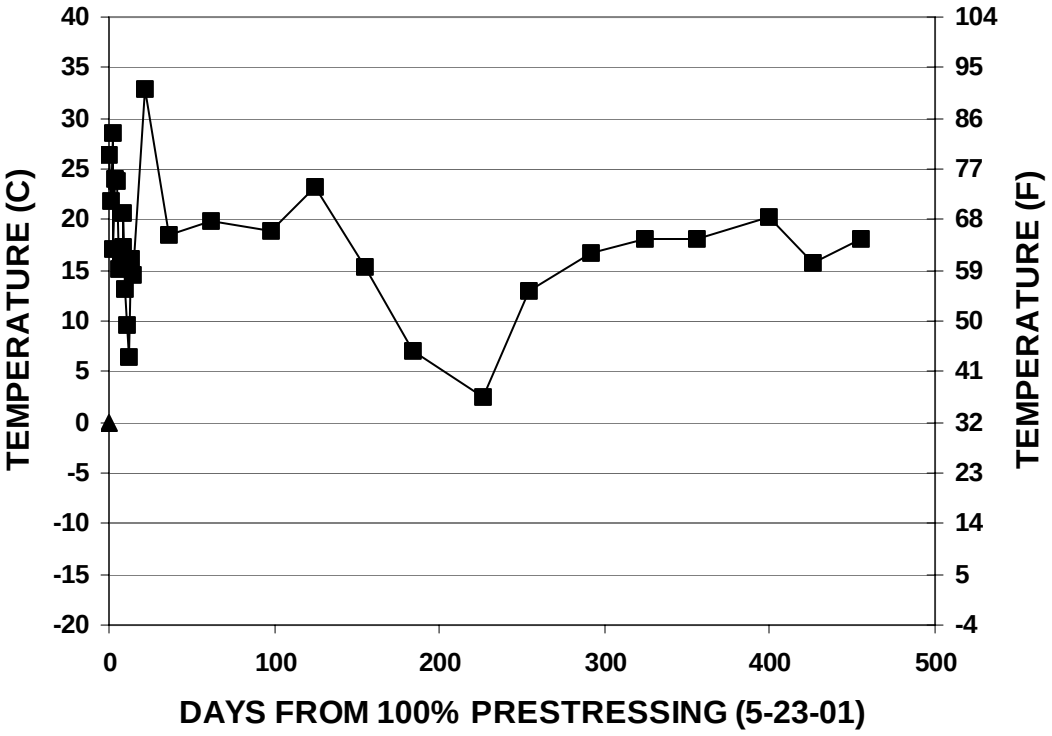

Figure 5.25 – Temperature Readings for the Reno Solid Beam Specimens

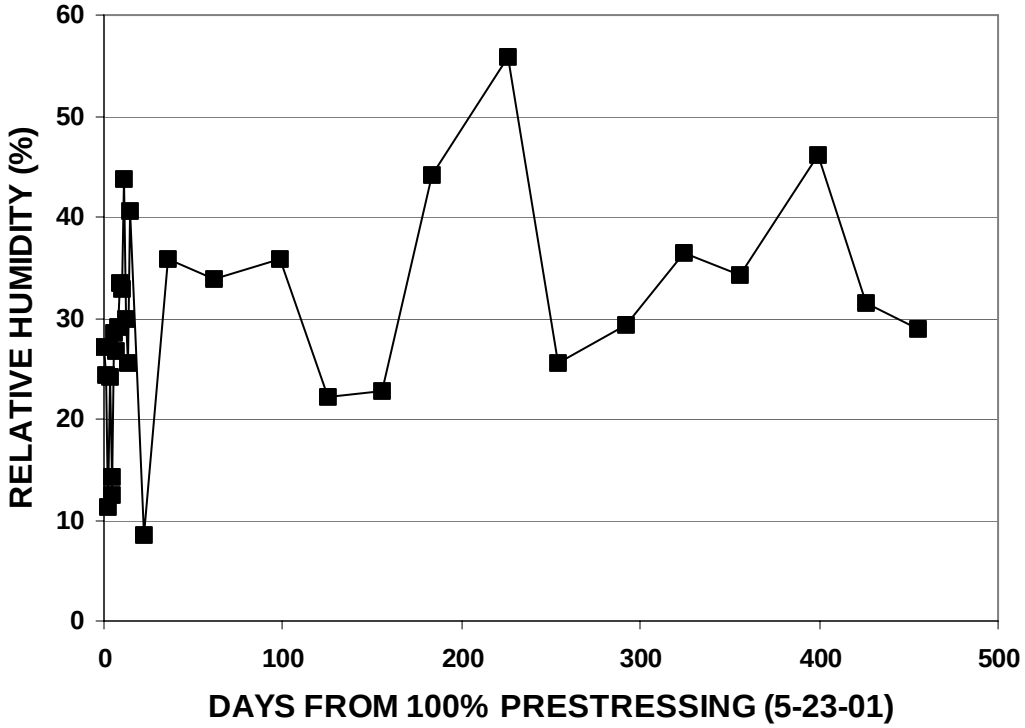

Figure 5.26 – Relative Humidity Readings for the Reno Solid Beam Specimens

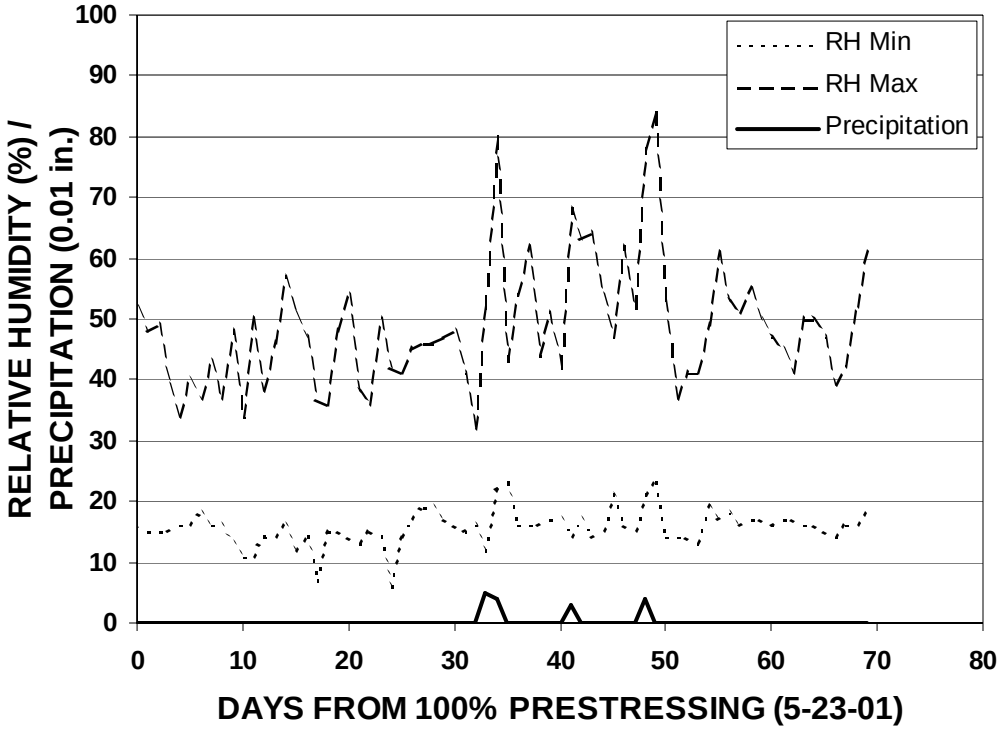

Figure 5.27 – Climate Data from the Reno Airport for the Three Months Following Tensioning of the Solid Beams

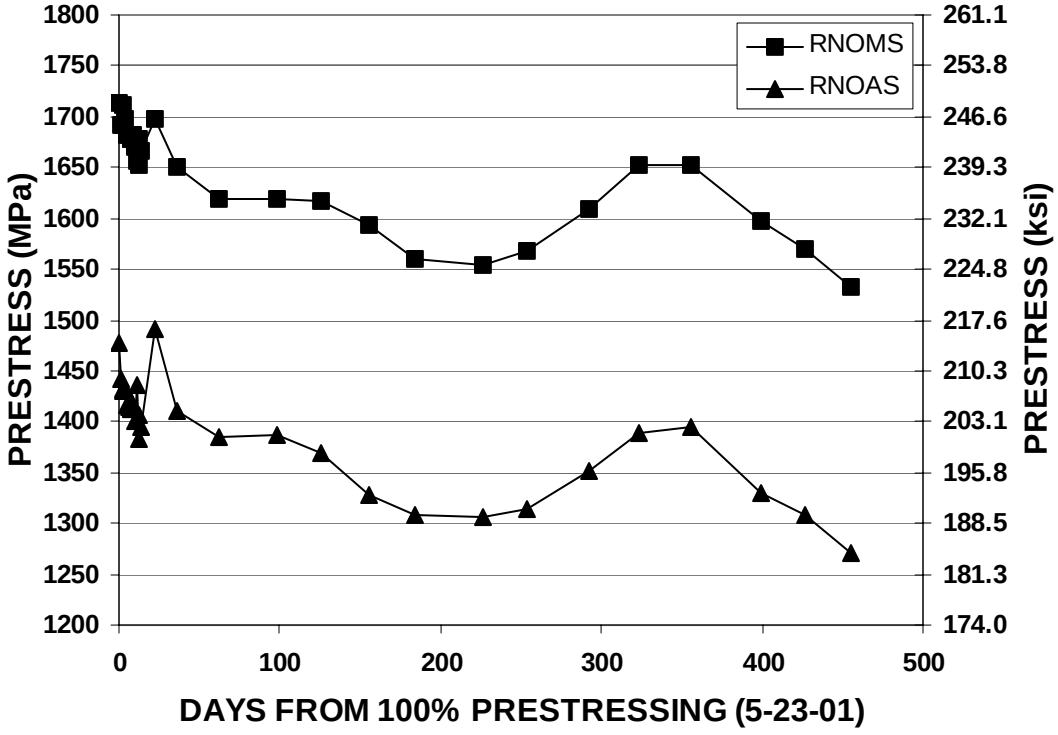

Figure 5.28 – Electric Gage Prestress Readings for the Reno Solid Beams

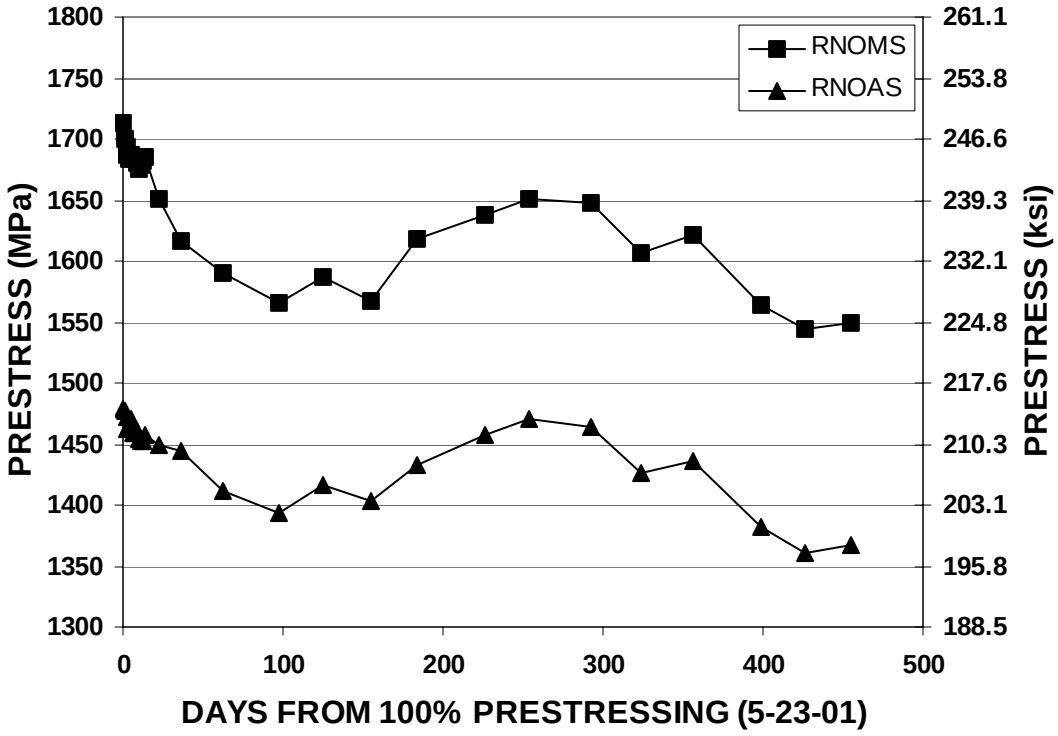

Figure 5.29 – Mechanical Gage Prestress Readings for the Reno Solid Beams

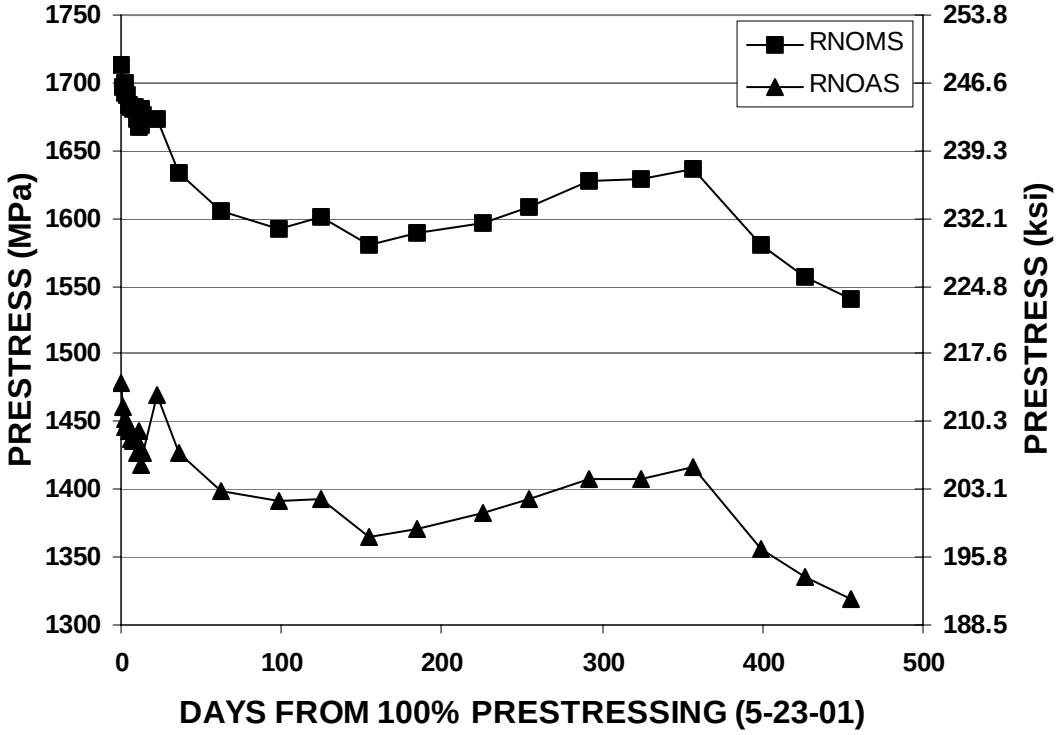

Figure 5.30 – Average Gage Readings for the Reno Solid Beams

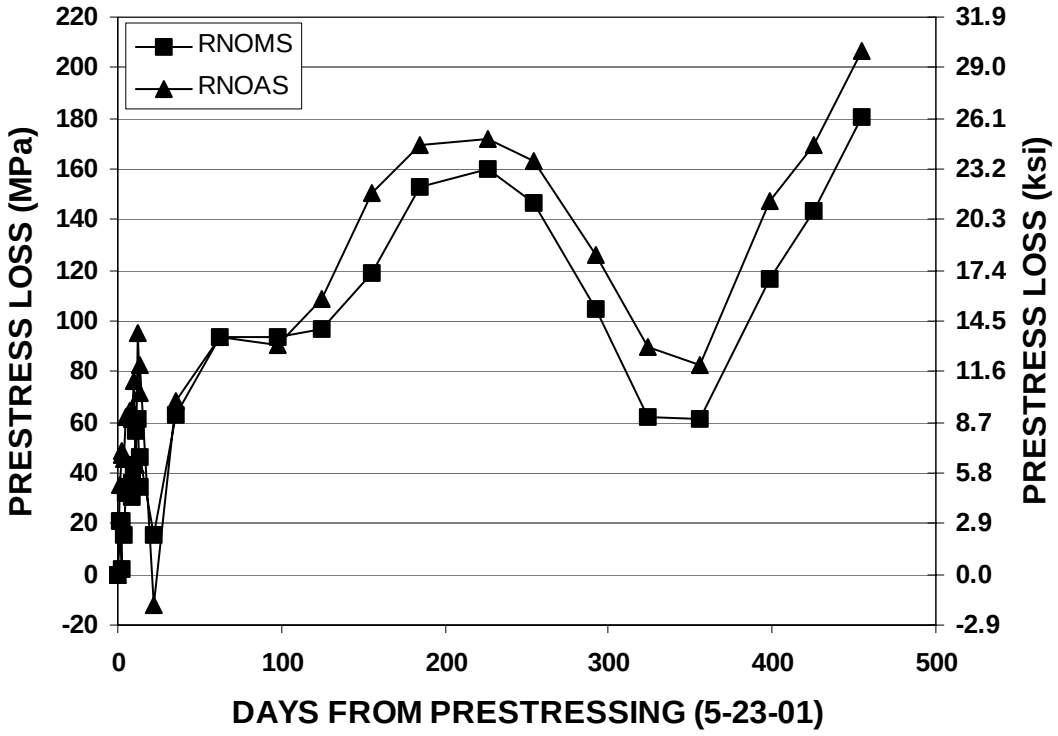

Figure 5.31 – Electric Gage Prestress Loss Readings for the Reno Solid Beams

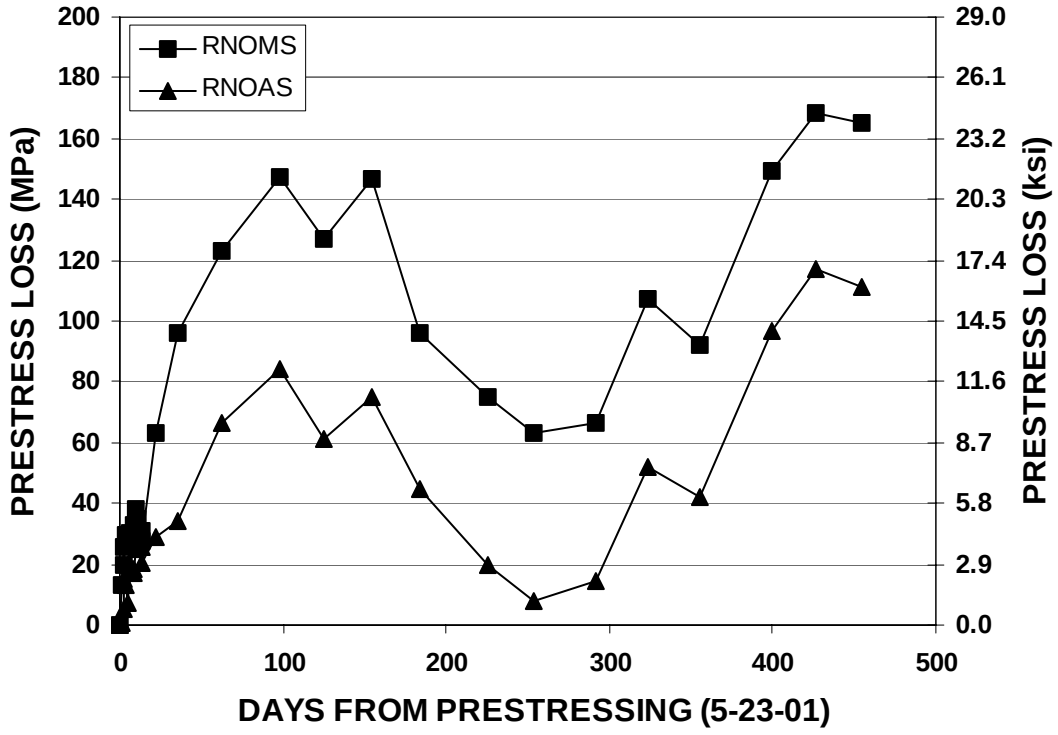

Figure 5.32 – Mechanical Gage Prestress Loss Readings for the Reno Solid Beams

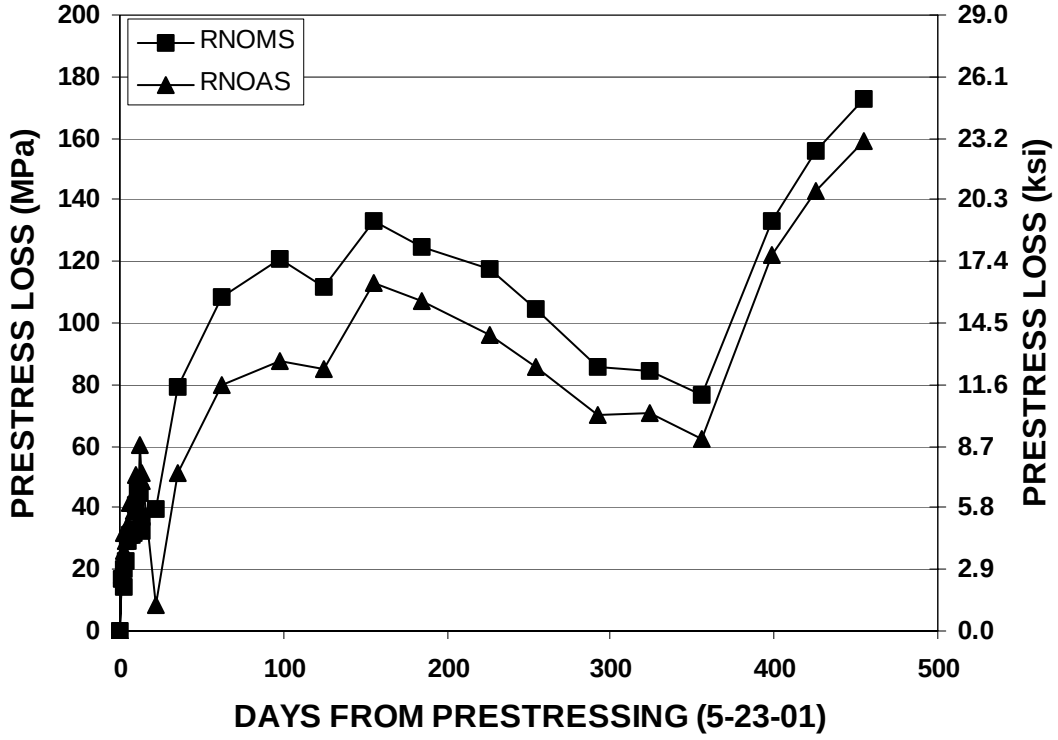

Figure 5.33 – Average Gage Prestress Loss Readings for the Reno Solid Beams

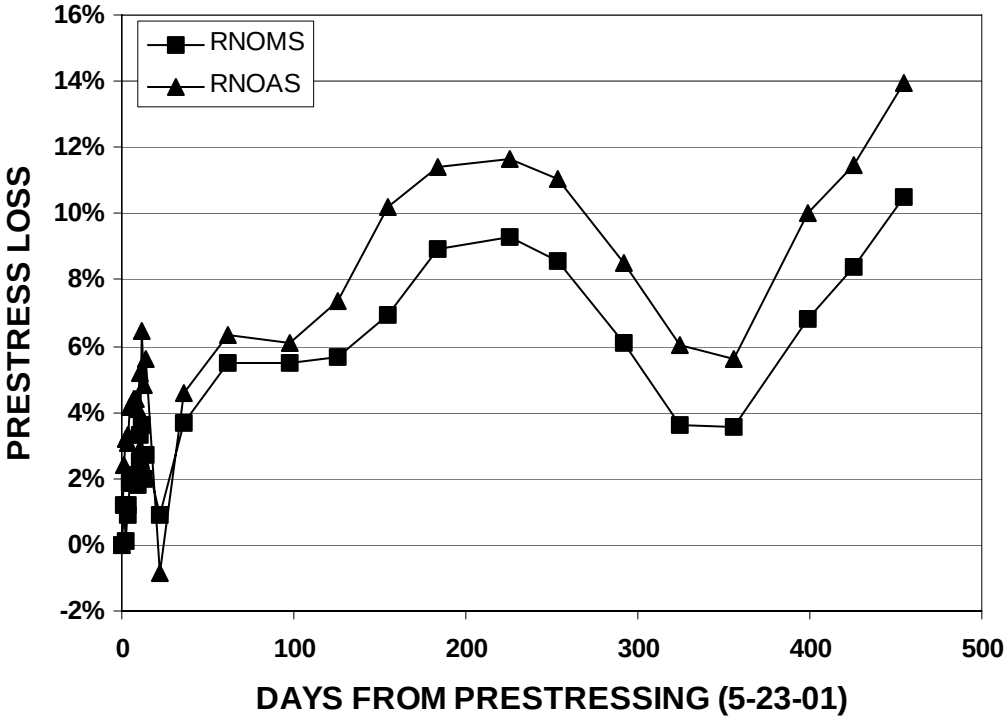

Figure 5.34 – Electric Gage Percentage Loss Readings for the Reno Solid Beams

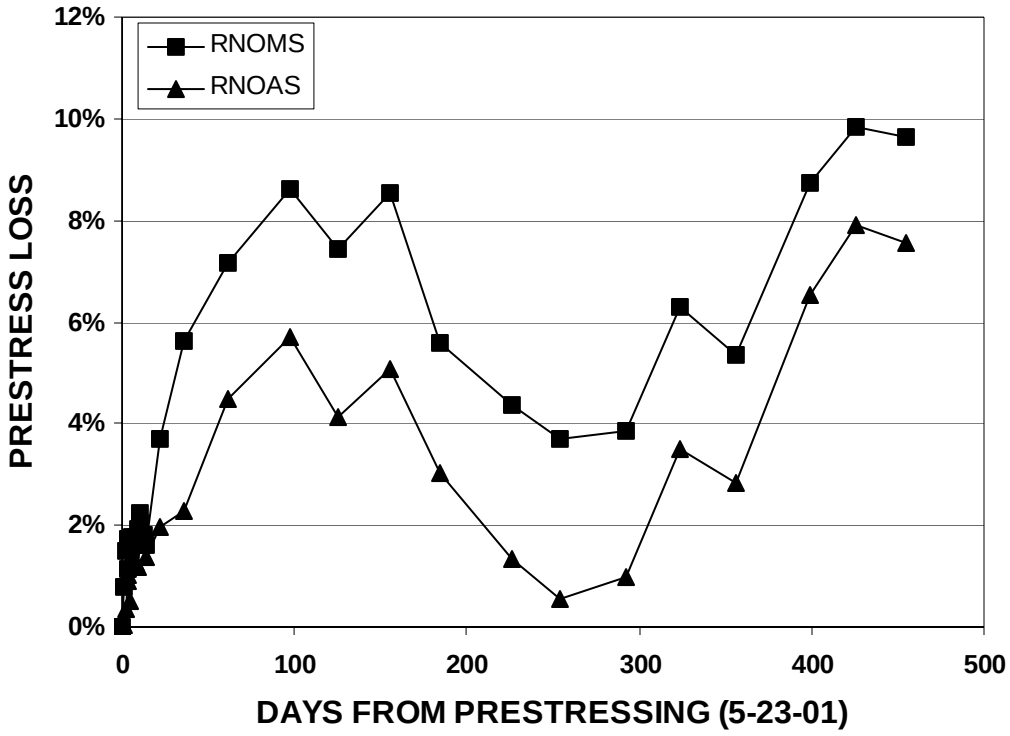

Figure 5.35 – Mechanical Gage Percentage Loss Readings for the Reno Solid Beams

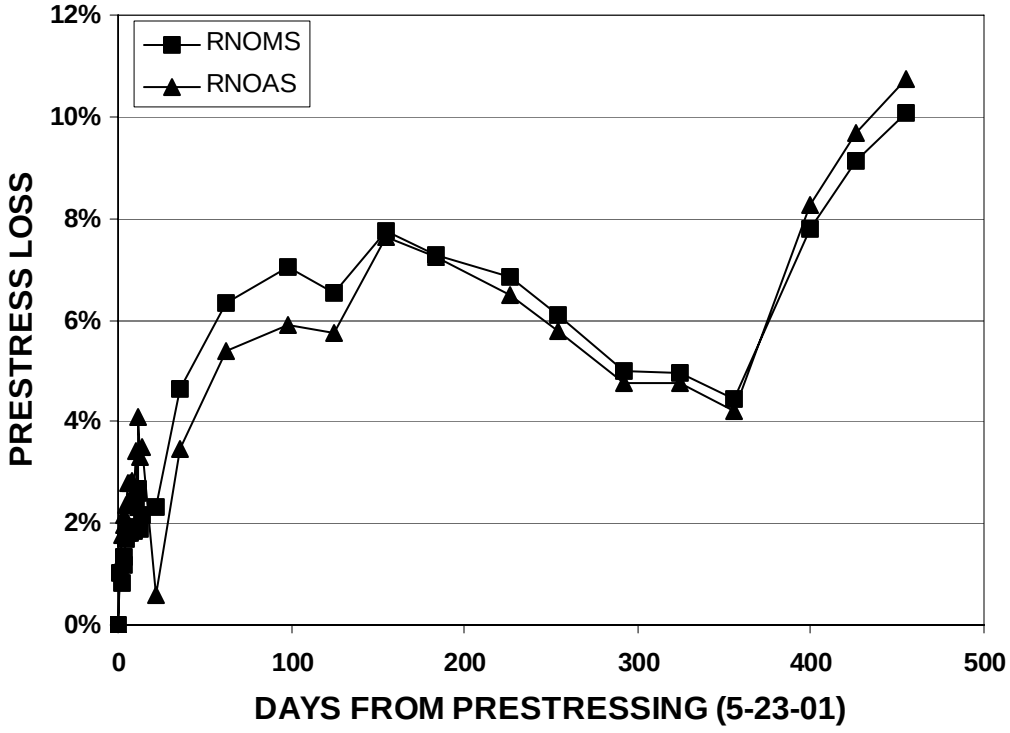

Figure 5.36 – Average Gage Percentage Loss Readings for the Reno Solid Beams

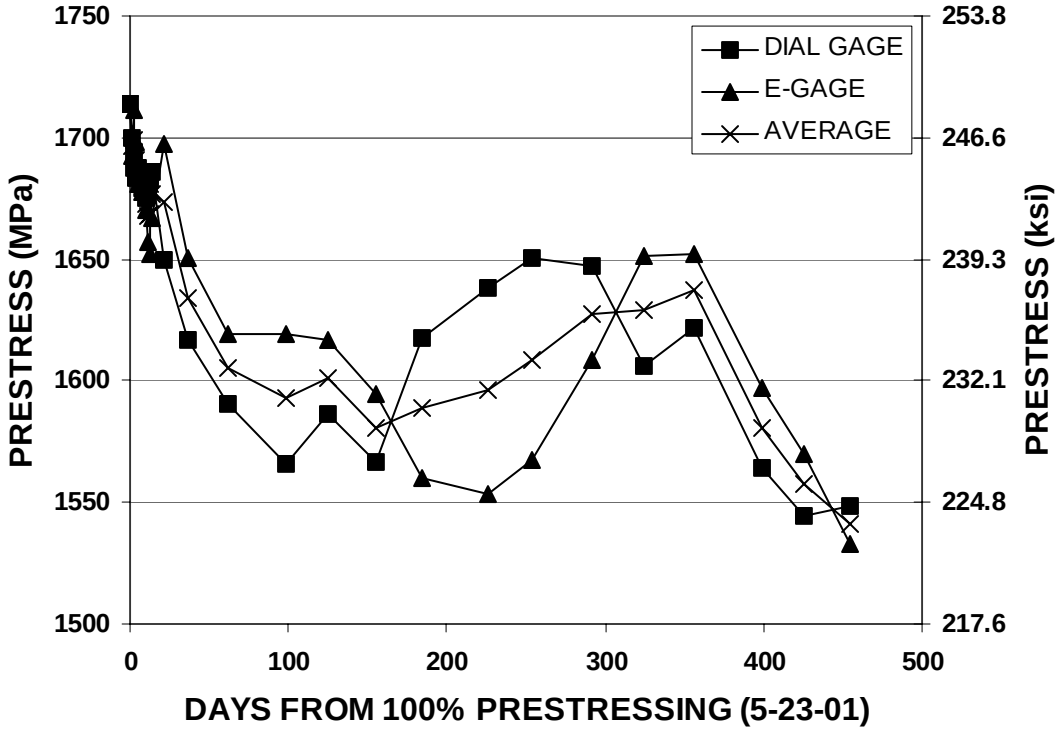

Figure 5.37 – RNOMS Gage Readings

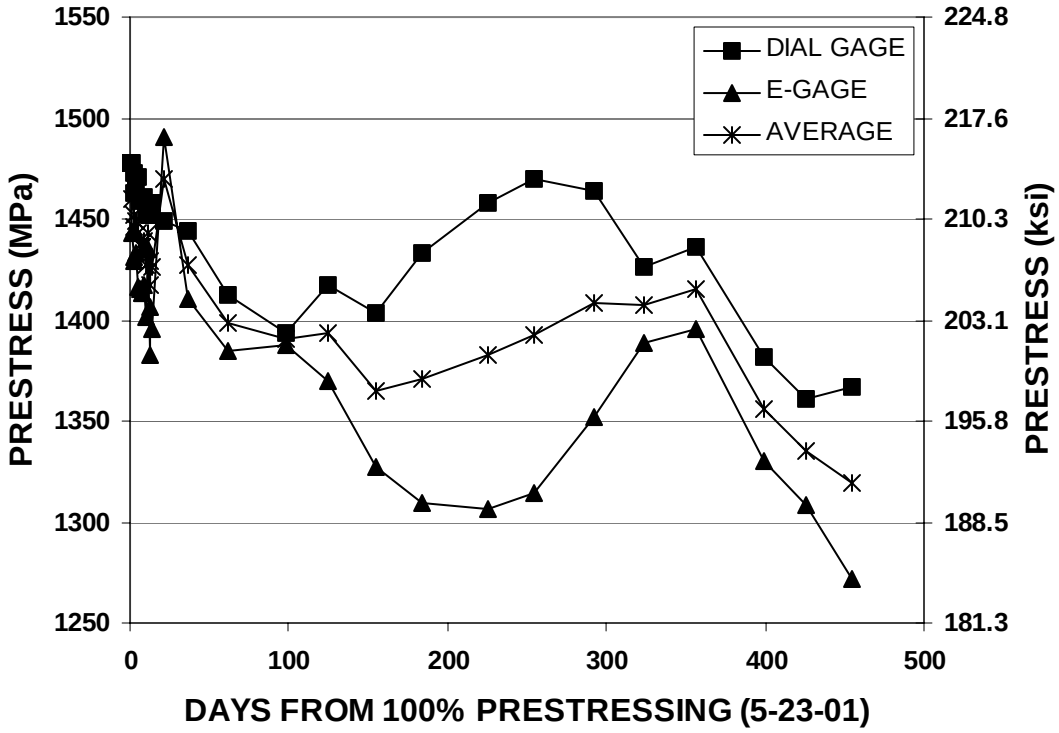

Figure 5.38 – RNOAS Gage Readings

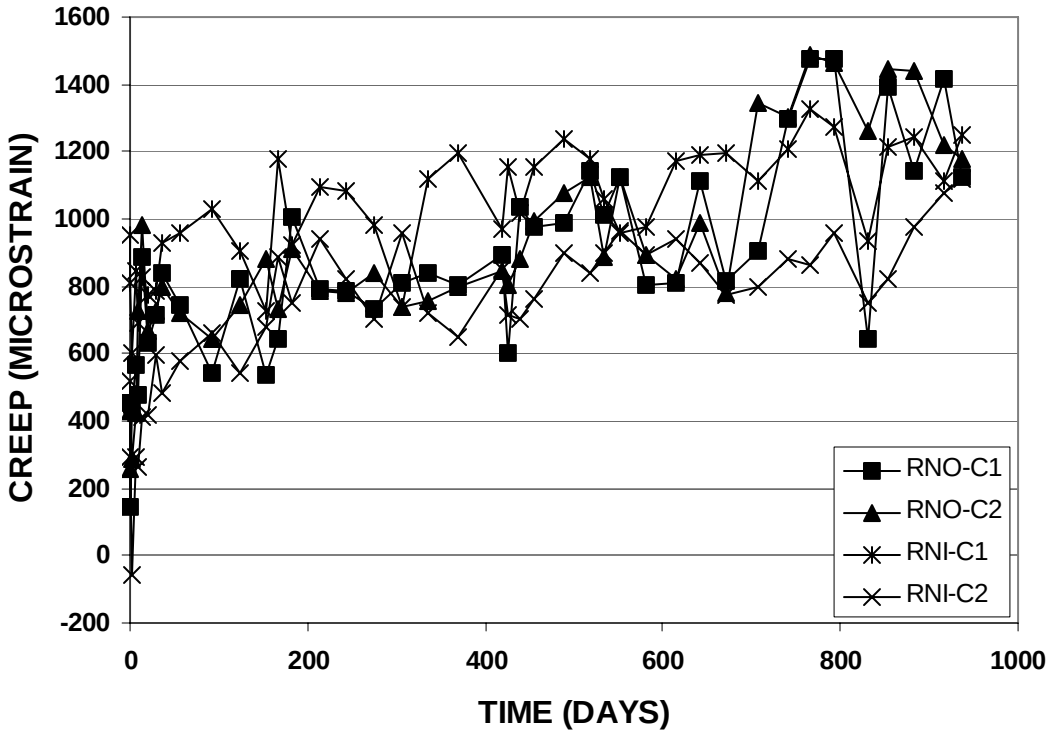

Figure 5.39 – Reno Box Girder Creep Cylinders

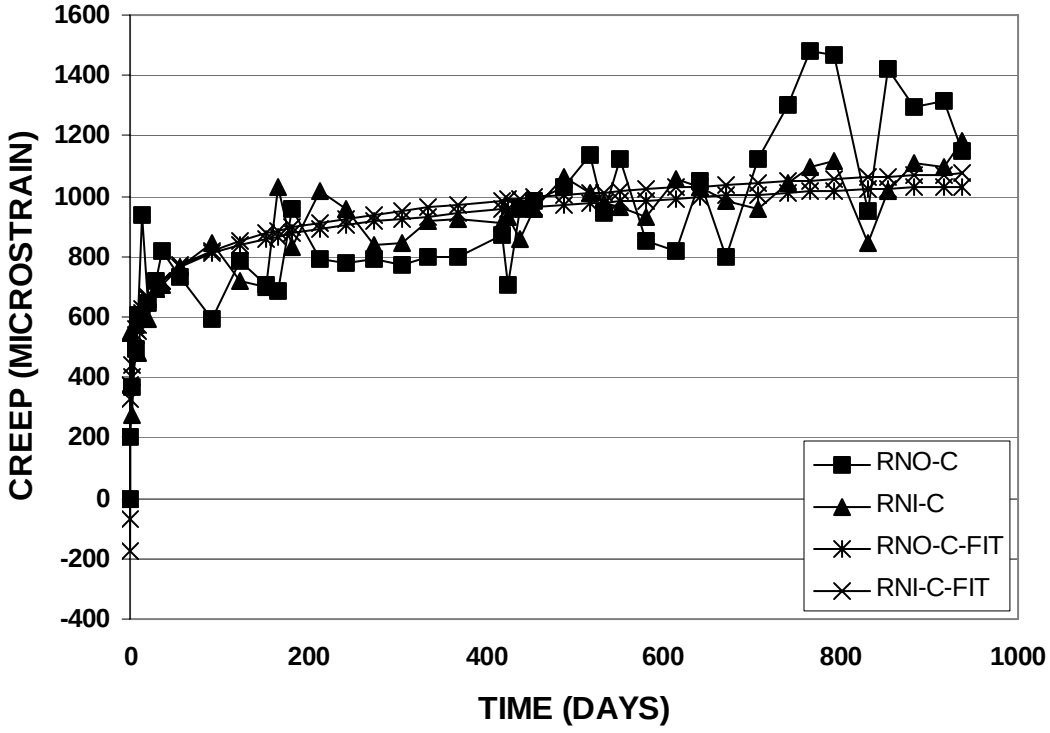

Figure 5.40 – Reno Box Girder Cylinder Creep Average and Log-Fit

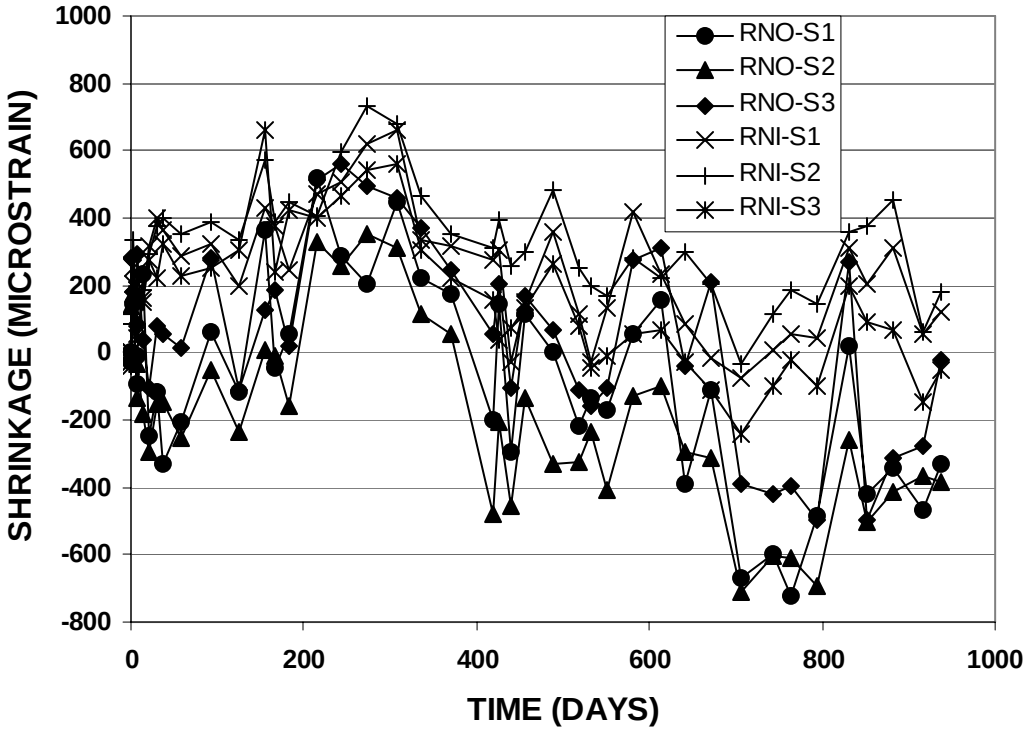

Figure 5.41 – Reno Box Girder Shrinkage Cylinders

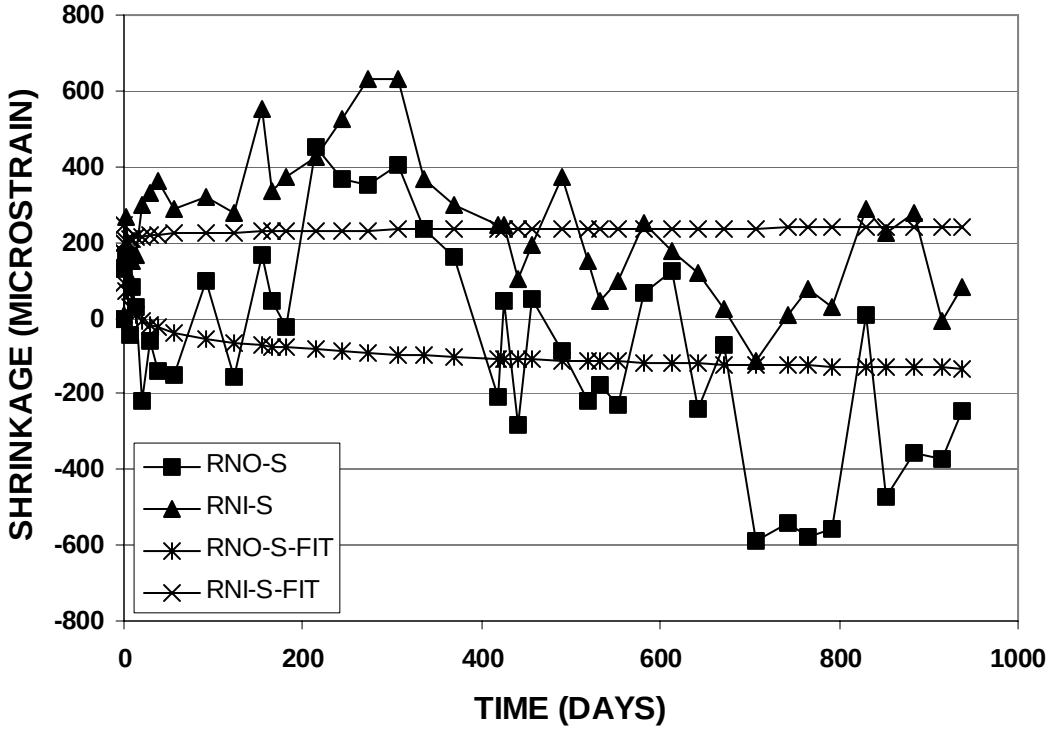

Figure 5.42 – Reno Box Girder Shrinkage Cylinder Average and Log-Fit

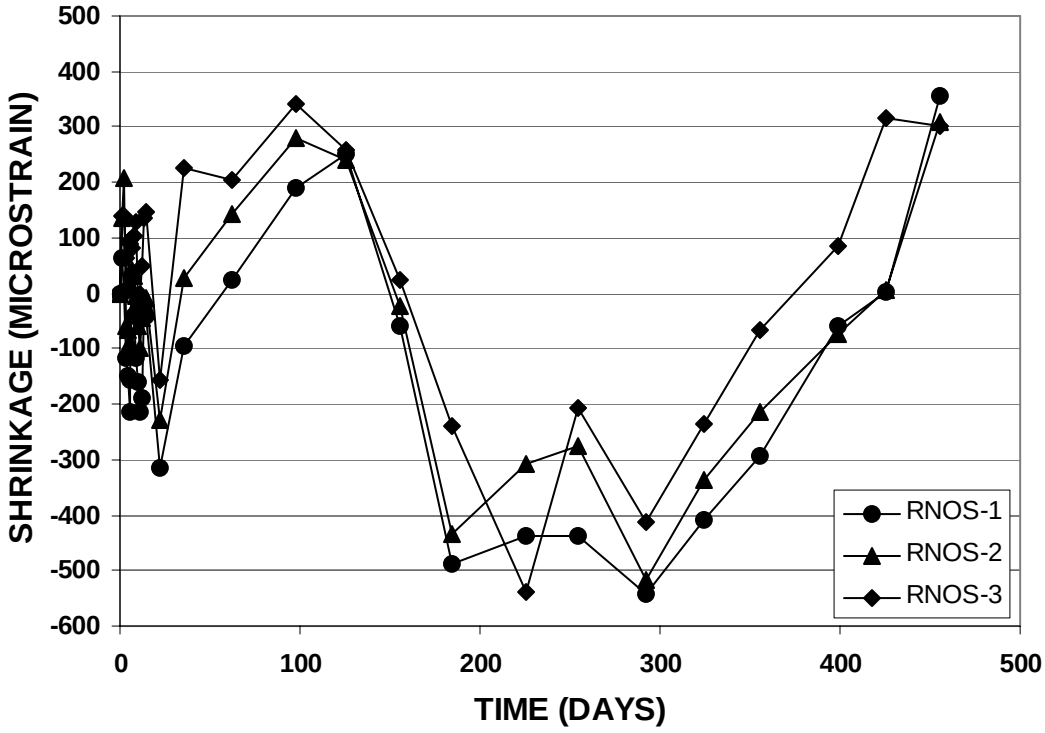

Figure 5.43 – Reno Solid Beam Shrinkage Cylinders

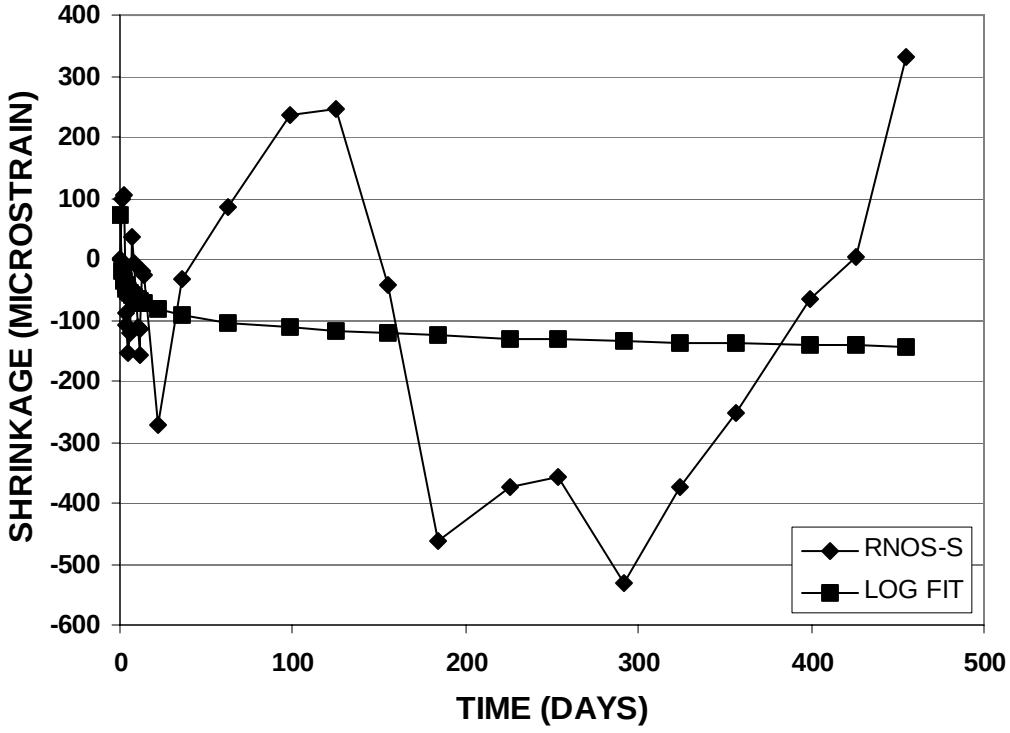

Figure 5.44 – Reno Solid Beam Shrinkage Average and Log-Fit

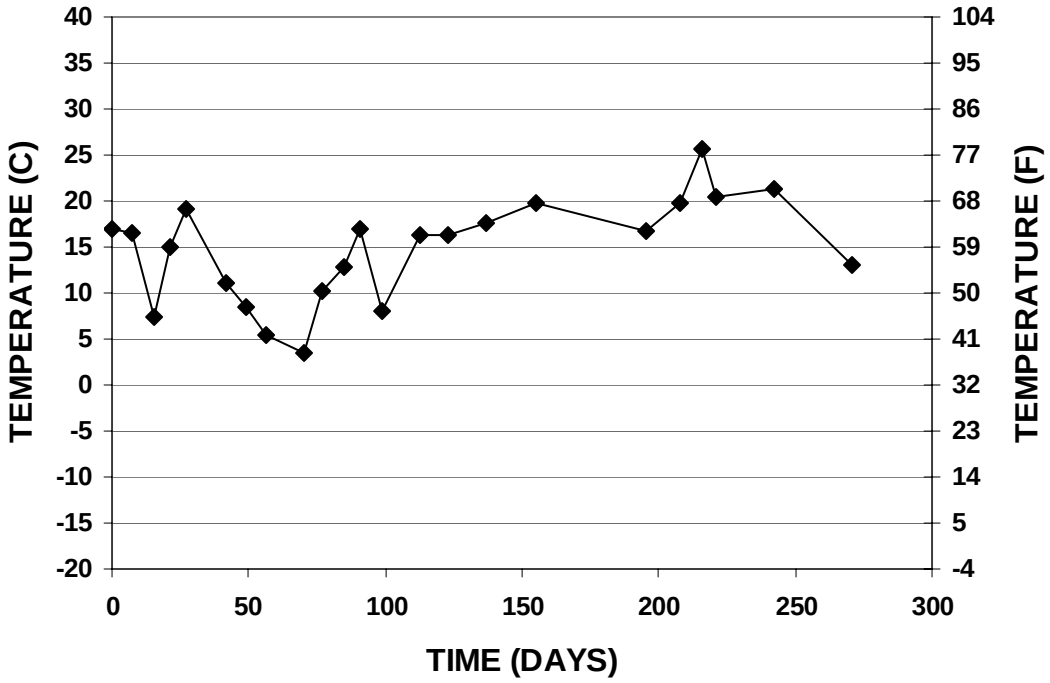

Figure 5.45 – Supplemental Reno Outdoor Shrinkage Cylinders Temperature Readings

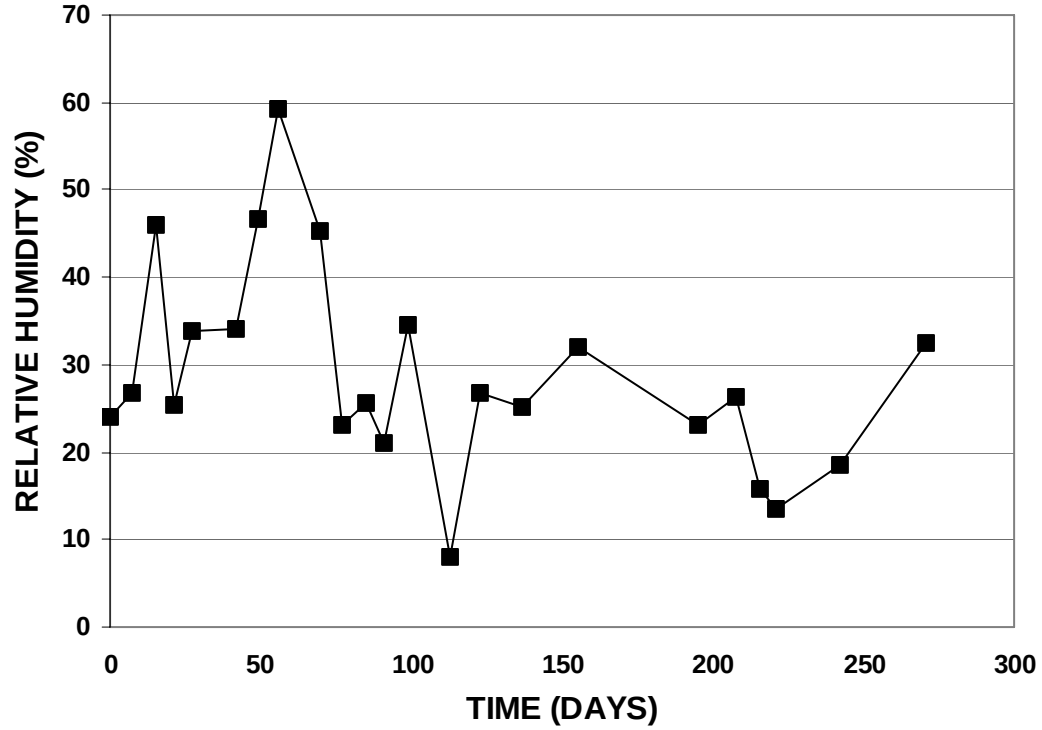

Figure 5.46 – Supplemental Reno Outdoor Shrinkage Cylinders Relative Humidity Readings

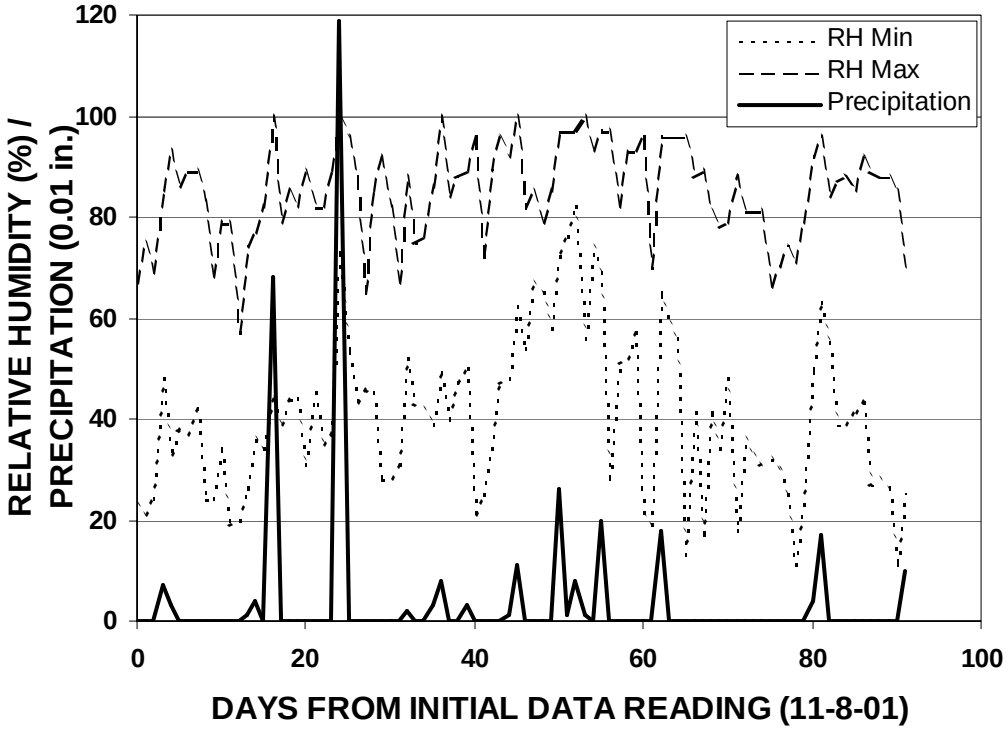

Figure 5.47 – Supplemental Outdoor Shrinkage Cylinders Climate Data from the Reno Airport for the First Three Months

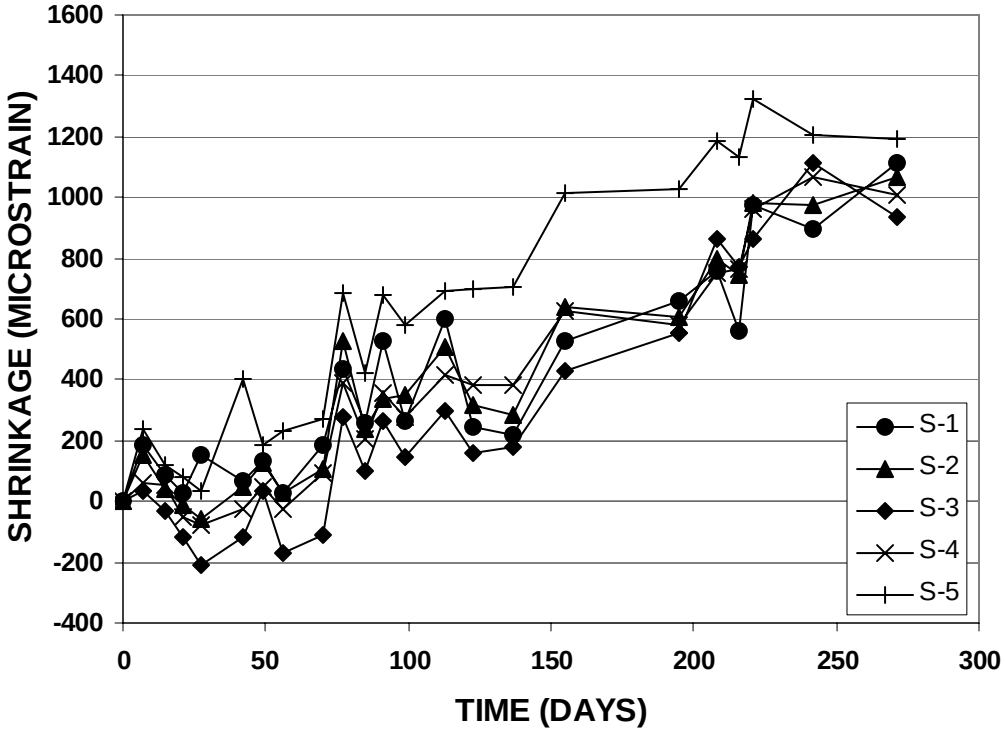

Figure 5.48 – Supplemental Reno Outdoor Shrinkage Cylinders

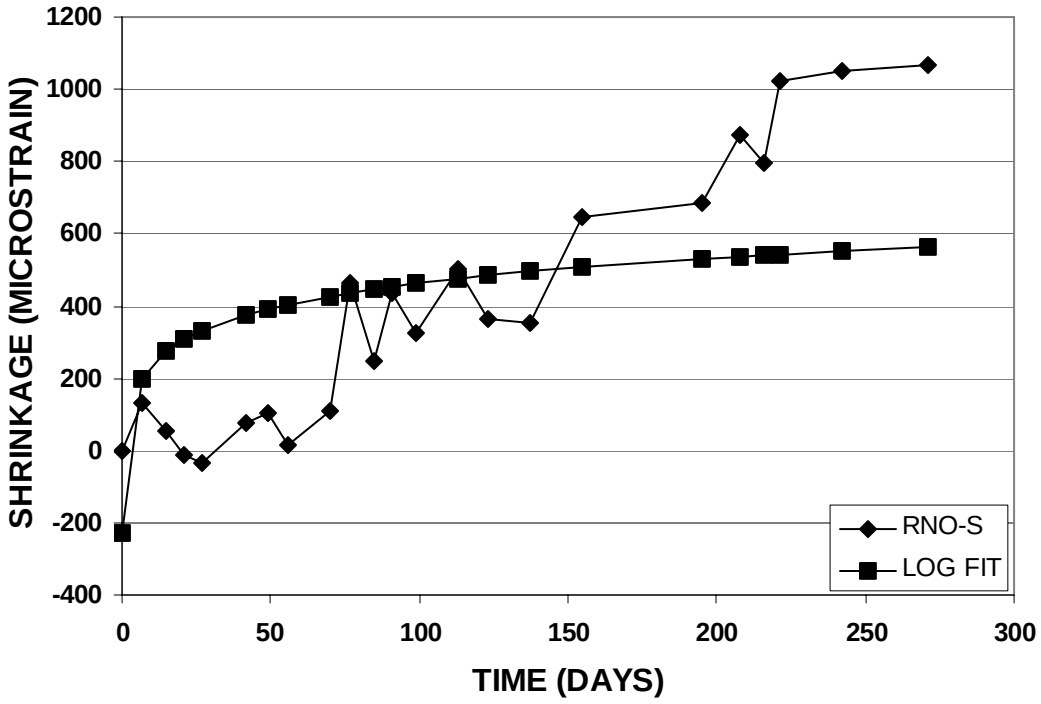

Figure 5.49 – Supplemental Reno Outdoor Shrinkage Cylinder Average and Log-Fit

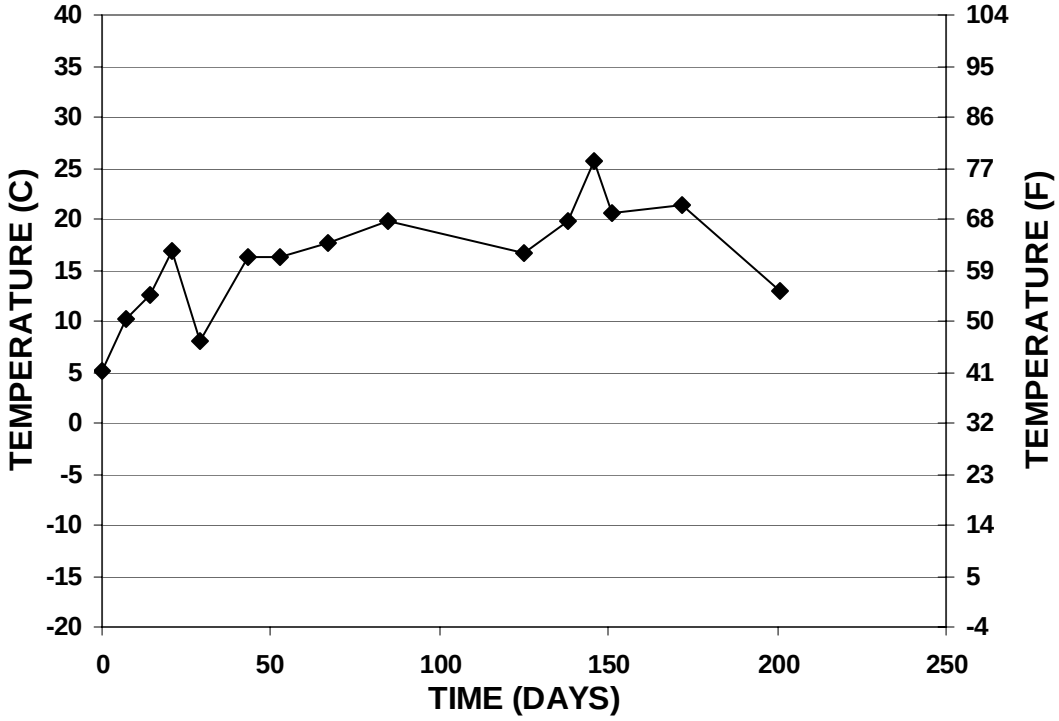

Figure 5.50 – Supplemental Reno Indoor Shrinkage Cylinder Temperature Readings

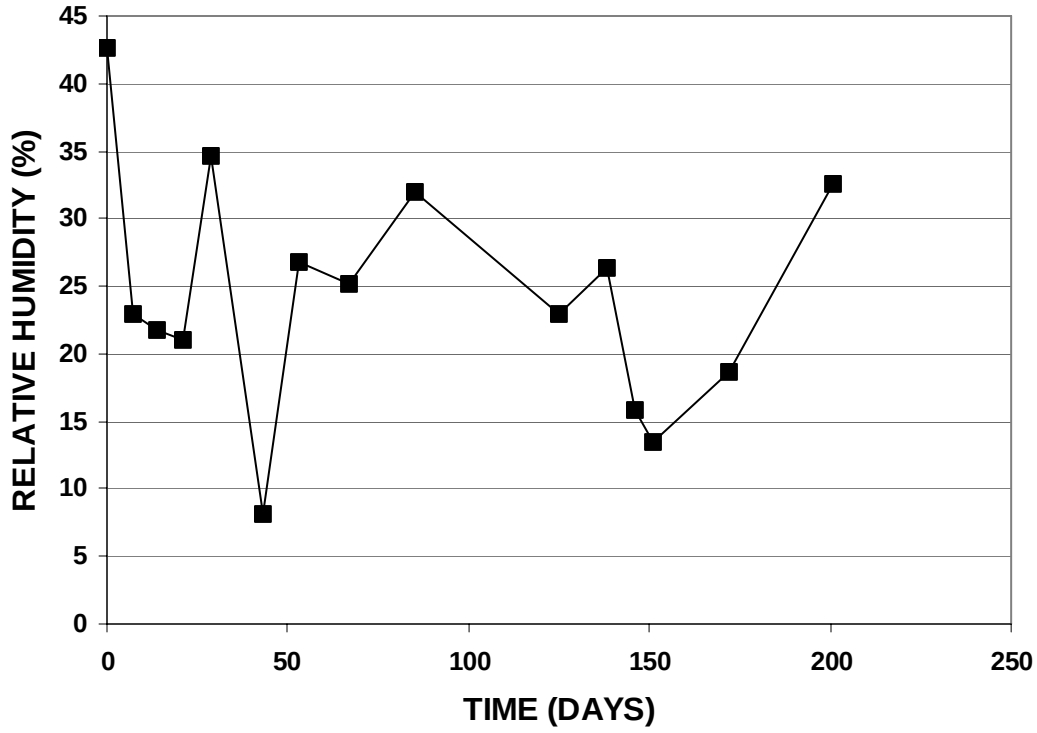

Figure 5.51 – Supplemental Reno Indoor Shrinkage Cylinder Relative Humidity Readings

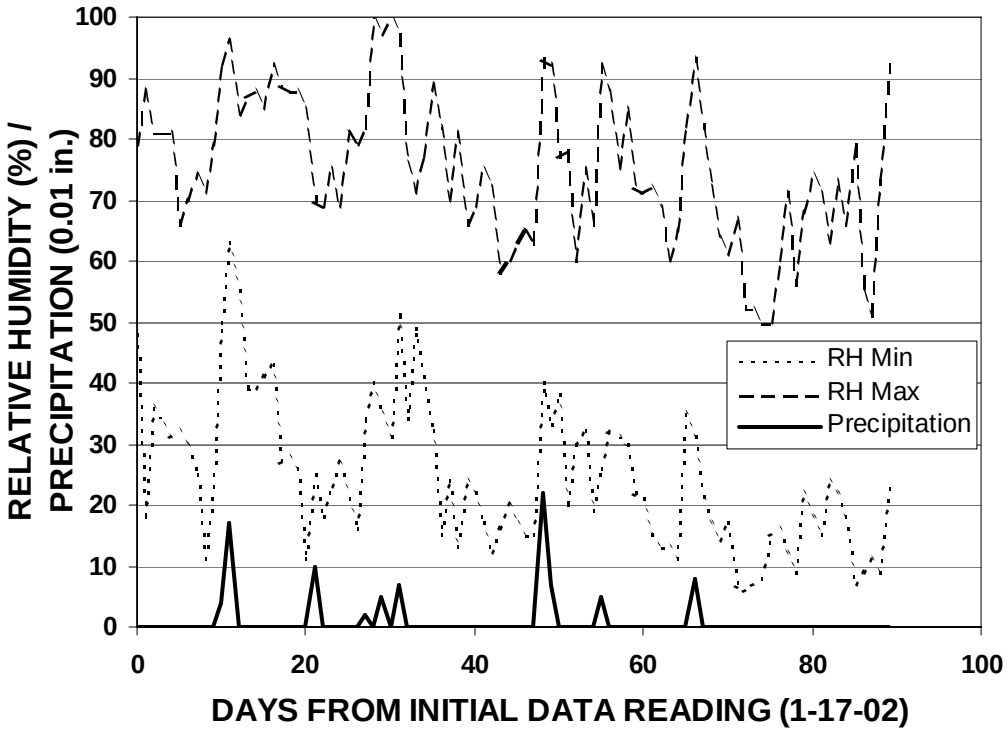

Figure 5.52 – Supplemental Indoor Shrinkage Cylinders Climate Data from the Reno Airport for the First Three Months

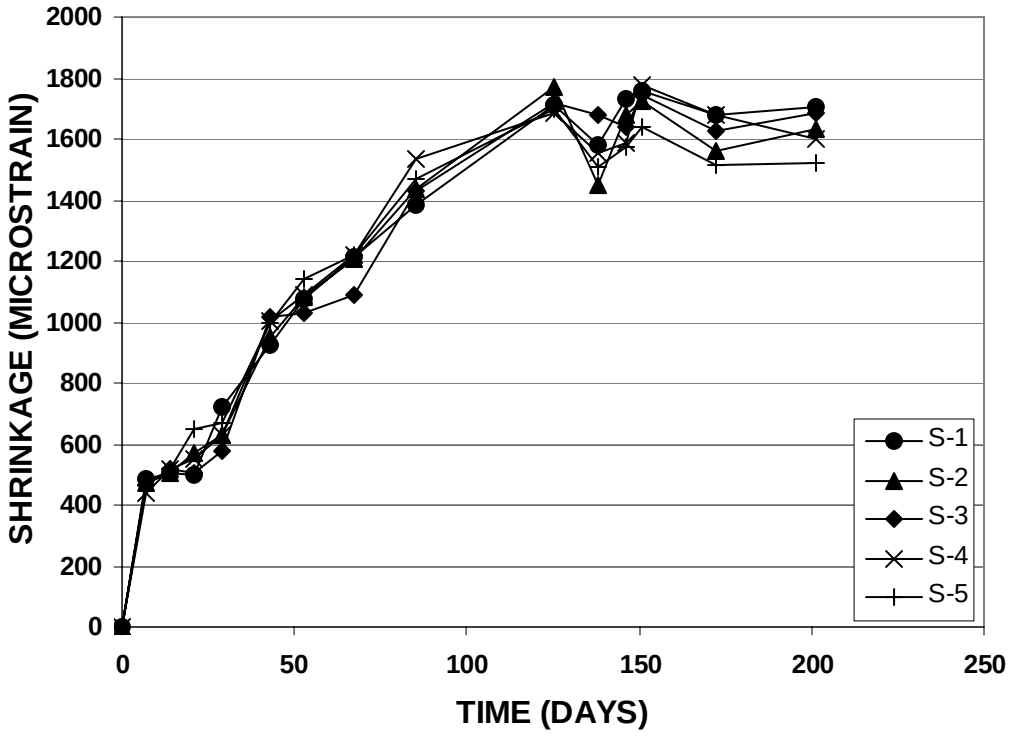

Figure 5.53 – Supplemental Reno Indoor Shrinkage Cylinders

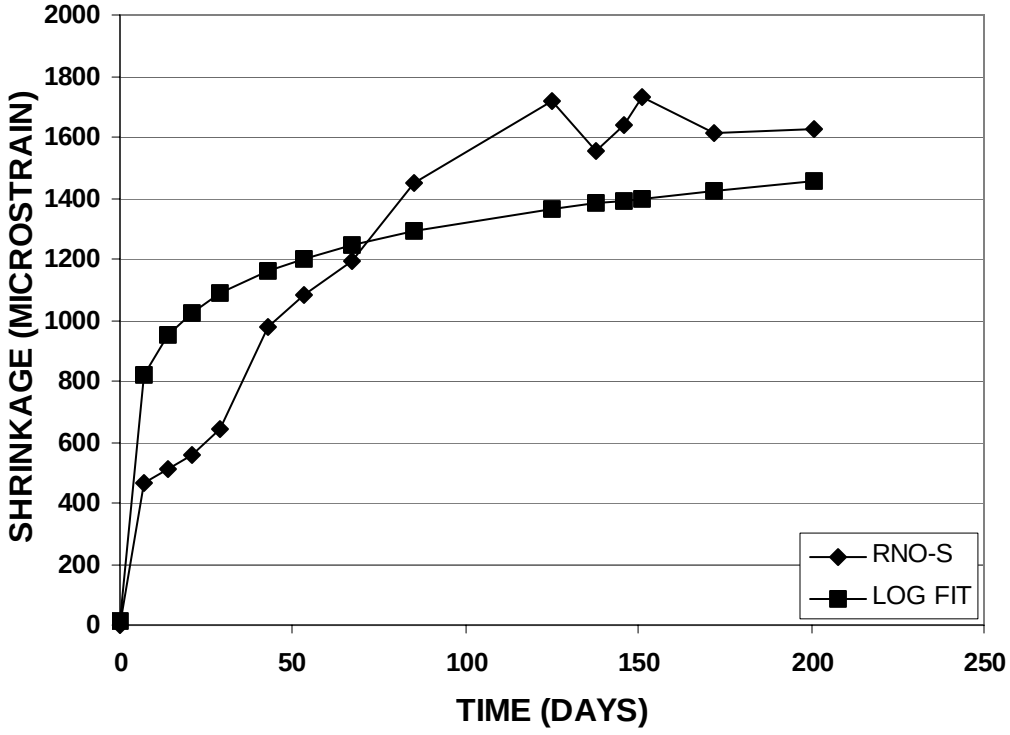

Figure 5.54 – Supplemental Reno Indoor Shrinkage Cylinder Average and Log-Fit

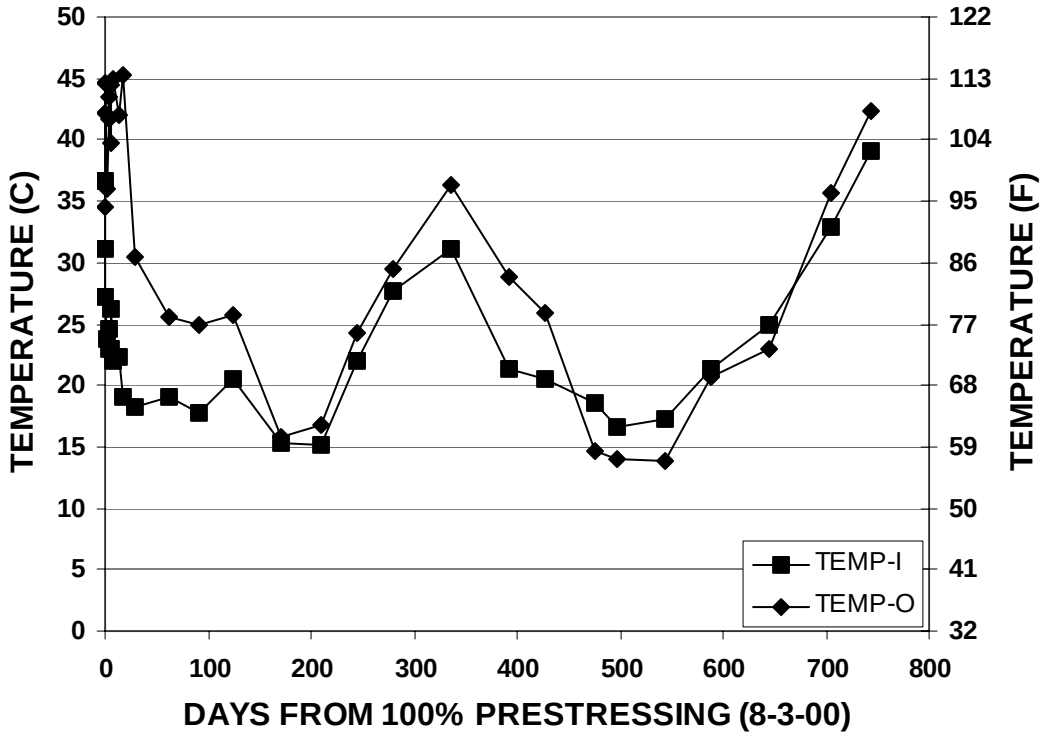

Figure 5.55 – Temperature Readings for the Las Vegas Box Girder Specimens

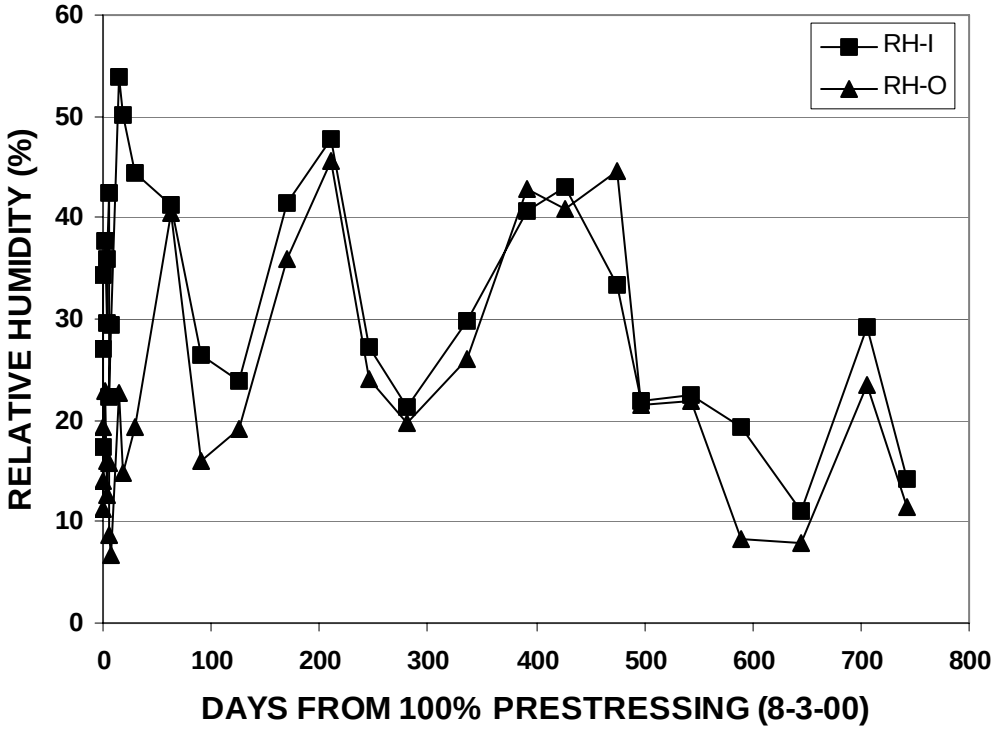

Figure 5.56 – Relative Humidity Readings for the Las Vegas Box Girder Specimens

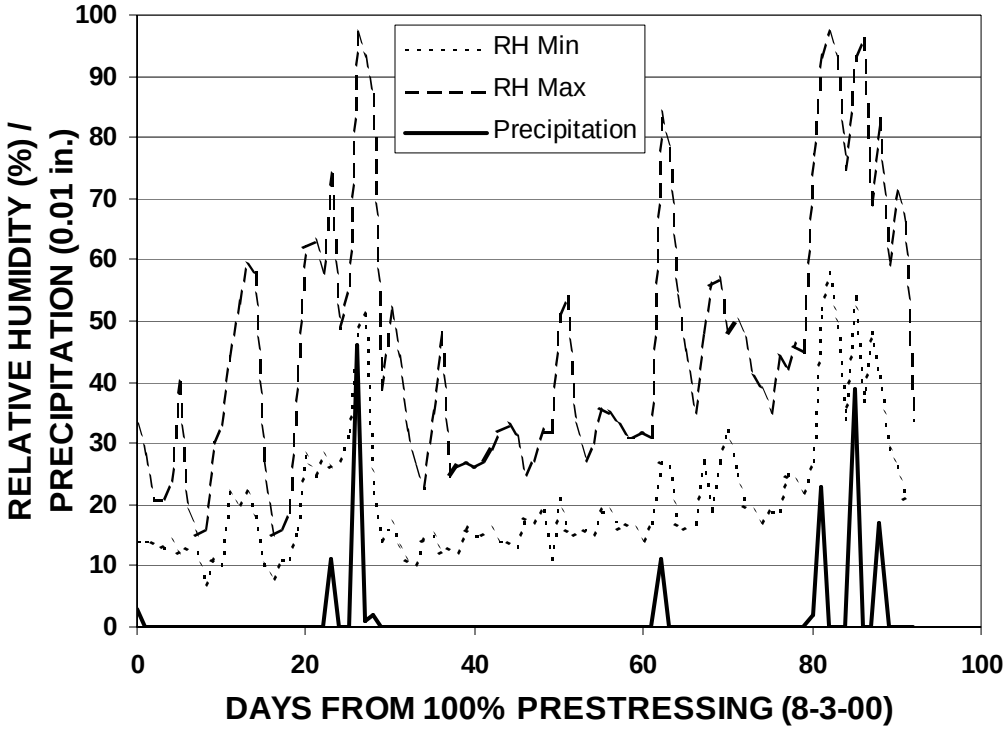

Figure 5.57 – Climate Data from the Las Vegas Airport for the Three Months Following Tensioning of the Box Girders

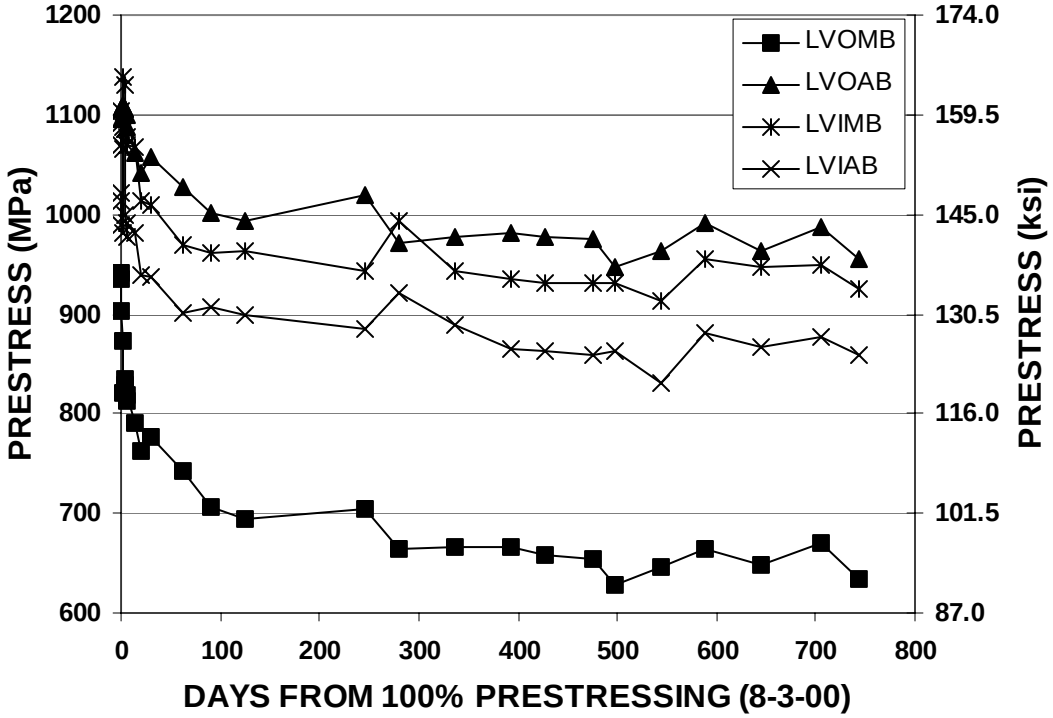

Figure 5.58 – Electric Gage Prestress Readings for the Las Vegas Box Girders

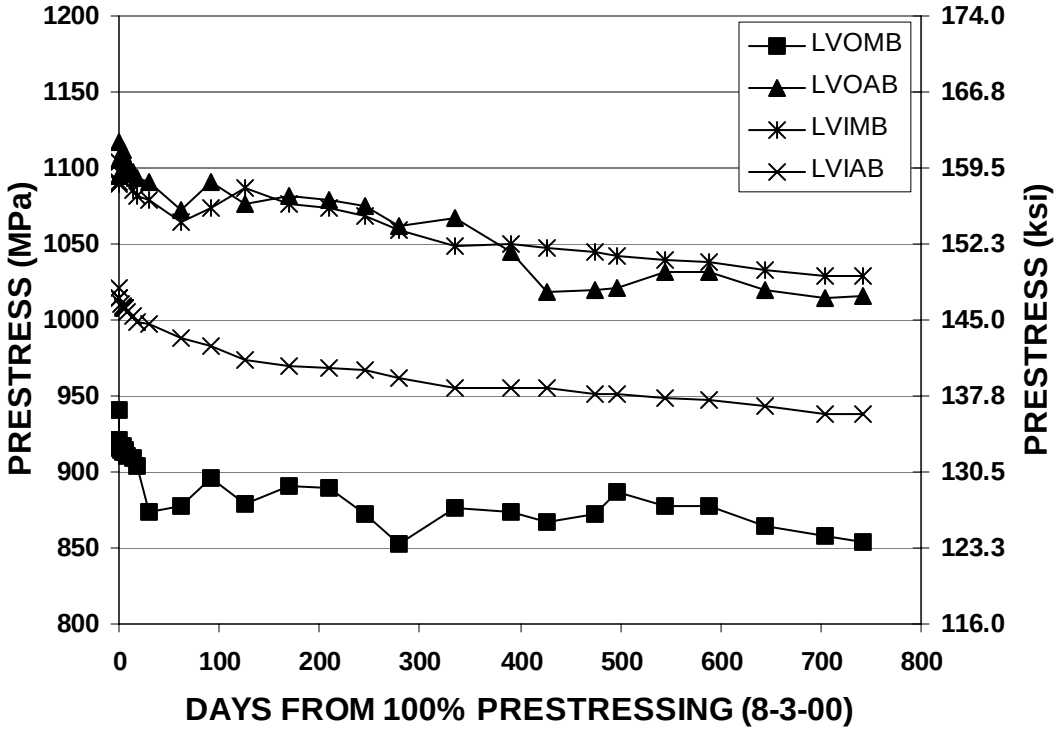

Figure 5.59 – Mechanical Gage Prestress Readings for the Las Vegas Box Girders

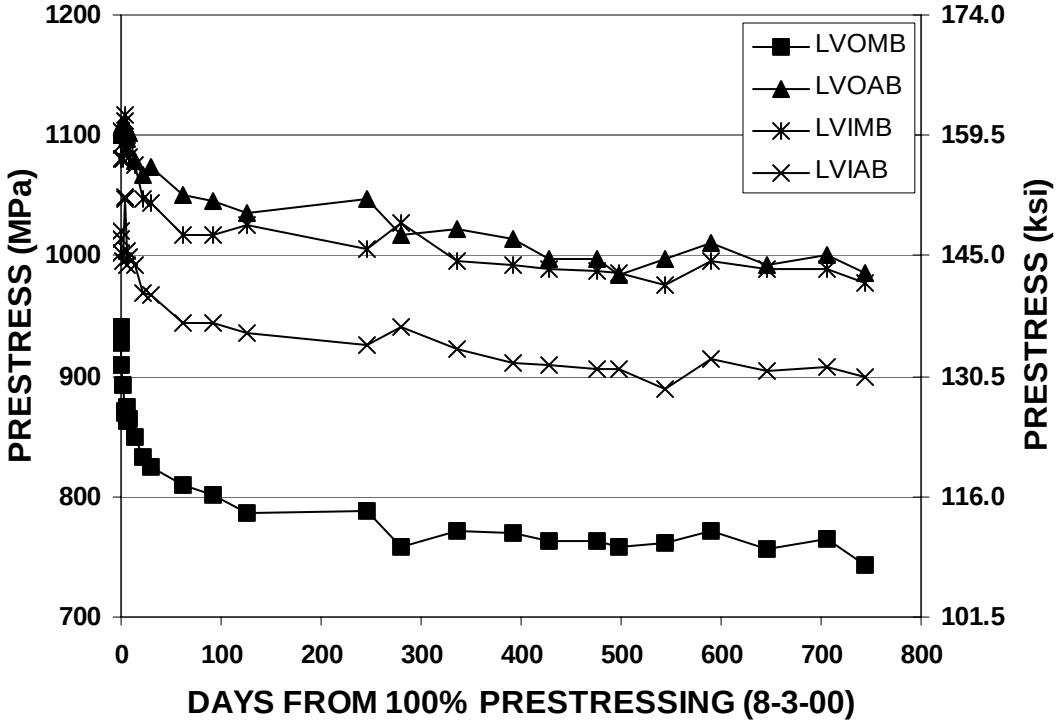

Figure 5.60 – Average Gage Readings for the Las Vegas Box Girders

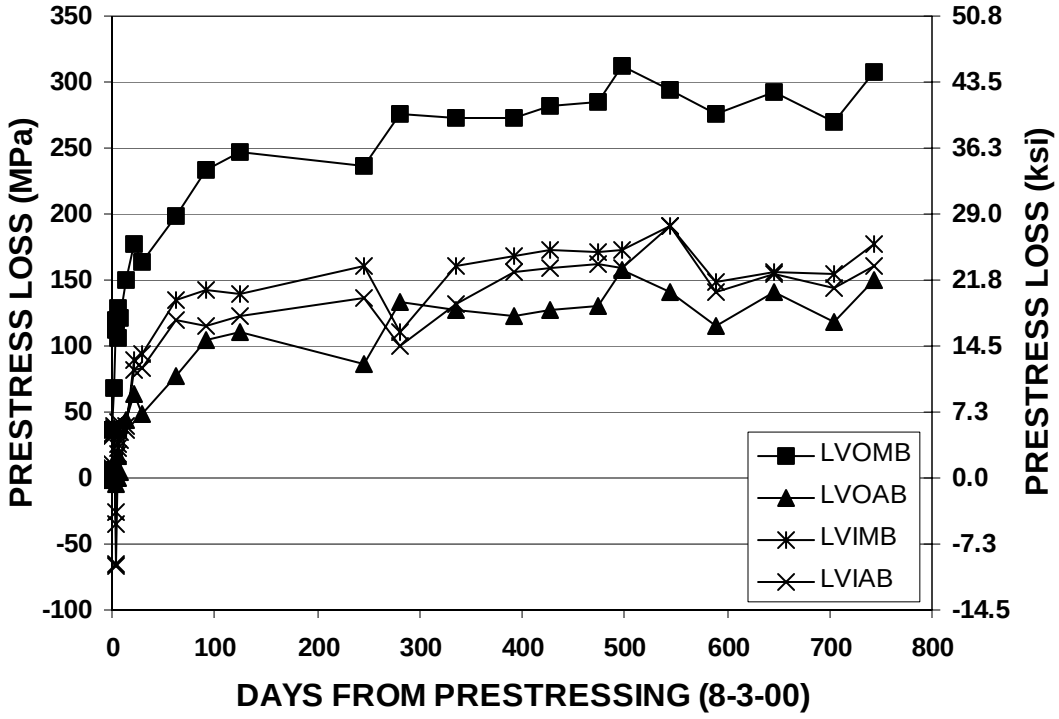

Figure 5.61 – Electric Gage Prestress Loss Readings for the Las Vegas Box Girders

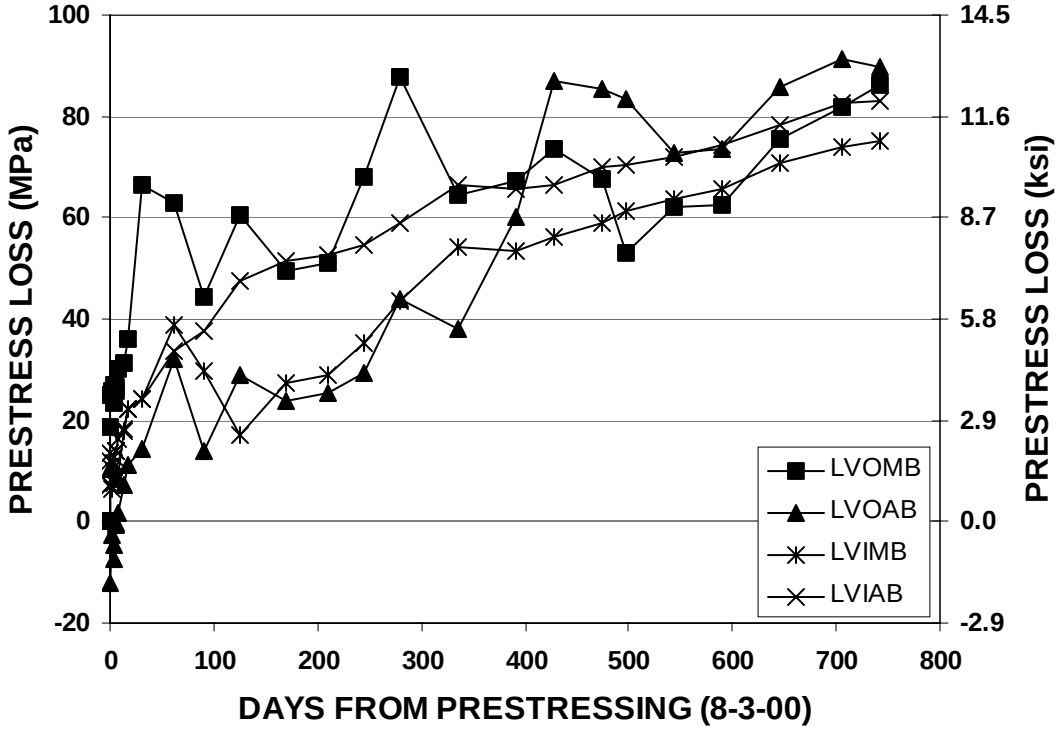

Figure 5.62 – Mechanical Gage Prestress Loss Readings for the Las Vegas Box Girders

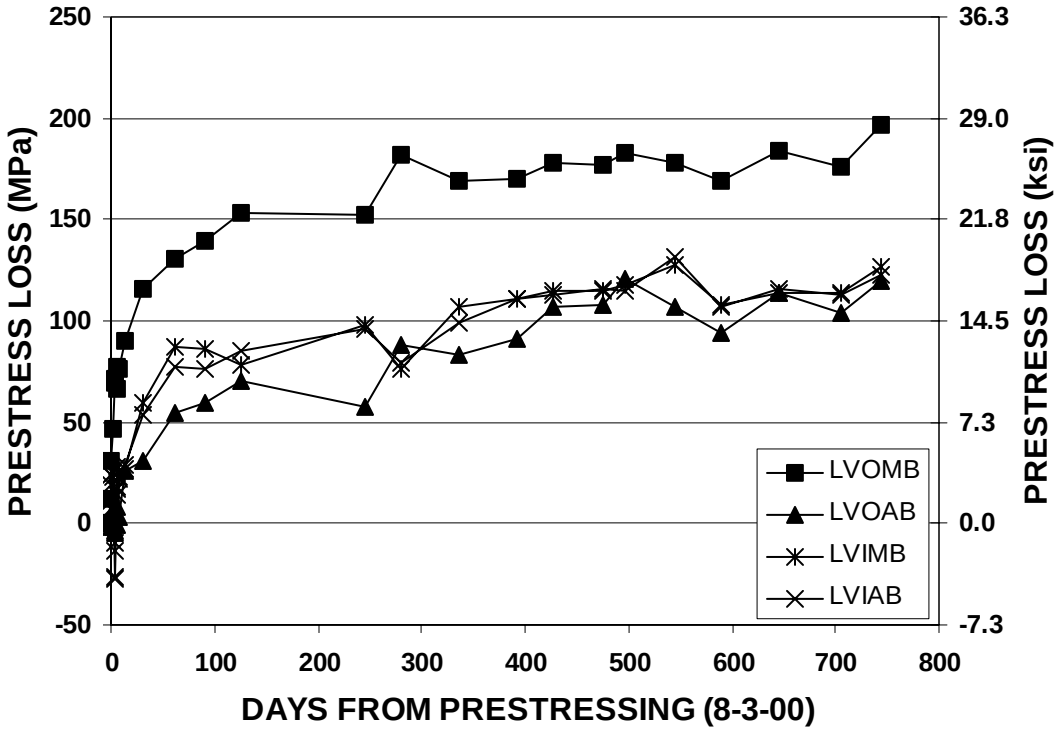

Figure 5.63 – Average Gage Prestress Loss Readings for the Las Vegas Box Girders

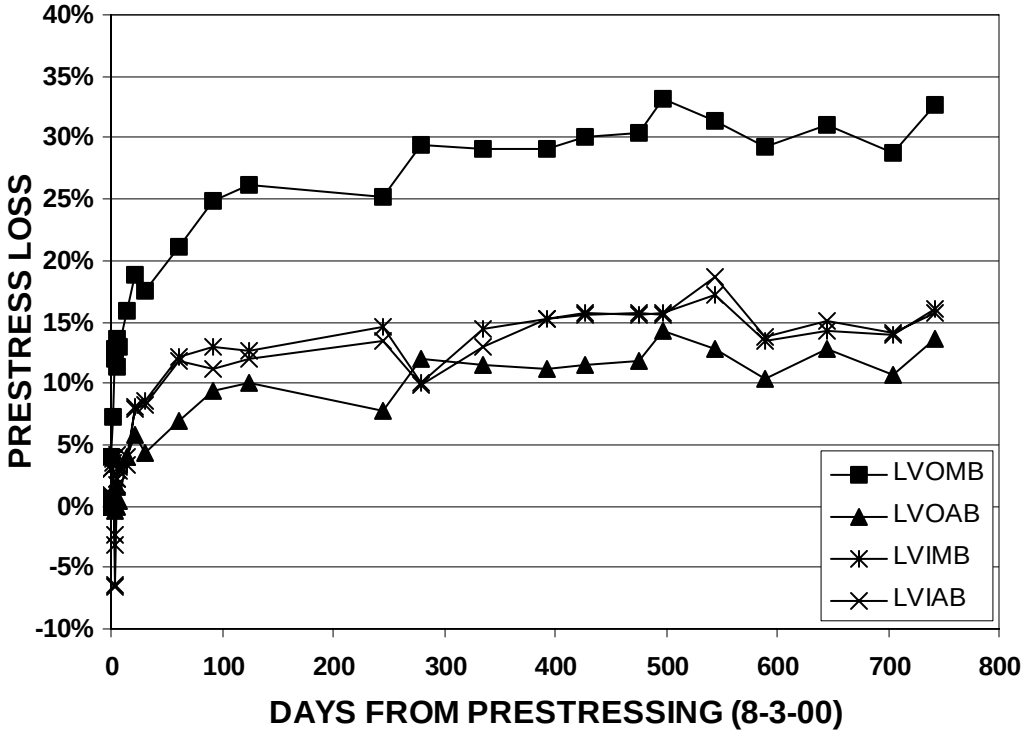

Figure 5.64 – Electric Gage Percentage Loss Readings for the Las Vegas Box Girders

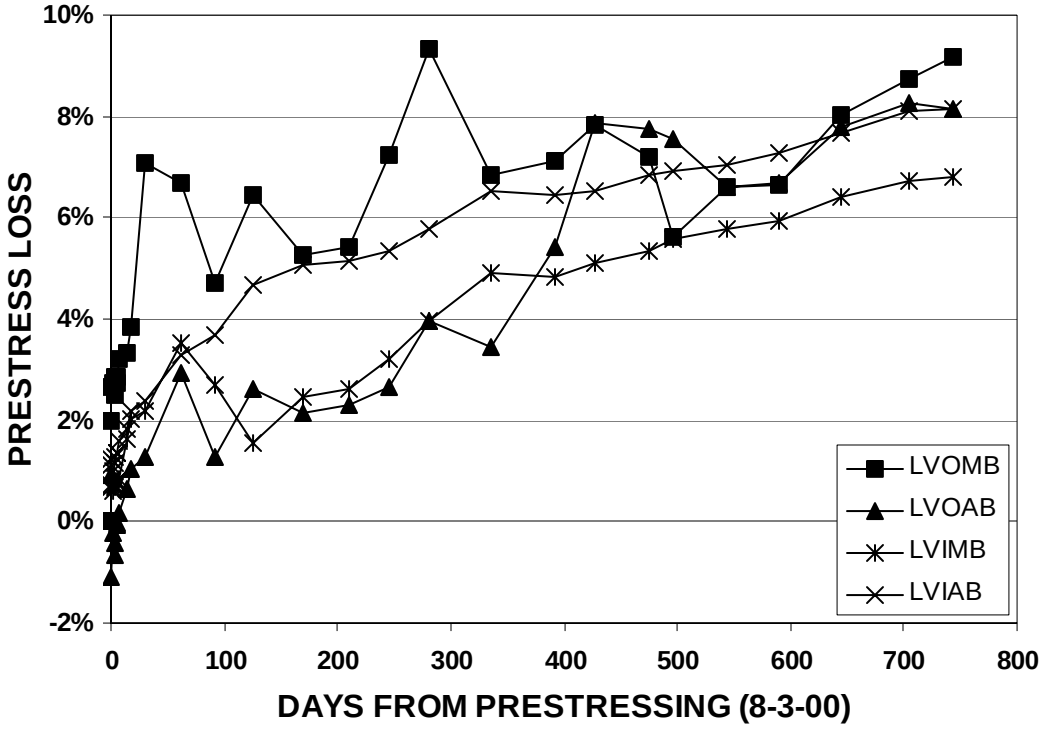

Figure 5.65 – Mechanical Gage Percentage Loss Readings for the Las Vegas Box Girders

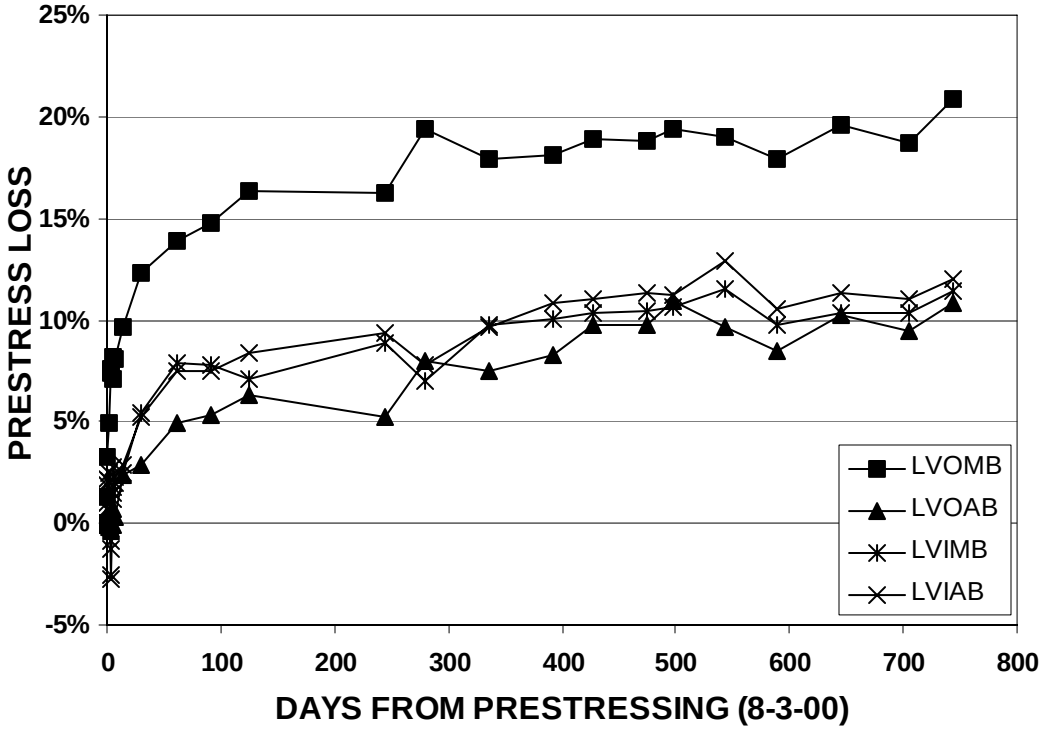

Figure 5.66 – Average Gage Percentage Loss Readings for the Las Vegas Box Girders

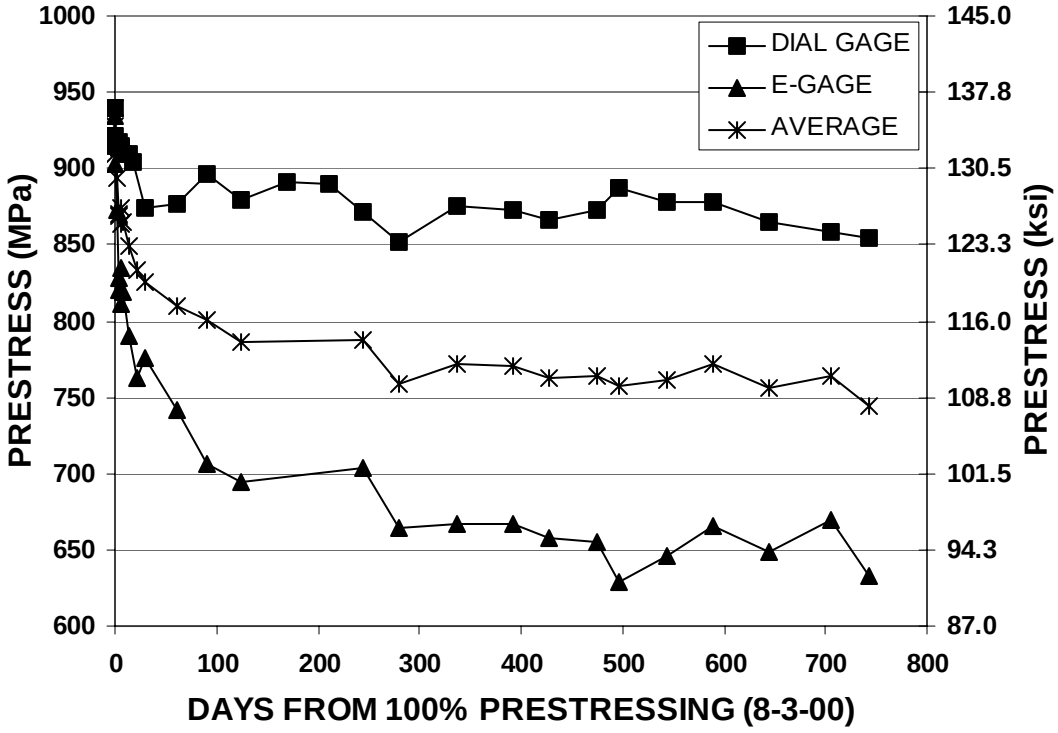

Figure 5.67 – LVOMB Gage Readings

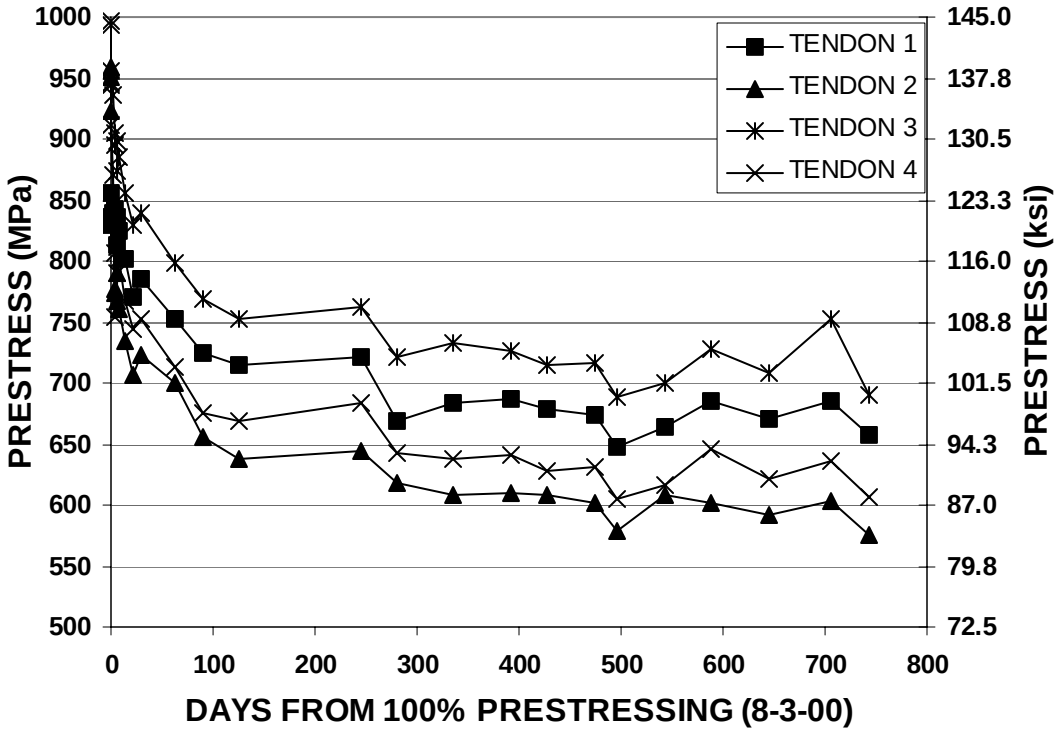

Figure 5.68 – LVOMB Electric Gage Readings Per Tendon

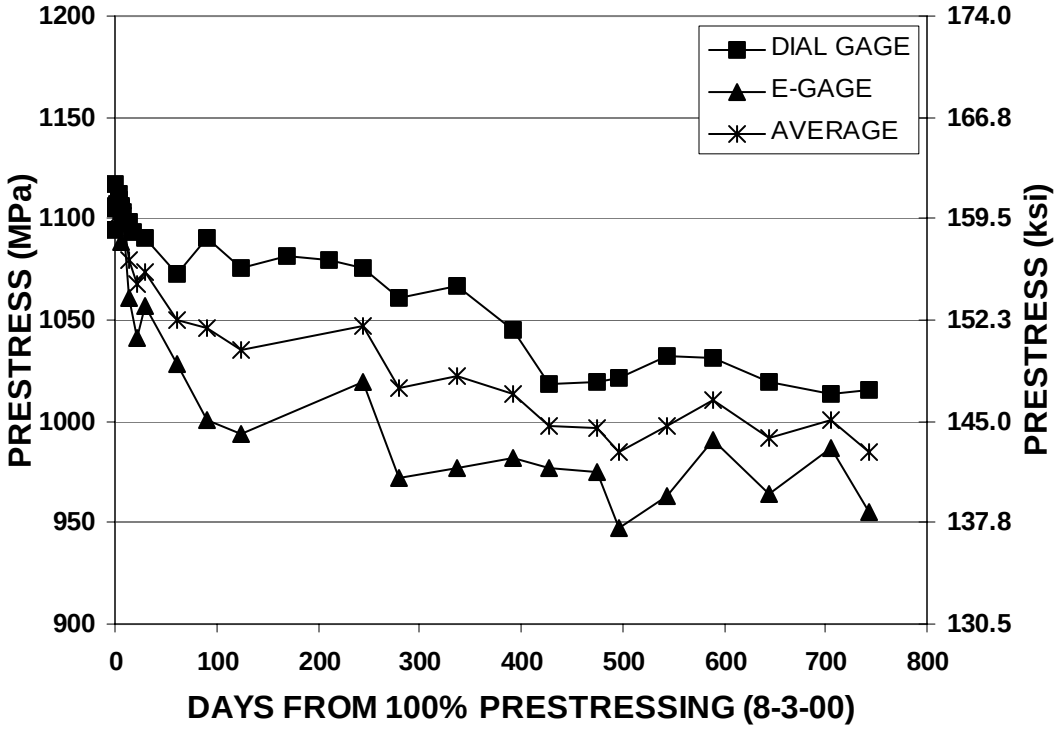

Figure 5.69 – LVOAB Gage Readings

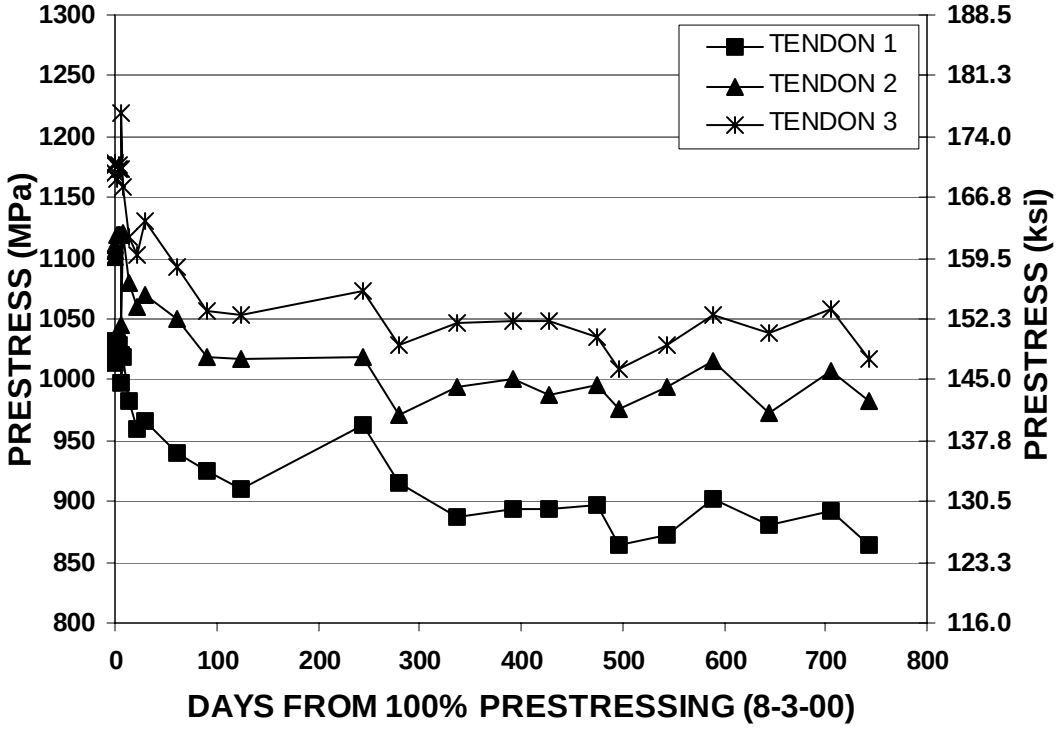

Figure 5.70 – LVOAB Electric Gage Readings Per Tendon

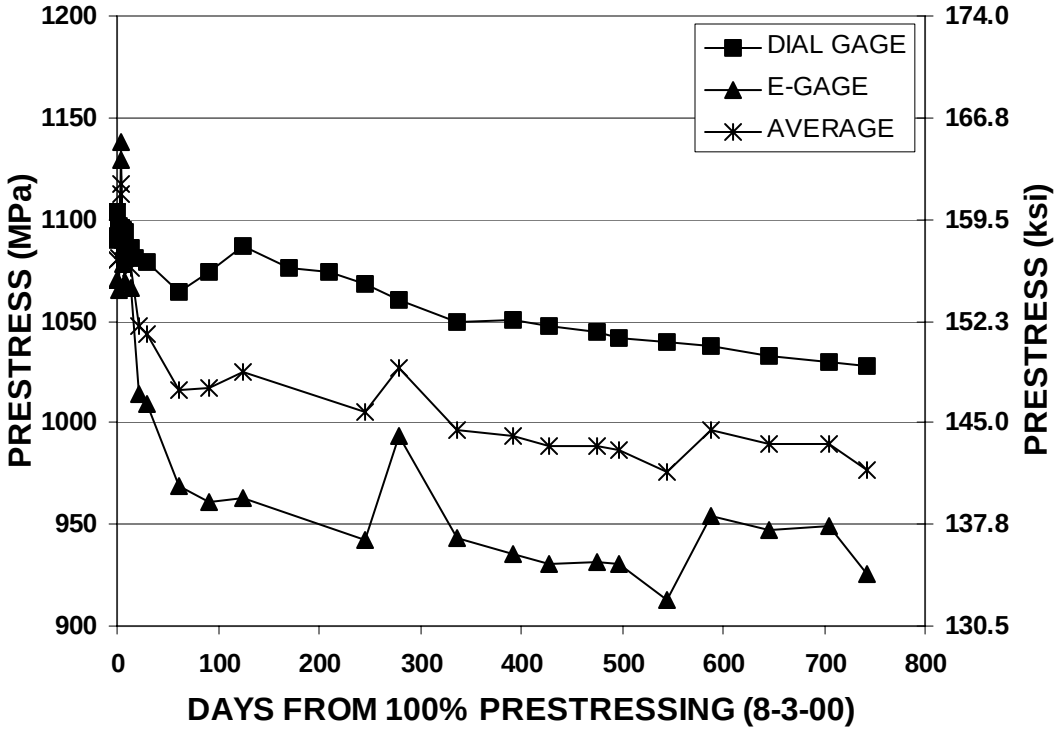

Figure 5.71 – LVIMB Gage Readings

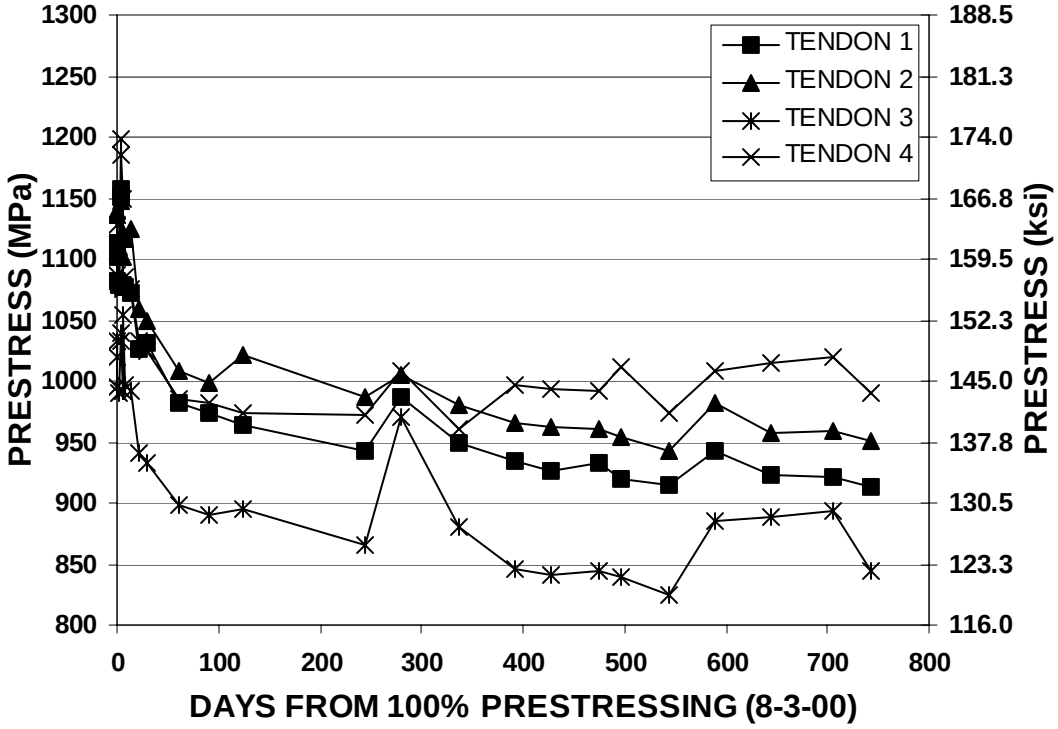

Figure 5.72 – LVIMB Electric Gage Readings Per Tendon

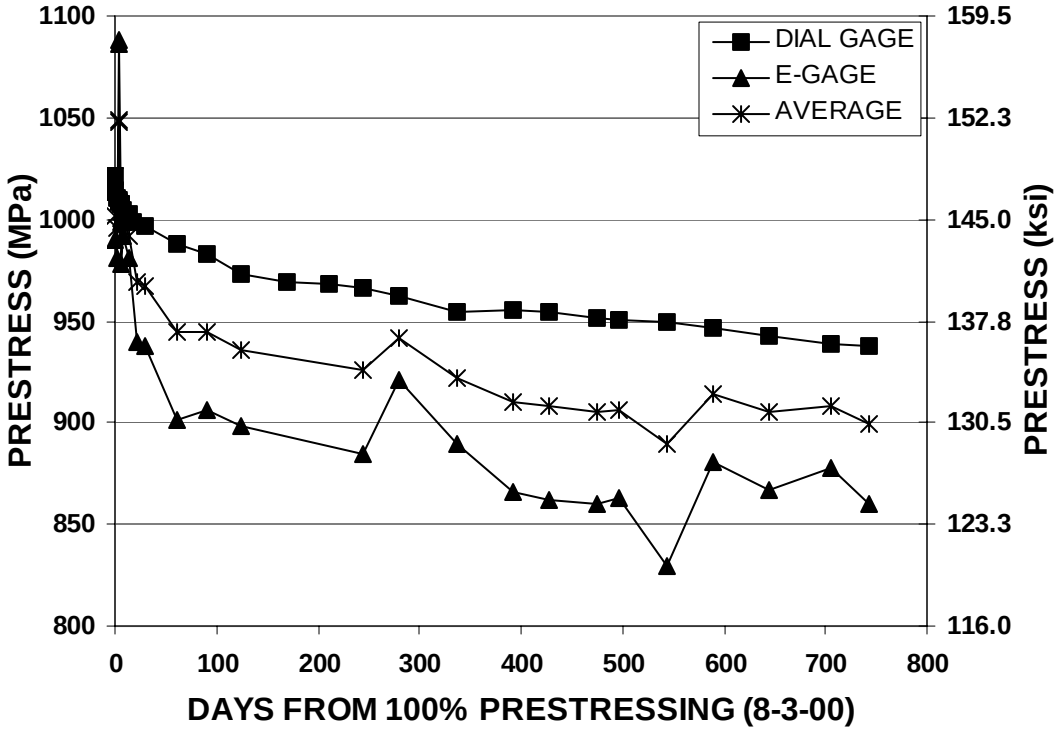

Figure 5.73 – LVIAB Gage Readings

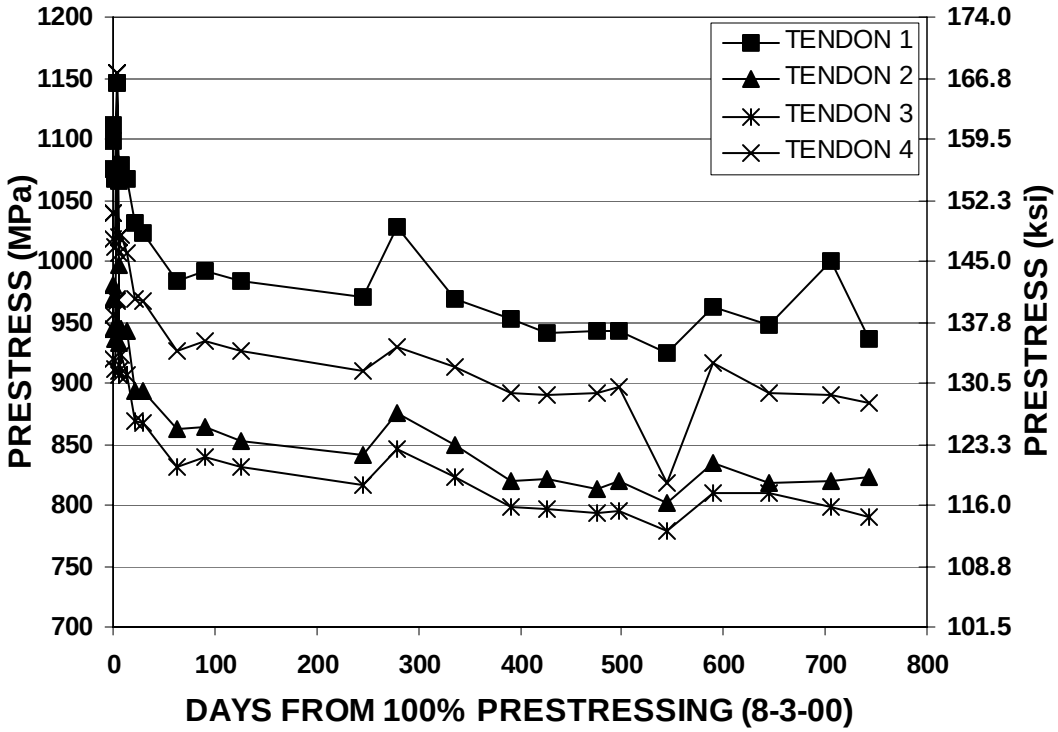

Figure 5.74 – LVIAB Electric Gage Readings Per Tendon

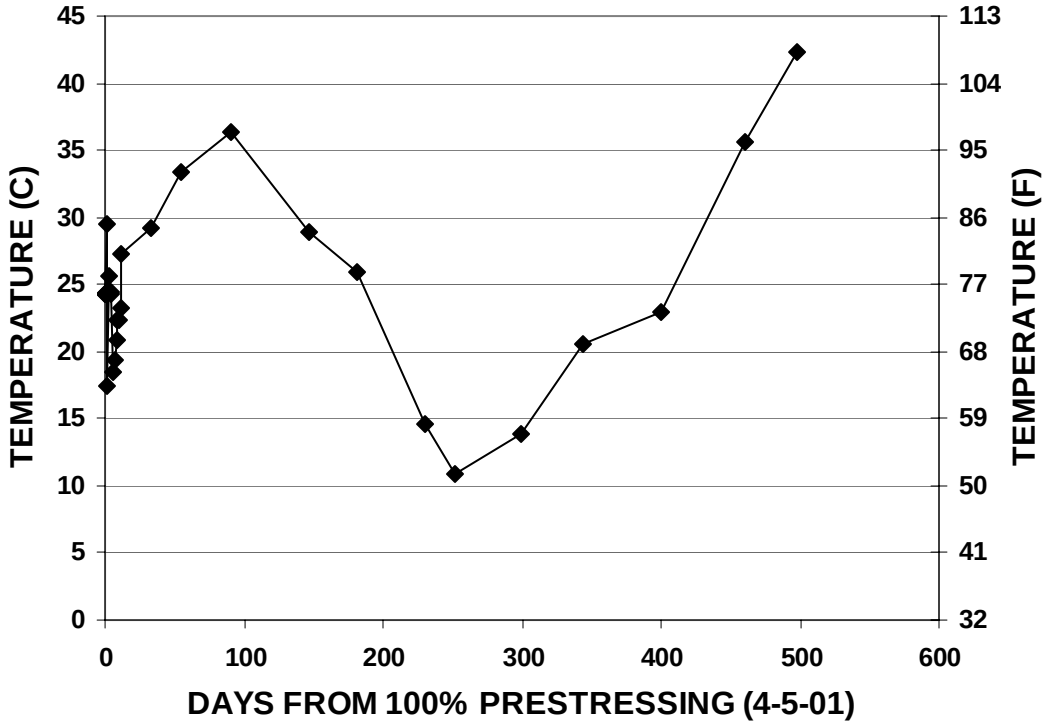

Figure 5.75 – Temperature Readings for the Las Vegas Solid Beam Specimens

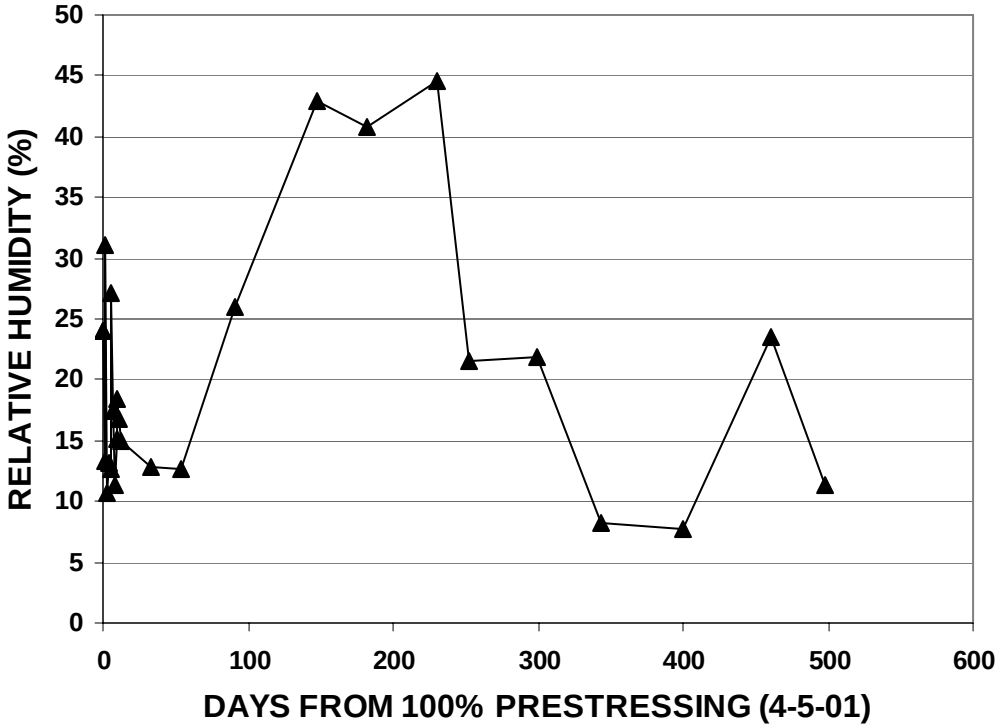

Figure 5.76 – Relative Humidity Readings for the Las Vegas Solid Beam Specimens

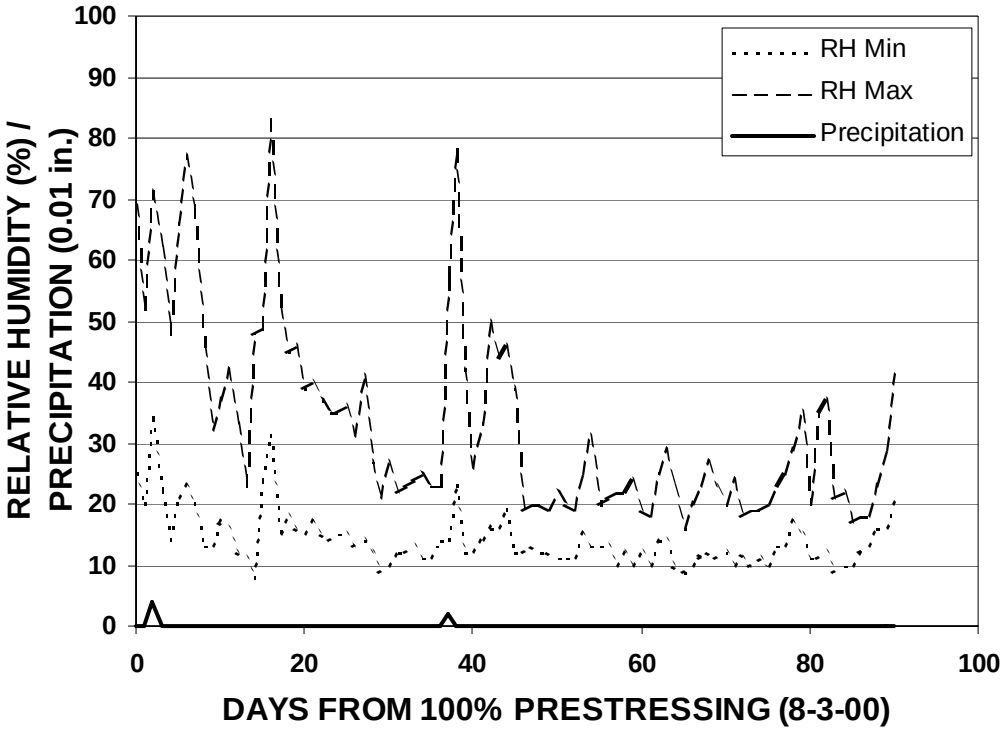

Figure 5.77 – Climate Data from the Las Vegas Airport for the Three Months Following Tensioning of the Solid Beams

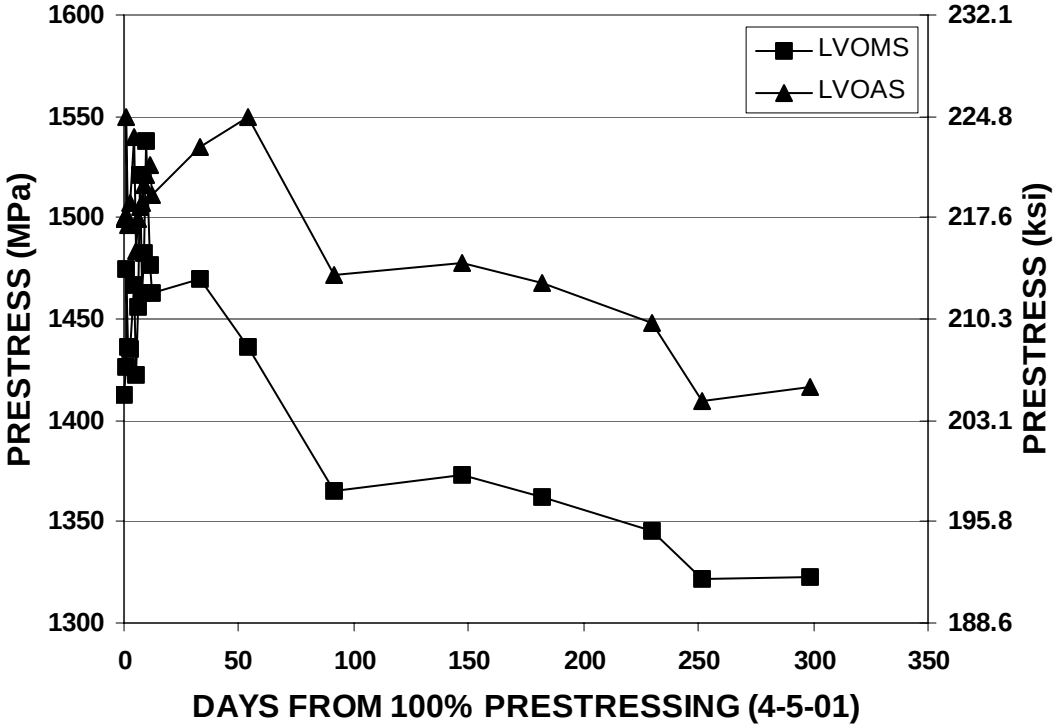

Figure 5.78 – Electric Gage Prestress Readings for the Las Vegas Solid Beams

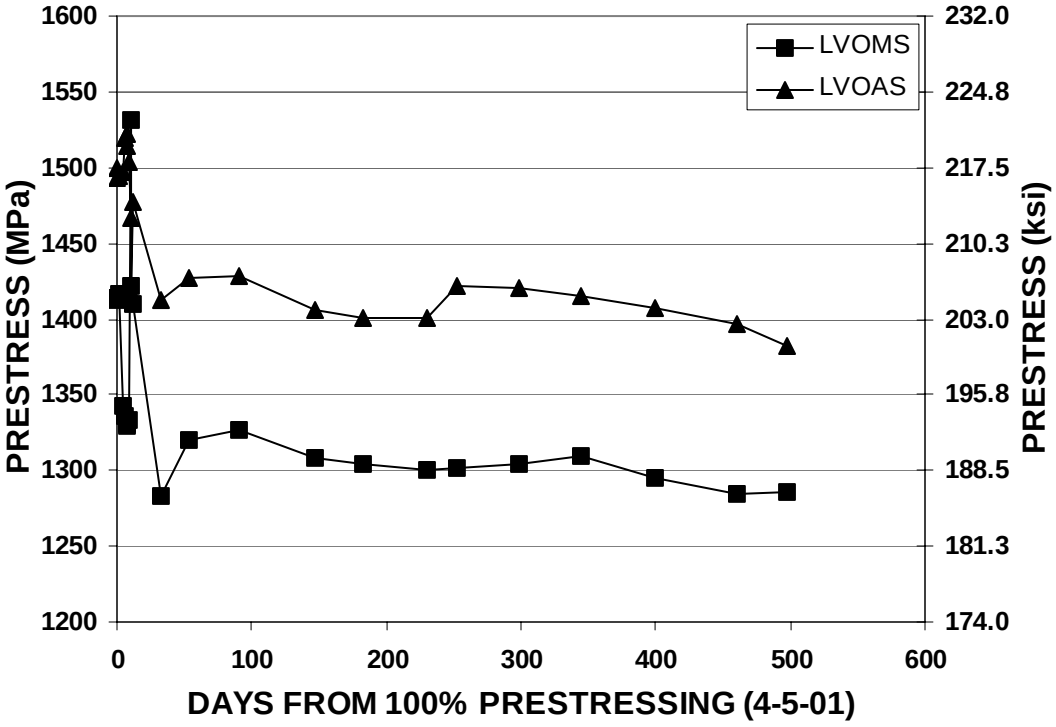

Figure 5.79 – Mechanical Gage Prestress Readings for the Las Vegas Solid Beams

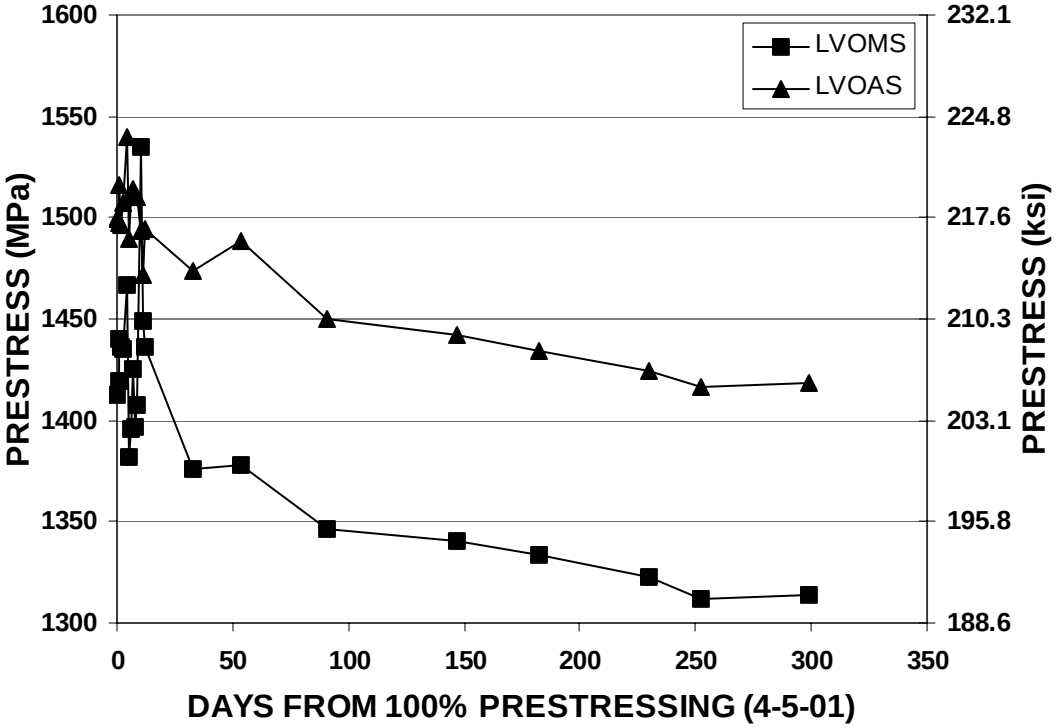

Figure 5.80 – Average Gage Readings for the Las Vegas Solid Beams

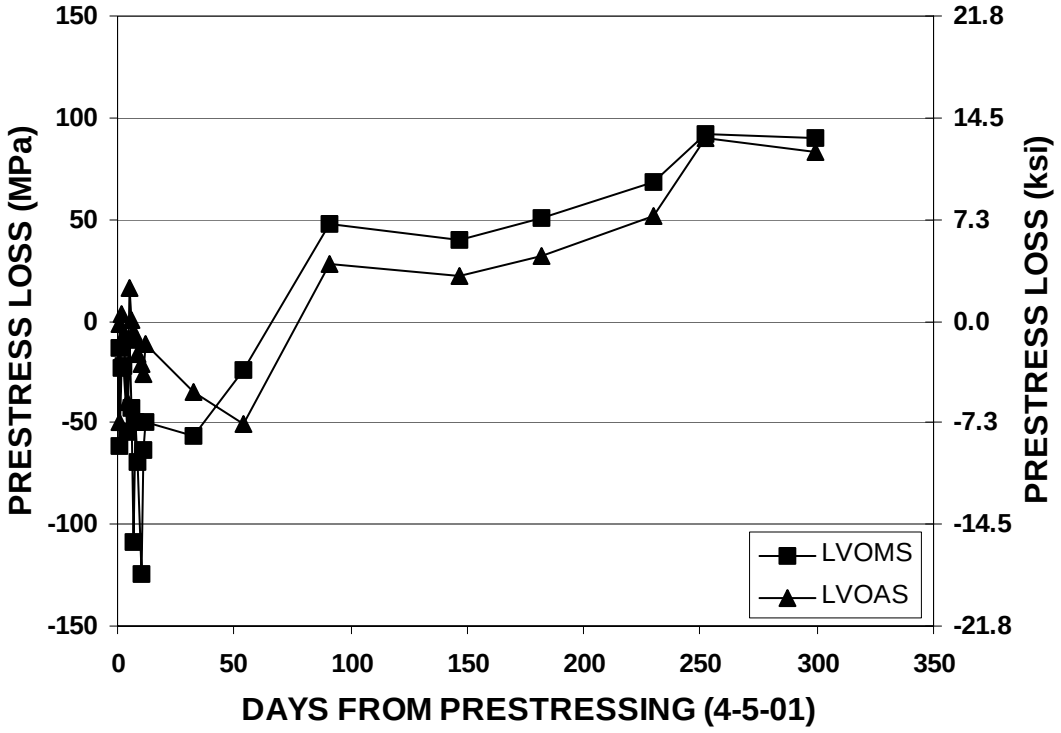

Figure 5.81 – Electric Gage Prestress Loss Readings for the Las Vegas Solid Beams

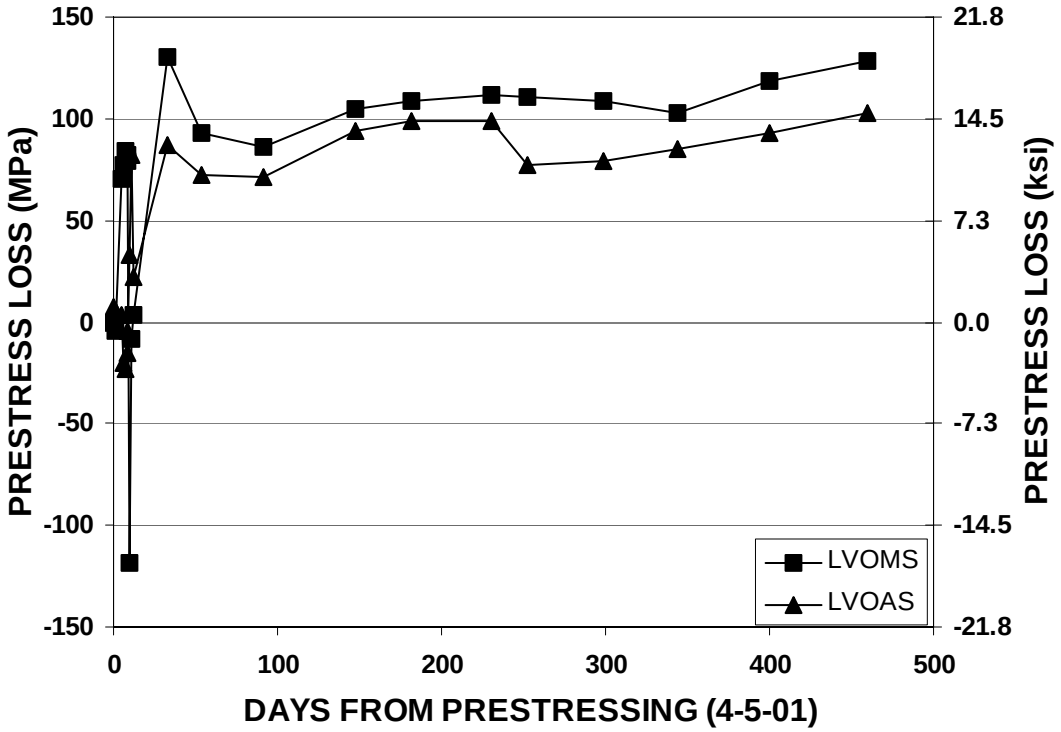

Figure 5.82 – Mechanical Gage Prestress Loss Readings for the Las Vegas Solid Beams

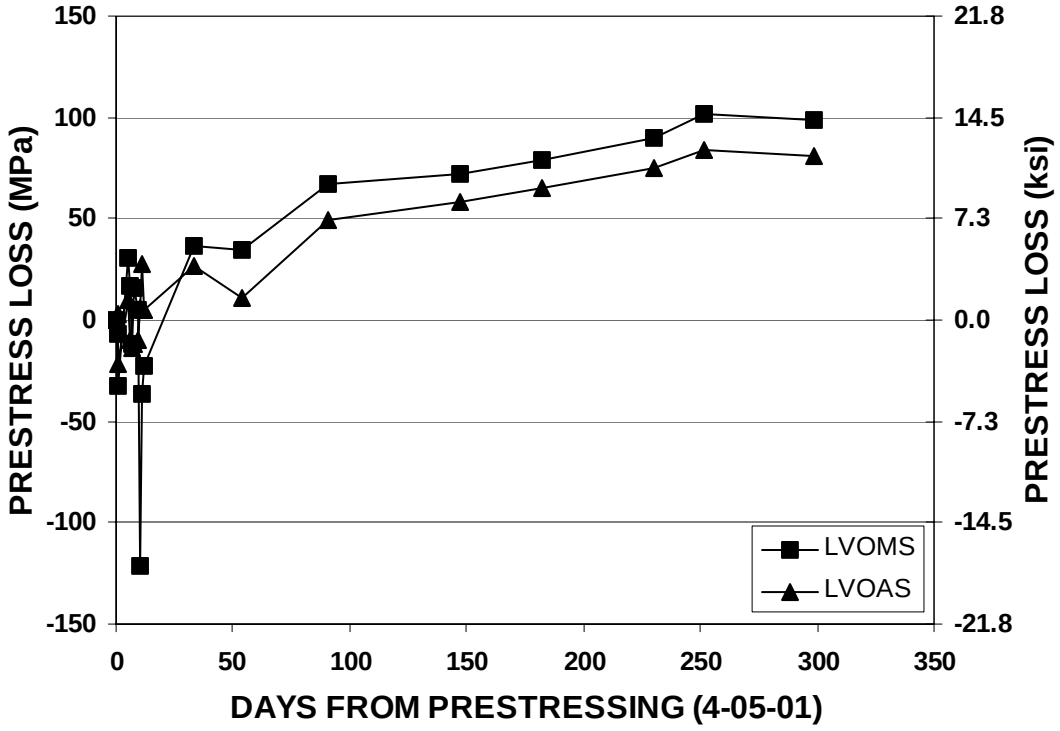

Figure 5.83 – Average Gage Prestress Loss Readings for the Las Vegas Solid Beams

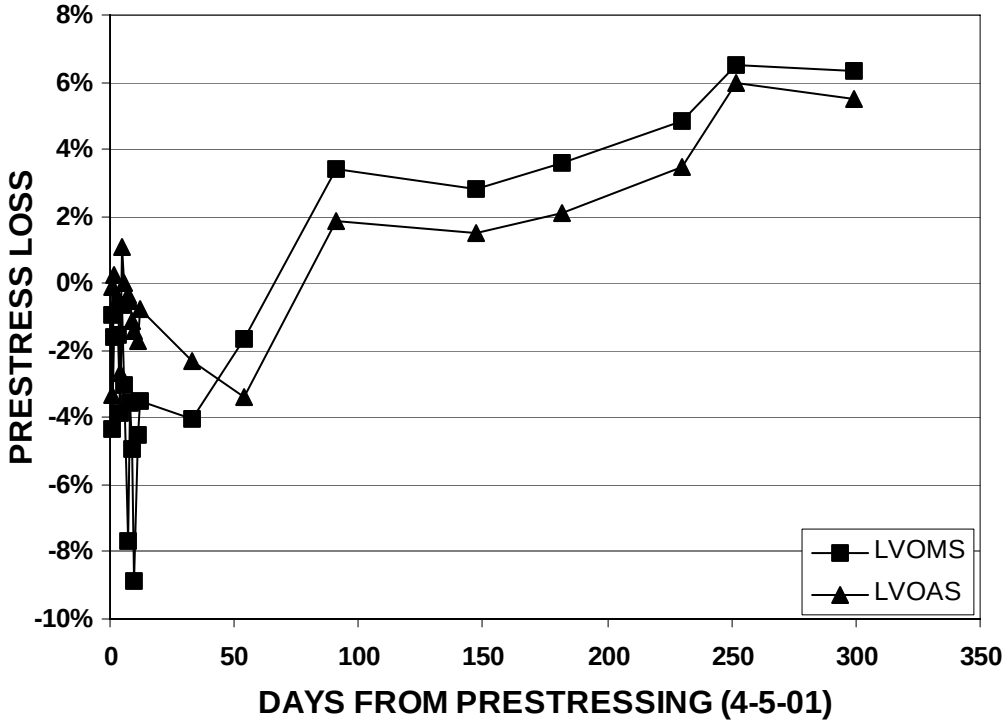

Figure 5.84 – Electric Gage Percentage Loss Readings for the Las Vegas Solid Beams

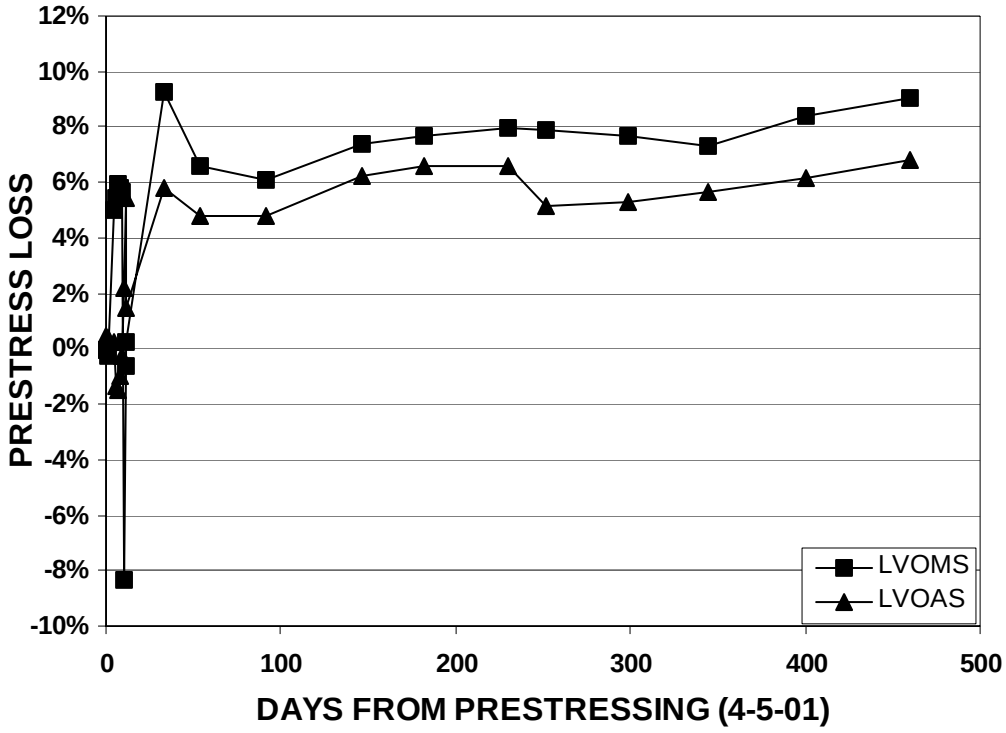

Figure 5.85 – Mechanical Gage Percentage Loss Readings for the Las Vegas Solid Beams

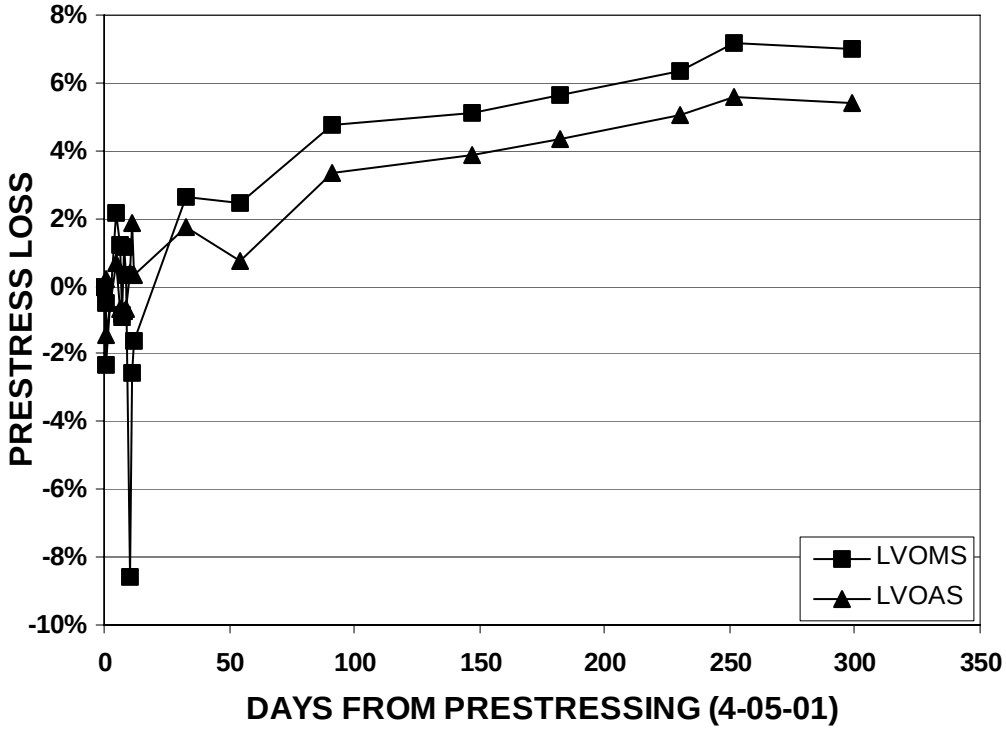

Figure 5.86 – Average Gage Percentage Loss Readings for the Las Vegas Solid Beams

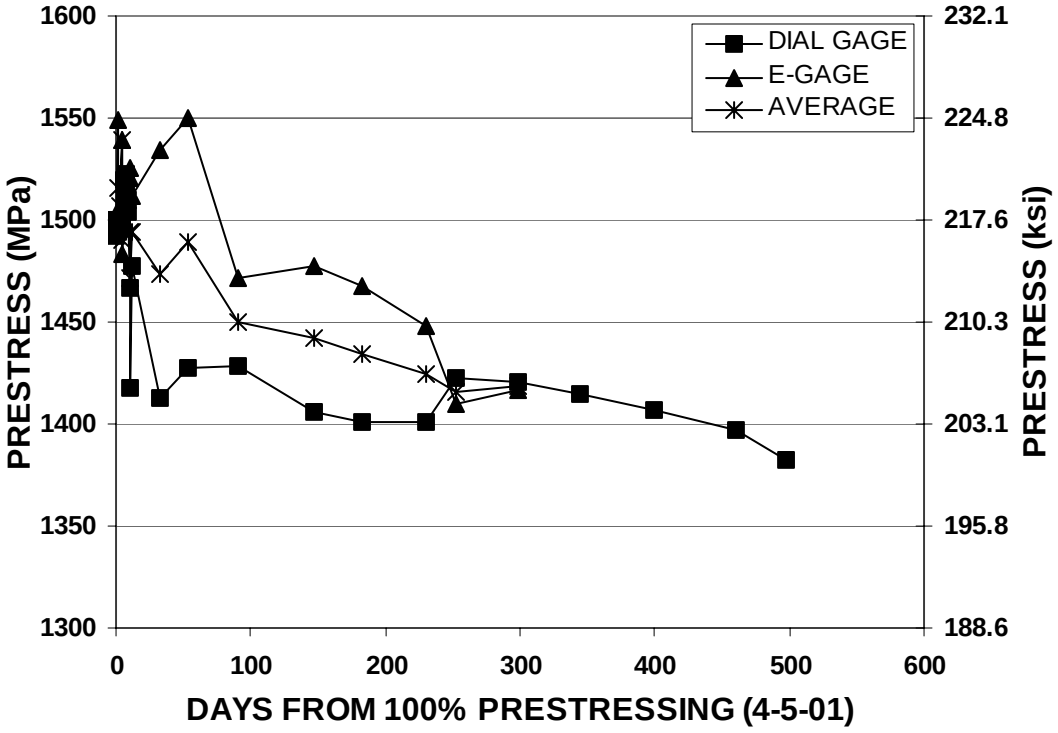

Figure 5.87 – LVOMS Gage Readings

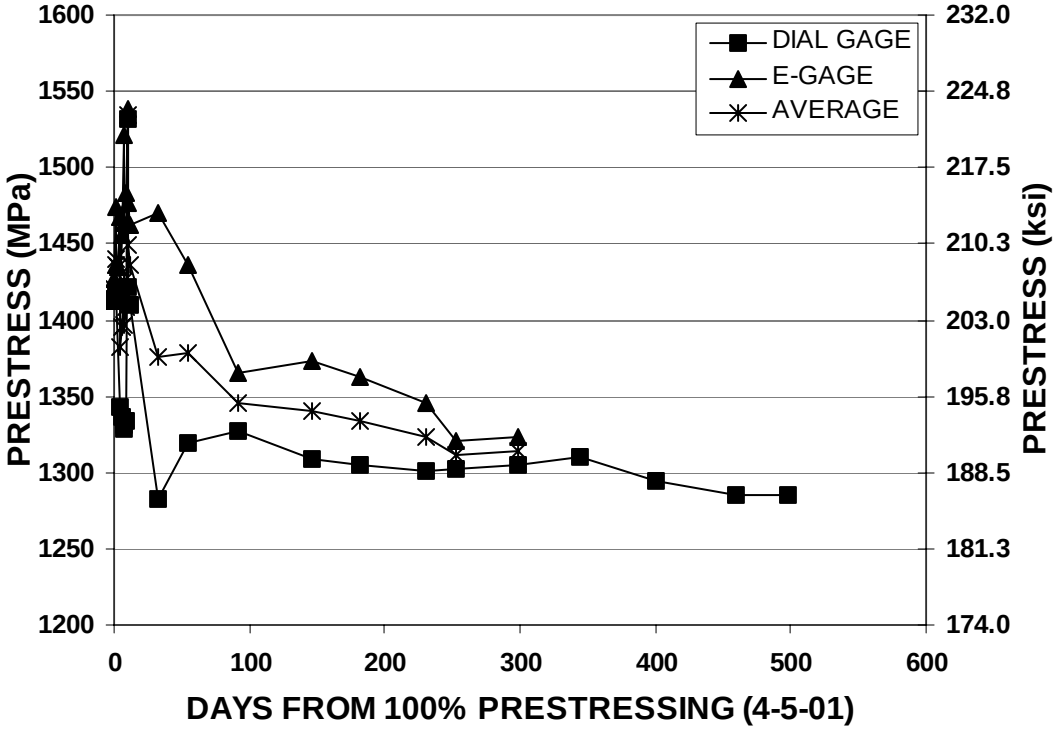

Figure 5.88 – LVOAS Gage Readings

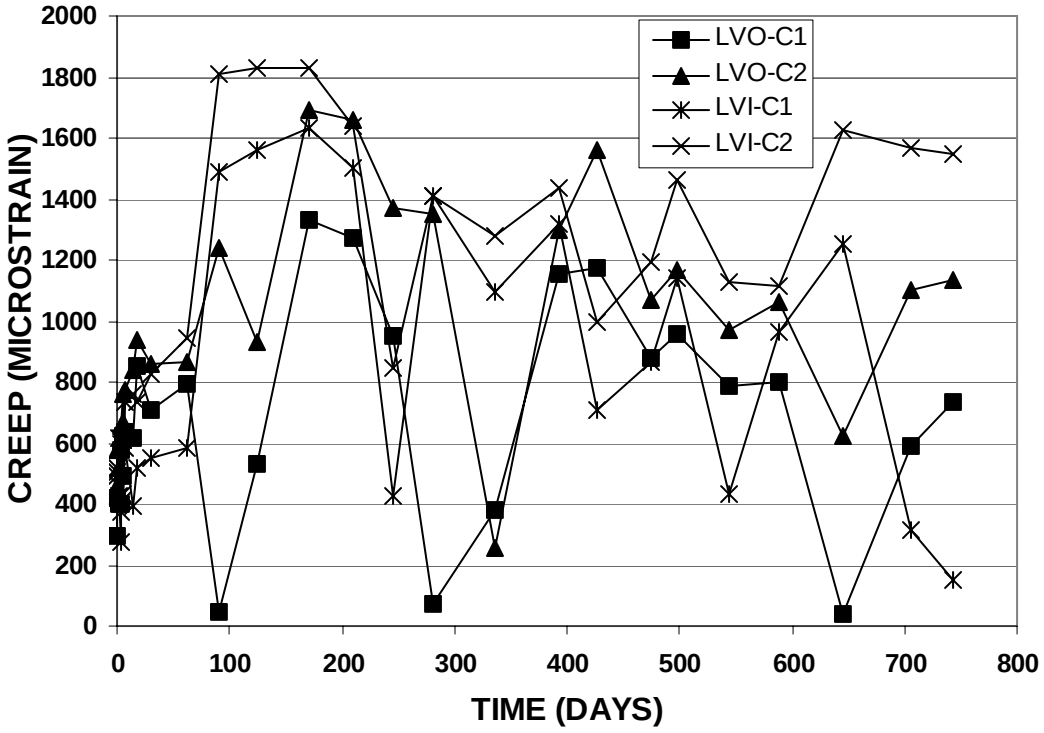

Figure 5.89 – Las Vegas Box Girder Creep Cylinders

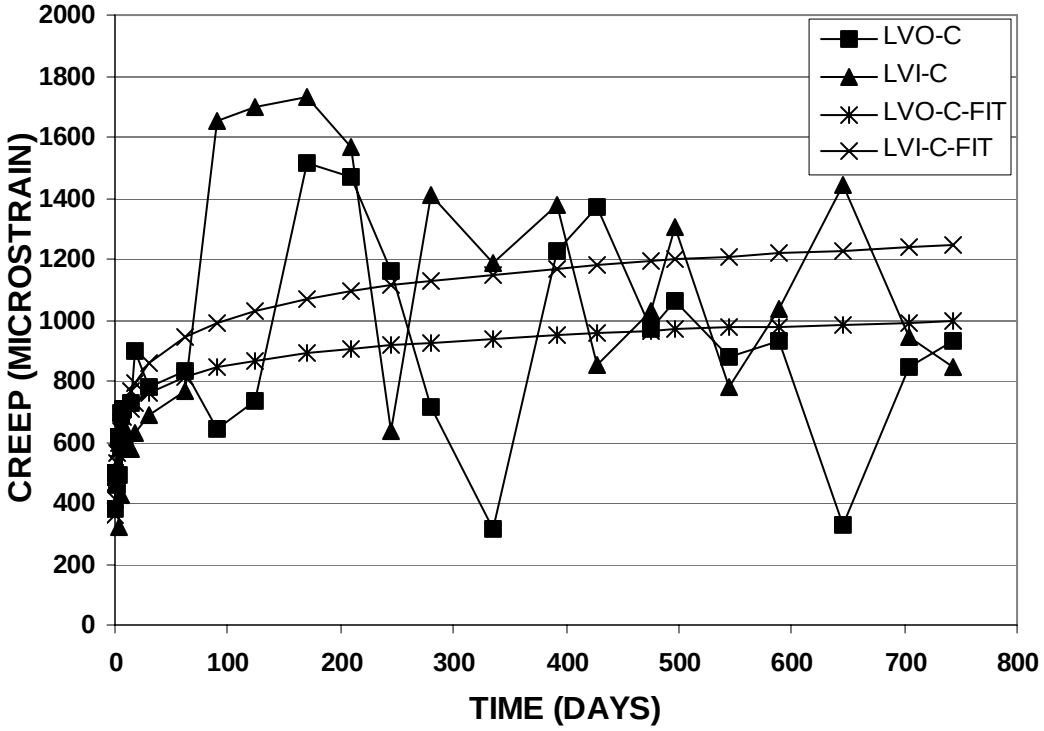

Figure 5.90 – Las Vegas Box Girder Cylinder Creep Average and Log-Fit

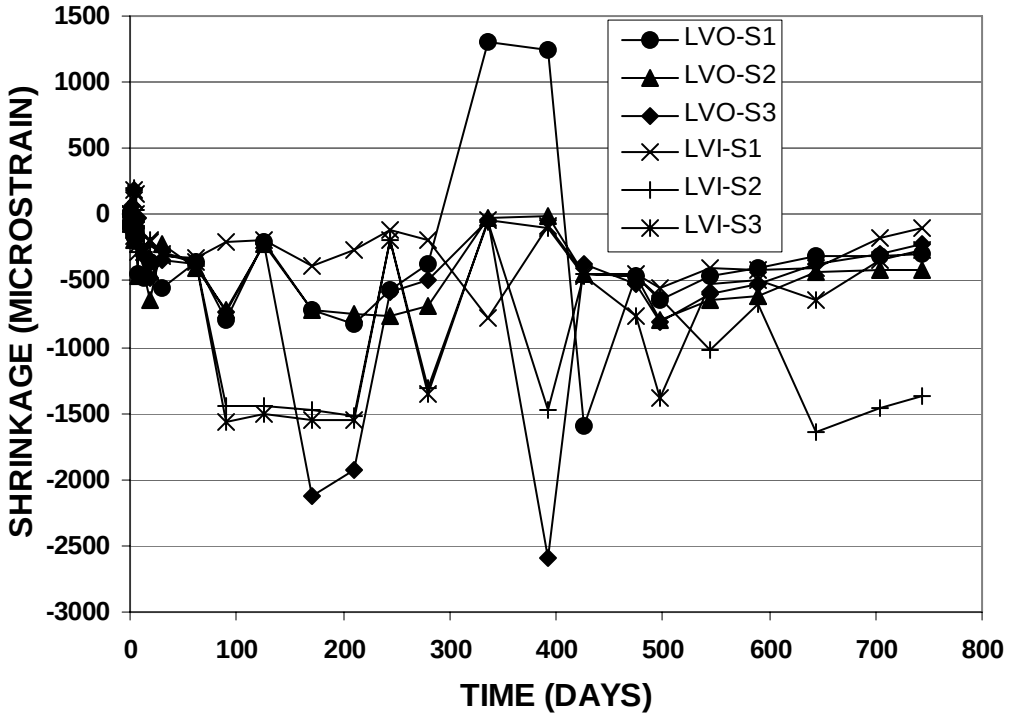

Figure 5.91 – Las Vegas Box Girder Shrinkage Cylinders

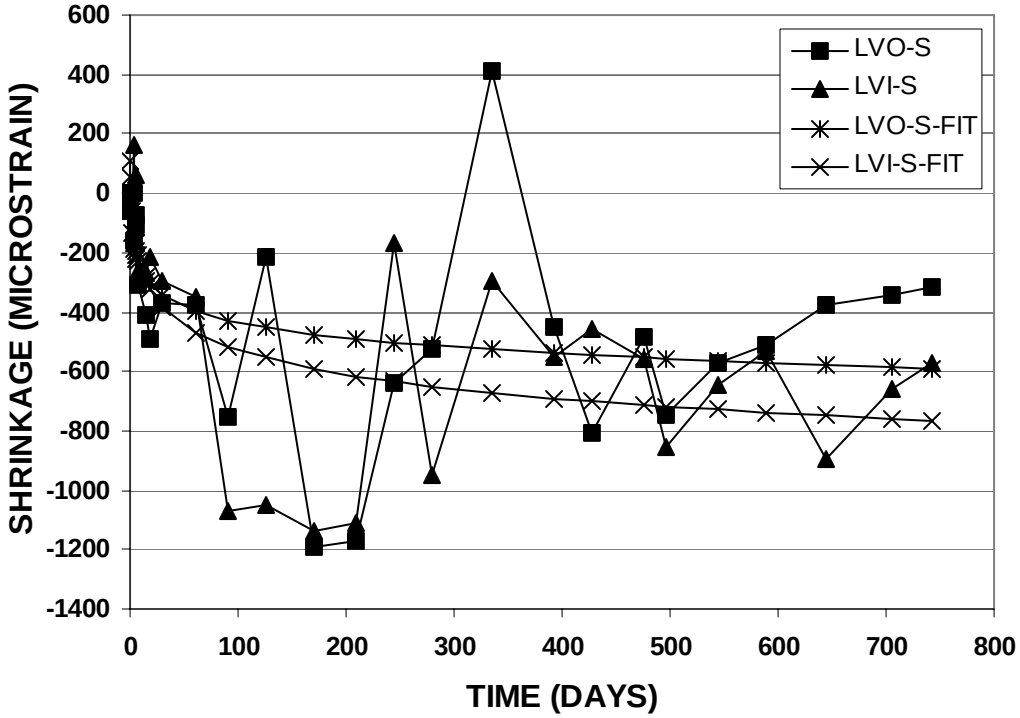

Figure 5.92 – Las Vegas Box Girder Shrinkage Cylinder Average and Log-Fit

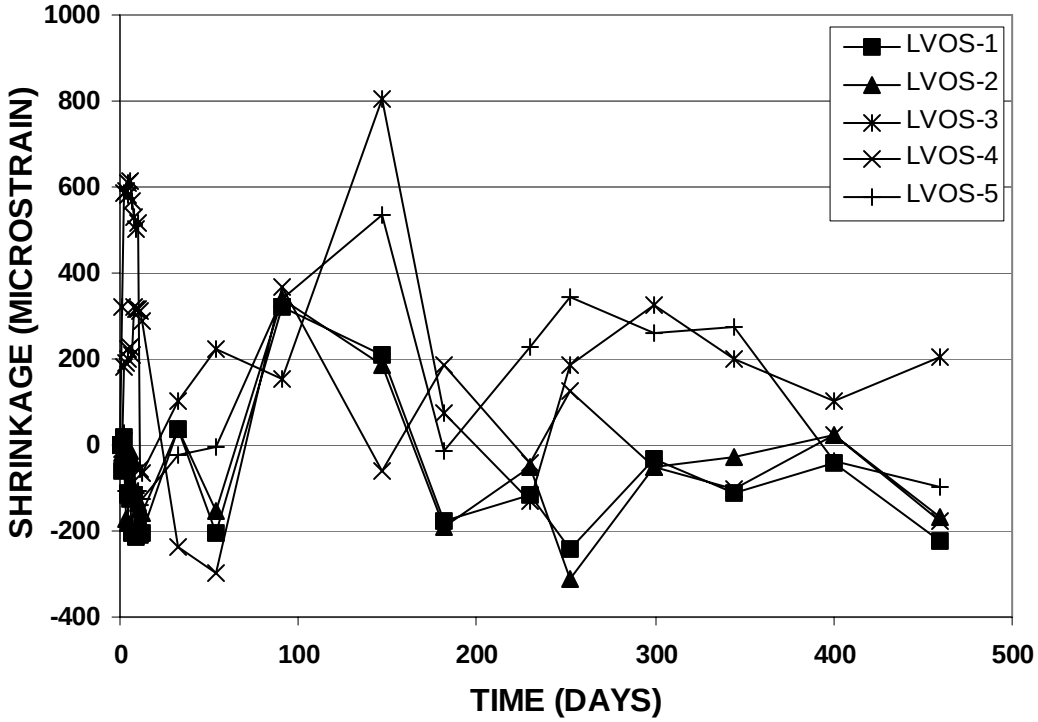

Figure 5.93 – Las Vegas Solid Beam Shrinkage Cylinders

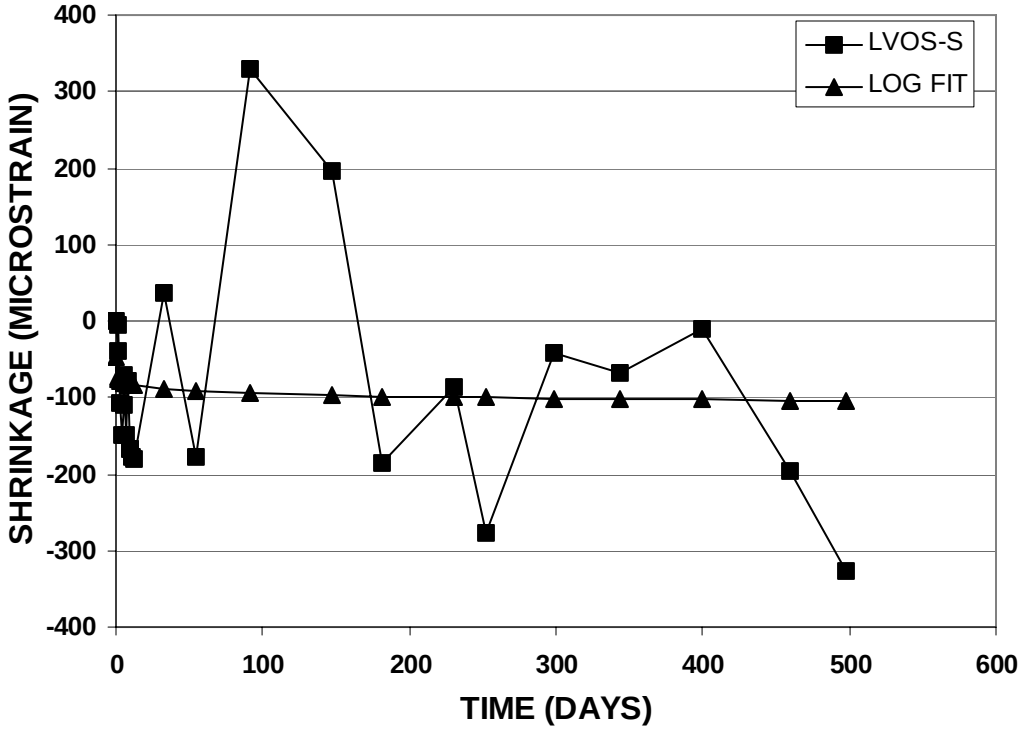

Figure 5.94 – Las Vegas Solid Beam Shrinkage Cylinder Average and Log-Fit

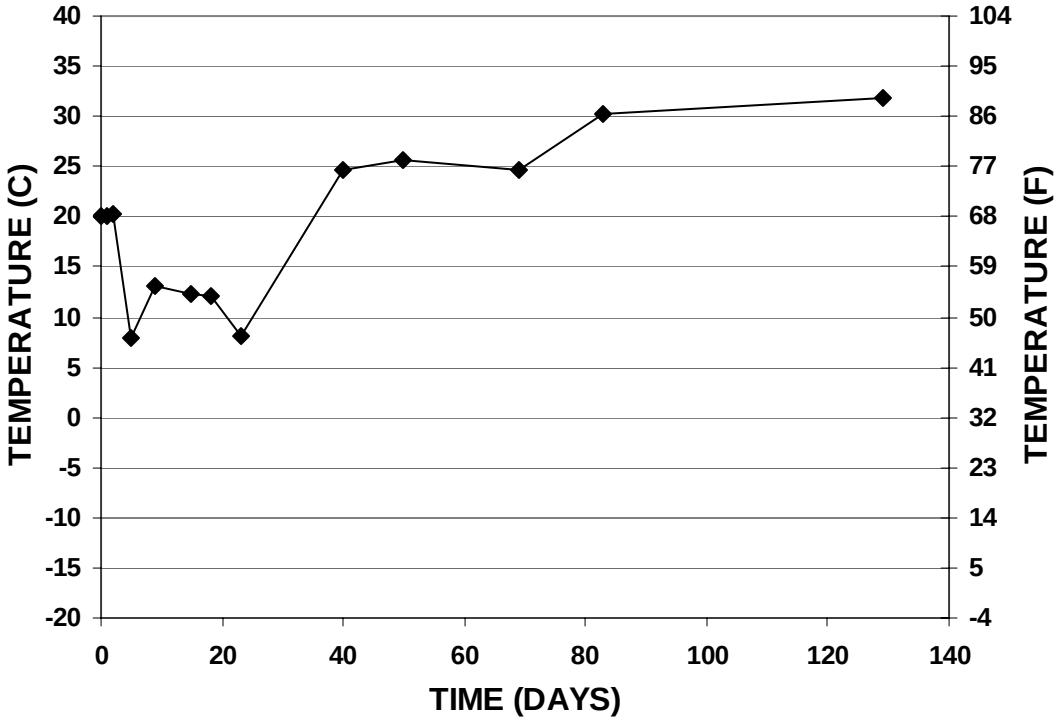

Figure 5.95 – Supplemental Las Vegas Outdoor Shrinkage Cylinders Temperature Readings

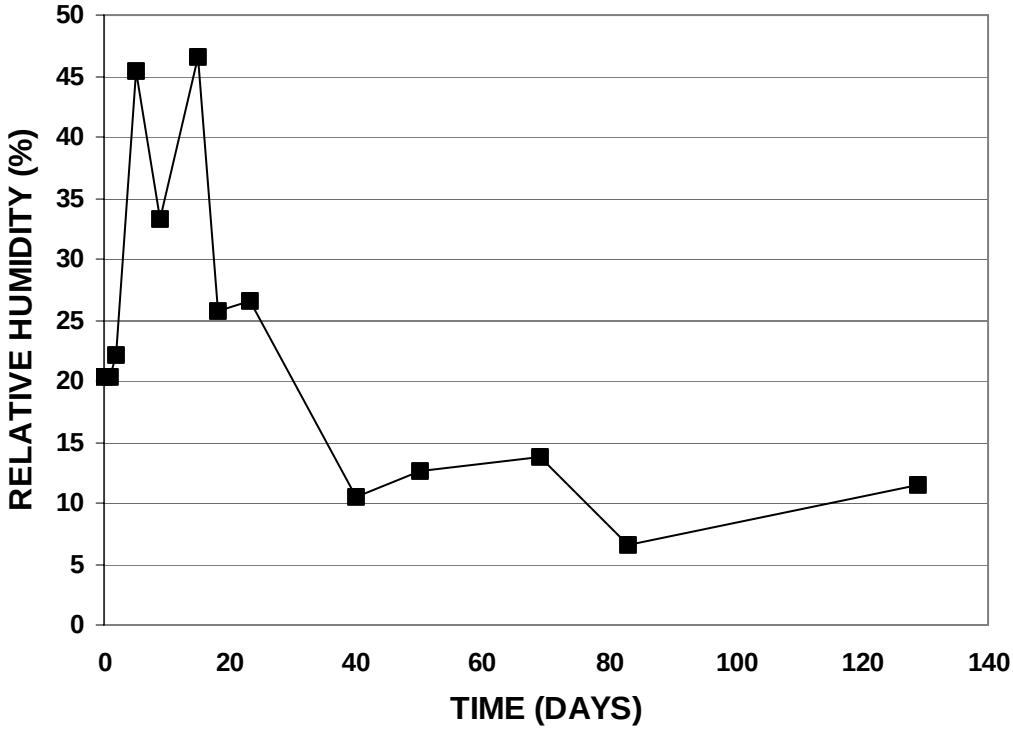

Figure 5.96 – Supplemental Las Vegas Outdoor Shrinkage Cylinders Relative Humidity Readings

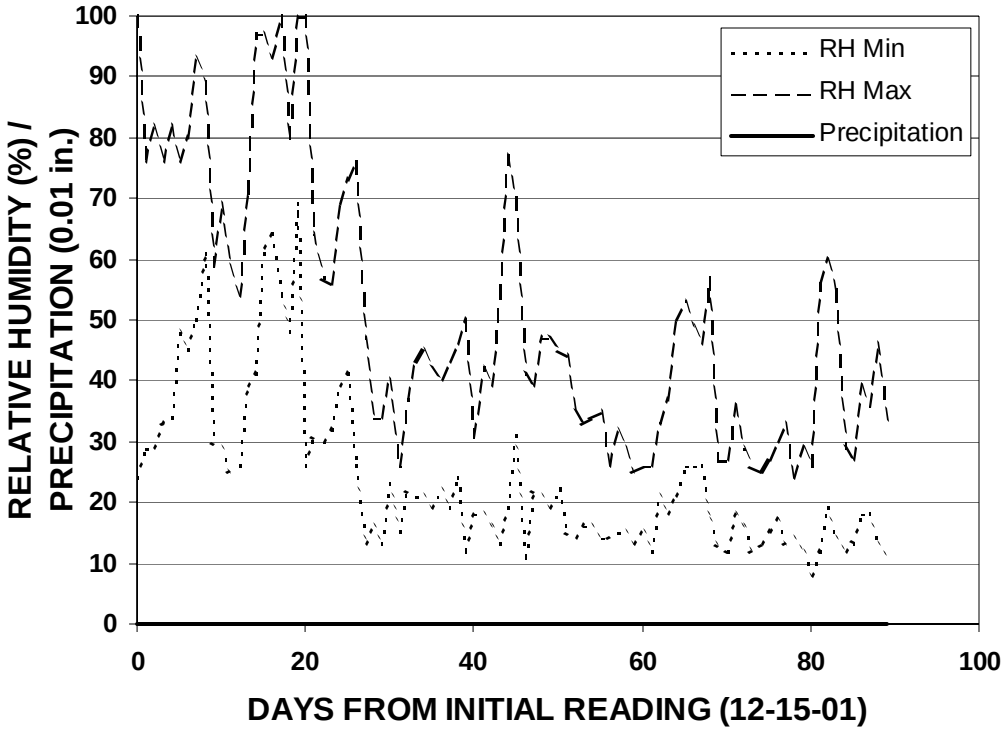

Figure 5.97 – Supplemental Shrinkage Cylinders Climate Data from the Las Vegas Airport for the First Three Months

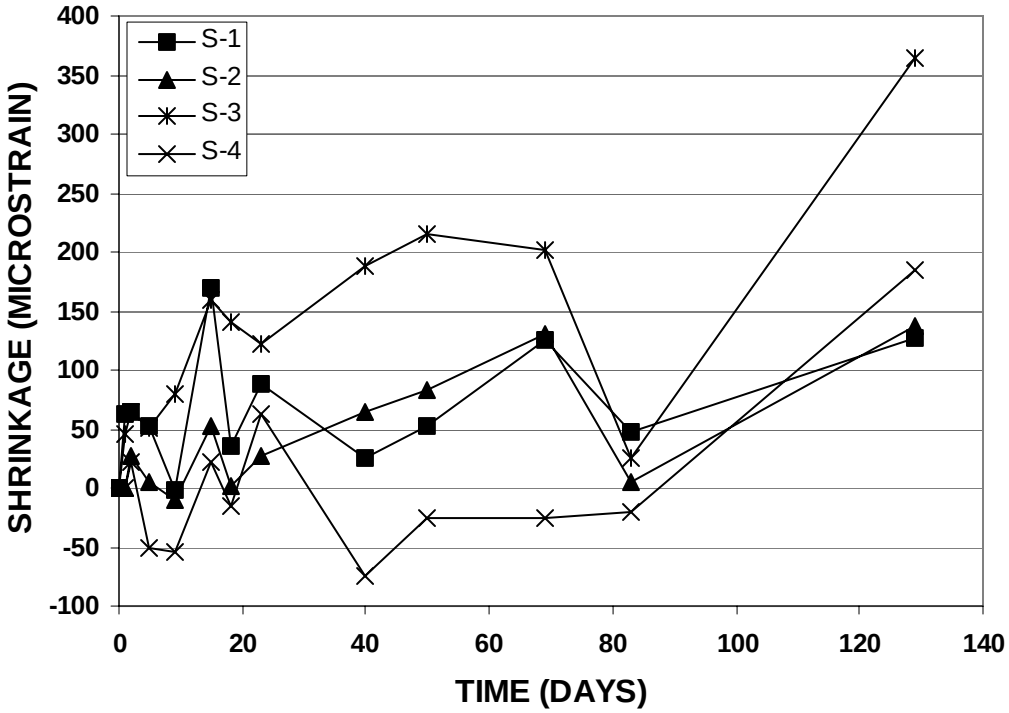

Figure 5.98 – Supplemental Las Vegas Outdoor Shrinkage Cylinders

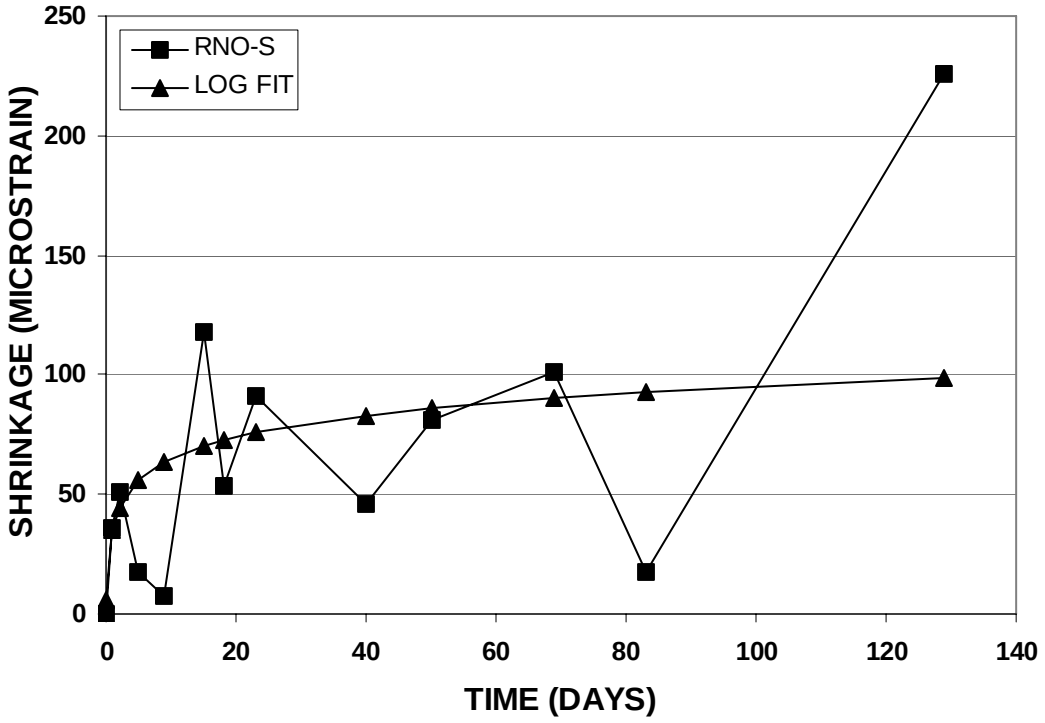

Figure 5.99 – Supplemental Las Vegas Outdoor Shrinkage Cylinder Average and Log-Fit

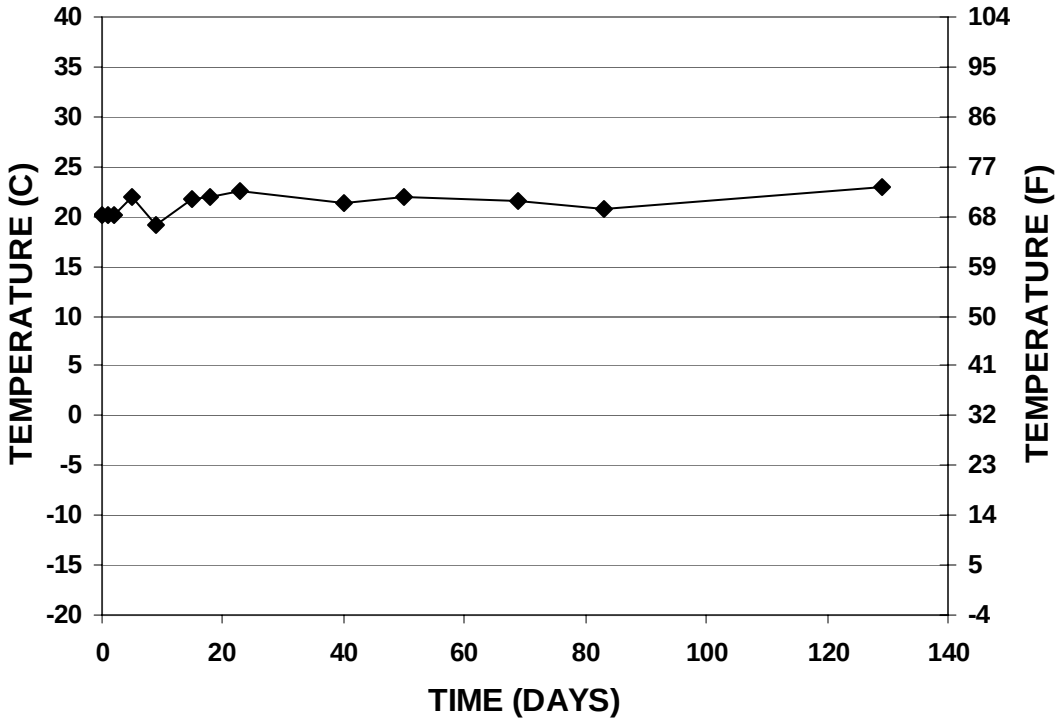

Figure 5.100 – Supplemental Las Vegas Indoor Shrinkage Cylinder Temperature Readings

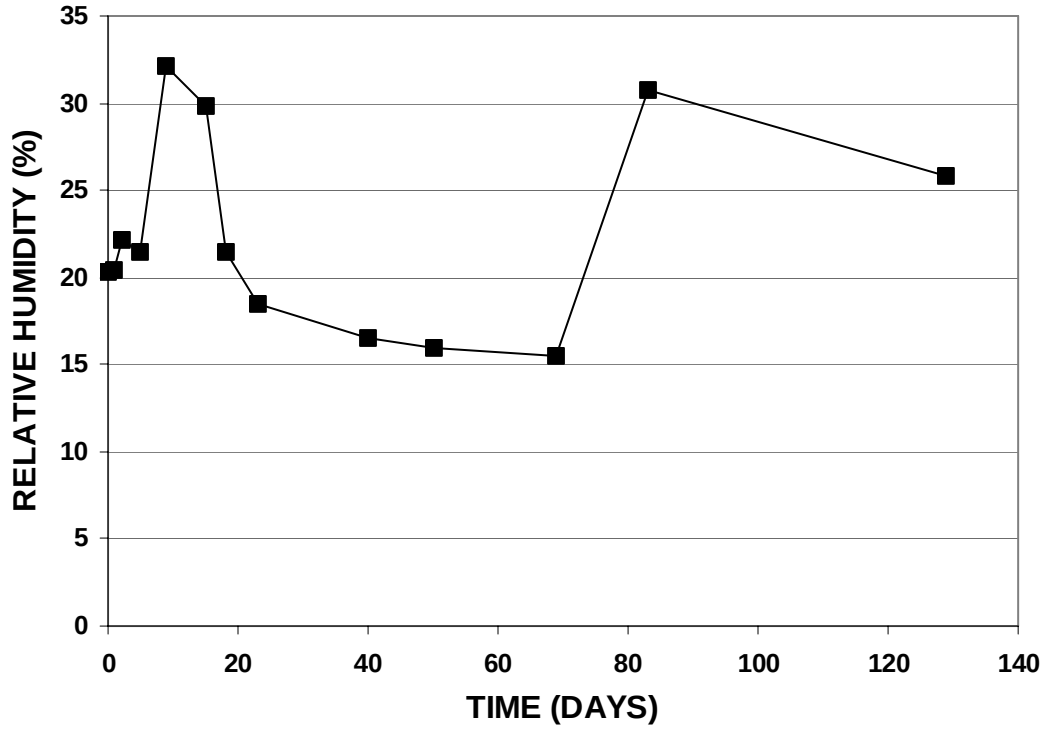

Figure 5.101 – Supplemental Las Vegas Indoor Shrinkage Cylinder Relative Humidity Readings

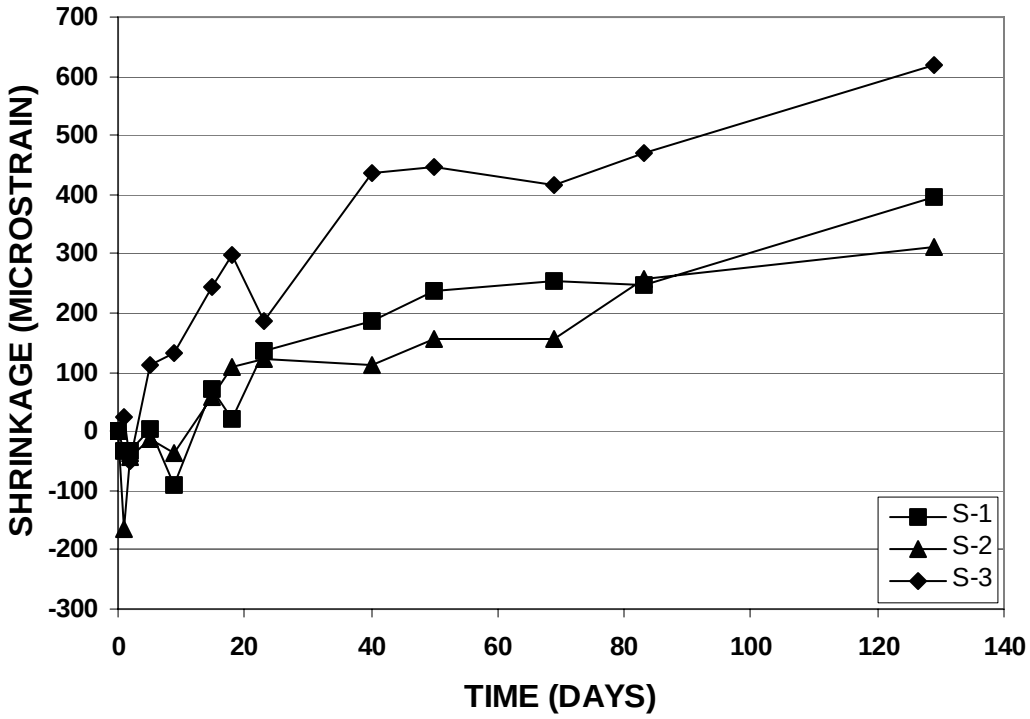

Figure 5.102 – Supplemental Las Vegas Indoor Shrinkage Cylinders

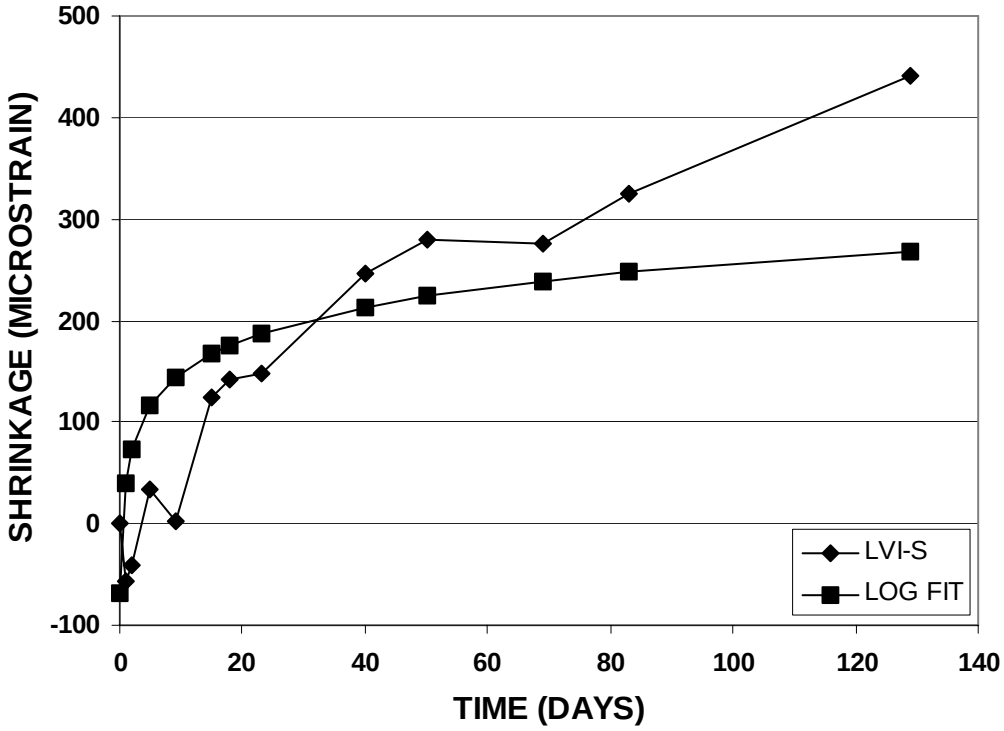

Figure 5.103 – Supplemental Las Vegas Indoor Shrinkage Cylinder Average and Log-Fit

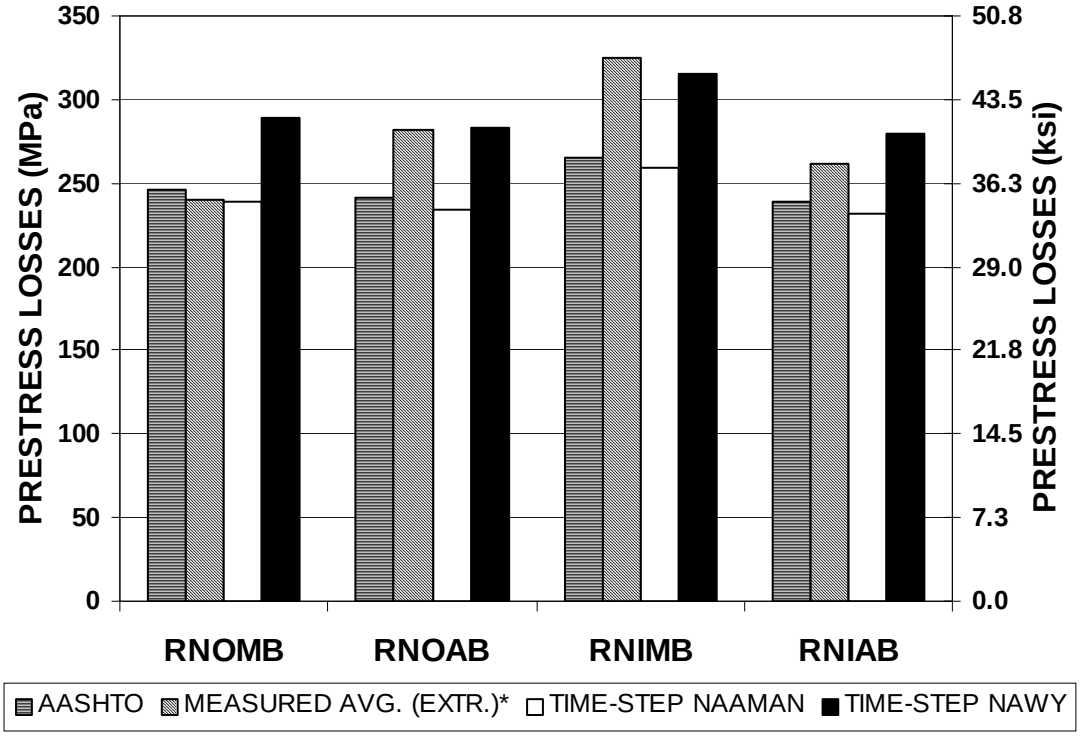

Figure 5.104 – Lifetime Loss Comparison – Reno Box Girders

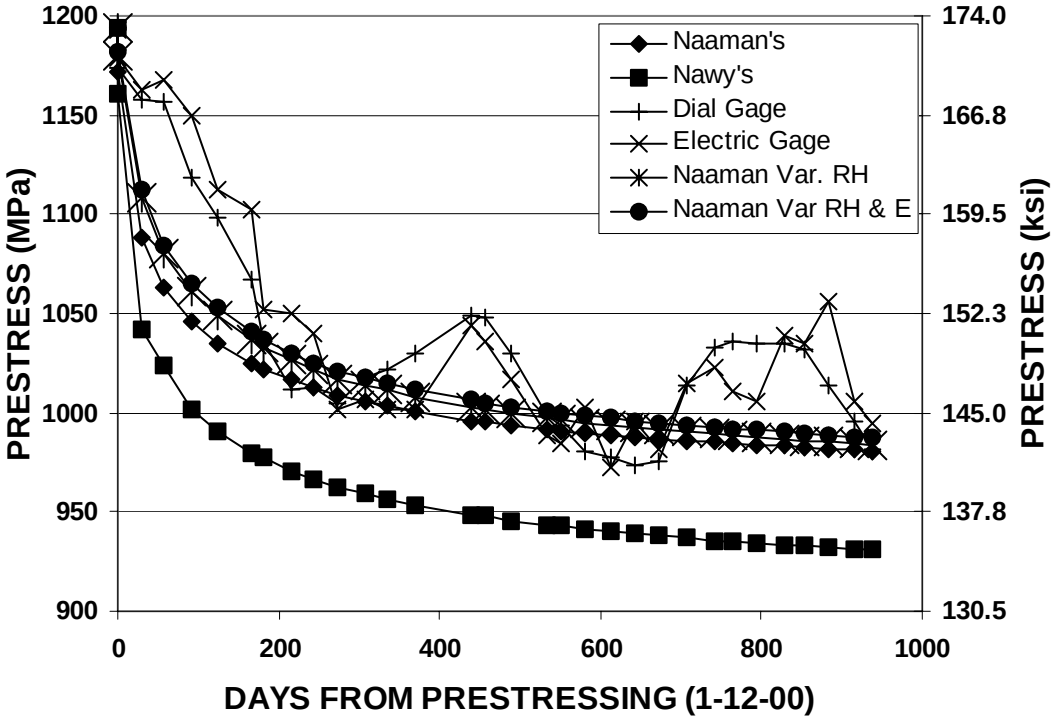

Figure 5.105 – Prediction Method Comparison - RNOMB

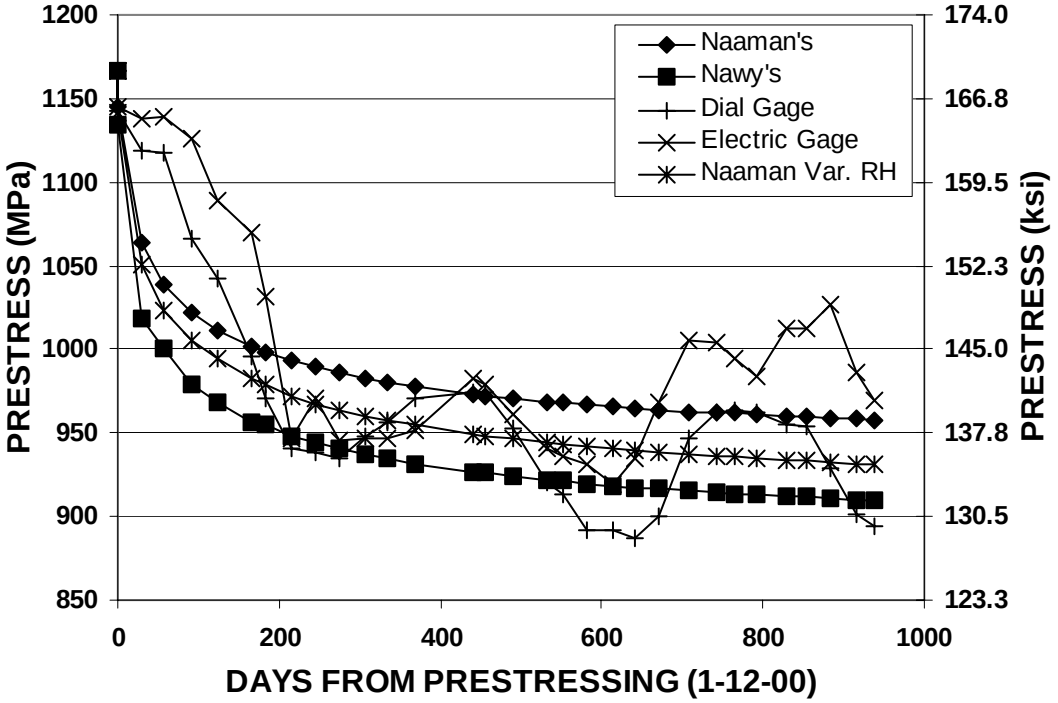

Figure 5.106 – Prediction Method Comparison - RNOAB

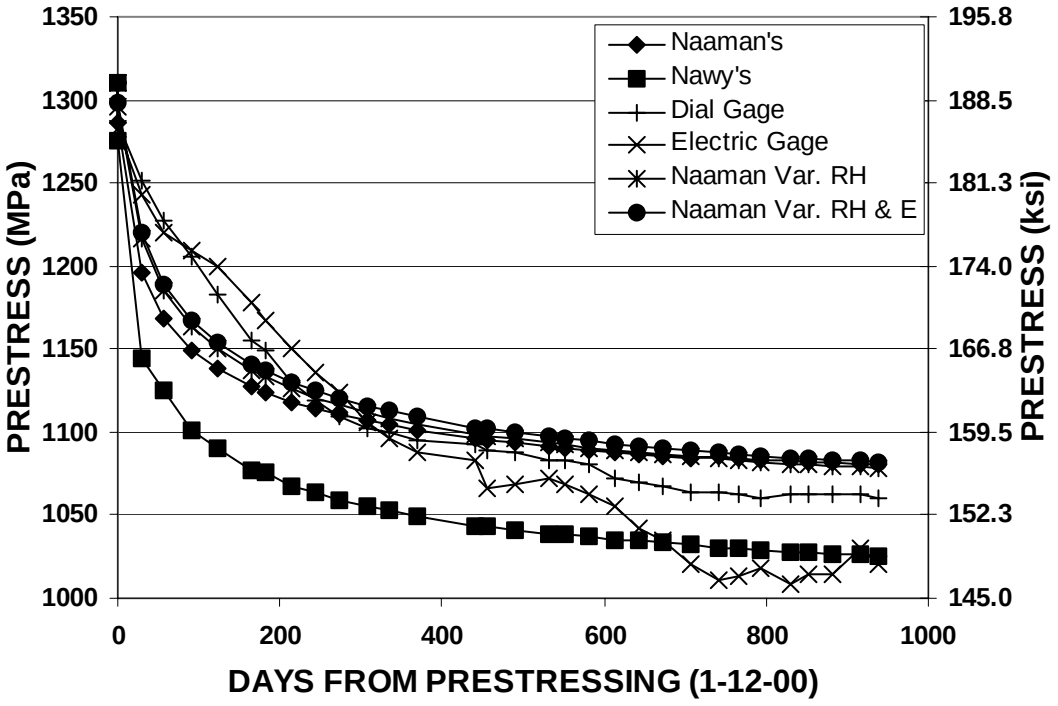

Figure 5.107 – Prediction Method Comparison - RNIMB

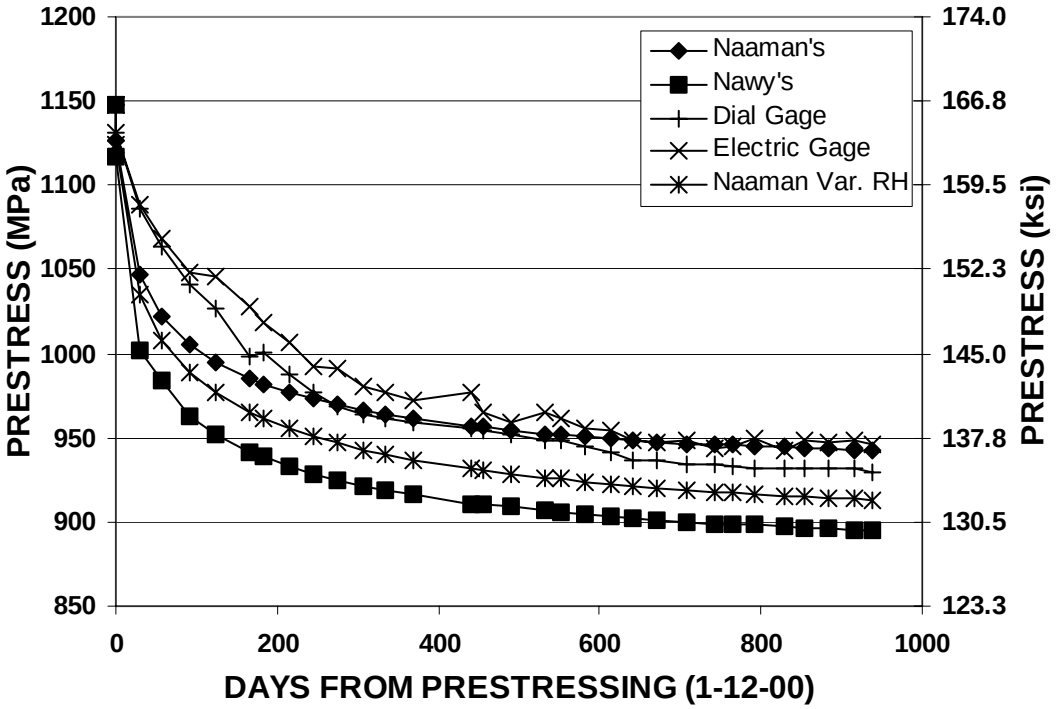

Figure 5.108 – Prediction Method Comparison - RNIAB

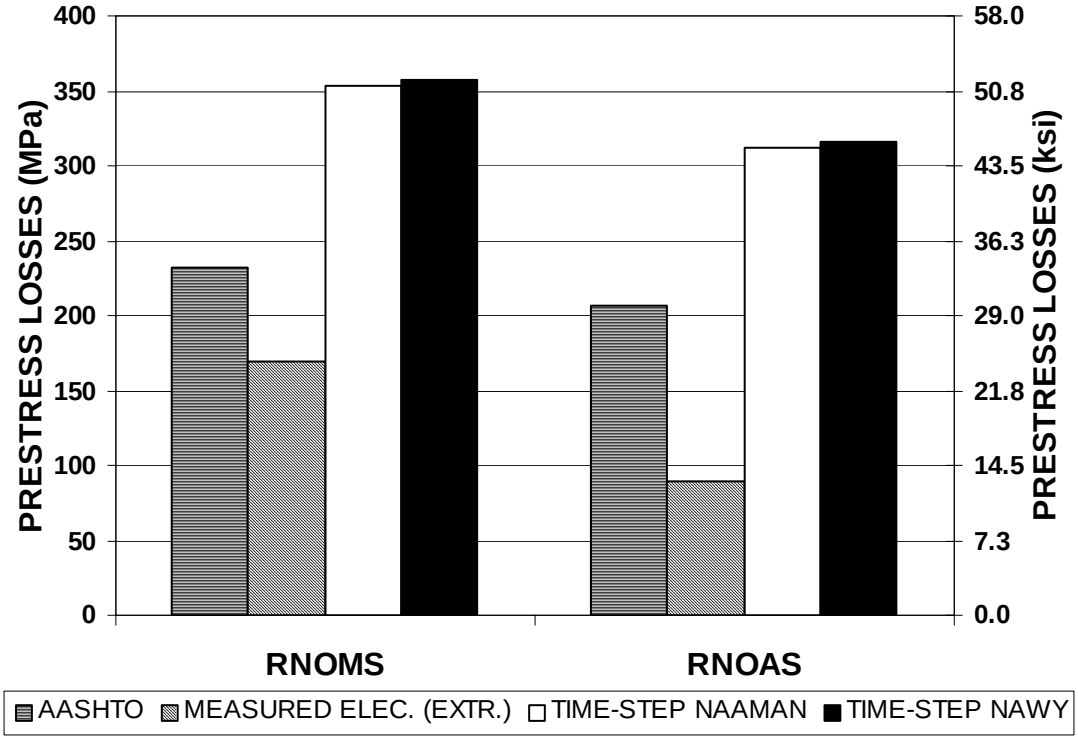

Figure 5.109 – Lifetime Loss Comparison – Reno Solid Beams

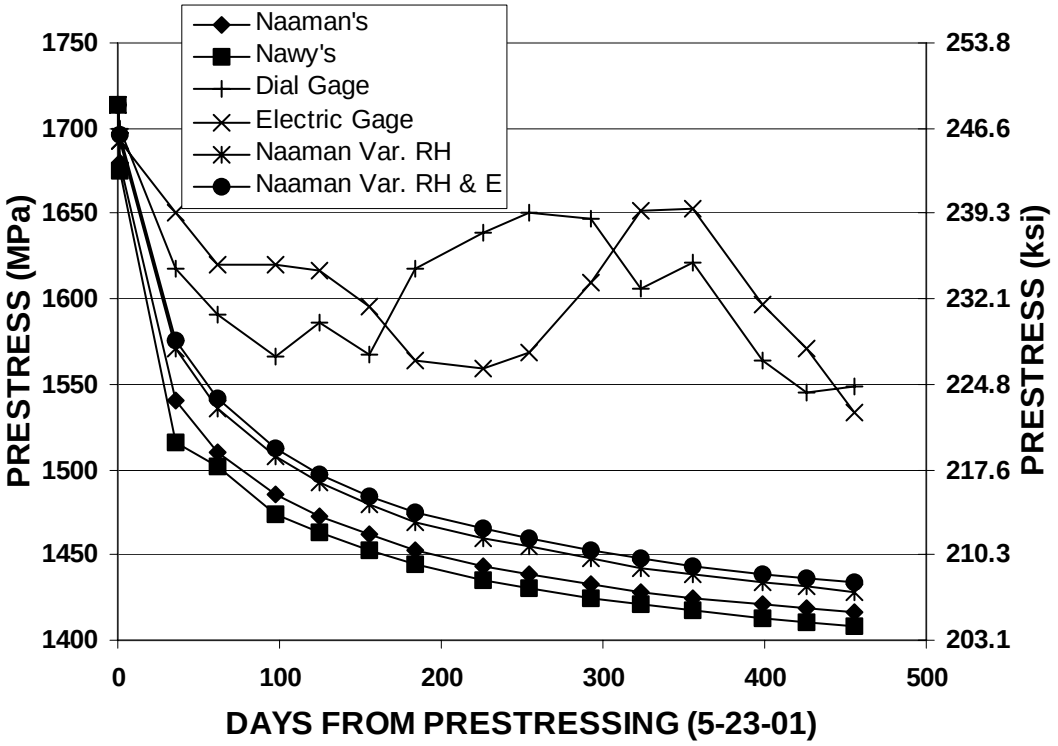

Figure 5.110 – Prediction Method Comparison - RNOMS

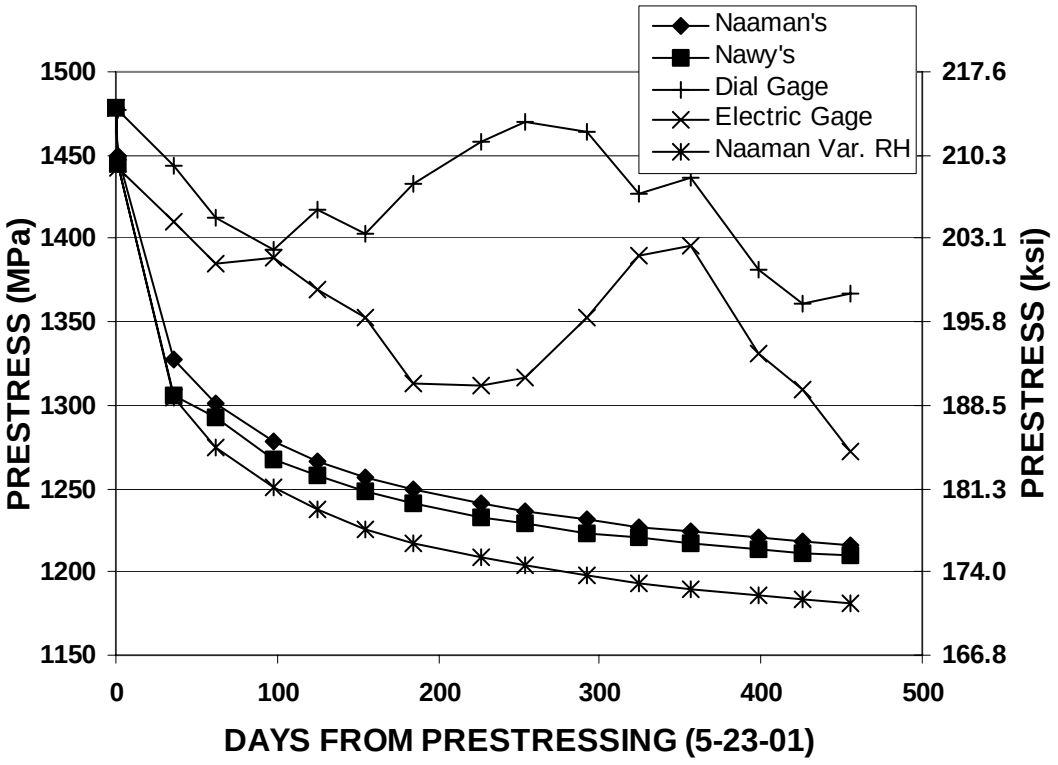

Figure 5.111 – Prediction Method Comparison - RNOAS

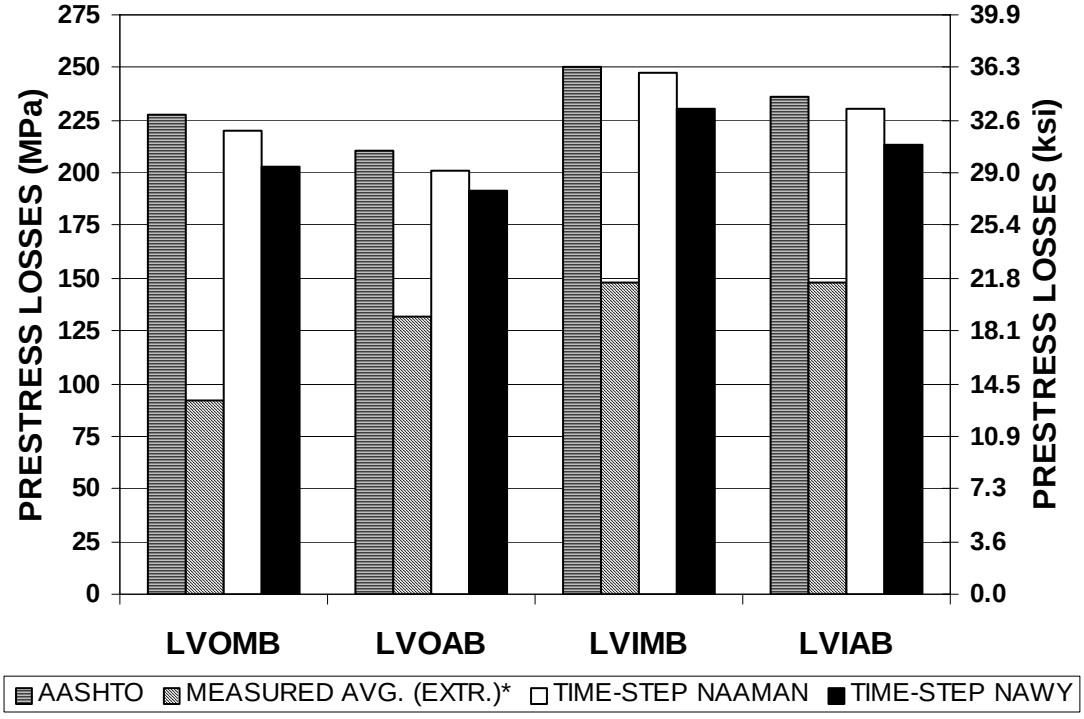

Figure 5.112 – Lifetime Loss Comparison – Las Vegas Box Girders

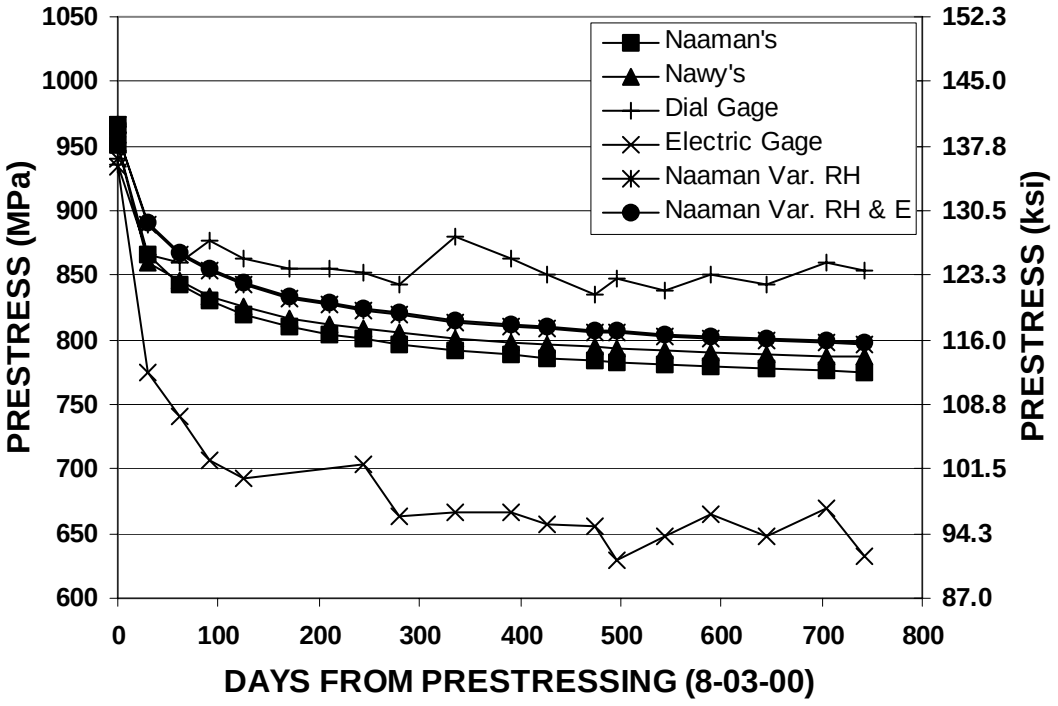

Figure 5.113 – Prediction Method Comparison - LVOMB

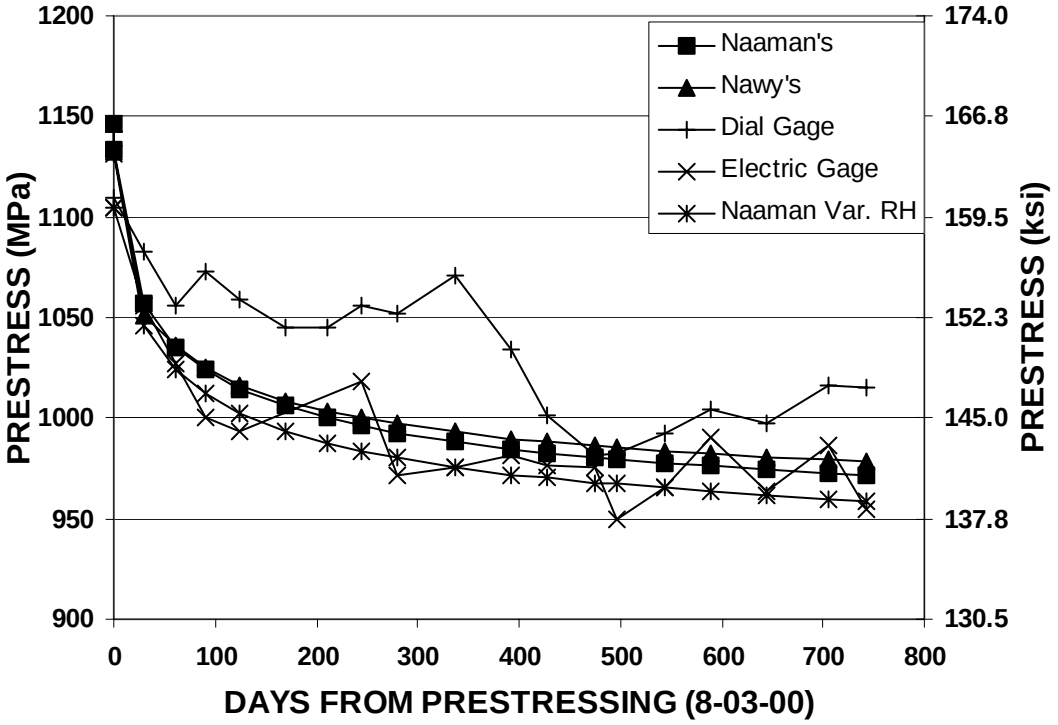

Figure 5.114 – Prediction Method Comparison – LVOAB

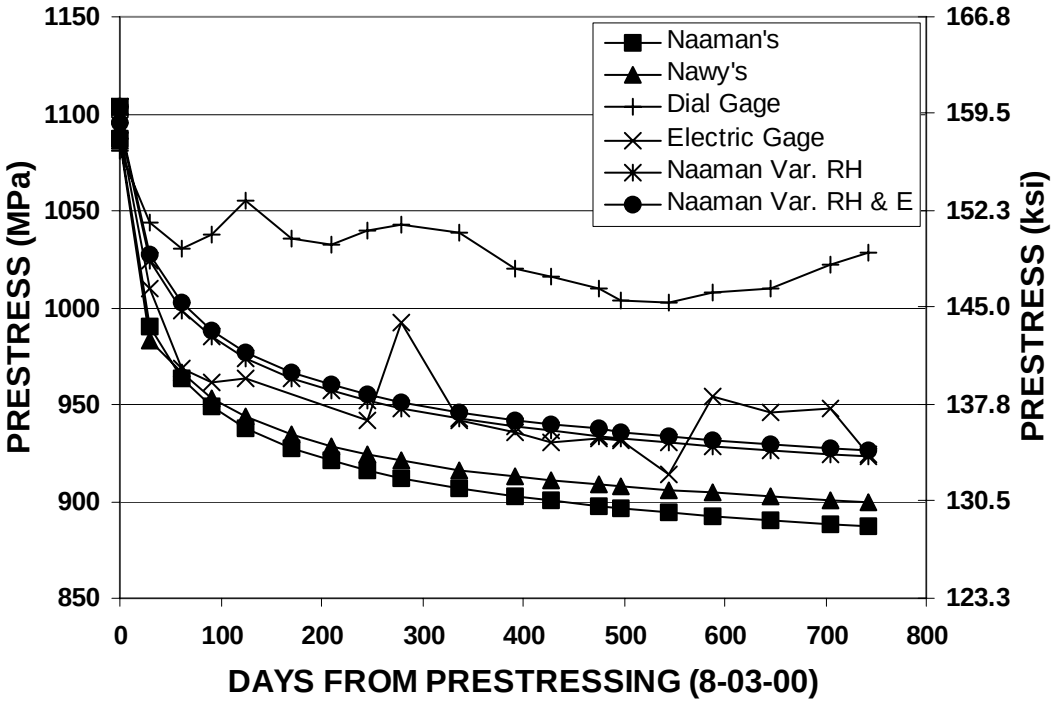

Figure 5.115 – Prediction Method Comparison - LVIMB

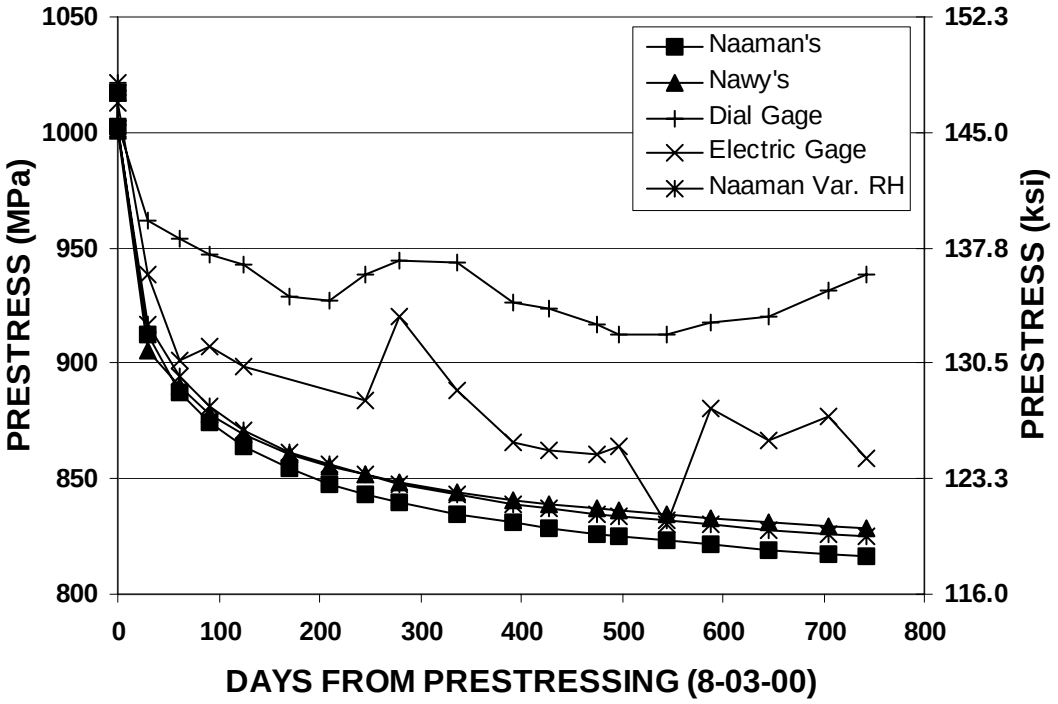

Figure 5.116 – Prediction Method Comparison – LVIAB

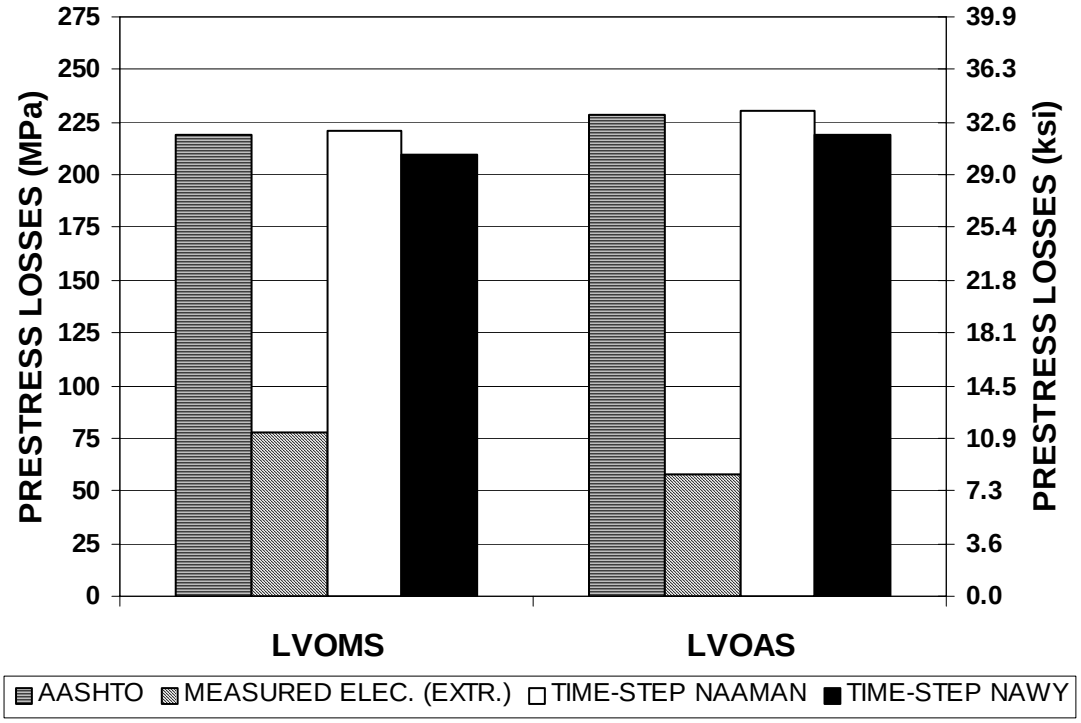

Figure 5.117 – Lifetime Loss Comparison – Las Vegas Solid Beams

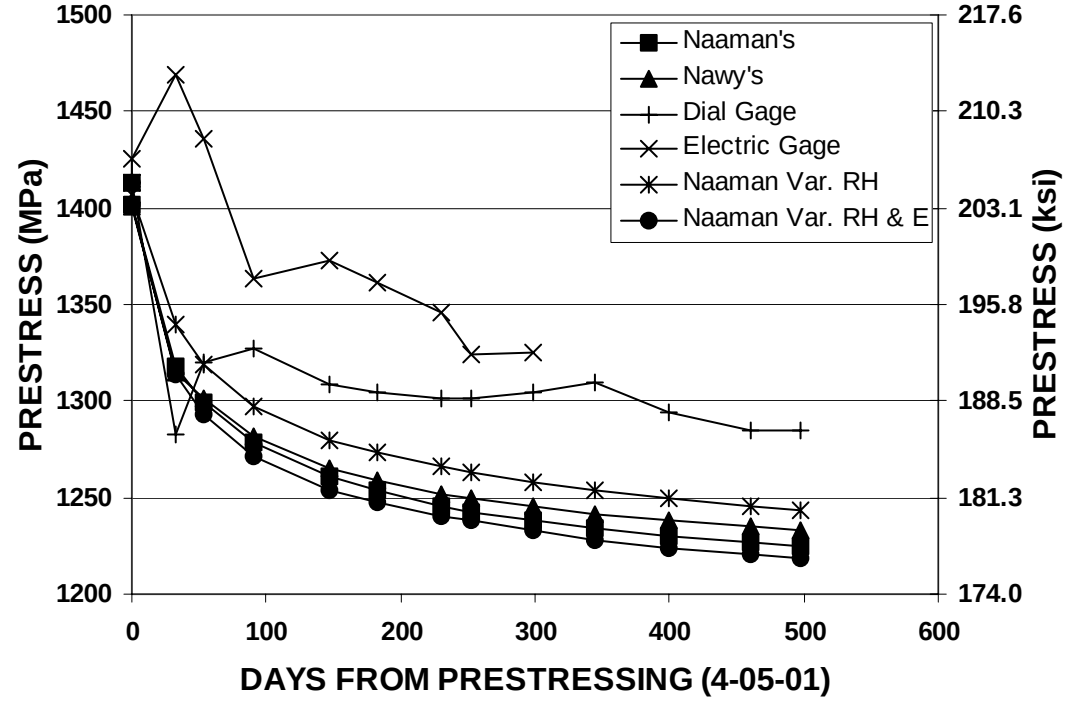

Figure 5.118 – Prediction Method Comparison - LVOMS

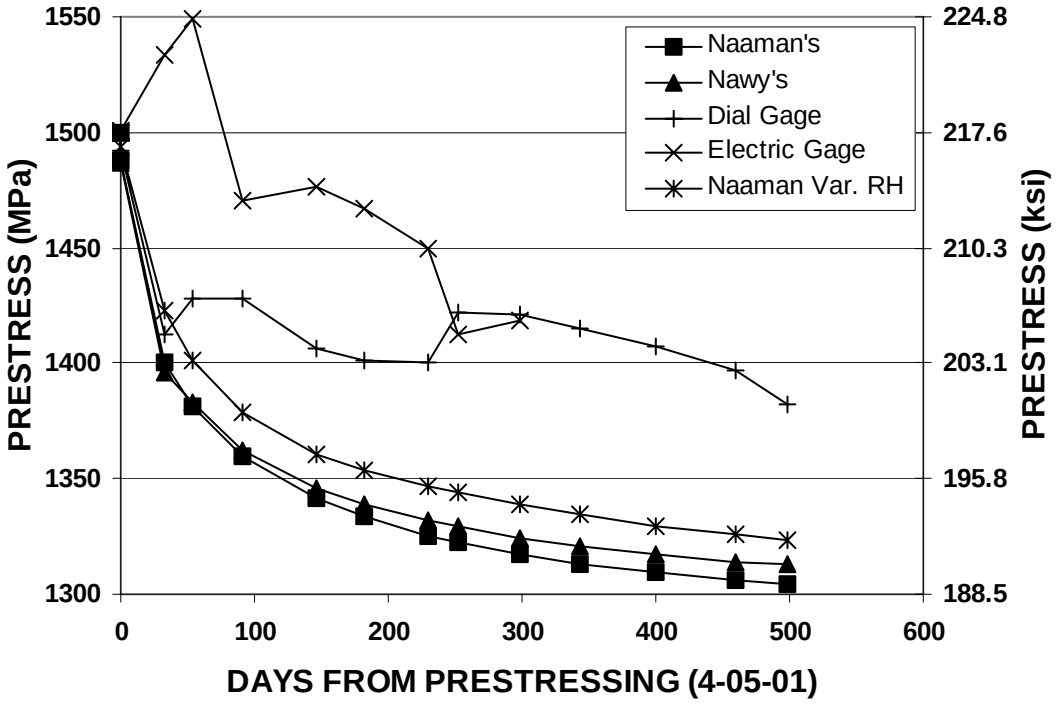

Figure 5.119 – Prediction Method Comparison - LVOAS

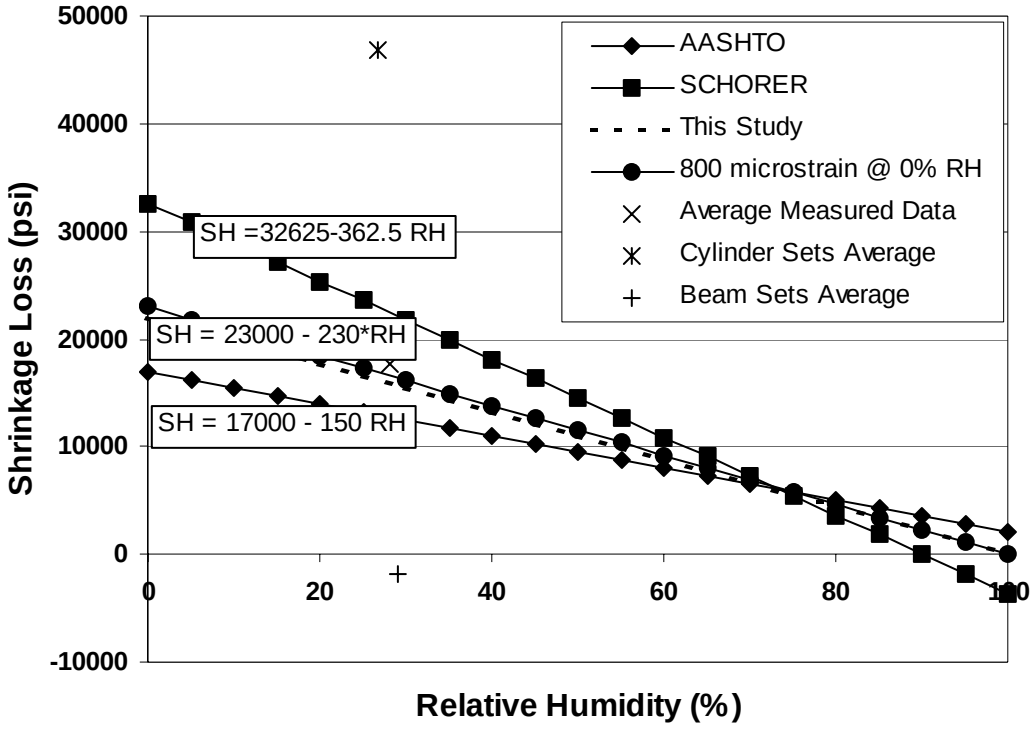

Figure 6.1 – Comparison of Shrinkage Losses

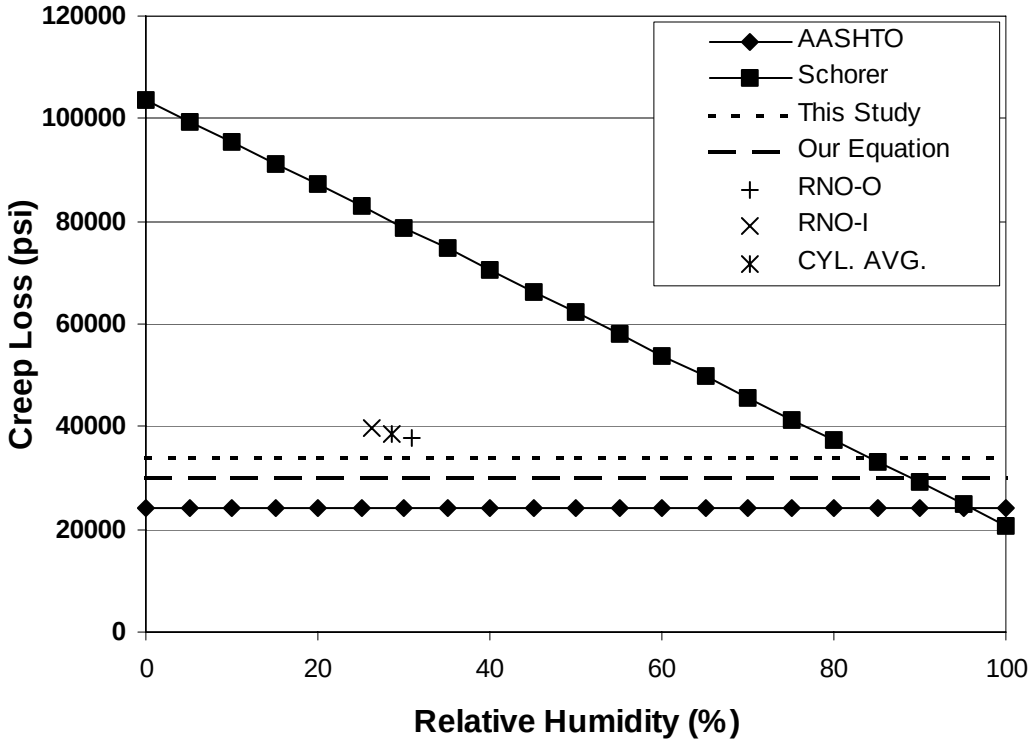

Figure 6.2 – Comparison of Creep Losses Using 30% Initial Stress

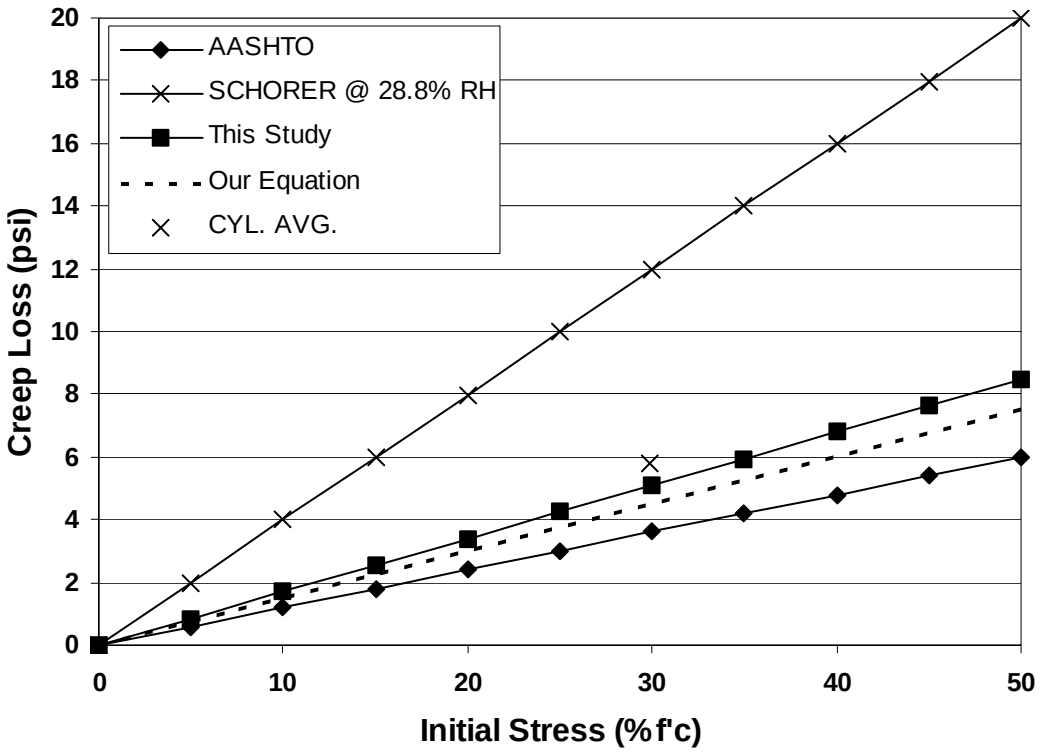

Figure 6.3 – Comparison of Creep Losses for Different Initial Stresses

Progress Report
June 1999

CREEP AND SHRINKAGE LOSSES IN NEVADA AGGREGATES

SELECTION OF AGGREGATES

Prepared by Catherine French and M. Saiid Saiidi

ABSTRACT

The overall objective of this study is to determine the effects of climate and aggregate type on prestress losses due to creep and shrinkage. Outlined in this report are three issues: a review of aggregate characteristics that affect creep and shrinkage losses, the identification of the aggregate sources that are used in bridge construction in Nevada, and recommended sources for the aggregates that are more likely to exhibit large creep and shrinkage losses. The recommended aggregate source in Northern Nevada is All-Lite Lockwood. Andesite, the aggregate rock type, experiences larger creep and shrinkage losses than the rock types from other aggregate sources. In the south, limestone was selected because it appears to be the only aggregate type used in bridges. A second parameter chosen for the study is the aggregate to cement ratio (a/c). Two batches of concrete, one with an a/c value of 4 and the other with an a/c value of 5 will be mixed at the university for eight beam specimens, four in the north and four in the south.

OBJECTIVES

The overall objective of this study is to determine the effects of climate and aggregate type on prestress losses due to creep and shrinkage. To accomplish the objectives, eight prestressed concrete beams will be constructed using different aggregates in Northern and Southern Nevada. The beams will be monitored to study the variation of prestress forces over a 30-month period. The objectives of the part of the study discussed in this report are to (1) review aggregate characteristics that affect creep and shrinkage losses, (2) identify the aggregate sources that are used in bridge construction, and (3) recommend sources for aggregate that are more likely to exhibit large creep and shrinkage losses.

RESEARCH PLAN

Literature Review

The focus of the literature review is on aggregates. In particular, aggregate properties that affect creep and shrinkage were of interest.

Aggregate Properties

Five major characteristics of aggregates affecting the magnitude of creep and shrinkage in concrete were identified:

1) Modulus of elasticity
2) Aggregate content
3) Absorption
4) Cleanness

5) Thermal expansion

1) Modulus of Elasticity

Modulus of elasticity (E) has the most significant effect on creep and shrinkage of concrete. As expected, the higher the E value, the lower the deformation of aggregate. The E value is mainly affected by aggregate density. Aggregates with higher density have a larger E[1]. In contrast, the higher porosity, the lower the E value[2].

2) Aggregate Content

Figure 1 illustrates the effect of aggregate content and water-cement ratio on shrinkage. It can be noted that as the aggregate content increases, shrinkage becomes less sensitive to the water-cement ratio. If the aggregate content is reduced, the water-cement ratio becomes critical because it increases shrinkage.

Note that the aggregate content also affects creep of concrete. The following equations demonstrate how both creep and shrinkage depend on aggregate content:

S_c = Shrinkage of concrete S_p = Shrinkage of paste
C_c = Creep of concrete C_p = Creep of paste

a = aggregate content (aggregate/cement)

(For the purposes of this relationship, n and α are arbitrary and are less than one.)

Shrinkage $Sc / Sp = (1-\mathbf{a})^n$
Creep $Cc / Cp = (1-\mathbf{a})^\alpha$

By increasing aggregate content of concrete from 71-74% (at same water/cement ratio) shrinkage is reduced by 20%[1]. The increase of the volumetric aggregate content from 65 to 70% can decrease the creep by 10%.

3) Absorption

Cracking contributes to increased permeability increasing the water absorption by the specimen. An increased absorption capacity of an aggregate creates a conducive environment for drying creep. This is provided by the transference of moisture held by aggregates with high porosities. Drying shrinkage and creep are both directly affected by capillary pores (range of 3-20nm), which facilitate more avenues for moisture. Admixtures contributing to pore-refinement also increase creep and shrinkage[2].

4) Cleanness

Clean aggregates are necessary because the presence of clay reduces the concrete's resistance to deformation. Clay-coated aggregates can increase shrinkage by

up to 70%. Aggregates with high absorption are also vulnerable to higher shrinkage and should be avoided[1].

5) Thermal Expansion

Thermal shrinkage strain is caused by a large temperature drop and is controlled by the coefficient of thermal expansion of concrete[2]. Limestone has the lowest coefficient of thermal expansion[2].

Comparison of Aggregate Types

References 2 and 3 present a comprehensive evaluation of creep and shrinkage properties of different aggregate types. Figures 2 and 3 summarize the shrinkage and creep strains as a function of time for several aggregate types, respectively2. It can be seen that sandstone is the most vulnerable aggregate type to both shrinkage and creep. The aggregate that leads to the least amount of shrinkage is quartz, with limestone also exhibiting relatively small shrinkage strains. Limestone shows the least amount of creep strains (Fig. 3), with quartz also having relatively small creep strains.

The results from Ref. 3 are similar to those of Ref. 2. Dolomite (limestone) and siltstone show the least and the most amount of shrinkage, respectively (Fig. 4). With respect to creep strains, granite and dolomite exhibit low strains, whereas andesite and some particular type of quartz show the highest strains.

Other Factors Affecting Creep and Shrinkage

Other considerations, aside from the aggregates, are noted in the following sections. These factors are mentioned to maintain a thorough investigation.

Cement paste is the material which actually undergoes creep and shrinkage. Therefore, the choice of the most appropriate cement paste is necessary in design. Creep and shrinkage generally increase with high cement content[2]. Cements deficient of gypsum exhibit greatly increased shrinkage and creep losses[1]. Higher shrinkage also occurs with the use of high-alumina cement.

Some concrete and cement chemical properties contributing to creep and shrinkage should also be heeded. Added calcium chloride increases the shrinkage of cement by 10 to 50%. Carbonation shrinkage, which occurs with high CO^2 concentrations, occurs to the greatest degree at intermediate humidities; however, it has no effect on shrinkage at high (100%) and low (25%) humidities[1].

Removing a specimen directly from water to an extremely dry environment causes cracks in the concrete[1]. Air entrainment has been shown to have no effect on shrinkage[1]. This should be considered because often in northern Nevada concrete is air-entrained to compensate for the effect of freeze-thaw action.

Aggregate Sources

Initially, a list of sieve analyses results was requested for the representative aggregates utilized most often by NDOT for bridge structures in northern and southern Nevada. In total, data from seven aggregate companies were received: three from the north and four from the south (Table 1). The type of rock each company supplied for use specifically in NDOT bridge construction was requested. Additionally, a sample copy of the concrete mix design used by each company was collected for the NDOT bridge projects. Based on the mix design and the rock type specific recommendations were made as to the aggregate sources to be used in the project.

Recommendations

Based on the material presented in the previous sections, aggregates sources were selected. Aggregates supplied by All-Lite Lockwood and Gopher Pit were selected for the construction of the beams in the north. The mineral of the aggregate produced from these sources is metamorphic andesite. As illustrated by Figs. 4 and 5 andesite contributes to shrinkage losses and, even more so, to creep losses. The sources in the south all supply limestone. Therefore, the aggregate choice from the south will be the limestone.

Aggregate content is another property that will be controlled for each specimen constructed. Low aggregate contents yield greater degrees of creep and shrinkage. The more critical, yet common, range representing the amount of aggregate is aggregate-cement ratios (a/c) of 4 to 5 (Table 1). Two batches of concrete for four beams will be constructed. One concrete batch will have an a/c value of 4 and the other will have and a/c value of 5. Because of the low concrete volume required and the necessary control for the mix designs, the concrete for the girders will be mixed at the university using the designated aggregate.

Notes:

One of the aggregate suppliers Rocky Ridge (coarse aggregate) and Stormy Canyon (sand) could not provide a concrete mix design. Steve Parker from Nevada Cement claims that the aggregate from these sources, namely Rocky Ridge, has only been used recently and only for asphalt pavement. Therefore, the decision was made to exclude the aggregates supplied from Rocky Ridge and Stormy Canyon.

REFERENCES

1. Neville, A.M., Properties of Concrete, Pitman Publishing Limited, London, 1981.

2. Mehta, P. Kumar and Monteiro, Paulo J.M., Concrete: Structure, Properties, and Materials, Prentice Hall, Englewood Cliffs, New Jersey, 1993.

3. Alexander, Mark G., "Aggregates and the Deformation Properties of Concrete," ACI Materials Journal, V. 93, No. 6, pp. 569-577, November-December 1996.

4. Popovics, Sandor, Concrete-Making Materials, Hemisphere Publishing Corporation, Washington, 1979.

Table 1. Mix Design Parameters Used for Aggregate Selection

Concrete Supplier	Pit Name	Weight of Aggregate (lbs.)	Wieght of Cement (lbs.)	Weight of Water (lbs.)	Ratio a/c (by weight)	Ratio w/c	A.C. by Total Volume (%)	Rock Type
	North							
CB Concrete	All-Lite Lockwood & Cashor Pit	2624	564	260	4.65	0.46	64.15	metamorphic andesite
?	Stormy Canyon & Rocky Ridge	No Mix Design Provided				0.44		basalt
Use Own	River Ranch Deposit	2974	611	300	4.87	0.49	68.18	dolometic limestone
	South							
Nevada Ready Mix	Lone Mountain Road Pit	4167	739	379	5.64	0.51	68.5	limestone
Eagle Ready Mix	Blue Diamond Materials	3290	480	187	6.85	0.39	71.19	dolometic limestone
Silver State Materials	Sloan Pit	2995	706	300	4.24	0.42	68	limestone
CSR	Buffalo Road Pit	3942	984	355	4.01	0.36	68	limestone

APPENDIX B
TIME-STEP METHODS

B.1 Naaman

The following section is a summary of the equations used from the time-step method suggested by Naaman. This method approaches prestress loss estimates by setting two points in time and then determining the loss over that period. The total loss is then produced by the summation of the losses from each time period.

Relaxation Loss, $\Delta f_{pR}(t_i, t_j)$

$$\Delta f_{pR}(t_i, t_j) = \frac{f_{ps}(t_i)}{45}\left(\frac{f_{ps}(t_i)}{f_{py}} - 0.55\right)\log\left(\frac{t_j}{t_i}\right)$$

Where:

$f_{ps}(t_i)$ = stress in the prestressing strands at the beginning of the interval
f_y = yield stress of the prestressing strands
t = time in hours

$$\frac{f_{ps}}{f_{py}} \geq 0.55$$

Shrinkage Loss, $\Delta f_{pS}(t_i, t_j)$

$$\Delta f_{pS}(t_i, t_j) = E_{ps}\varepsilon_{SU}K_{SH}K_{SS}\left[g(t_i) - g(t_j)\right]$$

Where:

E_{ps} = elastic modulus of prestressing steel
ε_{SU} = ultimate shrinkage strain of concrete material

$$= \left[2 + \frac{11}{230}(w - 220)\right]10^{-4}$$

$$= \left[2 + \frac{11}{1337}(w - 1279)\right]10^{-4}(\text{SI units})$$

Where:

w = water content in pounds per cubic yard (newtons per cubic meter)
K_{SH} = relative humidity correction factor (see Table B.1, B.3, and B.4)
K_{SS} = shape and size correction factor (see Table B.3 and B.4)

$$= 1.14 - 0.09\left(\frac{V}{S}\right)$$

Where:

$\frac{V}{S}$ = volume - to - surface ratio

$$g(t) = \frac{t}{b+t}$$

Where:

t = time in days
b = 35 for moist-cured concrete and 55 for steam-cured concrete

Creep Loss, $\Delta f_{pC}(t_i, t_j)$

$$\Delta f_{pC}(t_i, t_j) = E_{ps}\left[g(t_i) - g(t_j)\right]C_{CU}K_{CH}K_{CA}K_{CS}\varepsilon_{ci}$$

Where:

C_{CU} = ultimate creep coefficient (see Table B.2, B.3, and B.4)
K_{CH} = relative humidity correction factor (see Table B.1, B.3, and B.4)
$$= 1.27 - 0.0067H$$

Where:

H = relative humidity (%)
K_{CA} = age at loading correction factor (see Table B.1, B.3, and B.4)
K_{CS} = shape and size correction factor (see Table B.1, B.3, and B.4)
$$= 1.14 - 0.09\left(\frac{V}{S}\right)$$

Where:

$\frac{V}{S}$ = volume - to - surface ratio

$$\varepsilon_{ci} = \frac{f_{cgs}(t_i)}{E_c}$$

Where:

$f_{cgs}(t_i)$ = stress due to the dead load and prestressing force in the concrete at the centroid of the prestressing steel at time t_i

E_c = concrete modulus of elasticity

$$g(t) = \frac{t^{0.60}}{10 + t^{0.60}}$$

Where:

t = time in days

B.1.1 Calculation of Losses

The losses for the time-step methods were calculated using spreadsheets similar to Fig. B.1.

Where:

e = eccentricity of prestressing steel
L = length
SD = superimposed dead load
D = dead load
LL = live load
Anchorage = anchorage set losses
Friction = friction losses
M_{sd} = moment due to the superimposed dead load
M_d = moment due to the dead load
M_l = moment due to the live load
M_t = total moment

Figure B.2 shows how the spreadsheet was set up.

Where:

$$R_1 = f_{pi} * \left[1 - \frac{\log(t_1)}{45} \left(\left(\frac{f_{pi}}{f_{py}} \right) - .055 \right) \right]$$

$$R_n = \frac{f_p(t_{n-1})}{45} \left(\left(\frac{f_p(t_{n-1})}{f_{py}} \right) - 0.55 \right) \left(\log \left(\frac{t_n}{t_{n-1}} \right) \right)$$

$$\frac{f_p(t_n)}{f_{py}} = IF \left(\frac{f_p(t_{n-1})}{f_{py}} < 0.55, 0.55, \frac{f_p(t_{n-1})}{f_{py}} \right)$$

$$f_{cgs}(t_n) = -f_p(t_{n-1})\frac{A_{ps}}{A_c}\left(1+\frac{e^2}{\left(\frac{I_c}{A_c}\right)}\right)+M_t\left(\frac{e}{I_c}\right)$$

$$C_n = -f_{cgs}(t_n)C_{cu}K_{ca}K_{ss}K_{ch}\left(\left(\frac{t_n^{0.60}}{10+t_n^{0.60}}\right)-\left(\frac{t_{n-1}^{0.60}}{10+t_{n-1}^{0.60}}\right)\right)$$

$$S_n = E_{ps}\varepsilon_{su}K_{sh}K_{ss}\left(\left(\frac{t_n}{35+t_n}\right)-\left(\frac{t_{n-1}}{35+t_{n-1}}\right)\right)$$

B.2 Nawy

The following section is a summary of the equations used from the time-step method suggested by Nawy. Different from Naaman, this method determines the total prestress losses at anytime beyond the time of prestressing. See tables B.3 and B.4 for values used in estimating losses for beam specimens.

Relaxation Loss, Δf_{pR}

$$\Delta f_{pR} = f_{pi}\frac{\log(t_2-t_1)}{45}\left(\frac{f_{pi}}{f_{py}}-0.55\right)$$

In Which:

f_{pi} = initial stress in prestressing strands
f_y = yield stress of the prestressing strands
t = time in hours

$$\frac{f_{pi}}{f_{py}} \geq 0.55$$

Shrinkage Loss, Δf_{pSH}

$$\Delta f_{pSH} = \varepsilon_{SH}E_{ps}\left(\frac{t}{t+b}\right)$$

In Which:

ε_{SH} = ultimate shrinkage strain of concrete material taken as $780*10^{-6}$ microstrain
E_{ps} = elastic modulus of prestressing steel
t = time in days following when shrinkage would be considered
b = 35 for moist curing and 55 for steam curing

Creep Loss, Δf_{pCR}

$$\Delta f_{pCR} = K_{CR}\left(f_{cs} - \bar{f}_{csd}\right)\frac{E_{ps}}{E_c}$$

In Which:

$$K_{CR} = 2.35\left(\frac{t^{0.60}}{10 + t^{0.60}}\right)$$

In Which:

t = time in days
f_{cs} = initial stress in concrete immediately following prestressing
$\boldsymbol{f_{csd}}$ = stress in the concrete at the centroid of the prestressing steel due to all superimposed dead loads applied after prestressing
E_c = concrete modulus of elasticity

B.2.2 Calculation of Losses

The losses using Nawy's method were calculated using a spreadsheet similar to the one used for Naaman's method, but using the equations suggested by Nawy.

Table B.1 – Naaman Values for Prestress Loss Factors

		Moist-cured concrete	
Relative Humidity (*H*)		$40\% \le H \le 80\%$	$80\% \le H \le 100\%$
Shrinkage Loss Variables	t	≥ 7 days	≥ 7 days
	b	35	35
	K_{SH}	$=1.40-0.01*H$	$=3-0.03*H$
Relative Humidity (*H*)		$H \ge 40\%$	
Creep Loss Variables	t, t_A	≥ 7 days	
	K_{CA}	$= 1.25\ t_A^{-0.118}$	
	K_{CH}	$=1.27-0.0067*H$	
		Steam-cured concrete	
Relative Humidity (*H*)		$40\% \le H \le 80\%$	$80\% \le H \le 100\%$
Shrinkage Loss Variables	t	≥ 1 to 3 days	≥ 1 to 3 days
	b	55	55
	K_{SH}	$=1.40-0.01*H$	$=3-0.03*H$
Relative Humidity (*H*)		$H \ge 40\%$	
Creep Loss Variables	t, t_A	≥ 1 to 3 days	
	K_{CA}	$= 1.13\ t_A^{-0.095}$	
	K_{CH}	$=1.27-0.0067*H$	

Table B.2 – Naaman Ultimate Creep Coefficient

Concrete Compressive Strength (psi)	Ccu*
3000	3.10
4000	2.90
5000	2.65
6000	2.40
7000	2.20
8000	2.00

*Interpolation may be used for values in between.

Table B.3 – Specimen Properties and Factor Values For Time-Step Methods Reno Beams

PROPERTIES	RNOMB	RNOAB	RNIMB	RNIAB	RNOMS	RNOAS
Area of Concrete, A_c (in^2)	64				24.75	
Concrete Strength, f'_c (psi)	6693				4100	
Modulus of Elasticity of Concrete, E_c (psi)	4663213				3649781	
Area of Prestressing Steel, A_{ps} (in^2)	0.864				0.216	
Moment of Inertia, I (in^4)	596.33				62.39	
Yield Strength of Prestressing Steel, f_{py} (ksi)	243				243	
Modulus of Elasticity of Prestressing Steel, E_{ps} (ksi)	28000				28000	
Initial Stress in Prestressing Steel, f_{pi} (ksi)	173.1	169.2	190.1	166.5	248.5	214.4
Volume-Surface Ratio, $^V/_S$ (in)	0.75				1.25	
Relative Humidity, H (%)	50				50	
NAAMAN FACTORS						
e_{SU} (strain)	0.000773913				0.000773913	
K_{SH}	0.90				0.90	
K_{SS}	1.07				1.03	
C_{CU}	2.29				2.86	
K_{CH}	0.94				0.94	
K_{CA}	0.69				0.74	
K_{CS}	1.07				1.03	

Table B.4 – Specimen Properties and Factor Values For Time-Step Methods Las Vegas Beams

PROPERTIES	LVOMB	LVOAB	LVIMB	LVIAB	LVOMS	LVOAS
Area of Concrete, A_c (in^2)	64				24.75	
Concrete Strength, f'_c (psi)	6693				4100	
Modulus of Elasticity of Concrete, E_c (psi)	4663213				3649781	
Area of Prestressing Steel, A_{ps} (in^2)	0.864	0.648	0.864	0.864	0.216	
Moment of Inertia, I (in^4)	596.33				62.39	
Yield Strength of Prestressing Steel, f_{py} (ksi)	243				243	
Modulus of Elasticity of Prestressing Steel, E_{ps} (ksi)	28000				28000	
Initial Stress in Prestressing Steel, f_{pi} (ksi)	136.4	160.3	160	148.1	204.9	217.5
Volume-Surface Ratio, $^V/_S$ (in)	0.75				1.25	
Relative Humidity, H (%)	27				27	
NAAMAN FACTORS						
e_{SU} (strain)	0.000773913				0.000773913	
K_{SH}	1.13				1.13	
K_{SS}	1.07				1.03	
C_{CU}	2.29				2.86	
K_{CH}	1.09				1.09	
K_{CA}	0.64				0.78	
K_{CS}	1.07				1.03	

NAAMAN

INPUTS	in and kips
A_c	64
A_{ps}	0.864
I_c	596.33
f_{pu}	270
f_{pi}	173.1
f_{py}	243
E_{ps}	28000
f'_c	6693
E_c	2986.09
e	0
L (ft)	12
SD (k/ft)	0
D (k/ft)	0.0667
LL (k/ft)	0
RH	50
V/S	0.75
w/c (lbs/yd^3)	340
Anchorage	0
Friction	0

MOMENTS	
M_{sd}	0
M_d	57.6
M_l	0
Mt	57.6

BEAM: RNOM

Time from Curing Until Stressing (t_c): 146

C_{cu}	2.288
K_{ca}	0.694
K_{ss}	1.073
K_{ch}	0.935

ε_{su}	0.001
K_{sh}	0.900

							PRESTRESS	
TIME	**LOSSES**						**TOTAL**	**CR & SH**
0	**RELAX.**	**fpi/fpy**	**CR**	**fcs**	**SH**	**CR & SH**	173.1	173.1
1	0.86	0.71	3.17	-2.34	0.02	3.19	169.04	169.91
29	0.80	0.70	11.55	-2.28	0.54	12.09	156.15	157.82
57	0.09	0.64	3.18	-2.11	0.41	3.59	152.47	154.23
92	0.05	0.63	2.16	-2.06	0.39	2.56	149.86	151.67
124	0.03	0.62	1.27	-2.02	0.28	1.55	148.28	150.12
166	0.03	0.61	1.17	-2.00	0.29	1.46	146.80	148.66
182	0.01	0.60	0.35	-1.98	0.09	0.44	146.35	148.22
215	0.01	0.60	0.61	-1.98	0.17	0.78	145.55	147.44
244	0.01	0.60	0.45	-1.96	0.13	0.57	144.97	146.86
274	0.01	0.60	0.39	-1.96	0.11	0.51	144.45	146.36
307	0.01	0.59	0.37	-1.95	0.11	0.48	143.97	145.87
335	0.01	0.59	0.28	-1.94	0.08	0.36	143.60	145.52
370	0.01	0.59	0.30	-1.94	0.09	0.39	143.20	145.12
440	0.01	0.59	0.51	-1.93	0.15	0.66	142.54	144.47
456	0.00	0.59	0.10	-1.92	0.03	0.13	142.41	144.34
489	0.00	0.59	0.19	-1.92	0.06	0.25	142.15	144.09
533	0.00	0.58	0.23	-1.92	0.07	0.30	141.85	143.79
552	0.00	0.58	0.09	-1.92	0.03	0.12	141.73	143.67

Figure B.1 – Spreadsheet Calculations for RNOM Using Naaman

581	0.00	0.58	0.13	-1.91	0.04	0.17	141.56	143.50
614	0.00	0.58	0.14	-1.91	0.04	0.18	141.38	143.33
642	0.00	0.58	0.11	-1.91	0.03	0.14	141.24	143.19
672	0.00	0.58	0.11	-1.91	0.03	0.14	141.10	143.04
707	0.00	0.58	0.12	-1.90	0.03	0.15	140.94	142.89
742	0.00	0.58	0.11	-1.90	0.03	0.14	140.95	142.90
765	0.00	0.58	0.07	-1.90	0.02	0.09	140.86	142.81
793	0.00	0.58	0.08	-1.90	0.02	0.10	140.76	142.71
830	0.00	0.58	0.10	-1.90	0.03	0.13	140.63	142.58
853	0.00	0.58	0.06	-1.90	0.02	0.08	140.55	142.51
883	0.00	0.58	0.07	-1.90	0.02	0.09	140.46	142.41
916	0.00	0.58	0.08	-1.90	0.02	0.10	140.36	142.32
938	0.00	0.58	0.05	-1.89	0.01	0.06	140.30	142.25
1303	0.01	0.58	0.63	-1.89	0.16	0.79	139.49	141.46
1668	0.01	0.57	0.41	-1.88	0.10	0.51	138.97	140.95
2033	0.01	0.57	0.30	-1.88	0.07	0.36	138.61	140.59
2398	0.00	0.57	0.23	-1.87	0.05	0.27	138.33	140.32
2763	0.00	0.57	0.18	-1.87	0.04	0.21	138.11	140.10
3128	0.00	0.57	0.15	-1.86	0.03	0.17	137.93	139.93
3493	0.00	0.57	0.12	-1.86	0.02	0.14	137.79	139.78
3858	0.00	0.57	0.10	-1.86	0.02	0.12	137.66	139.66
4223	0.00	0.57	0.09	-1.86	0.02	0.11	137.55	139.56
4588	0.00	0.57	0.08	-1.86	0.01	0.09	137.46	139.46
4953	0.00	0.57	0.07	-1.86	0.01	0.08	137.38	139.38
5318	0.00	0.57	0.06	-1.85	0.01	0.07	137.30	139.31
5683	0.00	0.57	0.06	-1.85	0.01	0.06	137.24	139.25
6048	0.00	0.56	0.05	-1.85	0.01	0.06	137.18	139.19
6413	0.00	0.56	0.05	-1.85	0.01	0.05	137.12	139.14
6778	0.00	0.56	0.04	-1.85	0.01	0.05	137.07	139.09
7143	0.00	0.56	0.04	-1.85	0.01	0.04	137.03	139.04
7508	0.00	0.56	0.04	-1.85	0.00	0.04	136.99	139.00
7873	0.00	0.56	0.03	-1.85	0.00	0.04	136.95	138.96
8238	0.00	0.56	0.03	-1.85	0.00	0.04	136.91	138.93
8603	0.00	0.56	0.03	-1.85	0.00	0.03	136.88	138.90
8968	0.00	0.56	0.03	-1.85	0.00	0.03	136.85	138.87
9333	0.00	0.56	0.03	-1.85	0.00	0.03	136.82	138.84
9698	0.00	0.56	0.02	-1.85	0.00	0.03	136.79	138.81
10063	0.00	0.56	0.02	-1.85	0.00	0.03	136.77	138.78
10428	0.00	0.56	0.02	-1.85	0.00	0.02	136.74	138.76
10793	0.00	0.56	0.02	-1.85	0.00	0.02	136.72	138.74
11158	0.00	0.56	0.02	-1.85	0.00	0.02	136.70	138.72
11523	0.00	0.56	0.02	-1.85	0.00	0.02	136.68	138.70
11888	0.00	0.56	0.02	-1.85	0.00	0.02	136.66	138.68
14600	0.00	0.56	0.11	-1.84	0.01	0.12	136.53	138.56
			30.70		4.00	34.69		

Figure B.1 (continued) – Spreadsheet Calculations for RNOM Using Naaman

NAAMAN

INPUTS	in and kips
A_c	64
A_{ps}	0.864
I_c	596.33
f_{pu}	270
f_{pi}	173.1
f_{py}	=0.9*fpu
E_{ps}	28000
f'_c	6693
E_c	$=36.5*f'_c{}^{0.5}$
e	0
L (ft)	12
SD (k/ft)	0
D (k/ft)	0.0667
LL (k/ft)	0
RH	50
V/S	0.75
w/c (lbs/yd^3)	340
Anchorage	0
Friction	0

MOMENTS	
M_{sd}	0
M_d	57.6
M_l	0
Mt	57.6

BEAM: RNOM

Time from Curing Until Stressing (t_c): 146

C_{cu}	$=-0.00022f'_c+3.76$
K_{ca}	$=1.25t_c^{-0.118}$
K_{ss}	=1.14-0.09V/S
K_{ch}	=1.27-0.0067RH

ε_{su}	=(2+11/230(w/c-220))0.0001
K_{sh}	=IF(RH>80,3-0.03RH,1.4-0.01RH)

							PRESTRESS	
TIME	**LOSSES**						**TOTAL**	**CR & SH**
t_0	**RELAX.**	**fpi/fpy**	**CR**	**fcgs**	**SH**	**CR & SH**	173.1	173.1
t_1	R_1	$fp(t_0)/fpy$	C_1	$fcgs(t_1)$	S_1	C_1+S_1	$T(t_1)$	$Tcs(t_1)$
t_n	R_n	$fp(t_{n-1})/fpy$	C_n	$fcgs(t_n)$	S_n	C_n+S_n	$T(t_n)$	$Tcs(t_n)$
			$=\Sigma C_1+...+C_n$		$=\Sigma S_1+...+S_n$	$=\Sigma(C_1+S_1)+...+(C_n+S_n)$		

Figure B.2 – Spreadsheet Formulation for RNOM Using Naaman

Kenny C. Guinn, Governor

Nevada Department of Transportation
Jeff Fontaine, P.E. Director
Tie He, Research Division Chief
(775) 888-7220
the@dot.state.nv.us
1263 South Stewart Street
Carson City, Nevada 89712